METAL(II) SCHIFF BASE COMPLEXES AND THE INSULIN-MIMETIC STUDIES ON THE OXOVANADIUM(IV) COMPLEXES

BY

ADEOLA AYODEJI NEJO

206001421

B. Sc. (Hons), M. Sc. (Lagos)

A THESIS IN THE DEPARTMENT OF CHEMISTRY

SUBMITTED TO THE FACULTY OF SCIENCE AND AGRICULTURE IN PARTIAL FULFILMENT OF THE REQUIREMENTS FOR THE AWARD OF THE DEGREE OF

DOCTOR OF PHILOSOPHY

OF THE

UNIVERSITY OF ZULULAND

JUNE 2009

ABSTRACT

Sixteen symmetrical and four unsymmetrical tetradentate Schiff bases with the N_2O_2 chromophore were isolated in pure form and fully characterized by elemental analyses, melting point, IR and ^1H NMR. The appearance of two different peaks for each of the azomethine protons and phenolic protons confirm the asymmetry nature of the unsymmetrical Schiff bases. All the Schiff bases were successfully coordinated to oxovanadium(IV) ion to form the corresponding complexes. The unsymmetrical Schiff bases were also successfully coordinated to cobalt(II), nickel(II) and copper(II) ions to form their corresponding complexes. In all thirty-two metal(II) Schiff bases complexes were isolated. These complexes were characterized by elemental analyses, melting point, IR, EPR, cyclic voltammetry, magnetic susceptibility measurements, differential scanning calorimetry and electronic spectra. The isolation of the unsymmetrical tetradentate Schiff bases and their complexes as well as some of the symmetrical tetradentate Schiff bases and their complexes are considered to be novel. The purity and composition of both the Schiff bases and the metal(II) complexes were established by elemental analyses.

The comparison of the IR spectra of the Schiff-bases and their metal complexes indicated that the Schiff bases acted as tetradentate ligands. The observed shifts in the stretching frequencies of ν(C=N) and ν(C—O) are indicative of the formation of these complexes. Further conclusive evidence of the coordination of these Schiff-bases with the metal ions was shown by the appearance of new bands due to ν(M—N) and ν(M—O) in the metal complexes. Most of the oxovanadium(IV) complexes exhibit a strong band in the range 959−989 cm^{-1}, which have been assigned to ν(V=O) in a monomeric square pyramidal coordination environment. The

oxovanadium(IV) complexes with trimethylene bridge, in which their ν(V=O) appeared at 848−860 cm^{-1}, have been assigned polymeric structure with [V=O····V=O] interactions, which afforded distorted octahedral coordination geometry.

The electronic spectral and magnetic susceptibility measurements were used for assigning the stereochemistry of each metal complex. Electronic spectra indicate a square-planar geometry for all the cobalt(II), nickel(II) and copper(II) complexes. This was also corroborated by the effective magnetic moment of the complexes.

The electronic spectra of the oxovanadium(IV) complexes suggest a diversity of geometries. The electronic spectra indicate a square-pyramidal geometry for the five-coordinate species and distorted octahedral geometry for the six-coordinate species. The room temperature magnetic moments of 1.6–1.8 BM are normal for V(IV) d^1 configuration. The solution EPR spectra of the oxovanadium(IV) are consistent with square pyramidal geometry. The cyclic voltammetry of the oxovanadium(IV) complexes revealed only one quasi-reversible wave for each complex and they all showed redox couples with peak- to peak separation values (ΔEp) ranging from 74 to 83 mV, indicating a single step one electron transfer process.

In vitro glucose uptake was carried out on all the oxovanadium(IV) complexes using C2C12 cell line. All the complexes tested increased glucose utilization in C2C12 cells over basal values except two of the complexes whose percentage glucose uptake was lower than the basal glucose uptake (DMSO). Eighteen of the complexes significantly increased glucose uptake when compared to the basal glucose uptake of the solvent vehicle (DMSO). Cytotoxic test carried out on all the complexes using MTT assay showed that the complexes were not toxic to the cells

at both low and high concentrations. Two of the complexes showed activities comparable or greater than that of insulin.

Four unsymmetrical and five symmetrical Schiff base complexes of oxovanadium(IV) have been tested *in vivo* for their insulin mimetic activities. An acute oral administration of the four unsymmetrical Schiff base complexes of oxovanadium(IV) elicited a progressive reduction in plasma glucose over 6 h in STZ rats. Two of the unsymmetrical Schiff base complexes of oxovanadium(IV) induced a significant reduction in plasma glucose over a 6 h period. Oral administration of the five symmetrical complexes also elicited a progressive reduction in plasma glucose over 6hrs. Two of these complexes induced a significant reduction in plasma glucose during the 6 hour period.

ACKNOWLEDGMENTS

I am very much grateful to the Almighty God, the King of kings and the Lord of lords for enabling me to complete this work.

I wish to acknowledge my sincere thanks to my supervisors, Prof Gabriel Kolawole and Prof Andy Opoku for their invaluable help, thought-provoking guidance, encouraging attitude and pleasant behaviour throughout this study.

I wish to thank the National Research Foundation (NRF), South Africa for their generous financial support of this project.

The insulin-mimetic studies would also not have been possible without the help of Dr. Christo Muller of the Diabetic Discovery Platform (DDP), South African Medical Research Council. My sincere thanks also go to the other members of the group (DDP).

I also wish to thank Dr. Joanna Wolowska of School of Chemistry, The University of Manchester, UK for running the EPR and Dr. Paresh of Jackson state University, USA for use of DSC instrument.

I also wish to thank other lecturers in the department, especially Prof N. Revaprasadu and Mr. G Peckham, for their kind and cooperative behaviour throughout the course of this work.

I would like to thank my colleagues in the department, past and present. Special thanks go to Mr. O.M. Odeleye, Mr. O.A. Lawal, Mr. M. Chili, Miss. T. Xaba, Mr. N. Sosibo, Mr. N. Mlambo, Mr. P. Mdluli and Miss. M. Mdlolo. I extend a special thanks to the departmental support staff.

I also wish thank Pastor Foli and the members of the Redeem Christian Church of God (Empangeni branch) for their support and their prayers for successful completion of this work. I would like to thank Mrs. Kolawole for her encouragements and prayers throughout the course of this work.

I would like to thank my mum and my siblings for their moral support and prayers for successful completion of this work.

Special thanks to my dear wife for her patience and encouragement during the course of this work and my son Oluwaseyifunmi for his patience.

CERTIFICATION BY SUPERVISORS

We certify that this work was carried out by Mr. A.A. Nejo in the Department of Chemistry, University of Zululand and is approved for submission in fulfilment of the requirements for the award of the degree of Doctor of Philosophy in Chemistry.

.....
Promoter
G.A. Kolawole, B. Sc. (Hons), M. Ed, Ph.D (Ibadan), CChem, FRSC
Senior Professor of Inorganic Chemistry
Department of Chemistry, University of Zululand, Kwadlangezwa, South Africa

.....
Co-promoter
A.R. Opoku, B. Sc.(Hons) (Knust) Ph.D (Machester)
Professor of Biochemistry
Department of Biochemistry and Microbiology, University of Zululand, Kwadlangezwa, South Africa

DEDICATED

To my sons, Oluwaseyifunmi and Oluwatomisin;

To my wife, who inspired me a lot;

To my mum, who sacrificed every personal comfort to see me through my basic education

LIST OF PUBLICATIONS FROM THIS WORK

A A. Nejo, G A. Kolawole, A R. Opoku, J Wolowska, P O' Brien, "Synthesis, Characterization and preliminary Insulin-enhancing studies of symmetrical tetradentate Schiff Base Complexes of Oxovanadium(IV)" *Inorganica Chimica Acta 362* (2009) 3993-4001

A A. Nejo, G A. Kolawole, A R. Opoku, C Muller and J Wolowska, "Synthesis, Characterization and Insulin-enhancing studies of Unsymmetrical tetradentate Schiff Base Complexes of Oxovanadium(IV)" *Journal of Coordination Chemistry* 62:21 (2009) 3411-3424

ORAL COMMUNICATIONS AND POSTER PRESENTATIONS IN CONFERENCES

ORAL COMMUNICATIONS

5th International Symposium on Recent Advances in Environmental Health, Jackson, MS, USA
Nejo A. A., Kolawole G. A., and Opoku A. R. "Oxovanadium(IV) Complexes of Symmetrical Schiff Bases as possible Insulin enhancers" September 14th – 17th 2008.

39th SACI National Convention, Stellenbosch, SouthAfrica
Nejo A. A., Kolawole G. A., Opoku A. R. and Muller C. "Synthesis, Characterization and Insulin-enhancing studies of Unsymmetrical Tetradentate Schiff Base Complexes of Oxovanadium(IV)" November 30th – December 5th 2008.

POSTER PRESENTATIONS

2nd Annual Faculty of Science and Agriculture Research Symposium, Kwadlangezwa, South Africa
Nejo A. A., Kolawole G. A. and Opoku A. R "Synthesis, Characterization and Spectroscopic Studies of Symmetrical Tetradentate Schiff Base Oxovanadium(IV) Complexes as Part of Insulin mimetic Studies, November 1st 2007.

38th International Conference of Coordination Chemistry (Jerusalem-Israel)
Nejo A. A., Kolawole G. A. and Opoku A. R "Synthesis, Characterization and Insulin-enhancing Studies of Symmetrical Tetradentate Schiff Base Complexes of Oxovanadium(IV), July 20th – July 25th 2008.

TABLE OF CONTENTS

		PAGE
Abstract		i
Acknowledgements		iv
Certification		v
List of Publications from this work		vii
Oral Communications and Poster Presentations in Conferences		viii
Table of contents		ix
List of Figures		xvi
List of Tables		xix
List of Abbreviations		xxi
CHAPTER 1 INTRODUCTION		
1.1	Schiff bases	1
1.2	Biological Importance of Schiff Bases	3
1.3	Schiff base metal complexes	4
1.4	History and occurrence of vanadium	15
1.4.1	The chemistry of vanadium	17
1.5	Oxovanadium(IV) insulin enhancing agents	19
1.5.1	Pyronates and pyridinonates	20
1.5.2	Acetylacetonates	22
1.5.3	Picolinates	24
1.5.4	Oxovanadium(IV) salen-type derivatives	25
1.5.5	Dicarboxylate ester–oxovanadium(IV) complexes	26
1.6	Other metals used as insulin enhancing agents	27

1.6.1 Zinc compounds 27

1.6.2 Magnesium compounds 28

1.6.3 Chromium compounds 29

1.7 Toxicity of vanadium compounds 30

1.8 Accumulation of vanadium compounds in the body 30

1.9 Mechanism of action of insulin 31

1.10 Types of diabetes 33

1.11 Prevalence of diabetes in the World 34

1.12 Prevalence of diabetes in South Africa 35

1.13 Scope of this work 37

1.14 Aims and Objectives 37

1.15 Compounds covered in the project 38

CHAPTER 2 PHYSICAL TECHNIQUES USED FOR CHARACTERIZATION

2.1 Electron paramagnetic resonance (EPR) 42

2.1.1 The theory of EPR spectroscopy 43

2.1.2 The Effects of Point Symmetry 46

2.2 Magnetic susceptibility 47

2.2.1 The theory of magnetic susceptibility 48

2.2.2 Types of magnetic behaviour 49

2.2.3 Magnetic properties of transition metal complexes 50

2.3 UV-Visible spectrophotometry 51

2.3.1The Molecular Orbital Approach to bonding in oxovanadium(IV) ion 52

2.4 Thermal Analysis (TA) 56

2.4.1 Types of TA Instruments 57

2.5 Cyclic Voltammetry 60

CHAPTER 3 EXPERIMENTAL

3.1 Materials 62

3.2 Materials for insulin-mimetic test 62

3.3 Synthesis 62

3.3.1. Preparation of unsymmetrical Schiff bases 63

3.3.2 Preparation of symmetrical Schiff bases 63

3.3.3 Preparation of oxovanadium(IV) complexes 63

3.3.4. Preparation of the cobalt(II), nickel(II) and copper(II) Complexes 64

3.4 Characterization of the ligands and complexes 64

3.4.1 Microanalysis 65

3.4.2 Melting/decomposition points 65

3.4.3 ^{1}H NMR spectra 65

3.4.4 Infrared spectroscopy 65

3.4.5 Electronic absorption spectra 65

3.4.6 Electron paramagnetic resonance (EPR) 66

3.4.7 Magnetic moments 66

3.4.8 Cyclic voltammetry 66

3.4.9. Differential scanning calorimetry (DSC) 66

3.5 Insulin-mimetic activity 67

3.5.1 *In vitro* studies 67

3.5.1.1 Cell culture 67

3.5.1.2 Viable cell counts 68

3.5.1.3 Glucose uptake determination 68

3.5.1.4 Statistical analysis 69

3.5.2 *In vivo studies* 69

3.5.2.1 Animals 69

3.5.2.2 Experimental groups 70

3.5.2.3 Collecting of blood samples 70

3.5.2.4. Analysis of data 71

3.5.2.5 Gavage procedure 71

3.5.2.6 Statistical Analysis 71

CHAPTER 4 RESULTS AND DISCUSSION

4.1 Synthesis 72

4.1.1 Unsymmetrical Schiff bases 72

4.1.2 Unsymmetrical Schiff base metal(II) complexes 73

4.1.2.1 Unsymmetrical Schiff base complexes of cobalt(II) 74

4.1.2.2 Unsymmetrical Schiff base complexes of nickel(II) 74

4.1.2.3 Unsymmetrical Schiff base complexes of copper(II) 74

4.1.2.4 Unsymmetrical Schiff base complexes of oxovanadium(IV) 74

4.1.3 Symmetrical Schiff bases and complexes of oxovanadium(IV) 75

4.1.3.1 Benzophenoneimine 75

4.1.3.2 Naphthaldiimines 76

4.1.3.3 Chlorosalicylaldiimines 76

4.1.3.4 Methoxysalicylaldiimine 76

4.1.3.5 Ethoxysalicylaldiimine 77

4.2 ^{1}H NMR spectra of the Schiff bases 77

4.2.1 Unsymmetrical Schiff bases 78

4.2.2 Symmetrical Schiff bases 78

4.2.2.1 Benzophenoneimine 79

4.2.2.2 Naphthaldiimines 79

4.2.2.3 Chlorosalicylaldiimines 79

4.1.2.4 Methoxysalicylaldimine 80

4.1.2.5 Ethoxysalicylaldiimine 80

4.3 Infrared spectra 81

4.3.1 Unsymmetrical Schiff bases and their complexes 83

4.3.1.1 Unsymmetrical Schiff base complexes of cobalt(II) 83

4.3.1.2 Unsymmetrical Schiff base complexes of nickel(II) 83

4.3.1.3 Unsymmetrical Schiff base complexes of copper(II) 84

4.3.1.4 Unsymmetrical Schiff base complexes of oxovanadium(IV) 84

4.3.2 Symmetrical Schiff bases and their complexes 85

4.3.2.1 Benzophenoneimine 85

4.3.2.2 Naphthaldiimines 86

4.3.2.3 Chlorosalicylaldiimines 87

4.3.2.4 Methoxysalicylaldiimines 87

4.3.2.5 Ethoxysalicylaldiimines 88

4.4 Electronic spectra of the metal(II) complexes 89

4.4.1 Unsymmetrical Schiff base metal(II) complexes 91

4.4.1.1 Unsymmetrical Schiff base complexes of cobalt(II) 91

4.4.1.2 Unsymmetrical Schiff base complexes of nickel(II) 91

4.4.1.3 Unsymmetrical Schiff base complexes of copper(II) 92

4.4.1.4 Unsymmetrical Schiff base complexes of oxovanadium(IV) 92

4.4.2 Symmetrical Schiff base complexes of oxovanadium(IV) 93

4.4.2.1 Benzophenoneimine complexes 93

4.4.2.2 Naphthaldiimines complexes 94

4.4.2.3 Chlorosalicylaldiimines complexes 95

4.4.2.4 Methoxysalicylaldiimines complexes 96

4.4.2.5 Ethoxysalicylaldiimines complexes 97

4.5 Magnetic moment of the metal(II) complexes 98

4.5.1 Unsymmetrical Schiff base complexes of cobalt(II) 98

4.5.2 Unsymmetrical Schiff base complexes of nickel(II) 98

4.5.3 Unsymmetrical Schiff base complexes of copper(II) 99

4.5.4 Symmetrical and unsymmetrical Schiff base complexes of oxovanadium(IV) 99

4.6 EPR spectra of oxovanadium(IV) complexes 99

4.6.1 Unsymmetrical Schiff base complexes of oxovanadium(IV) 101

4.6.2 Symmetrical Schiff base complexes of oxovanadium(IV) 101

4.7 Cyclic voltammetry 103

4.8 Thermal analysis of oxovanadium(IV) complexes 103

4.8.1 Unsymmetrical Schiff base complexes of oxovanadium(IV) 104

4.8.2 Symmetrical Schiff base complexes of oxovanadium(IV) 105

4.8.2.1 Benzophenoneimine complexes 105

4.8.2.2 Naphthaldiimines complexes 105

4.8.2.3 Chlorosalicylaldiimines complexes 105

4.8.2.4 Methoxysalicylaldiimines complexes 106

4.8.2.5 Ethoxysalicylaldiimines complexes 107

CHAPTER 5 INSULIN-MIMETIC STUDIES ON THE OXOVANADIUM(IV) COMPLEXES

5.1 *In vitro* analysis 108

5.1.1 Unsymmetrical Schiff base complexes of oxovanadium(IV) 109

5.1.2 Symmetrical Schiff base complexes of oxovanadium(IV) 110

5.1.2.1 Benzophenoneimine complexes 110

5.1.2.2 Naphthaldiimines complexes 110

5.1.2.3 Chlorosalicylaldiimines complexes 111

5.1.2.4 Methoxysalicylaldiimines complexes 111

5.1.2.5 Ethoxysalicylaldiimines complexes 111

5.2 *In vivo* analysis 112

5.2.1 Unsymmetrical Schiff base complexes of oxovanadium(IV) 113

5.2.2 Symmetrical Schiff base complexes of oxovanadium(IV) 114

CHAPTER 6 CONCLUSIONS AND FUTURE PROSPECTS

6.1 Conclusions 116

6.2 Suggestion for future work 119

REFFERENCES 121

APPENDIX I

Tables of experimental results 135

APPENDIX II

Figures of spectroscopic spectra 153

Bar chart for *in vitro* analysis 186

Bar chart for *in vivo* analysis 188

LIST OF FIGURES

PAGE

Fig. 1.1 Some classes of Schiff base ligands 2

Fig. 1.2 Insulin-mimetic behaviour of vanadium compounds 32

Fig. 1.3 Worldwide map showing the prevalence of diabetes 35

Fig. 2.1 Energy levels for an unpaired electron in a magnetic field 45

Fig. 2.2 Energy level ordering of Ballhausen and Gray 55

Fig. 2.3 Changes in the ordering of the d orbitals in oxovanadium(IV) complexes 56

Fig. 4.1 Preparation of the unsymmetrical Schiff bases and their metal(II) complexes 73

Fig. 4.3.1 IR spectra of complex CoL^1 and its ligand H_2(naph-Clsal)opd: representative spectra for the unsymmetrical complexes of cobalt(II) and the ligands 153

Fig. 4.3.2 IR spectra of complex NiL^4 and its ligand H_2(naph-Clsal)opd: representative spectra for the unsymmetrical complexes of nickel(II) and the ligands 153

Fig. 4.3.3 IR spectra of complex CuL^1 and its ligand H_2(naph-Clsal)opd: representative spectra for the unsymmetrical complexes of copper(II) and the ligands 154

Fig. 4.3.4 IR spectra of complex VOL^1 and its ligand H_2(naph-Clsal)opd: representative spectra for the unsymmetrical complexes of oxovanadium(IV) and the ligands 154

Fig. 4.3.5 IR spectra of complex VOL^5 and its ligand H_2bp_2en: representative spectra for the benzophenoneimine 155

Fig. 4.3.6 IR spectra of complex VOL^8 and its ligand H_2naph_2en: representative spectra for the naphthaldiimine 155

Fig. 4.3.7 IR spectra of complex VOL^{13} and its ligand H_2Clsal_2tn: representative spectra for the chlorosalicylaldiimine 156

Fig. 4.3.8 IR spectra of complex VOL^{15} and its ligand $H_2Omesal_2en$: representative spectra for the methoxysalicylaldiimine 156

Fig. 4.3.9 IR spectra of complex VOL^{18} and its ligand $H_2Oetsal_2en$: representative spectra for the ethoxysalicylaldiimine 157

Fig. 4.4.1 Electronic spectra of the unsymmetrical cobalt(II) complexes 158

Fig. 4.4.2 Electronic spectra of the unsymmetrical nickel(II) complexes 159

Fig. 4.4.3 Electronic spectra of the unsymmetrical copper(II) complexes 160

Fig. 4.4.4 – 4.4.5 Electronic spectra of the unsymmetrical oxovanadium(IV) complexes 161–162

Fig. 4.4.6 – 4.4.7 Electronic spectra of the benzophenoneiminato oxovanadium(IV) complexes 163–164

Fig. 4.4.8 – 4.4.8 Electronic spectra of the napthaldiiminato oxovanadium(IV) complexes 165–166

Fig. 4.4.9 – 4.4.10 Electronic spectra of the chlorosalicylaldiiminato oxovanadium(IV) complexes 167–168

Fig. 4.4.11– 4.4.12 Electronic spectra of the methoxysalicylaldiiminato oxovanadium(IV) complexes 169–170

Fig. 4.4.13 – 4.4.14 Electronic spectra of the ethoxysalicylaldiiminato oxovanadium(IV) Complexes 171–172

Fig. 4.5.1 EPR spectra of oxovanadium(IV) complexes 1[VOL^1], 2[VOL^2], 3[VOL^3], and 4[VOL^4] 173

Fig. 4.5.2 EPR spectra of oxovanadium(IV) complexes 5[VOL^5], 6[VOL^6], 7[VOL^7] and 8[VOL^{12}] 174

Fig. 4.6 Cyclic voltammograph of the oxovanadium(IV) complexes 175

Fig. 4.7.1.1– 4.7.5.3 DSC curves of oxovanadium(IV) complexes VOL^1 – VOL^{20} 176–186

Fig. 5.1.1 Glucose uptake graph for the oxovanadium(IV) complexes VOL^1 – VOL^{10} 186

Fig. 5.1.2 Glucose uptake graph for the oxovanadium(IV) complexes VOL^{11} – VOL^{20} 187

Fig. 5.2.1 The effect of the unsymmetrical complexes on hyperglycemia in Wistar outbred rats with STZ-induced diabetes 188

Fig. 5.2.2 The effect of five symmetrical complexes on hyperglycemia in Wistar outbred rats with STZ-induced diabetes 189

LIST OF TABLES

PAGE

Table 1.1 List of countries with the highest numbers of estimated cases of diabetes for 2000 and 2030 36

Table 1.2 Prevalence estimates of diabetes in South Africa: comparison of years 2003 and 2025 36

Table 1.3 Nomenclature and formulae for the Schiff base ligands 39

Table 1.4 Nomenclature and formulae for the oxovanadium(IV) complexes 40

Table 2.1 Relationships between g and A tensors, EPR symmetry and the point symmetry of paramagnets 46

Table 2.2 The expected spin only moments for n unpaired electron system 51

Table 4.1.1 Physical properties and analytical data for the Schiff bases and oxovanadium(IV) complexes 135

Table 4.1.2 Physical properties and analytical data for cobalt(II), nickel(II) and copper(II)the compounds 137

Table 4.2 ^{1}H NMR data for free ligands 138

Table 4.3.1 Selected infrared spectral bands of the Schiff bases and oxovanadium(IV) complexes 139

Table 4.3.2 Selected infrared spectral bands of cobalt(II), nickel(II) and copper(II) complexes 141

Table 4.4.1 Electronic spectral data of the cobalt(II) complexes 142

Table 4.4.2 Electronic spectral data of the nickel(II) complexes 143

Table 4.4.3 Electronic spectral data of the copper(II) complexes 144

Table 4.4.4 Electronic spectral data of the oxovanaduim(IV) complexes 145

Table 4.5 Room temperature magnetic moments for the complexes 148

Table 4.6.1 EPR parameters for the oxovanadium(IV) complexes with axial symmetry 149

Table 4.6.2 EPR parameters for the oxovanadium(IV) complexes with

rhombic symmetry 149

Table 4.7 Cyclic voltammetric data for oxovanadium(IV) complexes 150

Table 4.8 DSC phenomenological data of the complexes 151

Table 5 Glucose uptake data for the oxovanadium(IV) complexes 152

LIST OF ABBREVIATIONS

AMPK	AMP-activated protein kinase
ATCC	American Type Culture Collection
β	Bohr magneton
BM	Bohr magneton
BEOV	Bis(ethylmaltolato)oxovanadium(IV)
BMOV	Bis(maltolato)oxovanadium(IV)
Co^{II}(salen)	N,N'-bis(salicylaldene)ethylenediaminatocobalt(II)
Co^{II}(salpn)	N,N'-bis(salicylaldene)propylenediaminatocobalt(II)
^{o}C	degree Celsius
CN^{-}	cyano
CV	Cyclic Voltammetry
DMF	dimethylformamide
DMSO	dimethylsulphoxide
DSC	differential scanning calorimetry
DTA	differential thermal analysis
EPR	electron paramagnetic resonance
FBS	fetal bovine serum
FFA	free fatty acid
GLUT	Glucose transporters
g	gyromagnetic ratio
h	Planck's constant
H	magnetic field
Hema	ethylmaltol, 3-hydroxy-2-ethyl-4-pyrone
Hdpp	1,2-dimethy-3-hydroxy-4-pyridinone

Hkoj	kojic acid, 5-hydroxy-2-hydroxymethy-2-pyrone
Hma	maltol, 3-hydroxy-2-methyl-4-pyrone
IDDM	insulin-dependent diabetes mellitus
IDF	International Diabetes Federation
IR	Infrared
LMCT	ligand to metal charge transfer
MeOH	methanol
M	molarity or metal ion
MIC	minimum inhibitory concentrations
NIDDM	non-insulin-dependent diabetes mellitus
NMR	nuclear magnetic resonance
nm	nanometre
Ni^{II}(salen)	N,N'-bis(salicylaldene)ethylenediiminatonickel(II)
Ni^{II}(salpn)	N,N'-bis(salicylaldene)propylenediiminatonickel(II)
PTK	protein–tyrosine kinase
PTP	protein tyrosine phosphatase
py	pyridine
STZ	streptozotocin
TGA	Thermogravimetric Analysis
TNAPY	N-(2-thienylmethylidene)-2-aminopyridine
μ_e	effective magnetic moment
UV	ultraviolet
$VO(acac)_2$	bis(acetylacetonato)oxovanadium(IV)
$VO(ma)_2$	bis(maltolato)oxovanadium(IV)
VOMPA	bis(6-methylpyridine-2-carboxylato)oxovanadium(IV)

$VO(pic)_2$	bis(picolinato)oxovanadium(IV)
Vis	visible
$Zn(6mpa)_2$	zinc(II)–6-methylpicolinate
$Zn(pa)_2$	zinc(II)–picolinate
$Zn(6mpa\text{-}ma)_2$	bis(6-methylpicolinemethylamido)zinc(II)

CHAPTER 1

INTRODUCTION

1.1 Schiff bases

Schiff bases are typically formed by the condensation of a primary amine and an aldehyde/ketone. The resultant compound, $R_1R_2C=NR_3$, is called a Schiff base (named after Hugo Schiff), where R_1 is an aryl group, R_2 is a hydrogen atom and R_3 is either an alkyl or aryl group. However, usually compounds where R_3 is an alkyl or aryl group and R_2 is an alkyl or aromatic group are also regarded as Schiff bases. Schiff bases that contain aryl substituents are substantially more stable and more readily synthesized, while those which contain alkyl substituents are relatively unstable. Schiff bases of aliphatic aldehydes are relatively unstable and readily polymerizable [1], while those of aromatic aldehydes having effective conjugation are more stable. In general, aldehydes react faster than ketones in condensation reactions, leading to the formation of Schiff bases as the reaction centre of aldehyde are sterically less hindered than that of ketone. Furthermore, the extra carbon of ketone donates electron density to the azomethine carbon and thus makes the ketone less electrophilic compared to aldehyde [2].

Schiff bases are generally bidentate (**1**), tridentate (**2**), tetradentate (**3**) or polydentate (**4**) ligands capable of forming very stable complexes with transition metals. They can only act as coordinating ligands if they bear a functional group, usually the hydroxyl, sufficiently near the site of condensation in such a way that a five or six membered ring can be formed when reacting with a metal ion (Fig. 1.1). The tetradentate Schiff base class is of the type reported in this thesis.

Schiff bases derived from aromatic amines and aromatic aldehydes have a wide variety of applications in many fields, *e.g.*, biological, inorganic and analytical chemistry [3, 4]. Applications of many new analytical devices require the presence of organic reagents as essential compounds of the measuring system.

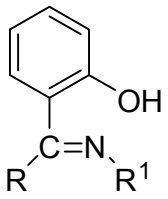

Bidentate (**1**)

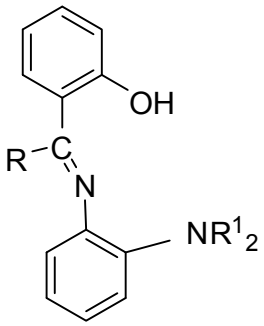

Tridentate (**2**)

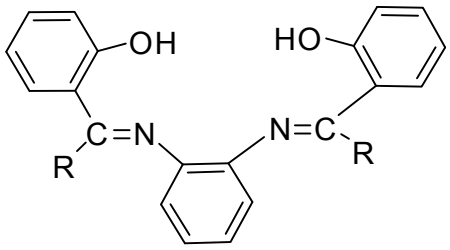

Tetradentate (**3**)

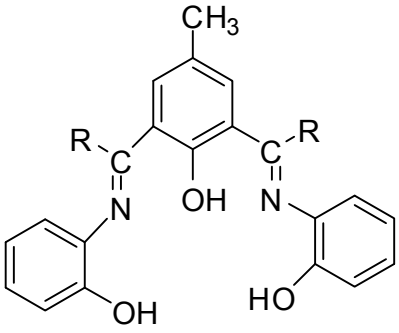

Pentadentate (**4**)

Fig. 1.1 Some classes of Schiff base ligands

Schiff bases are used, *e.g.*, in optical and electrochemical sensors, as well as in various chromatographic methods, to enable detection of enhanced selectivity and sensitivity [5-7]. Among the organic reagents actually used, Schiff bases possess excellent characteristics, structural similarities with natural biological substances, relatively simple preparation procedures and the synthetic flexibility that enables design of suitable structural properties [8, 9]. Schiff bases are widely applicable in

analytical determination, using reactions of condensation of primary amines and carbonyl compounds in which the azomethine bond is formed (determination of compounds with an amino or carbonyl group); using complex formation reactions (determination of amines, carbonyl compounds and metal ions); or utilizing the variation in their spectroscopic characteristics following changes in pH and solvent [10]. Schiff bases play important roles in coordination chemistry as they easily form stable complexes with most transition metal ions [11, 12]. In organic synthesis, Schiff base reactions are useful in making carbon-nitrogen bonds.

1.2 Biological Importance of Schiff Bases

Schiff bases appear to be important intermediates in a number of enzymatic reactions involving interaction of the amino group of an enzyme, usually that of a lysine residue, with a carbonyl group of the substrate [13]. Stereochemical investigations [14] carried out with the aid of molecular models showed that Schiff bases formed between methylglyoxal and the amino group of the lysine side chains of proteins can bend back in such a way towards the N atom of peptide groups that a charge transfer can occur between these groups and the oxygen atoms of the Schiff bases. Schiff bases derived from pyridoxal (the active form of vitamin B6) and amino acids are considered as very important ligands from biological point of view. Schiff bases are involved as intermediates in the processes of non-enzymatic glycosylations. These processes are normal during aging but they are remarkably accelerated in pathogeneses caused by stress, excess of metal ions or diseases such as diabetes, Alzheimer's disease, and atherosclerosis. Non-enzymatic glycosylation begins with an attack of sugar carbonyls or lipid peroxydation fragments on amino groups of proteins, aminophospholipids and nucleic acid,

causing tissue damages by numerous oxidative rearrangements. One of the consequences is cataract of lens proteins [15].

Many biologically important Schiff bases have been reported in the literature possessing, antimicrobial, antibacterial, antifungal, anti-inflammatory, anticonvulsant, antitumor and anti HIV activities [16-21]. Another important role of Schiff base structure is in transamination [22]. Transamination reactions are catalyzed by a class of enzymes called transaminases. Transaminases are found in mitochondria and cytosal of eukaryotic cells. All the transaminases appear to have the same prosthetic group, i.e., pyridoxal phosphate, which is covalently attached to them via an imino group. Schiff base formation is also involved in the chemistry of vision, where the reaction occurs between the aldehyde function of 11-*cis*-retinal and amino group of the protein (opsin) [23]. The biosynthesis of porphyrin, for which glycine is a precursor, is another important pathway, which involves the intermediate formation of Schiff base between keto group of one molecule of δ-aminolevulinic acid and ε-amino group of lysine residue of an enzyme.

1.3 Schiff base metal complexes

Transition metals are known to form Schiff base complexes and Schiff bases have often been used as chelating ligands in the field of coordination chemistry. Their metal complexes have been of great interest for many years. It is well known that N and S atoms play a key role in the coordination of metals at the active sites of numerous metallobiomolecules [24]. Schiff base metal complexes have been widely studied because they have industrial, antifungal, antibacterial, anticancer, antiviral and herbicidal applications [25-30]. They serve as models for biologically important species and find applications in biomimetic catalytic reactions. Chelating ligands containing N, S and O donor atoms show broad biological activity and are of special

interest because of the variety of ways in which they are bonded to metal ions. It is known that the existence of metal ions bonded to biologically active compounds may enhance their activities [28-30].

Schiff base metal complexes have been known since the mid nineteenth century [31] and even before the general preparation of the Schiff bases ligands themselves. Schiff base metal complexes have occupied a central place in the development of coordination chemistry after the work of Jørgensen and Werner [32]. However, there was no comprehensive, systematic study until the preparative work of Pfeiffer and associates [33]. Pfeiffer and his co-workers [34] reported a series of complexes derived from Schiff bases of salicylaldehyde and its substituted analogues.

Structure and mechanism of the formation of the Schiff base complexes and stereochemistry of four coordinate chelate complexes formed from Schiff bases and their analogues have been discussed in several reviews [35]. The configuration of the chelate group in the four coordinate complexes may be square-planar, tetrahedral, distorted tetrahedral or distorted trigonal pyramidal with the metal atom at the apex. The configuration depends primarily on the nature of the metal atom and also on the magnitude and symmetry of the ligand field. Metal complexes have also been reported with other ligands mixed with Schiff bases. Of all the Schiff base complexes, those derived from salicylaldiimines have been thoroughly studied so far. A variety of physiochemical investigations on these complexes provide a clear understanding of their stereochemical and electronic properties. The advantage of the salicylaldiimines ligand systems is the considerable flexibility of the synthetic procedures, which have resulted in the preparations of a wide variety of complexes with a given metal whose properties are often dependent on the ligand structure.

This review will concentrate on metal Schiff bases of some of the first row transition metals with emphasis on tetradentate Schiff base complexes of oxovanadium(IV), cobalt, nickel and copper

A number of structural studies on the effect of the number of CH_2 groups between the two azomethine moieties in VO^{2+}, Co^{2+}, Ni^{2+}, Cu^{2+} and Zn^{2+} complexes of tetradentate Schiff bases (**5**) derived from salicylaldehyde and a variety of diamines (1:2 ratio) have been reported [36-39]. They have been shown that an increase in the methylene chain length allows adequate flexibility for the complexes to change their structure from planar towards a distorted or pseudo-tetrahedral coordination depending on the magnitude of n. In addition, the longer chains cause the ligand field strength to decrease [36, 37]. Metal complexes of this type have been prepared for the series n = 2 to 10 for the bivalent cobalt, nickel, copper, zinc and manganese. For n = 2 most divalent first-row transition metals are expected to form square-planar complexes. However, a decrease in ligand field strength has been reported for nickel(II), copper(II) and zinc(II) derivatives as n is increased from 2 to 4. This decrease corresponds to an increase in distortion from planarity with increase in the length of the methylene bridge.

Kolawole and Patel [40] synthesized a series of [VO{OC_6H_4CH=N-$CR^1R^2(CH_2)_{n-1}$-N=CHC_6H_4O}] complexes, where n = 2–10. The ν(V=O) stretching frequencies fall in the range 861–994 cm^{-1} and the effective magnetic moments at room temperature of the complexes are between 1.64 and 1.81 BM. The complexes with [(n = 2; R^1 = R^2 = H), (R^1 = H, R^2 = CH_3), (R^1 = R^2 = CH_3)] are green, and their spectroscopic and magnetic properties suggest that they have tetragonal pyramidal structures. A corresponding complex (R^1 = R^2 = H, n = 3) is orange-yellow and its X-ray structure shows that it is polymeric, having a distorted octahedral geometry. The

electronic spectra in chloroform and pyridine and in the solid state indicate the possibility of an inversion of the ordering of energies of the e_π^* and b_1^* levels; consequently a diversity of geometries were observed as the methylene chain length increased. The stereochemistry of the complexes varies from distorted square-pyramidal to octahedral geometry.

In continuation of their study on oxovanadium(IV) ion, Kolawole, *et al* [41-43] also synthesized oxovanadium(IV) complexes of tetradentate 3-methoxysalicylaldiimine, 5-chlorosalicylaldiimine and naphthaldiimine Schiff bases containing the N_2O_2 chromophore and long-chain alkyl equatorial bridges. Their spectroscopic and magnetic properties suggest that the complexes are five-coordinate, except the trimethylene derivatives (having a six-membered equatorial ring size above V) are orange-yellow and polymeric. Substitution in the aromatic rings did not affect significantly the trend in the stereochemistry of the complexes. The 3-methoxysalicylaldiimine complexes of oxovanadium(IV) reported by Patel and Kolawole [41] is an isomeric form of 5-methoxysalicylaldiimine complexes reported in this thesis.

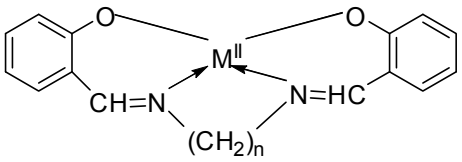

5

In general, Co(II) complexes have a higher tendency to assume a tetrahedral configuration than the corresponding Ni(II) complexes. The Co^{II}(salen) complex has a low spin square planar structure with a single unpaired electron and a magnetic moment of about 2.5 BM [39], and it is extremely oxygen sensitive. Increasing the

number of the methylene units in diamine chain of the Schiff base ligand (**5**) allows the Co(II) complexes to change from a square planar (n = 2) to a tetrahedral geometry [37, 38]. While the Co^{II}(salen) complex has no geometrical distortion with respect to the primary ligand, Co^{II}(salpn) has a distorted structure. This is in contrast to the Ni(II) series, which maintains a square planar geometry irrespective of increase in the number of the methylene groups, or adopts an octahedral geometry in the presence of donor solvents like MeOH, DMF, DMSO [36, 37]. The distortion about the cobalt centre is due to the extra methylene groups which causes an apparent weakening of the ligand field strength. In other words, the increasing chain length in salpn allows more flexibility to form a tetrahedral coordination geometry about the cobalt [the cobalt(II) shows a more pronounced tendency for the formation of tetrahedral complexes than either Ni(II) or Cu(II)] [44]. Therefore, Co^{II}(salpn) complex shows a low tendency to increase its coordination number by forming octahedral complexes in the presence of addition donors [44, 45]. However, relatively strong π-acceptor ligands (for example pyridine and its derivatives, or anions such as N_3^-, CN^-) increase effectively the ligand field strength.

Bis(N-alkyl- or bis(N-aryl-salicylideneiminato)nickel(II) complexes are basically 4-coordinate square-planar in the solid state. In chloroform or benzene Ni(II) salicylideneiminato-complexes become partially paramagnetic [46]. This effect arises through the monomeric planar speices being in equilibrium with dimeric or polymeric or tetrahedral form, which are paramagnetic [46]. Paramagnetic form of the complex of N-methylsalicyladiimine with Ni(II) has been isolated in solid state confirming that polymeric species are involved. As the length n increases from 2, the ligand field produced becomes much weaker, as indicated by the shift of the main *d–d* band towards lower wavenumbers and by lowering of the capacity of Ni(II) to bind

additional ligands, such as py, at the fifth and sixth coordination sites [46]. For instance, when dissolved in pyridine, [Ni^{II}(salen)] maintains 4-coordinate planar configuration binding no additional pyridine molecules, while [Ni^{II}(saltn)] binds two pyridine molecules to form 6-coordinate bis(pyridine)nickel(II) complex. Few studies have been reported where Ni(II) complexes are diamagnetic and planar. The Ni(II) complexes of N-isopropylsalicyladiimines and of its 5-ethyl derivative are tetrahedral and paramagnetic, whereas the complexes of 5-methyl-, 5-n-propyl-, 5-chloro- and 5-nitro-N-isopropyl salicyaldiimine are all planar and diamagnetic [46]. The presence of long side chains on the ligands tends to lower the symmetry of the nickel complexes, which in turn changes the stereochemistry of the complexes.

The complexity of stereochemistry of copper(II) complexes has been well documented, and many factors, such as ligand field stabilization energies, the Pauling electroneutrality principle, the Jahn-Teller effect, steric effects, *etc.,* have been invoked to account for the complicated structures [47]. Copper(II) complexes of (**5)** suffer greater increasing distortion from planarity towards tetrahedral geometry as n becomes large. X-ray diffraction studies have revealed that [N, N'-bis(salicylidene)ethylenediiminatocopper(II)] is dimeric, resulting in some out-of-plane distortion due to a weak intermolecular Cu—O bond [39]. This makes each copper atom five-coordinate with a near square-pyramidal arrangement of ligand donor atoms.

Many complexes of the Cu(sal·$R)_2$ type, where R denotes alkyl or aryl group have been reported and the complexes are considered to be square-planar [39]. Some of them, however, consist of binuclear units, in which there is very weak copper to copper bonds [39]. Cu-(Sal·$R)_2$, where R is alkyl or aryl groups, has square-planar configuration and is stable, but when there is considerable steric

hindrance, the distortion from the planarity may occur. Thus for R = tert-C_4H_9, iso-C_3H_7 and cyclohexyl, it was concluded from the electronic spectra that the complexes are distorted from the square plane [39]. It was also concluded that the distortion decreases in the following order tert-C_4H_9 > iso-C_3H_7 > C_6H_{11}. This was confirmed by X-ray studies, which showed that the angles between the two N-Cu-O planes is 80^o for the complex with R = tert-C_4H_9 and 60^o for the complex with R = iso-C_3H_7.

Schiff base of 4-aminoantipyrine and its complexes have a variety of applications in biological, clinical, analytical and pharmacological areas. Raman, *et al*. [48] prepared a new series of transition metal complexes of Cu(II), Ni(II), Co(II), Mn(II), Zn(II), VO(IV), Hg(II) and Cd(II) from the Schiff base derived from 4-aminoantipyrine, 3-hydroxy-4-nitrobenzaldehyde and o-phenylenediamine. Structural features were obtained from their elemental analyses, magnetic susceptibility, molar conductance, IR, UV–Vis, ^{1}H NMR and EPR spectral studies. The data show that these complexes have composition of ML type. The UV–Vis, magnetic susceptibility and EPR spectral data of the complexes suggest square–planar geometry around the central metal ion except VO(IV) complex which has square–pyramidal geometry. The redox behaviour of the copper and oxovanadium(IV) complexes was studied by cyclic voltammetry. Antimicrobial screening tests gave good results for the metal complexes. The nuclease activity of the above metal complexes shows that Cu, Ni and Co complexes cleave DNA through redox chemistry whereas other complexes were not effective.

The complexes of Cr(III), Fe(III), Co(II) and Ni(II) ions with a Schiff base derived from 4–dimethylaminobenzaldehyde and primary amines have been prepared and investigated using different physico-chemical techniques, such as

elemental analysis, molar conductance measurements, and infrared and electronic spectra. The chemical analysis data showed the formation of the complexes and a square planar geometry was suggested for Co(II) and Ni(II) complexes and an octahedral structure for Cr(III) and Fe(III) complexes [49].

Nair, *et al*. [50] synthesized two Schiff bases from 5-ethyl-2,4-dihydroxyacetophenone. Their copper, nickel, iron and zinc complexes were screened for antibacterial activity against some clinically important bacteria, such as *Pseudomonas aeruginosa*, *Proteus vulgaris*, *Proteus mirabilis*, *Klebsiella pneumoniae* and *Staphylococcus aureus*. The Schiff bases showed greater activity than their metal complexes. The metal complexes showed differential effects on the bacterial strains investigated and the solvent used, suggesting that the antibacterial activity is dependent on the molecular structure of the compound, the solvent used and the bacterial strain under consideration. Amongst the four metals, Zn complexes showed the best antibacterial activity followed by Fe in 1,4-dioxane while Ni followed by Zn and Fe showed the best antibacterial activity in DMF.

Metal complexes, ML_2Cl_2, where M is Fe(II), Co(II), Ni(II), Cu(II), Zn(II), or Cd(II), and L is the Schiff base formed by condensation of 2-thiophenecarboxaldehyde with 2-aminopyridine, N-(2-thienylmethylidene)-2-aminopyridine (TNAPY), have been prepared and characterized by elemental analysis and magnetic and spectroscopic measurements [11]. Elemental analysis of the chelates suggests the stoichiometry is 1:2 (metal-ligand). Infrared spectra of the complexes agree with the coordination to the central metal atom through the nitrogen of the azomethine (—HC=N—) group and the sulfur atom of the thiophene ring. Magnetic susceptibility data coupled with electronic and EPR spectra suggest a distorted octahedral structure for the Fe(II), Co(II), Ni(II), and Cu(II) complexes, and

a tetrahedral geometry for the Zn(II) and Cd (II) complexes. The Schiff base and its metal chelates were also screened for their *in vitro* antibacterial activity against *Escherichia coli, Staphylococcus aureus*, and *Pseudomonas aeruginosa.* The metal chelates were shown to possess more antibacterial activity than the uncomplexed Schiff-base.

Raman, *et al*. [51] have synthesized new Schiff base chelates of Cu(II), Co(II), Ni(II) and Zn(II) derived from benzil-2,4-dinitrophenylhydrazone with aniline. EPR spectral studies were carried out to suggest tentative structures for the complexes. The electronic absorption spectra of the Schiff base and its Cu(II), Co(II), Ni(II) and Zn(II) complexes were recorded at room temperature using acetone as solvent. The electronic spectra and magnetic susceptibility data of the complexes suggest octahedral geometry around the central metals ion.

Ni(II), Cu(II), Pd(II) and Pt(II) complexes of thiophene-2-carboxaldehyde Schiff bases of S-methyl- and S-benzyl dithiocarbazate have also been reported [52]. Magnetic and spectroscopic evidences support a square-planar structure for these complexes. The crystal structure of nickel and copper were determined by X−ray diffraction. Both complexes have a trans-planar structure in which the two Schiff base ligands are coordinated to the metal(II) ions as uninegatively charged bidentate ligands *via* the thiolate S and the azomethine N atoms. These complexes were also screened for their antifungal activity.

Ni(II) Schiff base complex derived from salicylaldehyde and *o*-aminobenzoic acid has been prepared and characterized [53]. The elemental analysis data show the formation of 1:1 [M:L] complex. The molar conductance measurement reveals a non-electrolytic nature. The electronic spectrum of the complex was typical of a square planar geometry. It was diamagnetic. The free Schiff base and its complex

were tested for antibacterial activities against several human pathogenic bacteria. They show no detectable activity against any of the bacteria screened [53].

Complexes of Ni(II), Co(II) and Cu(II) with Schiff base ligands derived from β-diketones and *p*-anisidine have been reported [54]. Spectral and magnetic studies on these complexes indicate that they are four coordinate, with square-planar geometry. It has been found that all the complexes are antimicrobially active and show higher activity than the free ligands.

Recently, there has been increasing interest in the synthesis and characterization of unsymmetrical Schiff base ligands and their metal complexes. This is due partly to the belief that the systematic investigation of these complexes may shed light on the nature of complexes of biological interest [55]. Unsymmetrical tetradentate Schiff base complexes are required to model the irregular binding of peptides because trace metals have been found to occur in metalloenzymes bound to a macrocycle such as the heme ring, or to donor atoms of peptide chains usually in a distorted environment [56]. Unsymmetrical ligands can clearly offer many advantages over their symmetrical counterparts in the elucidation of the composition and geometry of metal ion binding sites in metalloproteins and in the development leading to the duplication of enzymatic efficiency and selectivity of natural system with synthetic materials. A large percentage of enzymes have a metal atom at the active site. These metalloenzymes facilitate a variety of reactions, which include redox reaction (carried out by the oxidases and oxygenases), acid-catalysed hydrolysis (hydrolases) and rearrangement of carbon-carbon bonds (synthases and isomerases) [57, 58].

Osowole, *et al*. [59] prepared Ni(II), Cu(II) and Zn(II) complexes of unsymmetrical Schiff base derived from 2-hydroxy-1-naphthaldehyde, 2, 4-

pentanedione and *p*-phenylenediamine and their adducts with 2,2´-bipyridine and 1,10-phenanthroline. The magnetic moments and electronic spectra corroborate octahedral geometry for Ni(II) and Cu(II) complexes whereas the Zn(II) Schiff base complex analysed as 4-coordinate and the adduct as 6-coordinate. The antimicrobial properties of the ligand and complexes against *Staphlococcus aureus, Streptococcus faecalis, Bacillus sp, Escherichia coli, Pseudomonas aeruginosa, Salmonella tyhi, Klebsiella pneumonia, Acinetobacter sp, Flavobacterium sp, Enterococcus faecalis* and *Candida albicans* were reported. The compounds generally exhibited good activity against the selected organisms. The Cu(II) complex has comparable activity to gentamycin. The minimum inhibitory concentrations (MICs) of the sensitive compounds were also reported.

Copper(II) complexes of five new tetradentate unsymmetrical ligands, ethylene-N-(acetylacetoneimine)-N'-(ortho-hydroxyarylaldimine) (aryl = 3,5-dibromo phenyl, 3-methylphenyl, 3,6-dimethylphenyl, 3,5-dichlorophenyl, 3,5-dibromo acetophenone) have been reported [60]. The general coordination configuration was revealed by an X-ray crystallographic study of one of the complexes, ethylene-N-(acetylacetoneiminato)-N'-(ortho-hydroxy-3,5-dibromoacetophenoneiminato) copper(II), which exhibits an approximately square-planar geometry with a slight tetrahedron distortion. The substituent effect studied by EPR indicates that electronic factors have a profound effect on the central metal ions. Thermal analysis indicates that both salicylaldiiminato and acetylacetoneiminato donating moieties are thermally compatible.

Two series of novel unsymmetrical tetradentate Schiff bases derived from *o*-phenylenediamine and 1,3-naphthalenediamine and their oxovanadium(IV) complexes were synthesized by template and non-template methods and

characterized by elemental analysis, IR, ^{1}H and ^{13}C NMR and UV-Vis [61]. These complexes were used as catalysts for the selective aerobic oxidation of cyclohexene. The catalytic activity increases as the number of electron-donor groups decreases. Complexes containing the naphthylene-bridged ligands had similar redox potential. However, their catalytic activities were quite varied and the differences in their activities were strongly dependent on the fine structural data and redox potential. But in the complexes containing phenylene-bridged ligands, yield a good correlation between catalytic activity and redox potential.

1.4 History and occurrence of vanadium

Vanadium has atomic number 23. It is a soft, silvery grey, ductile transition metal. Vanadium was originally discovered by Andrés Manuel del Río, a Mexican mineralogist, in 1801. He first named it panchromium, because of the varied colours of its salts, but changed the name later on to erythronium (‘red’) as a reference to the red colour of its salts when treated with acids [62, 63]. However, soon he withdrew his discovery, since a French chemist incorrectly declared that this new element was only impure chromium. Vanadium was rediscovered in 1831 by the Swedish chemist Nils Gabriel Sefström (1787-1845) in remnants of iron ore quarried at the Taberg in Småland. He named the element vanadin, after the goddess of beauty, youth and love, Vanadis, referring to the beautiful multicoloured compounds [64]. After Sefström announced the discovery of vanadium, the brown lead ore from Mexico was reanalysed and it was shown that it really contained vanadium instead of chromium. Natural vanadium is a mixture of two isotopes, ^{51}V (99.76%) and ^{50}V (0.24%), the latter being slightly radioactive with a half-life of $>3.9 \times 10^{17}$ years. Today, vanadium is primarily obtained from the minerals vanadinite [$Pb_5(VO)_3Cl$] and

carnotite [$K_2(UO_2)_2(VO_4)_2$] by heating crushed ore in the presence of carbon and chlorine to produce vanadium trichloride. The vanadium trichloride is then heated with magnesium in an argon atmosphere. It is also present in some crude oils in the form of organic complexes.

Vanadium is corrosion resistant and is sometimes used to make special tubes and pipes for the chemical industry. Vanadium also does not easily absorb neutrons and has some applications in the nuclear power industry. A thin layer of vanadium is used to bond titanium to steel. Nearly 80% of the vanadium produced is used to make ferrovanadium or as an additive to steel. Ferrovanadium is a strong, shock resistant and corrosion resistant alloy of iron containing between 1% and 6% vanadium. Ferrovanadium and vanadium-steel alloys are used to make such things as axles, crankshafts and gears for cars, parts of jet engines, springs and cutting tools. Vanadium(V) oxide is perhaps vanadium's most useful compound. It is used as a mordant, a material which permanently fixes dyes to fabrics. Vanadium(V) oxide is also used as a catalyst in the contact process and in the manufacture of ceramics. Vanadium(V) oxide can also be mixed with gallium to form superconductive magnets.

Vanadium occurs with an abundance of 0.014% in the earth’s crust and is widespread [65]. The element is the second most abundant transition metal in the oceans (50 nM) [65]. Some aquatic organisms are known to accumulate vanadium. For instance, members of an order of tunicates (*Ascidiacea*) concentrate vanadium to 0.15 M in specialised blood cells [66]. However, the actual function of vanadium and the nature of the vanadium compounds present in these organisms remains unclear [62]. A naturally occurring vanadium-containing enzyme, vanadium

bromoperoxidase was discovered in the marine brown alga, *Ascophyllum nodosum* [67]. Since then, several vanadium haloperoxidases have been isolated and studied [68, 69]. Many of these enzymes have been detected in brown and red seaweeds [70, 71]. However, the accumulation of vanadium is not restricted to marine organisms, since vanadium containing haloperoxidases have also been isolated from terrestrial fungi [72] and a vanadium compound of low molecular weight (amavadin) has been isolated from the toadstool *Amanita muscaria* [73].

1.4.1 The chemistry of vanadium

Vanadium has an electronic configuration of $[Ar]3d^3 4s^2$ and can exist in eight oxidation states ranging from –3 to +5, but with the exception of –2 [74]. Only the three highest, +3, +4 and +5, are important in biological systems [75-77]. Under ordinary conditions, the +4 and +5 oxidation states are the most stable [74]. The coordination chemistry of vanadium is strongly influenced by the oxidation/reduction properties of the metal centre and the chemistry of vanadium ions in aqueous solution is limited to oxidation states of +2, +3, +4 and +5. Vanadium compounds of oxidation state of +2 and +3 are unstable to air and their compounds are predominantly octahedral. Many oxovanadium(V) complexes contain the VO_2^+ entity and the *cis* geometry in dioxo complexes have been confirmed by structural determination [78]. The oxo complexes of the halides, alkoxides, peroxides, hydroxamates and amino carboxylates have been characterized [79]. The oxidation of ligands by vanadium(V) prevents the isolation of a larger number of complexes. On the other hand, the oxidizing properties of vanadium(V) compounds are useful for many preparative reactions, namely for the catalysis of oxidations. Important

examples are catalyst used for the oxidation of SO_2 to SO_3 in the industrial production of sulphuric acid

Vanadium(IV) is the most stable oxidation state under ordinary conditions and majority of vanadium(IV) compounds contain the VO^{2+} unit (oxovanadium(IV) or vanadyl ion) which can persist through a variety of reactions and in all physical states. The VO^{2+} ion forms stable anionic, cationic and neutral complexes with several types of ligands and has one coordination position occupied by the vanadyl oxygen. A wide variety of oxovanaduim(IV) complexes have been prepared and characterized [74, 80]. A square pyramidal geometry has been well established with the oxovanadium(IV) oxygen apical and the vanadium atom lying above the plane defined by the donor atoms of the equatorial ligands. These square pyramidal complexes generally exhibit strong tendency to remain five coordinate [80]. However, orange polynuclear linear chain structures (···V=O···V=O···) [81, 82] and orange octahedral structures with a weak coordination of a solvent molecule are observed in the solid state for the Schiff base-oxovanadium(IV) complexes which have a six-membered N-N chelate ring. These complexes take a distorted-octahedral coordination. The absorption band due to V=O stretching vibration of oxovanadium(IV) complexes is usually observed at a higher wavenumber compared to those of vanadate(V) complexes. The V=O stretching vibration, however, is susceptible to a number of influences including electron donation from basal plane ligand atoms, solid-state effects, and coordination of additional molecules. Therefore, there has been considerable work done to assign the V=O stretching frequencies in oxovanadium(IV) compounds [83-85].

Electronic absorption spectra of oxovanadium(IV) complexes are normally interpreted in terms of the energy level scheme derived from a molecular orbital

treatment for a square-pyramidal structure with C_{4v} symmetry at the metal center, [86, 87] in which the z-axis is taken as the vanadium–oxygen double bond, and the x- and y-axes are taken along the equatorial bonds. In this scheme, b_2 (d_{xy}) < e_π* (d_{xz}, d_{yz}) < b_1* ($d_{x^2-y^2}$) < a_1* (d_{z^2}), three electronic transitions are predicted, and indeed three absorption bands due to the d–d transitions are usually observed for oxovanadium(IV) complexes [83, 84, 88]. However, in case of distorted oxovanadium(IV) complex, four absorption bands are observed owing to the splitting of d_{xz} and d_{yz} [88]. The absorption bands that have extinction coefficients in the thousands and which are assigned as ligand to metal charge transfer (LMCT) are sometimes observed. This is elaborated further in Chapter 2.

Due to the d^1 configuration of V(IV) ions, vanadium(IV) species are easily identified by EPR spectroscopy. Typical eight-line patterns are observed due to hyperfine interaction of the ^{51}V nucleus ($I = {}^7/_2$) [89].

1.5 Oxovanadium(IV) insulin enhancing agents

Before the discovery of insulin and its clinical trials for treating diabetes mellitus (DM), inorganic salts of vanadium have long been known to act as orally viable mimics or enhancing agents for increased activity of insulin *in vitro* and *in vivo*. The first report of vanadium salts being used as a metallotherapeutic agent appeared in 1899 [90]. Consistent with medical trials of that era, Lyonnet and his colleagues first tried the proposed drug on themselves, then on 60 of their patients (three of whom were diabetic) over a period of some months. They described what might be considered today a “Phase 0” clinical trial in somewhat vague terms: 4-5 mg sodium metavanadate (before meals) every 24 h, three times per week, with

resulting two out of the three diabetic patients said to have obtained a slight, transient, lowering of sugar levels. No ill effects were noted in any of their patients.

This result remained relatively unnoticed until much later in 1979 by Tolman, *et al.* [91] who demonstrated that a millimolar administration of sodium metavanadate to fat cells stimulated glucose uptake and inhibited lipid breakdown in a tissue-specific manner, similar to insulin. Although inorganic salts have been successful at enhancing the activity of insulin, the poor *in vivo* absorption and high dose requirement resulted in increased toxicity [92]. Since insulin is not orally active, great effort has therefore been made to synthesize oxovanadium(IV) complexes of organic ligands of high biological activity (hydro/lipophilicity) and low toxicity which are readily absorbed. Potent complexes with various coordination modes $VO(O_4)$, $VO(N_2O_2)$, $VO(N_2S_2)$, $VO(S_4)$, $VO(S_2O_2)$, and $VO(N_4)$, and the relationship between their structures and insulin-mimetic activities has been examined by evaluating both *in vivo* and *in vitro* results [93, 94].

1.5.1 Pyronates and pyridinonates

Maltol (Hma) (**6**) and related 3-hydroxy-4-pyrones are natural products (acetogenins) which occur as fungal carbohydrate metabolites, as well as being produced as byproducts of fementation. Both maltol and ethylmaltol (**7**) are by themselves approved food additives in many countries. In addition, maltol is well known for formation of stable, neutrally charged metal complexes which have an optimum combination of water-solubility, reasonable hydrolytic stability, and significant lipophilicity [95-97]. Pyrones and pyridinones can act as anionic chelating, bidentate *O*,*O*-ligands towards a number of biologically active metals [96-99]. Ligands structurally related to maltol include kojic acid (Hkoj) (**8**), and Hdpp (1,2-

dimethyl-3-hydroxy-4-pyridinone) (**9**), both of which have substituents that can alter selectively the water-solubility, hydrolytic stability and lipophilicity of their metal complexes [98].

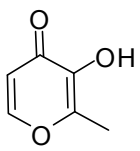

6

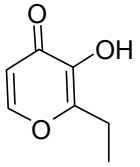

7

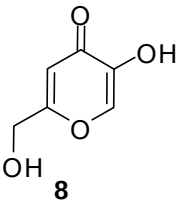

8

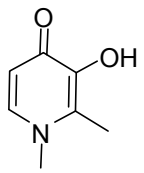

9

Bis(maltolato)oxovanadium(IV), BMOV or $VO(ma)_2$ (**10**), consists of vanadyl ion bound to the anion of maltol (3-hydroxy-2-methyl-4-pyrone, Hma) [99]. Interest in maltol and close analogues, such as ethylmaltol (3-hydroxy-2-ethyl-4-pyrone, Hema) and kojic acid (5-hydroxy-2-hydroxymethyl-4-pyrone, Hkoj), is partly due to their ability to deprotonate readily. The geometry in the solid state around the vanadium in BMOV is square pyramidal with the two maltolato ligands in a *trans* arrangement around the base of the square pyramid and the V=O unit axial.

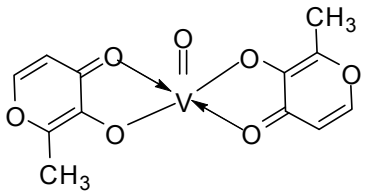

10

BMOV is the most widely and intensively tested of the many proposed insulin mimetic vanadium complexes [86, 99-102]. In addition to lowering glucose- and lipid-levels *in vivo*, BMOV delays or prevents long-term diabetes-induced pathology (including cardiomyopathy) and attenuates hyperinsulinemia and hyperlipidemia in genetically diabetic rats. The longest residence times for vanadium *in vivo* following

oral administration of ^{48}V-BMOV were in bone (31 days), followed by liver (7 h) and kidney (4 h) [101]. On average in these three tissues, vanadium uptake is 2–3 times greater after oral ^{48}V-BMOV administration, compared to the same dose of $^{48}VOSO_4$. Bis(ethylmaltolato)oxovanadium(IV), BEOV, $VO(ema)_2$ [103], with slightly greater hydrolytic stability and lipophilicity, has longer turnover times *in vivo*, especially in bone and liver. Solubility decreases only slightly, and stability to oxidation remains unchanged from BMOV. BEOV successfully completed phase I clinical trials in early 2000. The redox chemistry of BMOV demonstrates an impressive lability in oxidation and reduction [93].

1.5.2 Acetylacetonates

β-Diketones and related derivatives are considered a class of very important ligands in the growth of coordination chemistry. Their complexes have been thoroughly studied. Due to the presence of two oxygen donor atoms and facile keto-enol tautomerism they easily coordinate with metal ions after deprotonating the enolic hydrogen atom and provide stable metal complexes with six-membered chelate rings. Since the synthesis and characterization of bis(2, 4-pentanedionato) oxovanadium(IV), $VO(acac)_2$ (**11**), was first published in 1914 [104], the complex has been used extensively as a reagent in organic synthesis [105-107]. The physical properties of $VO(acac)_2$ have been examined by numerous workers [108-110]. A variety of derivatives, in which the terminal methyl group in the $acac^-$ ligands were substituted, have been prepared and studied [111, 112]. Such substitutions include both symmetric and asymmetric modifications of the parent $acac^-$ ligand and formation of the corresponding $VO(acac)_2$-type complexes [104, 113]. Both the 3-methyl- and 3-ethyl-2,4-pentanedionato oxovanadium(IV) complexes, $VO(Me\text{-}acac)_2$

(**12**) and VO(Et-acac)$_2$, (**13**) respectively, have been structurally characterized [114]. The vanadium atoms in these mononuclear complexes lie in distorted square pyramidal coordination environments. Both compounds have oxygen atoms coordinating in the equatorial plane; apical coordination by the oxo group completes the square pyramidal geometry in each case. As with the parent compound, VO(acac)$_2$, X-ray structural analysis shows that the vanadium atom lies above the basal plane.

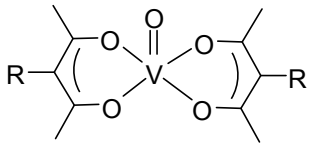

R= H **11**, R= CH_3 **12**, R= CH_2CH_3 **13**.

In an *in vitro* study of VO(acac)$_2$, 5–100 μM was found to be more effective than vanadyl sulphate in stimulating lipogenesis in isolated fat cells, and had identical effectiveness in stimulating activity of a cytosolic protein kinase [115]. Intraperitoneal injection (25 μmol kg^{-1}) of VO(acac)$_2$ lowered slightly plasma glucose levels in STZ-diabetic rats, though not to normal glucose levels; VO(Etacac)$_2$, at the same dose, was ineffective [100]. 0.4 mM of BMOV, VO(acac)$_2$, and VO(Etacac)$_2$, administererd orally , were equally (mildly) effective in glucose-lowering when given in the drinking water over an 8-week treatment period, but were significantly different from $VOSO_4$ at the same dose. In fact, the only clearly relevant physiological difference in this comparative group was between the ratio of vanadium intake/plasma vanadium levels, with $VOSO_4$ having a remarkably higher ratio compared to all oxovanadium(IV) complexes tested [100].

1.5.3 Picolinates

Several vanadium(IV) complexes with a $VO(N_2O_2)$ chromophore have been proposed as insulin mimics. One example is bis(pyridine-2-carboxylato) oxovanadium(IV), $VO(pic)_2$ (**14**), the synthesis of which was first reported in 1964 [116], but which was only recently characterized structurally [117] and tested biologically [117, 118]. $VO(pic)_2$ is slightly soluble in water and as an aqueous solution in an aerobic atmosphere, is susceptible to gradual oxidation. A methyl analogue of $VO(pic)_2$, bis(6-methylpyridine-2-carboxylato)oxovanadium(IV), VOMPA, has also been synthesized and characterized biologically, potentiometrically, and by a new blood circulation monitoring-EPR method (BCM-ESR) [119-121].

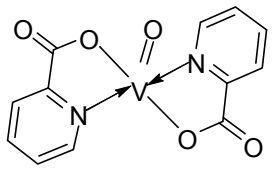

14

The insulin enhancing effects of picolinato chelates of oxovanadium(IV) have been clearly shown to be dependent on dose as well as delivery method. $VO(pic)_2$, administererd at 0.2 mmol kg^{-1} orally for 2 days and then at 0.1 mmol kg^{-1} for 11 days, normalized plasma glucose in STZ-diabetic rats, a model of insulin-dependent diabetes (IDDM) [122]. Plasma insulin levels increased significantly during this trial [122]. By comparison, when $VO(pic)_2$ was given to STZ-diabetic rats as a 2.4 mM solution (drinking water substitute), the calculated dose averaging 1.0 mmol kg^{-1} d^{-1} was accompanied by consistent glucose-lowering and no insulin elevation, but with considerable evidence of gastrointestinal irritation [117]. Intraperitoneal (i.p.)

administration of $VO(pic)_2$ at doses of 0.2, 0.1, and 0.06 mmol V kg^{-1} d^{-1} [117, 122] also lowered plasma glucose levels, accompanied by increased bilirubin at the highest dose. In comparison to its methylpicolinate analogue, the picolinate complex had a less sustained response and was less effective as an inhibitor of FFA release *in vitro*; thus VOMPA was chosen for continued investigation [119, 121, 122]. On the other hand, comparing $VO(pic)_2$ with BMOV [117], the picolinate complex had lower solubility and more gastrointestinal irritation for an equivalent dose, suggesting that there is room for further structural improvement in order to increase bioavailability and lessen side effects.

1.5.4 Oxovanadium(IV) salen-type derivatives

Several vanadium complexes of the tetradentate Schiff base ligand N,N'-bis(salicylidene)ethylenediamine (salen) (**15**) have been proposed for potential use as insulin mimetic agents [123]. These ligands are of particular interest because they provide coordination environments which efficiently stabilize different oxidation states of vanadium, while still providing active sites capable of binding other molecules. In addition these complexes exhibit catalytic reactivity towards organic substrates. Oxovanadium(IV) complexes have been shown to catalyze a variety of reactions such as the oxidation of alcohols and the conversion of sulphide to sulphur oxides and sulfones [124, 125]. Most oxovanadium(IV) complexes with a tetradentate Schiff base ligands like salen take green monomeric structures with square-pyramidal coordination geometry or orange linear chain structures (···V=O···V=O···) with distorted octahedral coordination in the solid state [81].

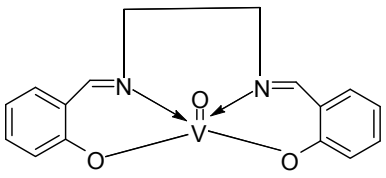

15

To date, only [VO(sal_2-en)] [126] and [VO(sal_2-1,3-pn)] [127] have been tested for insulin mimetic activity from among these complexes. Unlike most biological testing for new anti-diabetic agents, this was carried out in alloxan-diabetic rats, in which blood glucose levels decreased from hyperglycemic to hypoglycemic during oral intubation of [VO(salen)] (0.15 mmol V kg^{-1} d^{-1} for 30 days). Withdrawal of treatment brought an immediate reversion to hyperglycemia. Blood glucose levels were reduced over the treatment period; liver hexokinase activity was restored, and other carbohydrate metabolism enzymes in liver and kidney were normalized. On the other hand [VO(sal_2-1,3-pn)] normalized glucose and lipid values without an increase in insulin levels, and improved glucose tolerance.

1.5.5 Dicarboxylate ester–oxovanadium(IV) complexes

This class of complexes was investigated as models for the interaction of vanadium(IV) with bioligands. Complexes of oxovanadium(IV) with a series of dicarboxylate ligands (oxalate, glutarate, succinate, malonate) proved effective orally as insulin mimetic agents [128]. Only the cysteine methyl ester–oxovanadium(IV) complex, VCys, was characterized by X-ray structural analysis [129]. The oxovanadium(IV) in VCys appeared to be penta-coordinate around the central vanadium atom, thus assuming a square pyramidal geometry with two-fold symmetry and each pair of nitrogen and sulphur atoms mutually *trans*.

Insulin mimetic activity of these complexes at the doses for bioactivity (0.06 and 0.20 mmol V kg^{-1}) showed that VCys and the bis ligand analogues of malonate,

tartarate, and salicylaldehyde were indistinguishable from one another in terms of glucose-lowering ability in STZ-diabetic rats. The higher dose appeared to be significantly more effective than the lower dose in all cases. An oxalic acid analogue, bis(oxalato)oxovanadate(IV) dianion, was less effective than the others; significant glucose-lowering was seen only at the 0.20 mmol V kg^{-1} dose level [128].

1.6 Other metal complexes used as insulin enhancing agents

1.6.1 Zinc compounds

Zinc appears to play a role in modulating insulin receptor tyrosine kinase activity in the skeletal muscle of a genetic type 2 DM model mouse, similar to the action of vanadium [130]. In addition, zinc was proposed to affect carbohydrate metabolism through the insulin receptor, PTP1B, and other related proteins [131]. In fact, zinc and diabetes intersect at several points during metabolism in a cell [132, 133]. In 1980, zinc was found to stimulate rat adipocyte lipogenesis similar to the action of insulin [134], which was followed by the observations on *in vivo* antidiabetic effects of oral $ZnCl_2$ in STZ-rats and ob/ob mice in 1992 [135] and 1998 [136], respectively. Because the bioavailability of $ZnCl_2$ is relatively low, the coordination chemistry of zinc(II) ion was explored, and the first orally active insulin-mimetic and antidiabetic zinc(II)–picolinate complexes were discovered in 2002 [137]. Since then, a wide variety of zinc(II) complexes with different coordination structures have been synthesized [132, 138]. The determination of log β for zinc(II) complexes made it possible to discuss the relationship between the stability constant and the insulin-mimetic activity, e.g., zinc(II) complexes with log β lower than 10.5 *in vitro* exhibited higher insulin-mimetic activities than those of $ZnSO_4$ which was used as a control

[139, 140]. Similar to the vanadyl complexes, zinc(II)–picolinate complexes, such as [$Zn(pic)_2$] [141], [Zn(6-mpic)] [141], and bis(6-methylpicolinemethylamido)zinc(II) [$Zn(6\text{-}mpa\text{-}ma)_2$] [142], were prepared. The single X−ray crystal of [$Zn(6\text{-}mpic)_2(H_2O)]\cdot H_2O$ revealed the coordination geometry around the zinc(II) ion to be a distorted trigonal bipyramidal structure. Zinc(II)–picolinate complexes with log β lower than 10.5 exhibit higher *in vitro* insulin-mimetic activities than those of ZnSO4 and $VOSO_4$. And [$Zn(pic)_2$] with a log β = 9.52 showed higher activity than those of $ZnSO_4$ and $VOSO_4$. Based on the *in vitro* evaluation, both [$Zn(pic)_2$] and [$Zn(6\text{-}mpic)_2$] exhibited high hypoglycemic effects in KK-A^y mice that were subjected to a single *ip* injection and daily *ip* injections at a dose of 3.0 mg Zn kg^{-1} body weight for two weeks [137].

1.6.2 Magnesium compounds

The relationship between magnesium and diabetes has been studied for decades but it is not yet fully understood. Magnesium plays an important role in carbohydrate metabolism. It may influence the release and activity of insulin. Low blood levels of magnesium (hypomagnesemia) are frequently seen in individuals with Type 2 diabetes. Hypomagnesemia may worsen insulin resistance, a condition that often precedes type 2 diabetes, or may be a consequence of insulin resistance.

Studies suggest that a deficiency in magnesium may worsen blood glucose control in Type 2 diabetes. It is believed that a deficiency of magnesium interrupts insulin secretion in the pancreas and increases insulin resistance in the body's tissues. Evidence suggests that a deficiency of magnesium may contribute to certain diabetes complications. A recent analysis showed that people with higher dietary

intakes of magnesium (through consumption of whole grains, nuts, and green leafy vegetables) had a decreased risk of Type 2 diabetes. Supplementation with magnesium in patients of diabetes enhances insulin sensitivity and secretion. In rats predisposed in diabetes, supplementation with oral magnesium diminished the progression of the disease. Magnesium supplements can frequently overcome several serious blood pressure disorders as well. Magnesium supplements can be available in several varieties of salts, like magnesium citrate, magnesium gluconate or magnesium lactate.

1.6.3 Chromium compounds

The benefit of added chromium for diabetes control has been studied and debated for several years. Several studies report that chromium supplementation may improve diabetes control. Chromium is needed to make glucose tolerance factor, which helps insulin improve its action. The first chromium compound that has been used in the management of diabetes is chromium picolinate [143]. Studies carried out to investigate the carbohydrate metabolism in lean and obese rats when given chromium picolinate showed that the obese rats had more significant improvement in fasting insulin levels and glucose tolerance, but the lean rats did not experience any significant changes. The final conclusion was that the chromium picolinate may be beneficial in insulin resistance states but it appears to have no effects on the lean rats. The effectiveness of chromium picolinate is highly pronounced in pregnant women (gestational diabetes) and Type 2 DM. Other chromium compounds that have been tried are chromium chloride and chromium nicotinate. Because of insufficient information on the use of chromium to treat diabetes, no recommendations for supplementation yet exist.

1.7 Toxicity of vanadium compounds

Research carried out by many workers in different laboratories [144-146] have shown that vanadium toxicity depends on specific chemical form, oxidation state, administration route, period and doses, as well as types of organism studied. The concentration limit for which vanadium compounds become toxic also depends on the type of coordination environment. As a general rule, concentration below 1.0×10^{-5} M are estimated to be safe and still are able to maintain the biological activity, whereas those above 1.0×10^{-3} M are expected to be toxic for chronic use. The chronic toxic strength patterns of vanadium compounds follow the order: inorganic salts; soluble > insoluble > organic vanadium compounds; vanadium(V) organic compounds > vanadium(IV) organic compounds. In the case of vanadium organic compounds, the toxicity also depends on the donor atoms coordinated to vanadium; NN, OO, or NO are less toxic than compounds with donor sets NS, OS, or SS, irrespective of the vanadium oxidation state. The toxicity tends to decrease as the valence decreases. Typical clinical manifestations for acute toxicity are light diarrhea, vomiting, abdominal cramps, green tongue, severe *bronchospasm*, neurological and irreversible renal excretion damage [147].

1.8 Accumulation of vanadium compounds in the body

Vanadium tissue accumulation represents the major concern about vanadium use in the long-time administration [144]. It is noticeable that vanadium is stored in various organs with long half-lives in the body and its prolonged presence may potentially maintain some anti-diabetic activity [148]. Vanadium inorganic salts are not well absorbed by human organism; roughly 5 % of the ingested mass and only in certain condition can exceed 10 % [149]. Most ingested vanadium is apparently

unabsorbed and is thus excreted via the feaces. The distribution of vanadium in the body tissues after oral and intra-peritoneal administration follows the order: bone > kidney > spleen > heart > teste > lung > pancreas > brain after 24 h [150]. There is evidence that oxovanadium(IV) interacts with bone mineral, hydroxyapatite, but it is now known that the ions do not incorporate into the apatitic lattice and does not appear to affect bone strength or architecture [101]. On the other hand, vanadium organic complexes accumulation follows a pattern that is not quite different from inorganic salts. The principal sites of accumulation are bone, kidney and liver. However, the absorption of these compounds is highly improved, their retention time in plasma is also longer and their biological effects enhanced. Distribution and accumulation of vanadium is not due to increase in absorption, but depends strongly on the chemical structure [149].

1.9 Mechanism of action of insulin

Insulin is a hormone which is secreted by a group of cells within the pancreas called *Langerhans' islets*. It is a peptide hormone which regulates fat and carbohydrate metabolism. Insulin also serves to counteract catabolic hormone and suppress glucose production in the liver. The insulin receptor is tyrosine kinase embedded in the plasma membrane. It is composed of two alpha sub-units and two beta sub-units linked by disulfide bonds. The alpha chains house insulin binding domains while beta chains penetrate through the plasma membrane. The normal uptake and metabolism of glucose is initiated by a series of intracellular reaction known as the insulin-signaling cascade [151]. As insulin docks to the outside of the receptor, tyrosine at the inside is phosphorylated (**b** in Fig. 1.2), giving rise to a complicated signal transduction cascade (dashed arrow), which stimulates glucose

intake by a glucose carrier, symbolised by an “opening door”. This phosphorylation is counteracted by a protein tyrosine phosphatase (PTP), which catalyses the hydrolytic rupture of the phosphoester bond. This hydrolysis is fully effective in the absence of insulin (**c** in Fig. 1.2) or in the case of insulin tolerance.

Vanadate can enter the cell via phosphate and sulphate channels. Based on the well known fact that vanadate inhibits phosphatises [152], it has been proposed and evidenced that at least one possible mechanism works through an inhibition of PTP by vanadate, allowing the phosphoester bond (which also forms by autophosphorylation) and thus the signal transduction to remain intact; **d** in Fig. 1.2.

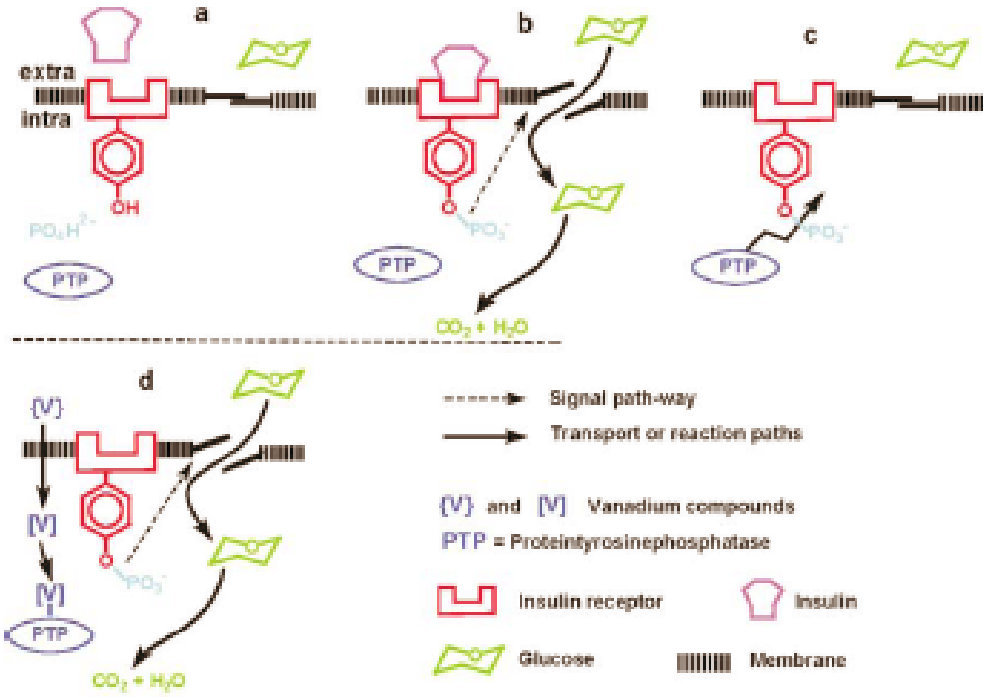

Figure 1.2 Insulin-mimetic behaviour of vanadium compounds. The scheme on the top represents a simplified signal path-way induced by insulin and vanadium, respectively [153]. Alternatively, a non-membrane protein–tyrosine kinase (PTK) may be activated by vanadium, or vanadate itself may esterificate effectively the tyrosines of the insulin receptor [147].

1.10 Types of diabetes

Diabetes mellitus is a group of diseases characterized by high levels of blood glucose resulting from defects in insulin production, insulin resistance, or both. Diabetes can be associated with serious complications and premature death, but people with diabetes can take steps to manage the disease and lower the risk of complications.

Type1 diabetes was previously called insulin-dependent diabetes mellitus (IDDM) or juvenile-onset diabetes. Type 1 diabetes develops when the body's immune system destroys pancreatic beta cells, the only cells in the body that make the hormone insulin that regulates blood glucose. This form of diabetes usually strikes children and young adults, although disease onset can occur at any age. Type 1 diabetes may account for 5 to 10% of all diagnosed cases of diabetes. Risk factors for Type 1 diabetes may include autoimmune, genetic, and environmental factors.

Type 2 diabetes was previously called non-insulin-dependent diabetes mellitus (NIDDM) or adult-onset diabetes. Type 2 diabetes may account for about 90-95% of all diagnosed cases of diabetes. It usually begins as insulin resistance, a disorder in which the cells do not utilise insulin efficiently. As the need for insulin rises, the pancreas gradually loses its ability to produce insulin. Type 2 diabetes is associated with older age (above 40 years old), obesity, family history of diabetes, history of gestational diabetes, impaired glucose metabolism, physical inactivity, and race/demography. Type 2 diabetes is increasingly being diagnosed in children and adolescents. This is attributed to changes in eating habits. Youths tend to feed more on junk foods which contain high fat content and less fiber.

Gestational diabetes is a form of glucose intolerance diagnosed in some women during pregnancy. Gestational diabetes is also more common among obese women and women with a family history of diabetes. During pregnancy, gestational diabetes requires treatment to normalize maternal blood glucose levels to avoid complications in the infant. After pregnancy, 5 – 10 % of women with gestational diabetes are found to progress to Type 2 diabetes. Women who have had gestational diabetes have a 20 - 50 % chance of developing diabetes in the next 5 - 10 years. Other specific types of diabetes result from specific genetic conditions (such as maturity-onset diabetes of youth), surgery, drugs, malnutrition, infections, and other illnesses. Such types of diabetes may account for 1 – 5 % of all diagnosed cases of diabetes.

1.11 Prevalence of diabetes in the World

The prevalence of diabetes for all age-groups worldwide was estimated to be 2.8 % in 2000 and expected to rise to 4.4 % in 2030 [154]. The total number of people with diabetes is projected to rise from 171 million in 2000 to 366 million in 2030. The major part of this numerical increase will occur in developing countries. There will be a 42 % increase (from 51 to 72 million) in the developed countries and a 170 % increase (from 84 to 228 million) in the developing countries. The greatest relative increases will occur in the Middle Eastern Crescent, sub-Sahara Africa and India. The greatest absolute increase in the number of people with diabetes will be in India. Globally, diabetes prevalence is similar in men and women but there are more women with diabetes than men (CIA World Factbook 2002).

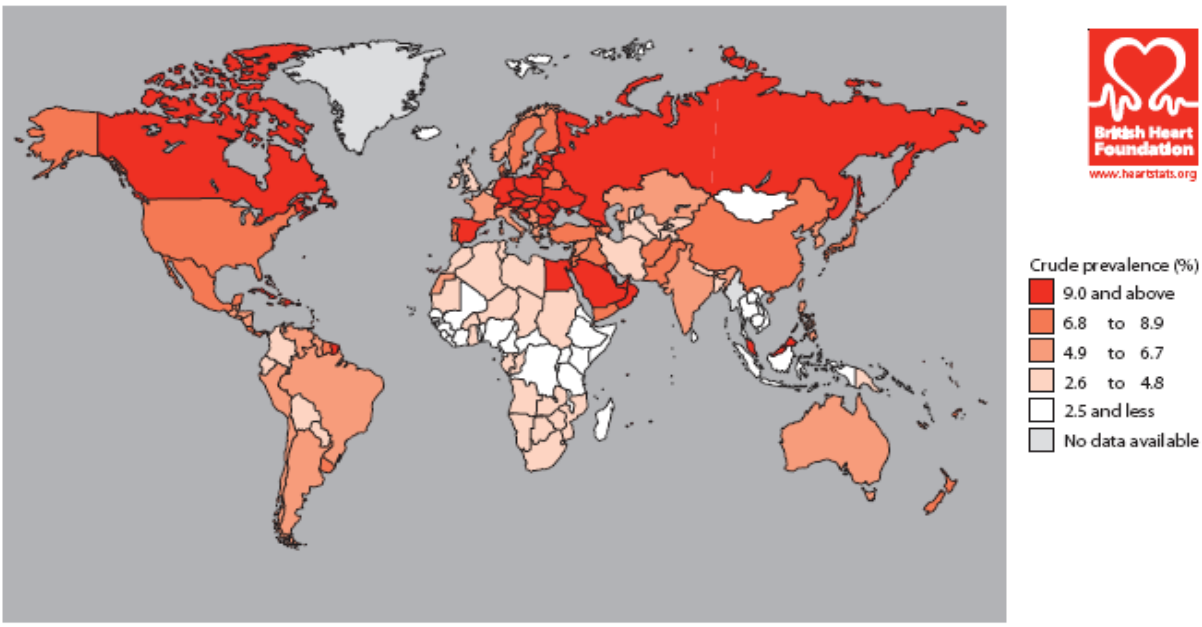

Figure 1.3 Worldwide map showing the prevalence of diabetes, 2003

Source: Diabetes Atlas, International Diabetes Federation (2003).

The ten countries estimated to have the highest numbers of people living with diabetes in 2000 and 2030 are listed in Table 1.1

1.12 Prevalence of diabetes in South Africa

Diabetes ranks the third in South Africa after ischemic heart disease and cancer in terms of morbidity and mortality. The prevalence in adults is 4% for whites, 5.8% for blacks and 13% for Indians [155]. Based on the revised WHO criteria, South African Indians show a high prevalence rate more than twice as that seen in the blacks or whites. The high prevalence of diabetes in South African Indians could be due to genetic susceptibility coupled with obesity.

Table 1.1 List of countries with the highest numbers of estimated cases of diabetes for 2000 and 2030 [154]

Ranking	2000		2030	
	Country	People with Diabetes (millions)	Country	People with Diabetes (millions)
1	India	31.7	India	79.4
2	China	20.8	China	42.3
3	US	17.7	US	30.3
4	Indonesia	8.4	Indonesia	21.3
5	Japan	6.8	Pakistan	13.9
6	Pakistan	5.2	Brazil	11.3
7	Russian Federation	4.6	Bangladesh	11.1
8	Brazil	4.6	Japan	8.9
9	Italy	4.3	Philippines	7.8
10	Bangladesh	3.2	Egypt	6.7

International Diabetes Federation (IDF) atlas reports a prevalence figure of 3.4% for 24 million South Africa between the age group 20-79 (2003) with an expected increase to 3.9% by 2025 as shown in Table 1.2. It is possible that the greater degree of obesity in females could account for the somehow higher prevalence of diabetes seen in females South African.

Table 1.2 Prevalence estimates of diabetes in South Africa: comparison of years 2003 and 2025

Year	Prevalence (20-79 y)		Distribution per population/1000							
	No.	%	Rural	Urban	Male	Female	20-39	40-59	60-79	Total
2003	24 741	3.4	272.1	569.1	322.7	518.5	127.1	489.6	224.5	841.2
2025	26 816	3.9	249.3	805.7	416.8	638.2	130.2	536.3	388.5	1 055.0

Source: Diabetes Atlas, International Diabetes Federation (2003).

1.13 Scope of this work

The scope of this work was to synthesise a series of novel symmetrical and unsymmetrical tetradentate Schiff bases derived from condensation of salicylaldehyde, substituted salicylaldehydes, 2-hydroxy-1-naphthaldehyde, and a series of aliphatic and aromatic diamines and to coordinate them with VO^{2+}, Co^{2+}, Ni^{2+}, and Cu^{2+}. The oxovanadium(IV) complexes would then be further investigated for their insulin-enhancing properties when administered as therapeutic agents.

1.14 Aims and Objectives

The aim of this research work will be directed toward the synthesis and characterisation of neutral symmetrical and unsymmetrical tetradentate Schiff base complexes of oxovanadium(IV) with high thermodynamic stability, adequate balance of hydrophilicity/lipophilicity and low toxicity that could be tested *in vitro* and *in vivo* for enhancement in the activity of insulin in lowering blood glucose levels. The work would also be extended to the synthesis and physicochemical characterisation of the cobalt(II), nickel(II), and copper(II) complexes of the unsymmetrical Schiff bases only because of the extensive attention that their symmetrical Schiff base complexes have attracted in the literature [39, 46, 51].

Specifically, the research objectives are:

(1) To synthesize and characterize a series of symmetrical and unsymmetrical tetradentate Schiff bases of the N_2O_2 donor sets, which are anticipated to provide stereochemical flexibility and stability to their metal(II) complexes.

(2) To coordinate the preformed ligands to the VO^{2+} and the unsymmetrical ligands to Co^{2+}, Ni^{2+} and Cu^{2+} ions.

(3) To establish the purity of the metal complexes and establish their stereochemistry.

(4) To screen the oxovanadium(IV) complexes as potential insulin-enhancing agents.

1.15 Compounds reported in the project

The compounds investigated in this project are listed, with their formulae, in Tables 1.3 and 1.4.

Table 1.3 Nomenclature and formulae for the Schiff bases

Name of ligand	Formulae
N-(naphthalidene)-N'-(5-chlorosalicylidene)orthophenylenediamine	H_2(naph-Clsal)opd
N-(naphthalidene)-N'-(3-ethoxysalicylidene)orthophenylenediamine	H_2(naph-Oetsal)opd
N-(naphthalidene)-N'-(5-nitrosalicylidene)orthophenylenediamine	H_2(naph-NO_2sal)opd
N-(naphthalidene)-N'-(salicylidene)orthophenylenediamine	H_2(naph-sal)opd
N,N'-bis(benzophenylidene)ethylenediamine	H_2bp_2en
N,N'-bis(benzophenylidene)-1-methylethylenediamine	H_2bp_2pn
N,N'-bis(benzophenylidene)trimethylenediamine	H_2bp_2tn
N,N'-bis(naphthalidene)ethylenediamine	H_2naph_2en
N,N'-bis(naphthalidene)trimethylenediamine	H_2naph_2tn
N,N'-bis(naphthalidene)orthophenylenediamine	H_2naph_2opd
N,N'-bis(5-chlorosalicylidene)ethylenediamine	H_2Clsal_2en
N,N'-bis(5-chlorosalicylidene))-1-methylethylenediamine	H_2Clsal_2pn
N,N'-bis(5-chlorosalicylidene) trimethylenediamine	H_2Clsal_2tn
N,N'-bis(5-chlorosalicylidene) orthophenylenediamine	H_2Clsal_2opd
N,N'-bis (5-methoxysalicylidene) ethylenediamine	$H_2Omesal_2en$
N,N'-bis(5-methoxysalicylidene) trimethylenediamine	$H_2Omesal_2tn$
N,N'-bis(5-methoxysalicylidene) orthophenylenediamine	$H_2Omesal_2opd$

N,N'-bis (3-ethoxysalicylidene)ethylenediamine	H_2Oetsal$_2$en
N,N'-bis (3-ethoxysalicylidene)-1-methylethylenediamine	H_2Oetsal$_2$pn
N,N'-bis (3-ethoxysalicylidene)orthophenylenediamine	H_2Oetsal$_2$opd

Table 1.4 Nomenclature and formulae for the oxovanadium(IV) complexes

Ref. No.	Name of complex	Formulae
VOL[1]	N-(naphthalidene)-N'-(5-chlorosalicylidene)orthopheny lenediiminato oxovanadium(IV)	[VO(naph-Clsal)opd]
VOL[2]	N-(naphthalidene)-N'-(5-nitrosalicylidene)orthophenylenediiminato oxovanadium(IV)	[VO(naphNO_2sal)opd]
VOL[3]	N-(naphthalidene)-N'-(3-ethoxysalicylidene)orthophenylenediiminato oxovanadium(IV)	[VO(naphOetsal)opd]
VOL[4]	N-(naphthalidene)-N'-(salicylidene)orthophenylenediiminato oxovanadium(IV)	[VO(naph-sal)opd]
VOL[5]	N,N'-bis(benzophenone)ethylenediiminatooxovanadium(IV)	[VObp$_2$en]
VOL[6]	N, N'-bis(benzophenone)-1,2-propylenediiminato oxovanadium(IV)	[VObp$_2$pn]
VOL[7]	N,N'-bis(benzophenone)trimethylenediiminatooxovanadium(IV)	[VObp$_2$tn]·MeOH
VOL[8]	N,N'-bis(naphthalidene)ethylenediiminatooxovanadium(IV)	[VOnaph$_2$en]
VOL[9]	N,N'-bis(naphthalidene)trimethylenediiminatooxovanadium(IV)	[VOnaph$_2$tn]
VOL[10]	N,N'-bis(naphthalidene)orthophenylenediiminato oxovanadium(IV)	[VOnaph$_2$opd]
VOL[11]	N,N'-bis(5-chlorosalicylidene)ethylenediiminatooxovanadium(IV)	[VOClsal$_2$en]
VOL[12]	N,N'-bis(5-chlorosalicylidene))-1,2-propylenediiminato oxovanadium(IV)	[VOClsal$_2$pn]
VOL[13]	N,N'-bis(5-chlorosalicylidene)trimethylenediiminato oxovanadium(IV)	[VOClsal$_2$tn]
VOL[14]	N,N'-bis(5-chlorosalicylidene)orthophenylenediiminato oxovanadium(IV)	[VOClsal$_2$opd]

VOL^{15}	N,N'-bis (5-methoxysalicylidene)ethylenediiminato oxovanadium(IV)	[$VO(Omesal_2en)$]
VOL^{16}	N,N'-bis (5-methoxysalicylidene)trimethylenediiminato oxovanadium(IV)	[$VO(Omesal_2tn)$].MeOH
VOL^{17}	N,N'-bis (5-methoxysalicylidene)orthophenylenediiminato oxovanadium(IV)	[$VO(Omesal_2opd)$]
VOL^{18}	N,N'-bis (3-ethoxysalicylidene) ethylenediiminato oxovanadium(IV)	[$VO(Oetsal_2en)$]
VOL^{19}	N,N'-bis (3-ethoxysalicylidene))-1,2-propylenediiminato oxovanadium(IV)	[$VO(Oetsal_2pn)$]
VOL^{20}	N,N'-bis (3-ethoxysalicylidene))orthophenylenediiminato oxovanadium(IV)	[$VO(Oetsal_2opd)$]
CoL^1	N-(naphthalidene)-N'-(5-chlorosalicylidene)orthopheny lenediiminato cobalt(II)	[Co(naph-Clsal)opd]
CoL^2	N-(naphthalidene)-N'-(5-nitrosalicylidene)orthophenylenediiminato cobalt(II)	[Co(naphNO_2sal)opd]
CoL^3	N-(naphthalidene)-N'-(3-ethoxysalicylidene) orthopheny lenediiminato cobalt(II)	[Co(naphOetsal)opd]
CoL^4	N-(naphthalidene)-N'-(salicylidene)orthophenylenediiminato cobalt(II)	[Co(naph-sal)opd]
CuL^1	N-(naphthalidene)-N'-(5-chlorosalicylidene)orthopheny lenediiminato copper(II)	[Cu(naph-Clsal)opd]
CuL^2	N-(naphthalidene)-N'-(5-nitrosalicylidene)orthopheny lenediiminato copper(II)	[Cu(naphNO_2sal)opd]
CuL^3	N-(naphthalidene)-N'-(3-ethoxysalicylidene)orthopheny lenediiminato copper(II)	[Cu(naphOetsal)opd]
CuL^4	N-(naphthalidene)-N'-(salicylidene)orthophenylenediiminato copper(II)	[Cu(naph-sal)opd]
NiL^1	N-(naphthalidene)-N'-(5-chlorosalicylidene)orthopheny lenediiminato nickel(II)	[Ni(naph-Clsal)opd]
NiL^2	N-(naphthalidene)-N'-(5-nitrosalicylidene)orthophenylenediiminato nickel(II)	[Ni(naphNO_2sal)opd]
NiL^3	N-(naphthalidene)-N'-(3-ethoxysalicylidene)orthopheny lenediiminato nickel(II)	[Ni(naphOetsal)opd]
NiL^4	N-(naphthalidene)-N'-(salicylidene)orthophenylenediiminato nickel(II)	[Ni(naph-sal)opd]

CHAPTER 2

PHYSICAL TECHNIQUES USED FOR CHARACTERIZATION

2.1 Electron paramagnetic resonance (EPR)

EPR, also called electron spin resonance (ESR), is a form of magnetic resonance spectroscopy used for measuring the absorption of electromagnetic radiation by a molecular system containing one or more unpaired electrons [156, 157]. The sample is usually placed in a magnetic field and the transitions monitored are between two electron energy levels. Most experiment uses 9-9.5 GHz microwaves radiation in the X-band, for which the free electron resonance occurs at about 3200-3400 G. This sensitive technique has proved useful in the study of the electronic structures of many species, including organic free radicals, biradicals, triplet excited states and most transition metals and rare-earth metals. Important biological applications include the use of 'spin labels' as probes of molecular environment in enzyme-active sites and membranes [156]. EPR has also been used to examine interior defects in solid state chemistry and to study reactive chemical species on catalytic surfaces.

EPR gives the chemical information regarding the structure of paramagnetic substances. The number of lines, their spacing and their relative intensities unequivocally indicate a characteristic structure of a species. It is observed that when a molecule or ions containing one or more unpaired electrons are placed in a magnetic field, the effect of the magnetic field is to lift the spin degeneracy, i.e., to make the energy of the electrons differ for its two M_s values, +½ and -½. The electron lines up its field with the magnetic field and results in an increase of

potential energy. A quantum-mechanical treatment shows that the energy difference between these two electron spin alignments is equal to $g\beta H$, where g is the gyromagnetic ratio, β is the Bohr magneton and H is the strength of magnetic field.

For EPR investigation, transition metal ions are the simplest example. To understand the spectrum of an ion requires a detailed consideration both of the individual ion and of its environment. The result may provide:

i) Identification of the elements, its specific valence state and composition;

ii) The symmetry of the crystalline electric field to which an ion is subjected, and

iii) Numerical values for parameters in spin Hamiltonian.

When the ions are placed in condensed media, their behavior in a magnetic field is profoundly altered. In evaluation of an EPR spectrum, the most important parameter is the g value, which is also known as spectroscopic splitting factor.

2.1.1 The theory of EPR spectroscopy [157]

The theory of EPR spectroscopy shares much in common with that of nuclear magnetic resonance spectroscopy (NMR). However, the magnetic moment of the electron is about 1000 times as large as the nuclear moment and the constants employed in NMR theory frequently are different in magnitude and sign. The electron is a charged particle with angular momentum (orbital and spin) and as such, it possesses a magnetic moment, μ_e, given by

$$\mu_e = -g\beta J \text{ ----------} \textbf{\textit{Equation 1}}$$

Here J (in units of $h/2\pi$) is the total angular momentum vector, h = Planck's constant, g is a dimensionless constant (the g-values, g-factor, or spectroscopic splitting factor), and β is a constant, the Bohr magneton. The negative sign in Eq. 1 is a

consequence of negative electronic charge. Neglecting orbital angular momentum and considering only the total spin angular momentum S, Eq. 1 can be written as

$$\mu_e = -g\beta S \text{ ----------} \textbf{\textit{Equation 2}}$$

The g-value for the free electron, g_e, is 2.0023. The approximation made in Eq. 2 is valid for most discussions of the EPR spectra of transition-metal complexes whose orbital angular momentum can be considered to be ''quenched''. Treating the g-value as an experimental quantity does not harm the present discussion, since deviation of g-values from g_e can be accounted for by introduction of spin-orbital coupling.

Magnetic moments can be detected by their interactions with magnetic fields. In zero field, the magnetic moments of unpaired electrons in a sample are randomly oriented. In the presence of a magnetic field, it gives rise to 2S+1 energy states (Zeeman splitting). The measurable components of μ_e are $g\beta m_s$ where m_s is the magnetic spin quantum number, which can take the values +S, +(S−1),...., − (S −1), -S. The application of a magnetic field to an S=½ or larger system is said to remove the spin degenerancy.

The energy of an electron moment in a magnetic field is given by

$$E = -\mu_e H \text{ ----------} \textbf{\textit{Equation 3}}$$

Combining Eq. 2 and 3, the expression

$$E = g\beta m_s \text{ ----------} \textbf{\textit{Equation 4}}$$

where S = ±½, yields two energy levels

$$E_{ms = +1/2} = +½\, g\beta H \text{ ----------} \textbf{\textit{Equation 5}}$$

and

$$E_{ms = -1/2} = -½\, g\beta H \text{ ----------} \textbf{\textit{Equation 6}}$$

whose energy is linearly dependent on H. The separation between these energy levels at a particular value of the magnetic field, H is

$$\Delta E = +½\, g\beta H_R - (-½\, g\beta H_R) = g\beta H \text{ ----------} \textbf{\textit{Equation 7}}$$

In an EPR experiment, an oscillating magnetic field perpendicular to the H induces transition between the $m_s = -½$ and $m_s = +½$ levels, provided the frequency, ν, is such that the resonance condition,

$$\Delta E = h\nu = g\beta H \text{ ----------} \textbf{\textit{Equation 8}}$$

is satisfied. The frequency is held constant and the magnetic field is varied. At a particular value of the magnetic field, H, resonance absorption of energy occurs, resulting in a peak in the spectrum (Fig. 2.1).

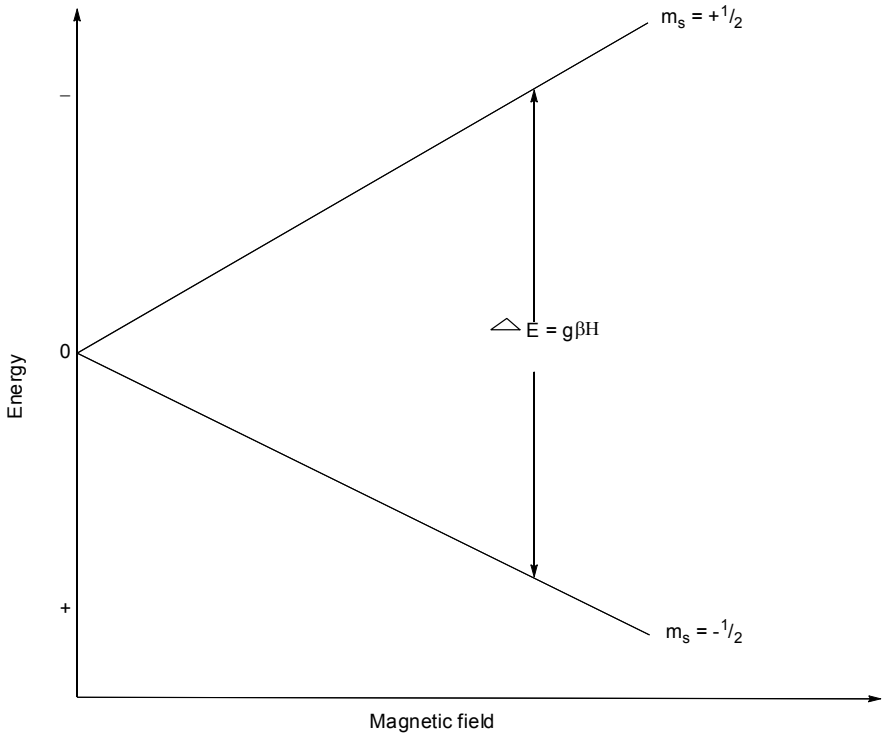

Fig. 2.1 Energy levels for an unpaired electron in a magnetic field

The EPR spectrum of oxovanadium(IV) complexes consists of eight-line signal (2I+1) arising from the interaction of a single unpaired electron (S =½) with the quenched orbital angular momentum of vanadium nucleus of spin I = $^7/_2$ [158, 159].

2.1.2 The Effects of Point Symmetry

The point symmetry at the metal determines whether or not any of the principal values of g or of hyperfine splitting constant (A) are required to be equal to each other. Also it determines whether or not any of the principal axes of *g* and A are required to be coincident. These criteria are summarized in Table 2.1, along with the accepted nomenclature for EPR behaviour and their associated point symmetries. The importance of these relationships is that each type of EPR behaviour is associated with a restricted number of point symmetries. This in turn places constraints upon the geometrical structures of the paramagnet [160].

Table 2.1 Relationships between g and A tensors, EPR symmetry and the point symmetry of paramagnets [160]

EPR Symmetry	*g* and *A* Tensors	Coincidence of Tensors Axes	Molecular Point Symmetry
Isotropic	$g_x = g_y = g_z$ $A_x = A_y = A_z$	All coincident	O_h, T_d, O, T_h, T
Axial	$g_x = g_y \neq g_z$ $A_x = A_y \neq A_z$	All coincident	D_{4h}, C_{4v}, D_4, D_{2d}, D_{6h}, C_{6v}, D_6, D_{3h}, D_{3d}, C_{3v}, D_3
Rhombic	$g_x \neq g_y \neq g_z$ $A_x \neq A_y \neq A_z$	All coincident	D_{2h}, C_{2v}, D_2
Monoclinic	$g_x \neq g_y \neq g_z$ $A_x \neq A_y \neq A_z$	One axis of g and A coincident	C_{2h}, C_s, C_2
Triclinic	$g_x \neq g_y \neq g_z$ $A_x \neq A_y \neq A_z$	Complete non-coincident	C_2, C_1
Axial Non-collinear	$g_x = g_y \neq g_z$ $A_x = A_y \neq A_z$	Only g_x and A_z coincident	C_3, S_6, C_4, S_4 C_{4h}, C_6, C_{3h}, C_{6h}

2.2 Magnetic susceptibility

For studying the electronic structure of a transition metal complex, the measurement of magnetic moment is a very useful method. It provides fundamental information about the bonding and stereochemistry of metal complexes. The magnetic properties of coordination compounds are based on the effect of ligands on the spectroscopic terms of metal ions [161]. The Gouy method is the simplest method of measuring magnetic moments. It consists of a suspension of a uniform rod in a non-homogeneous magnetic field of about 5000 Oersteds and measuring the force exerted on it by a conventional weighing technique. The caliberants usually used are $Hg[Co(SCN)_4]$ and $[Ni(en)_3S_2O_3]$ which are easy to prepare, do not decompose or absorb moisture and pack well in the sample tube. Their susceptibilities at 20 °C are; 16.44×10^{-6} and 11.03×10^{-6} c. g. s. units, respectively and may decrease from 0.05×10^{-6} to 0.04×10^{-6} per degree rise in temperature.

All substances possess magnetic properties and are affected by the application of a magnetic field [162]. The substances may be diamagnetic when an apparent reduction in mass is caused in the applied magnetic field and paramagnetic when an apparent increase in mass is caused in the magnetic field. The molar susceptibility, a measure of magnetic field, of a substance is an algebraic sum of the susceptibilities of the constituent atoms, ions or molecules. The susceptibility per gram atom of a paramagnetic metal ion in a particular compound is determined by measuring the molar susceptibility of the compounds and applying diamagnetic corrections for the other ions or molecules in the compound. The diamagnetic corrections can be estimated by various methods [163]; Pascal's correction gives satisfactory results for inorganic compounds.

2.2.1 The theory of magnetic susceptibility [162, 164]

When a substance is placed in a magnetic field of strength H, the magnetic induction or density of lines of force, B, within the substance is given by:

$$B = H + 4\pi I \quad \text{----------} \quad \textit{Equation 9}$$

where I is the intensity of magnetization or magnetic moment per unit volume and the term $4\pi I$ is a contribution to B by the substance itself. Dividing eq. 9 by H gives:

$$P = 1 + 4\pi\kappa \quad \text{----------} \quad \textit{Equation 10}$$

where P and κ are the magnetic permeability of the material and the magnetic susceptibility per unit volume respectively, which may be considered dimensionless. Thus the volume susceptibility of a vacuum is zero, since in a vacuum B/H = 1. The volume susceptibility of a diamagnetic substance is negative while paramagnetic substances have positive susceptibilities. In practice, susceptibility is usually expressed per unit mass (gram susceptibility) rather than per unit volume.

$$\chi_g = \kappa/\rho \quad \text{----------} \quad \textit{Equation 11}$$

where χ_g = gram susceptibility

ρ = density of the substance in gcm^{-1}

$$\chi_m = \chi_g M \quad \text{----------} \quad \textit{Equation 12}$$

where M is the molar mass of the sample. Similarly, χ_a and χ_{a+} refer to the atomic and ionic susceptibilities respectively and can be obtained from equation 13.

$$\chi_a = \chi_m - \Sigma\chi_L \quad \text{----------} \quad \textit{Equation 13}$$

where χ_L is the molar susceptibility of all other constituents of the ligands (diamagnetic correction).

The magnetic moment is given by

$$\mu_{eff} = 2.828\sqrt{\chi_a T}\ BM \quad \text{----------} \quad \textit{Equation 14}$$

where T is the temperature in K. Experimental values of χ_a are very small and are generally independent of both field strength and temperature.

2.2.2 Types of magnetic behaviour

If P<1 (i.e. I, κ and χ are negative) the substance is said to be diamagnetic. It causes a reduction in the intensity of the magnetic field and in an inhomogenous field moves to the region of lowest field strength. The molar susceptibility of diamagnetic substances is very small and negative (-1 to 100 × 10^{-6} c.g.s. e.m.u) and are usually independent of field strength and temperature. Diamagnetism is a property of all matter and arises from the interaction of paired electron with the magnetic field. Diamagnetic susceptibilities of atoms in molecule are additive; and this is of particular use in estimating the diamagnetic susceptibilities of ligand atoms and counter-ions in a transition metal complex.[162] Additivity of atomic susceptibility is contained in the Pascal's constants.

Paramagnetism results when P>1 i.e. I, κ and χ are positive, and it causes an increase in the intensity of the field and in an inhomogenous field it moves to the region of highest fields strength. Paramagnetic susceptibilities are positive and relatively large (100 to 100, 000 × 10^{-6} c.g.s. e.m.u). They are independent of field strength but depend inversely as temperature. However, temperature independent paramagnetism (TIP) can arise in system containing unpaired electron due to the coupling of the ground states with the excited states under the influence of a magnetic field.

Ferromagnetism and anti-ferromagnetism are both special classes of paramagnetism. They arise from the interaction of individual paramagnetic species with one another. In anti-ferromagnetism, the magnetic vectors of the neighbouring

centres tend to couple anti-parallel so as to cancel one another. It reduces the susceptibility and hence magnetic moment of a compound while in ferromagnetic substances the moments of the separate ions tend to align themselves parallel and thus to reinforce one another. They are both temperature and field strength dependent [161].

2.2.3 Magnetic properties of transition metal complexes

For ions of the first transition series, the magnetic moments due to electron spin (spin only moment) is given by the formula:

$$\mu_{s.o} = [4S(S+L)]^{½} \text{ ----------} \textbf{\textit{Equation 15}}$$

where S = sum of the spin quantum numbers, s = $\pm$ ½ , hence the number of unpaired electrons n = 2S

Equation 15 can therefore be rewritten as:

$$\mu_{s.o} = [n(n+1)]^{½} \text{ ----------} \textbf{\textit{Equation 16}}$$

Where there is orbital motion, the magnetic moment can be written as:

$$\mu_{S+L} = [4S(S+L) + L(L+1)]^{½} \text{ ----------} \textbf{\textit{Equation 17}}$$

Table 2.2 The expected spin only moments for n unpaired electron system

No. of unpaired electron	$\mu_{s.o}$ (B.M)	S
1	1.7	½
2	2.83	1
3	3.87	$^3/_2$
4	4.90	2
5	5.92	$^5/_2$
6	6.39	3
7	7.94	$^7/_2$

2.3 UV-Visible spectrophotometry

The excitation of a molecule from its electronic ground state to an electronic excited state corresponds to absorption of light in the near-infrared, visible or ultraviolet regions of the spectrum. For transition metal complexes, the absorption bands in the first two of these regions (infrared and visible) are relatively weak and are associated with transitions largely localized on the metal atom. The ultraviolet bands are intense and they are associated with the transfer of an electron from one atom to another and so are called charge-transfer bands.

The spectra of transition metal complexes depend on the transition of unpaired electrons from the ground state to an excited state. Transitions may occur between the split d-levels of the central atom, giving rise to the d-d or ligand field spectra. The spectra region where these bands occur spans the near infra-red, visible and UV. Most of the transition metal complexes are coloured due to d-d transitions in the visible region. The atomic overlap in metal—ligand bonds allows d

electrons to penetrate from the central atom to the ligand, and *vice versa*. The transitions are affected by the effect of ligands on the energies of the d orbital of the metal ions. Since octahedral, square-planar and tetrahedral fields cause splitting of d orbitals in different ways, the geometry will have a pronounced effect on the d-d transitions in a metal complex. Thus spectral data of transition metals provide useful information about the structure of complexes.

The optical spectra of oxovanadium(IV) complexes are characterized by three d-d transitions. These transitions have been assigned using the energy level scheme by Ballhausen and Gray [87]. In this scheme, band I is assigned as $b_2 \rightarrow e_\pi^*$ (11,000-16,000), band II as $b_2 \rightarrow b_1^*$ (14,500-19,000) and band III as $b_2 \rightarrow a_1^*$ (21,000-30,000). An overlap between band III and charge transfer bands has always been a problem in being able to make a definitive assignment of band III. It tends to 'borrow' intensity from a nearby charge transfer transition, which in many instances reduces it to a shoulder [165].

2.3.1 The Molecular Orbital Approach for oxovanadium(IV), $[VO(H_2O)_5]^{2+}$, ion

In an attempt to developed appropriate energy level scheme for oxovanadium(IV) ion, earlier theory using crystal field models of the ion were proposed by Furlani and Jørgensen [32, 166]. Furlani's calculations were restricted to $C_{\infty v}$ symmetry of oxovanadium(IV) ion and therefore could not account for all the observed energy levels. Considering the tetragonal molecular ion, $[VO(H_2O)_5]^{2+}$, with axial destabilization, Jørgensen obtained a scheme of energy levels which quantitatively accounted for the 'crystal field' part of the spectrum. The weakness of these early models was first pointed out by Palma-Vittorelli, *et al.* [167] and later by Ballhausen and Gray [87]. They concluded from their magnetic and spectral data

that a pure crystalline field model, that is, a model which only considers σ-bonding to be present, could not provide adequate description of the electronic structure of VO^{2+}. For accurate description of the electronic structure of oxovanadium(IV) ion and its complexes, provisions have to be made for π-bonding between vanadium and oxygen. This was achieved by the molecular orbital treatment of Ballhausen and Gray [87].

Ballhausen and Gray treated the molecular ion, $[VO(H_2O)_5]^{2+}$, in a sophisticated and detailed calculation, necessarily with many approximations. They arrived at the energy level scheme shown in Figure 2.1**.** The orbitals involved in bonding are the 3d, 4s and 4p of the metal, along with the 2s, $2p_\sigma$ ($2p_z$) and $2p_\pi$ ($2p_x$, $2p_y$) of the oxygen and the sp_σ hybrid orbitals for the water oxygens.

The crystal field transitions involve promoting the b_2 electron to the e_π^*, b_1^*, a_1^*, molecular orbitals which are essentially the 3d metal orbitals resulting in $^2E(I)$, $^2B_1$ and $^2A_1$ excited states respectively. The b_2 level is presumed to be purely vanadium $3d_{xy}$ orbital, while the e_π^* orbital is made up of a linear combination of vanadium $3d_{xz}$ and $3d_{yz}$ orbitals with oxygen $2p_x$ and $2p_y$ orbitals. The e_π^* energy level should therefore be sensitive to any perturbation that changes the axial compression in the vanadium-oxygen bond. A strong axial perturbation would be expected to reduce the vanadium-oxygen interaction thus lowering the e_π^* level with respect to b_2^*. The b_1^* level is made up of a linear combination of the $3d_{x^2-y^2}$ metal orbital and ligand orbitals concentrated in the equatorial plane. It is therefore expected that while any axial perturbation will only affect this level indirectly, it will be sensitive to electronic changes in the equatorial coordinating atoms. The a_1^* level involves an admixture of the $3d_{z^2}$ orbitals with the metal 4s and ligand orbitals. One

might expect to observe shifts in the band position on trans-ligation and with changes in the solvent.

The Ballhausen and Gray scheme has been used extensively by other workers to interprete optical, EPR and magnetic properties of oxovanadium(IV) complexes. However, many experimental results are being reported which tend to question the universality of the scheme. Selbin was the first to question the general applicability of the Ballhausen and Gray scheme. The basic assumptions of a C_{4v} symmetry and an O=V— equatorial ligand angle of 90 ^{o}C were in error as X−ray measurements later showed [168, 169]. Band III was observed at 25,000 cm^{-1} for bis(acetylacetonato)oxovanadium(IV) which has a higher V=O bond order [170] than the same bond in $[VO(H_2O)_5]^{2+}$. Ballhausen and Gray did not observe any band between 16,000 and 41,000 cm^{-1}.

Measurements at low temperature and on low-symmetry compounds are strengthening these doubts about the universality of the Ballhausen and Gray scheme.

Selbin has suggested that the ground level is the singly occupied, nonbonding b_2 orbital but that the e_π* and b_1* levels may be very close in energy such that they may cross one another from complex to complex. Kolawole, *et al*. [40, 41] did provide experimental evidence for the inversion of e_π* and b_1* in a series of symmetric Schiff base complexes of oxovanadium(IV) as the methylene bridge increases from 2 to 10 and proposed an energy level which incorporates Ballhaussen and Gray, and Selbin's schemes.

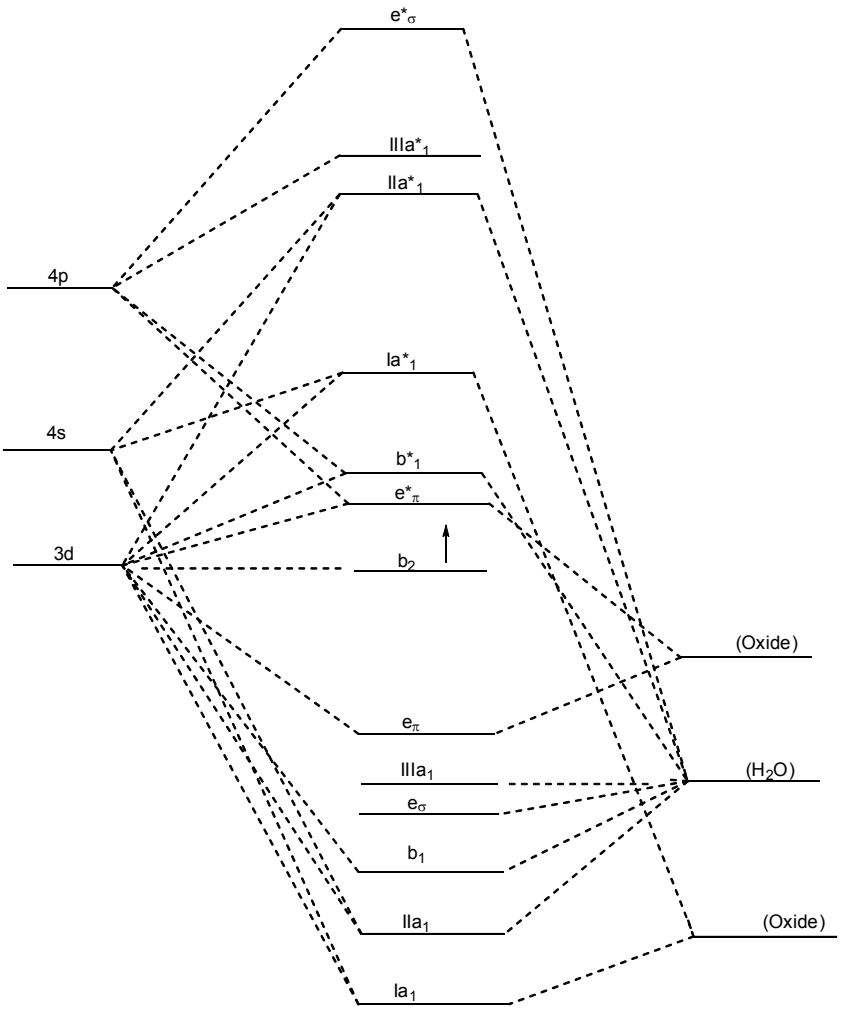

Fig. 2.2 Energy level ordering of Ballhausen and Gray [87]

Patel and Kolawole [41] provided an energy level that show the changes in the ordering of the d orbitals in oxovanadium(IV) complexes as shown in Fig. 2.2, which can be used to account for the electronic spectra of not only different square pyramidal complexes but also of octahedral ones.

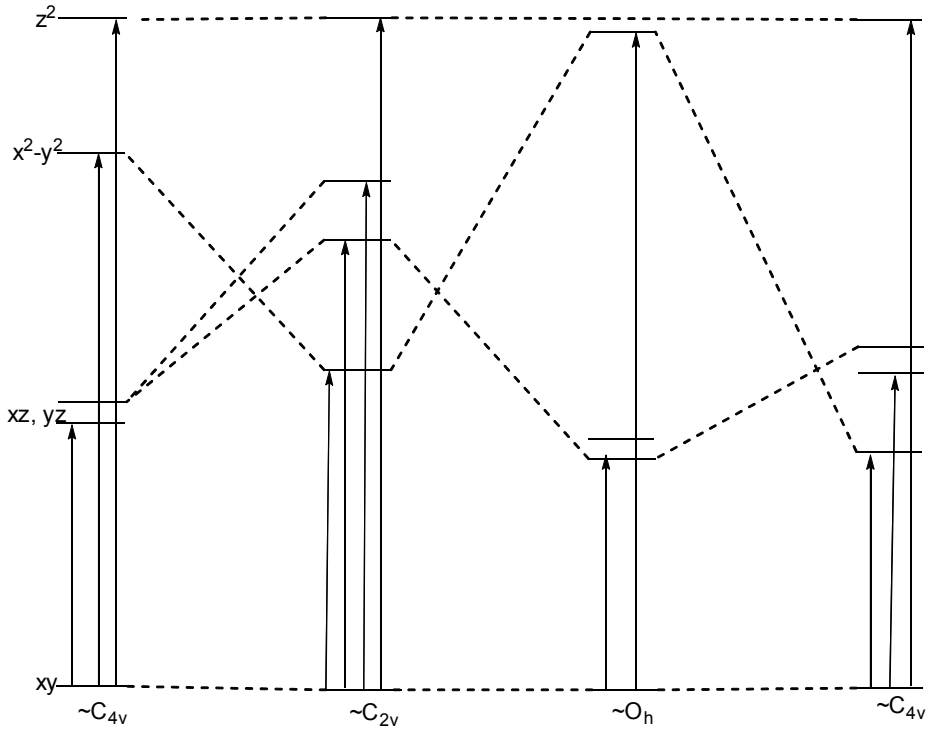

Fig. 2.3 Changes in the ordering of the d orbitals in oxovanadium(IV) complexes

2.4 Thermal Analyses (TA)

Thermal analyses refer to a group of techniques in which a property of a sample is monitored against time or temperature while the temperature of the sample, in a specified atmosphere, is programmed. Thermal analyses are based upon the detection of changes in the enthalpy or the specific heat of a sample as temperature is increased. As thermal energy is supplied to the sample its enthalpy increases and its temperature rises by an amount determined, for a given energy input, by the specific heat of the sample. The specific heat of a material changes slowly with temperature in a particular physical state, but alters discontinuously at a change of state. The supply of thermal energy may induce physical or chemical processes in the sample, e.g. melting or decomposition, accompanied by a change in enthalpy, the latent heat of fusion, heat of reaction, phase transformation, etc.

Such enthalpy changes may be detected by different thermal analyses and related to the processes occurring in the sample.

2.4.1 Types of TA Instrumentation

Thermal analyses encompass a wide variety of techniques such as:

(a) Thermogravimetric analysis (TGA)

(b) Differential thermal analysis (DTA)

(c) Differential scanning calorimetry (DSC)

(d) Thermal mechanical analysis (TMA)

(e) Temperature resolved X-ray diffraction

(f) Thermomagnetometry

(g) Thermoconductometry

(h) Dilatometry

The first three on the list are the most common types of thermal analyses used and discussion will be centred on them.

Thermogravimetric analysis (TGA) is an analytical technique used to determine a material's thermal stability and its fraction of volatile decomposition products by monitoring the weight change that occurs as a specimen is heated. The measurement is normally carried out in air or in an inert atmosphere, such as helium or argon, and the weight is recorded as a function of increasing temperature. Sometimes, the measurement is performed in a lean oxygen atmosphere (1 to 5% O_2 in N_2 or He) to slow down oxidation. In addition to weight changes, some instruments also record the temperature difference between the specimen and one or more reference pans (differential thermal analysis, or DTA) or the heat flow into the specimen pan compared to that of the reference pan (differential scanning

calorimetry, or DSC) [171]. The latter can be used to monitor the energy released or absorbed *via* chemical reactions during the heating process.

In thermogravimetry the change in mass of the sample is recorded as a function of temperature. It provides the analyst with quantitative measurements of change in weight associated with any transition. TG can directly record the loss in weight with time or temperature due to dehydration or decomposition. Thermogravimetric curves are characteristic of a given compound or system because of the unique sequence of physiochemical reactions which occur over definite temperature ranges [172]. In order for a mass change to be detected, a volatile component must he evolved or absorbed by the sample. The former is the usual mode of measurement, but many examples are also known for the latter. Since elevated temperatures are normally required for the evolution of volatile materials, mass-change measurements are made at increasing rather than decreasing temperatures. Routine measurements can be made at temperature range from ambient to 1500°C under inert atmosphere.

Differential thermal analysis (DTA) is a method of measuring the temperature difference between a sample and a reference sample under a controlled temperature-time programme. The instrument is composed of two identical cells in which the sample and a reference (often an empty pan) are placed. Both cells are heated with a constant heat flux, Q, using a single heater, and the temperatures of the two cells are measured as a function of time. If the sample undergoes a thermal transition such as melting, glass transition, chemical reactions, phase changes or structural changes occurring in the sample, liberation or absorption of energy by the sample with the corresponding deviation of its temperature from that of the reference is registered. The difference in temperature is represented by equation 18,

$$\Delta T = T_{sample} - T_{reference} \quad \text{---------- Equation 18}$$

Negative ΔT indicates an endotherm for a heating cycle. DTA curves are useful for both quantitative and qualitative estimate of energies associated with different transformations in thermal processes.

The positions and shapes of the peaks can be used to determine the changes in composition of the sample due to dehydration, decomposition and polymerization. The shape of the DTA curve can also be used in evaluating the kinetics of the reaction under carefully controlled conditions. It is important to note that thermal analysis is affected by experimental conditions and deviations caused by instrumental factors.

Quantitative analysis of DTA data is complicated and the instrument is usually viewed as a fairly crude sibling of a differential scanning calorimeter (DSC) discussed below. Recent instrumental advancements have improved the quantitative use of DTA instruments. A DTA instrument is generally less expensive than a DSC. Determinations of transition temperatures are accurate in a DTA. Estimates of enthalpies of transition are generally not accurate. In the DTA heat is provided at a constant rate and temperature is a dependent parameter.

Differential scanning calorimetry (DSC) is a technique in which the difference in energy inputs into a substance and a reference material is measured as a function of temperature while the substance and the reference material are subjected to a controlled temperature program. DSC is the most widely used thermoanalytical technique. It enables to determine a number of parameters connected with the physical or chemical processes in condensed phase. DSC monitors heat effects associated with phase transitions and chemical reactions as a function of temperature. In a DSC the difference in heat flow to the sample and a reference at

the same temperature is recorded as a function of temperature. The reference is an inert material such as alumina, or just an empty aluminum pan. The temperature of both the sample and reference are increased at a constant rate.

$$\Delta dH/dt = (dH/dt)_{sample} - (dH/dt)_{reference} \quad \textbf{\textit{Equation 19}}$$

The heat flow difference can be either positive or negative. In an endothermic process, such as most phase transitions, heat is absorbed and, therefore, heat flow to the sample is higher than that to the reference. Temperatures of phase transition, enthalpies of phase transitions, polymorphism in food and pharmaceuticals, liquid crystalline transitions, phase diagrams, thermoplastic polymer phase changes, glass temperatures, purity measurements and kinetic studies can be mentioned as examples where DSC is highly efficient.

2.5 Cyclic Voltammetry

Cyclic voltammetry (CV) is perhaps the most effective and versatile electroanalytical technique available for the mechanistic study of redox systems. It enables the electrode potential to be rapidly scanned in search of redox couples [173]. Once located, a couple can then be characterized from the potentials of peaks on the cyclic voltammogram and from changes caused by variation of the scan rate. In cyclic voltammetry, the electrode potential ramps linearly versus time. This ramping is known as the experiment's scan rate (V/s). The potential is measured between the reference electrode and the working electrode and the current is measured between the working electrode and the counter electrode. This data is then plotted as current (*i*) vs. potential (*E*). The forward scan produces a current peak for any analytes that can be reduced (or oxidized, depending on the initial scan direction) through the range of the potential scanned. The current will

increase as the potential reaches the reduction potential of the analyte, but then falls off as the concentration of the analyte is depleted close to the electrode surface. If the redox couple is reversible then when the applied potential is reversed, it will reach the potential that will reoxidize the product formed in the first reduction reaction, and produce a current of reverse polarity from the forward scan. This oxidation peak will usually have a similar shape to the reduction peak. As a result, information about the redox potential and electrochemical reaction rates of the compounds is obtained. For instance if the electronic transfer at the surface is fast and the current is limited by the diffusion of species to the electrode surface, then the current peak will be proportional to the square root of the scan rate.

The important parameters of cyclic voltammetry are the magnitude of the peak currents, i_{pa} and i_{pc}, and the potentials at which peaks occur, E_{pa} and E_{pc}. Reversible peaks have a distinct absolute potential difference between the reduction (E_{pc}) and oxidation peak (E_{pa}). In an ideal system $|E_{pc}-E_{pa}|$ would be 59 mV for a 1 electron process and 30 mV for a 2 electron process [174]. In addition th e ratio of the currents passed at reduction (i_{pc}) and end oxidation (i_{pa}) is near unity ($i_{pa}/i_{pc}=1$) for a reversible peaks. When such reversible peaks are observed thermodynamic information in the form of half cell potential $E^0_{1/2}$ can be determined. When waves are semi-reversible such as when i_{pa}/i_{pc} is less than or greater than 1, it can be possible to determine even more information especially kinetic processes like following chemical reaction. When waves are non-reversible it is impossible to determine what their thermodynamic $E^0_{1/2}$ is with cyclic voltammetry. .

CHAPTER 3

EXPERIMENTAL

3.1 Materials

All reagents and chemicals purchased from Aldrich-Sigma were of analytical/spectroscopic grade and used without further purification. Chemicals and solvents used for the preparation of Schiff base ligands and metal complexes are: salicylaldehyde, 5-chlorosalicylaldehyde, 5-nitrosalicylaldehyde,3-ethoxysalicyl aldehyde, 5-methoxysalicylaldehyde, 2-hydroxy-1-naphthaldehyde, ethylenediamine, 1,2-diaminopropane, 1,3-diaminopropane, 2-hydroxybenzophenone, 1,2-phenylene diamine, oxovanadium(IV)sulphate hydrate, tetrabutylammoniumperchlorate, cobalt(II) acetate, nickel(II) acetate, copper(II) acetate, ethanol, methanol, triethylamine, chloroform, dimethsulphoxide, toluene, and dichloromethane.

3.2 Materials for insulin-mimetic test

The following materials were used for the insulin-mimetic test: C2C12 mouse skeletal muscle cells were obtained from the American Type Culture Collection (ATCC number CRL-1772) and adult male Wistar rats (400-450g) were obtained from the Experimental Animal house of Diabetes Discovery Platform, South African Medical Research Council, Cape Town. Dulbecco modified Eagle's medium (DMEM), L-glutamine, sodium bicarbonate and glucose were purchased from Lonza (USA) while fetal bovine serum (FBS) and horse serum were purchased from Highveld Biological (South Africa).

3.3 Synthesis

3.3.1. Preparation of unsymmetrical Schiff bases

Ethanolic solutions of 2-hydroxy-1-naphthaldehyde (3.444 g, 20 mmol), 1,2-phenylenediamine (2.163 g, 20 mmol) and salicylaldehyde or substituted salicylaldehyde (20 mmol) in absolute ethanol (75 mL each) were prepared and chilled in the refrigerator at 4 ^{o}C for 15 min. To a stirred solution of the cold 2-hydroxy-1-naphthaldehyde, cold solution of 1, 2-phenylenediamine was added dropwise followed by the addition of cold solution of salicylaldehyde (or substituted salicylaldehyde) over a period of 2 min. The mixture was kept stirred at room temperature for 4 days, after which the mixture was warmed to, and kept at, 70 ^{o}C for 20 min with stirring to dissolve any unreacted reactants and to complete the reaction. The product was filtered hot and washed twice with ice cold ethanol. The orange product obtained was purified by digesting in hot ethanol, filtered hot, and dried in a desiccator over silica gel.

3.3.2 Preparation of symmetrical Schiff bases

The ligands were prepared according to established procedures [175]. A typical procedure for the synthesis of the symmetrical Schiff base is as follows: To a stirred solution of 0.08 mole of the appropriate 2-hydroxycarbonyl compound (aldehyde and ketone) in 60 mL absolute ethanol was added, drop wise, 0.04 mol of an ethanolic solution of aliphatic or aromatic diamines. This mixture was then stirred for 2 h at 50 ^{o}C. Afterwards the mixture was cooled to room temperature, or in ice, and the products formed were collected by filtration. The crystals were washed with cold absolute ethanol and re-crystallized from ethanol-chloroform (1:3 v/v) mixture. The yellow crystals were dried in a desiccator over silica gel.

3.3.3 Preparation of oxovanadium(IV) complexes

The following general procedure was used in the synthesis of all the oxovanadiun(IV) complexes [41]. Oxovanadium(IV) sulphate (6 mmol, 0.978 g) was dissolved in hot absolute methanol (300 mL) and a mixture of triethylamine (12 mmol, 1.214 g) and the corresponding Schiff bases (6 mmol), dissolved in methanol (20 mL), was added with stirring, which resulted in an instant colour change to green/orange. The mixture was stirred for 3 h at 50 ^{o}C and then concentrated to half of its volume using a rotary evaporator. The product was filtered and washed twice with cold absolute ethanol and allowed to dry in a desiccator over silica gel.

3.3.4. Preparation of the cobalt(II), nickel(II) and copper(II) complexes

The various complexes were prepared by addition of 3 mmol of $Co(CH_3COO)_2.4H_2O$ (0.53 g), $Ni(CH_3COO)_2.4H_2O$ (0.75 g) or $Cu(CH_3COO)_2.H_2O$ (0.60 g) dissolved hot absolute methanol (60 mL) to a stirring 3 mmol of the respective unsymmetrical Schiff bases in methanol (40 mL). The colour of the mixture changed instantly. The mixture was refluxed for 3 h and the precipitated solids were filtered, washed with cold methanol and allowed to dry in a desiccator over silica gel.

3.4 Characterization of the ligands and complexes

The ligands were characterized by elemental analysis, infrared and ^{1}H NMR while the metal complexes were characterized by elemental analyses, infrared, and electronic spectral, cyclic voltammetry, electron paramagnetic resonance, and room temperature magnetic susceptibility measurements, and differential scanning calorimetry.

3.4.1 Microanalysis

Carbon, hydrogen and nitrogen analysis was done in house on a Perkin-Elmer automated model 2400 Series II CHNS/O analyzer.

3.4.2 Melting/decomposition points

The melting/decomposition points were determined in house by placing a finely powered sample in a glass capillary and heating by using Barnstead/electrothermal digital melting point apparatus and are uncorrected.

3.4.3 ^{1}H NMR spectra

The ^{1}H NMR spectra of the ligands, in $CDCl_3$ with tetramethylsilane (TMS) as an internal standard, were obtained using a Bruker Avance III 400 MHz spectrophotometer at University of KwaZuluNatal Westville campus. All chemical shifts are given in ppm versus tetramethylsilane.

3.4.4 Infrared spectroscopy

Infrared spectra were recorded on a Bruker FT-IR tensor 27 spectrophotometer directly on small samples of the compounds in the range 200-4000 cm^{-1}. The infrared spectra measurements were carried out in house.

3.4.5 Electronic absorption spectra

Electronic absorption spectra in the UV-Visible region were recorded on a Cary Model 50 spectrophotometer between 200-1100 nm in both chloroform and DMSO as solvents. These measurements were also carried out in house.

3.4.6 Electron paramagnetic resonance (EPR)

EPR spectra were measured using a Bruker EMX Micro Premium X Spectrometer at X-band (9.4 GHz) on the powder and on the fluid and frozen solutions in toluene/dichloromethane (90/10 v/v). The EPR spectra measurements were run by Dr. J Wolowska of the University of Manchester, United Kingdom.

3.4.7 Magnetic moments

Magnetic susceptibility measurements done in house were made on powdered samples using a Sherwood Scientific magnetic susceptibility balance. $Hg[Co(SCN)_4]$ was used as the calibrant and corrections for diamagnetism were estimated from Pascal's constants.

3.4.8 Cyclic voltammetry

The cyclic voltammetry was run by Professor Kolawole during his sabattical visit to the Jackson State University, USA on CHI 832 electrochemical detector. Glassy carbon electrode, platinum wire and Ag/Ag^+ were used as working, supporting and reference electrodes respectively. Sample solutions were 10^{-3} M of each complex in spectroscopic grade DMSO containing 0.1 M tetrabutylammonium perchlorate as the supporting electrolyte. Each solution was degassed with ultra pure N_2 gas for 5 min before each measurement was made.

3.4.9. Differential scanning calorimetry (DSC)

Thermal analysis was carried out by Professor Kolawole during his sabattical visit to the Jackson State University, USA on Netzsch Thermal Analysis DSC 200

F3. The sample and reference pan are in separate furnaces heated by separate heaters. Both the sample and reference are maintained at the same temperature and the difference in thermal power required to maintain them at the same temperature is measured and plotted as a function of temperature or time. The differential heat flow is therefore only due to the heat capacity associated with heating the sample. Small samples (5-10 mg) were weighed in an aluminium pan and the mass noted. The pan was then covered with its cover, usually slightly smaller. The pans are then crimped close using TA's Blue DSC sample press. The enclosed sample was placed in the furnace side by side with the crimped closed empty aluminium pan as reference. The instrument is purged with ultra pure N_2 gas at regulated pressure between 100 and 140 kPa gauge (15 and 20 psig). The gas flow rate was set at 50 mL per min. Experiments were run from room temperature to 500 ^{o}C at scan rates of 10 ^{o}C/min.

3.5 Insulin-mimetic activity

Insulin-mimetic studies were carried at the Diabetic Discovery Platform, South African Medical Research Council, Tygerberg, South Africa under the direction of Dr. Christo Muller**.**

3.5.1 *In vitro studies*

3.3.1.1 Cell culture

Cells were cultured in Dulbecco modified Eagle's medium (DMEM) with 4 mM L-glutamine adjusted to contain 1.5 g/L sodium bicarbonate and 4.5 g/L glucose (Lonza, USA) and 10 % fetal bovine serum (Highveld Biological, South Africa) in a humidified atmosphere of 5 % CO_2 and 95% air at 37 ^{o}C. C2C12 cells were sub-

cultured in log phase to 70 % confluence and seeded at a density of 5000 cells/well into 96-well culture plates. To limit batch-to-batch variation cell subcultures were limited to ten passages. After three days culture myotube formation was induced by replacing the fetal bovine serum (FBS) in the medium with 10% horse serum (Highveld Biological, South Africa). All experiments were done in 5 days when more than 75% of the cells were differentiated morphologically.

3.5.1.2 Viable cell counts

The cells were suspended in a trypan blue (0.1% w/w) phosphate buffered saline solution and the ratio of stained to non-stained cells was determined after 5 min of incubation time. Viable cell counts were performed by using a hemocytometer.

3.5.1.3 Glucose uptake determination

Three hours prior to the glucose uptake, cells were incubated in glucose and serum free media. On the 5^{th} day, the medium was removed and replaced with 50 µL modified DMEM without phenol red supplemented with 8 mM glucose and 0,1% BSA (Sigma, USA) containing either the oxovanadium(IV) complexes at concentration of 0.05 µg/µL or the positive controls, insulin or metformin at concentration of 1 µM was added to the 96-well plate. The plate was then incubated for 2 h at 37 ^{o}C and 5 % CO_2. After incubation, 4 µL media was removed from each well and transferred to a new 96-well plate to which 196 µL deionized water was added in each well. 50 µL of this diluted medium was transfer to a new 96-well plate and 50 µL of the prepared glucose assay reagent (Biovision Inc., USA) was added per well and incubated for 30 min at 37 ^{o}C. Absorbance reading was measured at

wavelength 570 nm on a 96-well plate reader (Bio-Tek model ELx800, USA). The glucose concentration per well was calculated from a standard curve. Glucose utilisation was determined by subtracting the glucose concentration left in the medium of the relevant wells following incubation to media not exposed to cells during incubation. All assays were performed in triplicate.

3.5.1.4 Statistical analysis

Statistical analysis of data was performed by means of the student's t-test. The values are presented as means ± SD.

3.5.2 *In vivo studies*

3.5.2.1 Animals

Adult male Wistar rats (400-450g), obtained from the Experimental Animal house of Diabetes Discovery Platform, South African Medical Research Council were bred in an air-conditioned room with controlled lighting 12:12 h light/dark cycle. Rats were allowed free access to standard solid food for laboratory animals and tap water. Diabetes was induced by a single intraperitoneal injection of STZ**,** at a dose of 36 mg /kg**,** to reduce or deplete the numbers of insulin producing cells and to induce hyperglycaemia at levels typical of type 1, or late stage T2D. Rats were fasted for 3 h but were provided with drinking water ad libitum. Blood samples were taken from the tail vein 72 h after STZ injection. Plasma glucose concentrations were determined with a glucometer (Accu-Check®, Roche Diagnostics, Mannheim, Germany). Rats with a blood glucose level of more than 300% of the fasting level were considered diabetic and were selected for the studies. Diabetic rats were divided into 10 experimental groups each containing five rats.

3.5.2.2 Experimental groups

- **Control:** given the solvent vehicle only i.e. water and DMOS 15% v/v,
- **VOL^{1}:** was given 0.2 mM/kg of compound VOL^{1}.
- **VOL^{2}:** was given 0.2 mM/kg of compound VOL^{2}.
- **VOL^{3}:** was given 0.2 mM/kg of compound VOL^{3}.
- **VOL^{4}:** was given 0.2 mM/kg of compound VOL^{4}.
- **VOL^{5}:** was given 0.2 mM/kg of compound VOL^{5}.
- **VOL^{6}:** was given 0.2 mM/kg of compound VOL^{6}.
- **VOL^{7}:** was given 0.2 mM/kg of compound VOL^{7}.
- **VOL^{12}:** was given 0.2 mM/kg of compound VOL^{12}.
- **VOL^{13}:** was given 0.2 mM/kg of compound VOL^{13}

The unsymmetrical Schiff base complexes of oxovanadium(IV) (VOL^{1}-VOL^{4}) were selected for exploratory *in vivo* analyses to establish the effect of the substituents observed under the *in vitro* analyses since the two cases of Schiff base complexes reported in literature for their insulin mimetics were on the symmetrical analogues [126-127]. Furthermore in vitro studies are expensive and highly controlled and the selection of this class of complexes is to cut down on cost.

3.5.2.3 Collecting of blood samples

0.2 mmol/kg solutions of the complexes in DMSO were administered orally to STZ-diabetic induced rats. Blood samples were taken from the tail vein and plasma glucose was measured at intervals of 0, 1, 2, 3, 4, 5 and 6 hours.

3.5.2.4. Analysis of data

The percentage changes in the plasma glucose values of the treatment groups in the STZ rat model were calculated for each hour and then subtracted from the percentage changes in the control values (normalized against the control) at each time-point.

3.5.2.5 Gavage procedure

Diabetic rats were lightly anaesthetized by inhalation of 98 % oxygen and 2 % fluothane (AstraZeneca Pharmaceuticals) until the rats were sufficiently anaesthetized to allow safe and stress-free handling while retaining their swallow-reflex. A teflon gavage catheter was placed into the stomach**,** via the mouth and esophagus, and 1 mL of water and DMSO (15 % v/v) containing the VOL compound was injected directly into the stomach. An additional volume of approximately 200 µL of water was then injected to flush any remaining extract from the gavage catheter. The catheter was then promptly removed and the rat placed in its cage for recovery.

3.5.2.6 Statistical analysis

Results were entered into an Excel spreadsheet and statistically analysed against the control at each time-point using the parametric t-test (Graphpad software). A bar-graph with SEM error bars represents the hourly percentage changes in the whole blood glucose values over the 6-h monitoring period. A statistical significance of $p \leq 0.05$ is indicated by *, statistical significance 0.01 – 0.0001 is indicated by ** and statistical significance $p \leq 0.0001$ is normally indicated by ***.

CHAPTER 4

RESULTS AND DISCUSSION

4.1 Synthesis

4.1.1 Unsymmetrical Schiff bases

A series of new structurally novel unsymmetrical Schiff base ligands were prepared by the condensation reaction in a 1:1:1 molar ratio of 2-hydroxy-1-naphthaldehyde, o-phenylenediamine, and substituted salicylaldehyde or salicylaldehyde and kept stirring at room temperature for four days. All ligands formed were orange-yellow and melted at 134-195 ^{o}C. They were also obtained in high yield and in high purity (Table 4.1). The procedure for the preparation of the unsymmetrical Schiff bases was developed in our laboratory. The sequence of reaction is shown as part of the Scheme presented in Figure 4.1. The following factors were found to affect the course of the synthesis: (i) the sequence of addition of the reagents, (ii) temperature of the solution of the starting reagents (solution chilled to about 4 ^{o}C), (iii) the nature of the diamine (aliphatic or aromatic) used and (iv) the reaction time. A change of amine from o-phenylenediamine to 1, 3-diaminopropane led to the formation of symmetrical Schiff base, N, N'-bis(2-hydroxy-1-naphthalidene)-1, 3-diaminopropane, following the same procedure. From the above observation, it may be concluded that the resonance stabilization energy, arising from extended conjugation, reinforces the formation of the *o*-phen-bridged Schiff base as against the symmetrical Schiff base formed with the aliphatic diamine. A change in reaction time from four days to just three hours or the use of warm solutions of the starting reagents produced mixed products. From the above observations, it seems that the condensation reactions occurred stepwise.

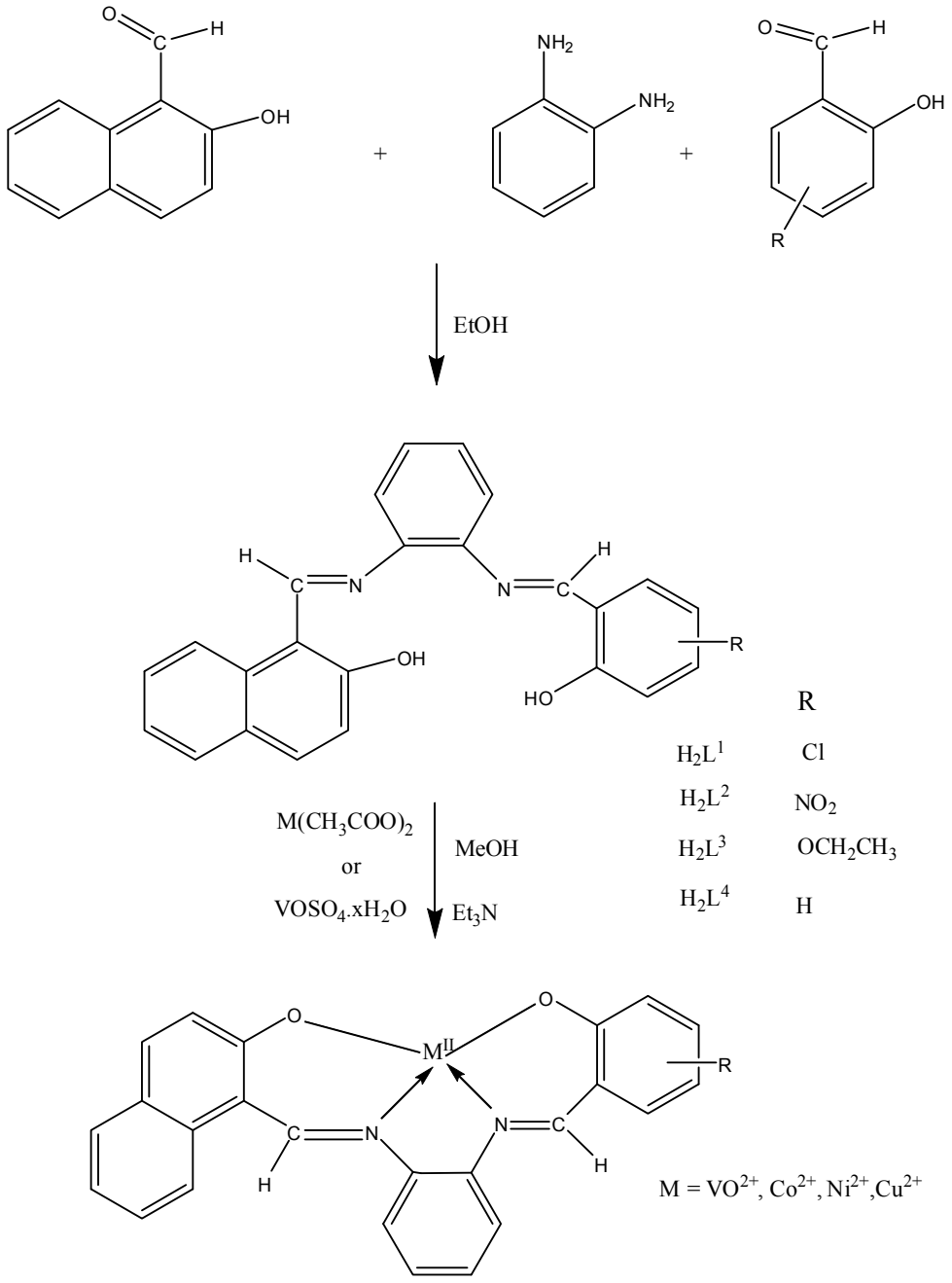

Fig. 4.1 Preparation of the unsymmetrical Schiff bases and their metal(II) complexes

4.1.2 Unsymmetrical Schiff base metal(II) complexes

A series of new structurally novel unsymmetrical tetradentate Schiff base metal(II) complexes of oxovanadium(IV), cobalt(II), nickel(II), and copper(II) were prepared by refluxing together the relevant unsymmetrical Schiff bases with the corresponding oxovanadium(IV) sulphate (or metal(II) acetate for other metals) in

methanolic medium and is shown as part of the Scheme presented in Figure 4.1. They were isolated pure from methanol in very good yields. The purity of the metal complexes was established by microanalyses as formulated. All the unsymmetrical Schiff base complexes did not melt or decompose when heated up to 250 ^{o}C. The analytical data, colour, percentage yields, and melting points of the complexes are presented in Table 4.1.1− 4.1.2.

4.1.2.1 Unsymmetrical Schiff base complexes of cobalt(II)

The cobalt(II) complexes were prepared by refluxing the relevant unsymmetrical Schiff bases with $Co(CH_3COO)_2 \cdot 4H_2O$ in methanol. The resulting brown solid are stable in air.

4.1.2.2 Unsymmetrical Schiff base complexes of nickel(II)

The nickel(II) complexes were synthesized by reacting the respective unsymmetrical Schiff bases with $Ni(CH_3COO)_2 \cdot 4H_2O$ in 1 : 1 molar ratio in methanol. All the nickel(II) complexes formed were red in colour.

4.1.2.3 Unsymmetrical Schiff base complexes of copper(II)

The copper(II) complexes were prepared by refluxing appropriate amount of $Cu(CH_3COO)_2 \cdot H_2O$ and the respective unsymmetrical Schiff bases in methanol. All the complexes were pale brown in colour.

4.1.2.4 Unsymmetrical Schiff base complexes of oxovanadium(IV)

The oxovanadium(IV) complexes were prepared by heating a mixture of each ligand and oxovanadium(IV) sulphate in 1:1 metal:ligand ratio, buffered with

triethylamine at 50 ^{o}C. All the oxovanadium(IV) complexes formed were green in colour as shown in Table 4.1.1.

4.1.3 Symmetrical Schiff bases and their complexes

The symmetrical ligands and their oxovanadium(IV) complexes were isolated pure from ethanol and methanol respectively, and in very good yields. All the ligands involving aliphatic bridges are yellow while those involving aromatic diamine are either orange or orange-yellow in colour. All the trimethylene-bridged complexes are orange. VOL^{10} and VOL^{17} are brown and others are green in colour. All the complexes did not melt/decompose up to 250 ^{o}C except VOL^{19} which melted at 239-240 ^{o}C. The high melting points of these complexes reflect some molecular complexity. Complexes VOL^{7} and VOL^{17} were formed with associated MeOH to form distorted octahedral complexes. The analytical data, colour, percentage yields, and melting points of the ligands and complexes are contained in Table 4.1.1

4.1.3.1 Benzophenoneimine

The Schiff bases were prepared by refluxing equimolar (0.08 mol) quantities of 2-hydroxybenzophonone in 60 mL absolute ethanol and the respective aliphatic diamine (0.04 mol) in ethanol (10 mL) for 2 h. All the ligands were yellow and melted at 123-165 ^{o}C. The oxovanadium(IV) complexes were isolated from the reaction of $VOSO_4$ with the preformed Schiff bases in methanol in 1:1 metal to ligand ratio, buffered with triethylamine. They were all green except the complex involving the trimethylene bridge, which gave an orange colour and was also formed with associated MeOH

4.1.3.2 Naphthaldiimines

The Schiff bases were prepared by heating equimolar (0.08 mol) quantities of 2-hydroxy-1-naphthylaldehyde in 60 mL absolute ethanol and the respective aliphatic/aromatic diamine (0.04 mol) in ethanol (10 mL) under reflux for 2 h. All the Schiff bases in this series were yellow except the one with the aromatic amine bridge which gave an orange product. All the Schiff bases melted at 222-234 ^{o}C except H_2naph_2-en which melted over 250 ^{o}C. Reactions of the Schiff bases with $VOSO_4$ in methanol in 1:1 metal to ligand ratio, buffered with triethylamine, gave green powders of VOL[8], orange powders of VOL[9] and brown powders of VOL[10].

4.1.3.3 Chlorosalicylaldiimines

The Schiff bases were prepared by condensation reaction of 5-chloro salicylaldehyde (0.08 mol) with the respective diamine (0.04 mol) in absolute ethanol for 2 h and recrystallized from ethanol-chloroform (1:3 v/v) mixture. All the ligands were yellow except H_2Clsal_2opd which was orange-yellow in colour. All the Schiff bases melted at 61- 220 ^{o}C. The oxovanadium(IV) complexes were isolated from the reaction of $VOSO_4$ with the preformed Schiff bases in methanol and buffered with triethylamine. Complexes VOL[11] and VOL[12] are green, and VOL[14] and VOL[13] are yellow and orange-yellow respectively.

4.1.3.4 Methoxysalicylaldiimine

The Schiff bases were prepared by heating equimolar (0.08 mol) quantities of 5-methoxysalicylaldehyde in 60 mL absolute ethanol and the respective aliphatic/aromatic diamine (0.04 mol) in ethanol (10 mL) under reflux for 2 h. The ligands in this series were all yellow except $H_2Omesal_2opd$ which gave an orange

product. All the Schiff bases melted at 82-166 ^{o}C. The oxovanadium(IV) complexes of the series were formed by the reactions of the Schiff bases with $VOSO_4$ in methanol and was buffered with triethylamine. The products gave green powders for VOL^{15}, orange powders for VOL^{16} and brown powders for VOL^{17}.

4.1.3.5 Ethoxysalicylaldiimine

The Schiff bases in this series were prepared by refluxing equimolar (0.08 mol) quantities of 3-ethoxysalicylaldehyde in 60 mL absolute ethanol and the respective aliphatic/aromatic diamine (0.04 mol) in ethanol (10 mL) for 2 h. All the ligands were yellow except H_2Oetsal$_2$opd, which gave an orange product and their melting points were in the range of 70-139 ^{o}C. The oxovanadium(IV) complexes were isolated from the reaction of $VOSO_4$ with the preformed Schiff bases in methanol, buffered with triethylamine. All the complexes in this series were green and they did not melt/decompose below 250 ^{o}C, except the methylethylenediamine-bridged complex which melt at 239-240 ^{o}C.

4.2 ^{1}H NMR spectra of the Schiff bases

The ^{1}H NMR spectral data of the free ligands recorded in $CDCl_3$ against tetramethylsilane (TMS) as internal reference are presented in Table 4.2. The ^{1}H-NMR spectra of the Schiff bases displayed the O—H protons of the phenolic groups and azomethine protons (H—C=N) at 12.7-15.3 and 8.3-9.5 ppm, as singlets, respectively. The aromatic protons, which appeared as a multiplet, were observed at 6.6-8.1 ppm. The signal due to the methyl protons were observed at 1.3-3.8 ppm while the CH_2 protons were observed between 2.0 and 4.1 ppm. The C—H protons present only in methylethylenediamine-bridged ligands were observed at 3.5-3.8

ppm. The chemical shifts obtained were similar to those of Schiff bases reported in the literature [60, 61, 176, 177].

4.2.1 Unsymmetrical Schiff bases

The appearance of two different peaks for each of the azomethine protons and phenolic protons confirm the unsymmetrical nature of the Schiff bases in this series. The higher of the two signals for both the azomethine and phenolic protons is assigned to the azomethine/phenolic proton attached to the naphthaldehyde ring while the lower signals is assigned to the azomethine/phenolic proton attached to salicylaldehyde ring. Signals for the methine proton of the azomethine group were observed between 8.2 and 9.0 ppm. The peaks in the region 6.8-8.1 ppm, which appeared as a multiplet, are assigned to chemical shifts for aromatic protons. The O—H protons of the phenolic group were observed as a singlet between 12.0 and 15.5 ppm and were generally shifted downfield due to intramolecular hydrogen bonding [60]. The signal due to the methyl protons on the ethoxy substituent in H_2L^3 appeared as a triplet at 1.5 ppm while the signal at 4.1 ppm is assigned to the CH_2 proton.

4.2.2 Symmetrical Schiff bases

The ^1H NMR spectral of the symmetrical Schiff bases showed single peaks for each of the azomethine protons and phenolic protons. This is attributed to the symmetrical nature of these ligands.

4.2.2.1 Benzophenoneimine

The signal corresponding to the azomethine protons were absent in this series because the hydrogen atom is replaced by the phenyl group. ^{1}H NMR spectra gave the aromatic protons in the range of 6.6-7.5 ppm and the O—H protons of the phenolic groups in the range of 15.2-15.5. Signals for the methyl protons were observed at 1.3 ppm while the CH_2 protons were observed between 2.1 and 3.7 ppm. The CH proton of the methylethylenediamine ligand was observed at 3.5 ppm.

4.2.2.2 Naphthaldiimines

The O—H protons of the phenolic groups and the azomethine protons of this series appeared at 14.3-15.1 and 8.2-9.5 ppm respectively, as a singlet. The peaks for the aromatic protons were observed at 7.0-8.1 ppm as a multiplet. The CH_2 protons of the trimethylenediamine bridged ligand appeared as two different peaks corresponding to two different proton environments. The middle CH_2 protons appeared as a multiplet at 2.2 ppm and others appeared as a triplet at 3.8 ppm. The CH_2 protons for the ethylenediamine bridged ligand were observed at 4.0 ppm as a singlet.

4.2.2.3 Chlorosalicylaldiimines

The ^{1}H NMR spectral of this series showed the aromatic protons as a multiplet in the range 6.6-7.4 ppm and the O—H protons of the phenolic groups in the range 13.0-13.4 ppm. The azomethine protons appeared as a strong singlet in the range 8.3-8.6 ppm. The peaks for the methyl protons were observed at 1.3 ppm while the CH_2 protons were observed between 2.1 and 4.0 ppm. The CH proton of the methylethylenediamine bridged ligand was observed at 3.7 ppm.

4.1.2.4 Methoxysalicylaldiimine

In the ^{1}H NMR spectral of this series, the signals due to the azomethine protons appeared as a singlet at 8.3-8.6 ppm while the O—H protons of the phenolic groups were observed at 12.7-12.9 ppm. The signal due to the methoxy protons was observed as a singlet at 3.8 ppm. Three peaks were observed for the CH_2 protons at 2.2, 3.7 and 4.0 ppm, corresponding to a multiplet, a triplet and a singlet respectively.

4.1.2.5 Ethoxysalicylaldiimine

The ^{1}H-NMR spectra of the Schiff bases in this series exhibit a multiplet signals at 6.7–7.3 ppm which are attributed to the aromatic protons. The methyl protons of the ethoxy substituent were observed as a triplet at 1.5 ppm while its CH_2 protons appeared as a quadruplet at 4.1-4.2 ppm. The methyl protons of the methylethylenediamine bridged ligand were observed as a duplet at 1.4 ppm while its CH_2 protons were observed as a doublet at 3.9 ppm. The signals due the azomethine protons and the O—H protons of the phenolic groups were observed as a singlet at 8.3-8.6 and 13.1-13.8 ppm respectively

. For the unsymmetrical Schiff bases, the observed difference in the signal of the phenolic proton is attributed to the greater electron withdrawing effect of the naphthaldehyde ring and hydrogen bonding between the phenolic proton and the azomethine nitrogen. The deshielding effect of electron withdrawing groups and hydrogen bonding are responsible for the proton signal being moved further downfield. Similarly, the same trend is observed for the azomethine proton of the

unsymmetrical Schiff bases. The difference observed in the methyl proton signals of the methoxy and the ethoxy groups is attributed to the closeness of the protons from the deshielding effect of the electron withdrawing oxygen atom in the group while the methyl proton of the methylethylenediamine bridged is observed upfield because it is well shielded. The shift in the phenolic proton of the benzophenoneimines downfield can be accounted for by either the presence of hydrogen bonding between the phenolic proton and the azomethine nitrogen or tautomerism in the 2-hydroxy substituted imines.

4.3 Infrared spectra

The important infrared spectral bands of the ligands and the metal(II) complexes are presented in Table 4.3.1−4.3.2 and Fig. 4.3.1-4.3.6. The tentative assignments of the observed bands for the compounds were made by comparing the spectra with those reported in the literature on similar systems [40, 41, 59]. The absorption bands due to the amino group disappeared in the IR spectra of all the ligands, which showed that the amino groups in the diamine condensed with the aldehyde/ketone. The band appearing at 1567-1640 cm^{-1} due to azomethine group in the ligands is shifted to lower frequency at 1573-1634 cm^{-1} in the metal(II) complexes, indicating the participation of the azomethine nitrogen in interaction with the metal ion. Similarly, the ν(C—O) band of the ligands, which occurs at 1257-1334 cm^{-1}, shifted to 1277-1366 cm^{-1} in the complexes indicated deprotonation and coordination of the phenolic oxygen to the metal atom. Thus, it can be concluded that the Schiff bases acted as tetradentate ligands coordination via the azomethine *N* and the phenolic *O*. Further conclusive evidence of the coordination of the Schiff-bases with the metal ions was shown by the appearance new bands at 435-583 and

410-581 cm^{-l} assigned to the metal nitrogen (M—N) and metal-oxygen (M—O) vibrations, respectively. These bands were absent in the spectra of the uncomplexed Schiff bases, thus confirming participation of the O and N atoms in the coordination. It has been established that the metal-ligand vibrational modes are very sensitive to substituent effects [178, 179]. This was proposed on the basis of isotopic labelling studies (^{15}N- and ^{18}O-labelling). The substituent effects were based on the position of substitution rather than on the nature of the substituents. The ν(M—O) bands are observed to exhibit higher vibrational frequencies than the ν(M—N) bands for the meta-substituents while the order is reversed for the para-substituents regardless of the nature of the substituents. It was suggested that the transmission of the substituent effects in the Schiff base complexes are propagated largerly by a mesomeric mechanism. The important bands along with their assignments are listed in Table 4.3.1.-4.3.2 and representative spectra are shown in Fig. 4.3.1-4.3.6.

Oxovanadium(IV) complexes of Schiff bases can give rise either to monomeric structures with square pyramidal/trigonal bipyramidal/octahedral coordination geometry or to polymeric structures, involving ····O=V····V=O···· linkages, with a distorted octahedral geometry [40]. However, on the basis of the location of the ν(V=O) band it is possible to distinguish between monomeric and polymeric complexes. In the present work, most of the oxovanadium(IV) complexes exhibit a strong band in the region 959-988 cm^{-1}, which have been assigned to ν(V=O) with a monomeric square pyramidal coordination geometry. All the orange-yellow coloured complexes, with the trimethylene bridge in which the ν(V=O) appeared at 848-860 cm^{-1}, have been assigned polymeric species with ····O=V····V=O···· interactions, which afforded a distorted octahedral coordination geometry.

4.3.1 Unsymmetrical Schiff bases and their complexes

The infrared spectra of both the ligands and complexes have no bands between 3100 and 4000 cm^{-1}, indicating the absence of the uncondensed N—H and uncoordinated —OH groups. Due to the unsymmetrical nature of the ligangs and the complexes, two bands were observed for each of the following bonds: ν(C=N), ν(C—O), ν(V—N) and ν(V—O), taking their origin from the different aldehydes.

4.3.1.1 Unsymmetrical Schiff base complexes of cobalt(II)

The position of ν(C=N) bands of the ligands appeared at 1610−1621 and 1567−1583 cm^{-1}. These are shifted to lower frequencies at 1603−1606 and 1571−1578 cm^{-1} respectively upon complexation indicating the involvement of the nitrogen atom of the azomethine group in coordination [176]. On the other hand, the (C—O) stretching frequencies, which occur at 1313−1333 and 1276−1289 cm^{-1} for the ligands was moved to higher frequencies by 12−30 cm^{-1} after complexation, which indicates that the shifts are due to coordination of the phenolic oxygen of the ligand to the metal ion [175]. The new bands observed in the complexes in the region 453−580 and 508−554 cm^{-1} were assigned to ν(Co—N) while 463−575 and 423−428 cm^{-1} are attributed to ν(Co—O) [176, 179].

4.3.1.2 Unsymmetrical Schiff base complexes of nickel(II)

The spectra of the ligands show two different C=N stretching frequency at 1610−1621 and 1567−1583 cm^{-1}, which are shifted to lower frequencies in the spectra of all the nickel complexes at 1603−1609 and 1577−1582 cm^{-1} respectively indicating the involvement of azomethine nitrogen in coordination to the metal ion

[176]. The corresponding phenolic C—O stretching frequency occurs at 1313−1333 and 1276−1289 cm^{-1} for the ligands and at 1331−1366 cm^{-1} and 1287−1311 cm^{-1} for the complexes. The shift to a higher frequency of this band confirms the participation of the phenolic oxygen in bonding [177]. Assignment of the proposed coordination sites is further supported by the appearance of new bands at 457−583 and 507−554 cm^{-1} which are assigned to ν(Ni—N) while 463−577 and 431 cm^{-1} are attributed to ν(Ni—O) [176, 179].

4.3.1.3 Unsymmetrical Schiff base complexes of copper(II)

The ligands exhibited the characteristic C=N stretching frequency at 1610−1621 and 1567−1583 cm^{-1}. The shifting of ν(C=N) band to lower values by 10−12 cm^{-1} indicates the participation of the two azomethine nitrogen atoms in bonding [176]. The corresponding phenolic C—O stretching frequency occurs at 1313−1333 and 1276−1289 cm^{-1} for the ligands and at 1325−1363 cm^{-1} and 1290−1317 cm^{-1} for the complexes. The shift in C—O stretching frequency confirms the participation of the phenolic O in C—O—M bond formation [175]. The bands due to ν(Cu—N) observed only in the complexes occurred at 460−574 and 501−548 cm^{-1} while 460−574 cm^{-1} and 416−463 are attributable to ν(Cu—O) bond [176, 179]. These bonds were observed in the spectra of the metal complexes and not in the spectra of the Schiff bases.

4.3.1.4 Unsymmetrical Schiff base complexes of oxovanadium(IV)

The ligands exhibited the characteristic C=N stretching frequency at 1610-1621 and 1567-1583 cm^{-1}. These are shifted to lower frequencies at 1604-1607 and 1573-1576 cm^{-1} respectively upon complexation indicating the involvement of the

nitrogen atom of the azomethine group in coordination [176]. The corresponding phenolic C—O stretching frequency occurs at 1313-1333 and 1276-1289 cm^{-1} for the ligands and at 1361-1366 cm^{-1} and 1312-13424 cm^{-1} for the complexes. The shift in C—O stretching frequency confirms the participation of the phenolic O in C—O—M bond formation [175].

A significant change observed in the infrared spectra of the complexes is the appearance of strong absorption band due to νV=O, which is absent in the ligands. The frequency spread observed for a large number of oxovanadium(IV) complexes was put at 985±50 cm^{-1} [165]. All the complexes exhibited a strong V=O stretching band at 970-988 cm^{-1}, which confirms that the complexes are monomeric [158]. The bands observed in the complexes in the region 483-558 and 536-541 cm^{-1} were assigned to ν(V—N) while 488-581 and 455-458 cm^{-1} are attributed to ν(V—O) [176].

Provisionally, the lower frequency bands of the azomethine group may be assigned to the $\nu C{=}N_{naph}$ and the higher frequency bands to the $\nu C{=}N_{sal}$ of the unsymmetrical Schiff bases.

4.3.2 Symmetrical Schiff bases and their complexes

4.3.2.1 Benzophenoneimine

All the Schiff bases reported gave a sharp and strong band due to ν(C=N) of the azomethine group at 1604-1607 cm^{-1} while the corresponding bands in the complexes were observed in the 1599-1601 cm^{-1} range. The observed shift to a lower frequency of the ν(C=N) in the complexes indicates a decrease in the bond order of C=N due to the coordination of the azomethine nitrogen to the metal ion [29]. Similarly, the ν(C—O) band of the ligands, which occurs at 1331-1334 cm^{-1},

shifted to 1336-1337 cm^{-1} in the complexes which suggests the coordination of the phenolic oxygen with the metal ion.

All the oxovanadium(IV) complexes in this series exhibit a strong band in the range 959-986 cm^{-1}, which has been assigned to ν(V=O) in a monomeric square pyramidal coordination geometry. The complex [VO(bp_2-tn)MeOH], behaves differently as the ν(V=O) occurs at 959 cm^{-1} confirming that the MeOH behaves as an adduct and excludes polymerization. The bands due to ν(V—N) and ν(V—O), observed only in the complexes, occurred at 495-528 and 406-489 cm^{-1} respectively [41].

4.3.2.2 Naphthaldiimines

IR spectra of these Schiff bases were also compared with the spectra of the metal complexes. The bands at 1615–1634 cm^{-1} due to the azomethine group of the Schiff base underwent a shift to lower frequency (1600–1618 cm^{-1}) after complexation, indicating the coordination of azomethine nitrogen to metal atom. The ν(C—O) band of the ligands, which occurs at 1257-1287 cm^{-1}, shifted to 1281-1343 cm^{-1} in the complexes confirming coordination of the phenolic oxygen with the metal ion. VOL^8 and VOL^{10} exhibit a strong band in the range 979-988 cm^{-1}, which have been assigned to ν(V=O) in a monomeric square pyramidal coordination geometry. The orange coloured complex, with a trimethylene bridge in which the ν(V=O) appeared at 852 cm^{-1}, has been assigned a polymeric structure with ····O=V····V=O···· interactions, which afforded a distorted octahedral coordination geometry [40].

New bands, absent in the spectra of Schiff bases, appeared at 549-577 and 466-506 cm^{-1} and are attributed to ν(V—-N) and ν(V—O) vibrations, respectively.

The appearance of ν(V—N) and ν(V—O) vibrations supports the involvement of nitrogen and oxygen atoms in complexation [41, 176].

4.3.2.3 Chlorosalicylaldiimines

The band at 1615-1636 cm^{-1} in the ligands, which shifts to 1612-1630 cm^{-1} in the complexes, is assigned to ν(C=N) frequency. The ν(C=N) frequency is displaced to lower frequency, indicating a decrease in the C=N bond order due to the coordinate bond of the metal with the lone pair of the azomethine nitrogen. The ν(C—O) band of the ligands, which occurs at 1277-1280 cm^{-1}, was slightly displaced to higher frequencies (1297-1322 cm^{-1}) on coordinated to the metal complexes. The characteristic ν(V=O) stretching frequency in the oxovanadium(IV) complex appears as a strong band at 960-988 cm^{-1}, within the range 960±50 cm^{-1} reported for square pyramidal oxovanadium(IV) complexes [165]. The ν(V=O) stretching frequency of the trimethylene derivative occurs at 860 cm^{-1}, which is consistent with polymeric system involving ····O=V····V=O···· bridge.

Assignment of the proposed coordination sites is further supported by the appearance of new bands at 516-554 and 435-498 cm^{-1} which are attributed to ν(V—O) and ν(V—N) respectively [41]. These bands are observed as new absorption peaks of the complex that are not present in the spectra of the free ligand.

4.3.2.4 Methoxysalicylaldiimines

The ligands exhibited the characteristic C=N stretching frequency at 1622-1640 cm^{-1} and are shifted to lower frequencies (1599-1634 cm^{-1}) upon complexation indicating the involvement of the nitrogen atom of the azomethine group in

coordination [59]. The phenolic C—O stretching frequency occurs in the 1272-1285 cm^{-1} for the ligands and in the 1277-1307 cm^{-1} region for the complexes. The C—O stretching frequency is generally shifted to a higher frequency, indicating the participation of phenolic oxygen in C—O—M bond formation [175].

A significant change observed in the infrared spectra of the complexes compared to their respective ligands is the appearance of strong absorption band due to V=O stretching frequency in the complexes. All the complexes exhibited a strong V=O stretching band at 979-981 cm^{-1}, which suggests monomeric square pyramidal structures. The ν(V=O) stretching frequency of the trimethylene derivative occurs at 848 cm^{-1}, which is also consistent with polymeric system involving ····O=V····V=O···· bridge. Other bands observed in the complexes in the regions 544-573 and 476-497 cm^{-1} are due to ν(V—O) and ν(V—N) respectively [41]. These bands were absent in the spectra of the ligands.

4.3.2.5 Ethoxysalicylaldiimines

The spectra of the Schiff bases show ν(C=N) bands in the region 1614-1637 cm^{-1}, which is shifted to lower frequencies in the spectra of all the complexes (1602-1631 cm^{-1}) indicating the involvement of nitrogen in coordination to the metal ion. The ν(C—O) band of the ligands, which occurs at 1272-1283 cm^{-1}, was slightly displaced to higher frequencies (1304-1315 cm^{-1}) on coordinated to the metal complexes. The characteristic ν(V=O) stretching frequency in the oxovanadium(IV) complex appears as a strong band at 960-988 cm^{-1}, which is consistent with monomeric square pyramidal structures. The nature of metal–ligand bonding is confirmed by the newly formed band at 541-614 and 448-483 cm^{-1} in the spectra of

the complexes which are tentatively assigned to ν(V—O) and ν(V—N) respectively [41].

4.4 Electronic spectra of the metal(II) complexes

The electronic absorption spectra are often very helpful in the evaluation of results furnished by other methods of structural investigation. The electronic spectral measurements were used for assigning the stereochemistries of metal complexes based on the positions and number of *d–d* transition peaks. The electronic absorption spectra of metal(II) complexes were recorded in 10^{-3} M and 10^{-5} M solutions of each complex in DMSO and chloroform in the range 200−1100 nm at room temperature. The electronic absorption spectra of cobalt(II), nickel(II) and copper(II) in 10^{-3} M solutions did not form homogeneous solutions and the spectra were noisy in both the visible and the UV regions. The results of the solution spectra are presented in Figure 4.4.1−4.4.4 and Table 4.4.1−4.4.2.

For four-coordinate cobalt(II), nickel(II) and copper(II) complexes, either a square planar or a tetrahedral configuration is possible. On the basis of electronic spectra, together with the magnetic moments, it is possible to differentiate between these two configurations.

The optical spectra of square pyramidal oxovanadium(IV) complexes are characterized by three d-d transitions. These transitions have been assigned using the energy level scheme proposed by Ballhausen and Gray for C_{4v} symmetry [87]. In this scheme band I is assigned as $b_2 \rightarrow e_\pi^*$ (11 000–16 000), band II as $b_2 \rightarrow b_1^*$ (14 500–19 000) and band III as $b_2 \rightarrow a_1^*$ (21 000–30 000). As mentioned earlier, Selbin[165] has questioned the general applicability of the Ballhausen and Gray scheme and has suggested that the ground level is the singly occupied, nonbonding

b_2 orbital but that the e_π^* and b_1^* levels may be very close in energy such that they may cross one another from complex to complex. Kolawole, *et al*. [40, 41] did provide experimental evidence for the inversion of e_π^* and b_1^* in a series of symmetric Schiff base complexes of oxovanadium(IV) as the methylene bridge increases from 2 to 10 and proposed an energy level which incorporates Ballhaussen and Gray, and Selbin's schemes.

An overlap between band III and charge transfer has always been a problem in being able to make a definitive assignment of band III. It tends to 'borrow' intensity from a nearby charge transfer transition, which in many instances reduces it to a shoulder. It has been possible to assign the three bands in most of the complexes reported in this work, except that band III, expectedly, appears as a shoulder in some of the complexes. In the complexes where the intensity of band I is lower than the intensity of band II inversion in the energies levels of b_1^* and e_π^* has been invoked. Only bands II and III could be observed in the solutions spectra of the unsymmetrical Schiff base complexes.

Complexes of oxovanadium(IV) with coordination numbers 5 and 6 are usually square pyramidal/trigonal bipyramidal and distorted octahedral, respectively. Due to a strong axial field, the energy levels associated with these structures do not differ considerably and the same scheme has been used for the interpretation of the spectra of oxovanadium(IV) complexes. In five-coordinate complex band I is simply shifted towards lower wavelengths and only the complexes with C_{2v} symmetry display four absorption bands between 400 and 860 nm. A reduction in the molar absorptivity of band II in spectra run in a coordinating solvent or its disappearance could be indicative of some sixth-coordination in such solvent.

4.4.1 Unsymmetrical Schiff base metal(II) complexes

4.4.1.1 Unsymmetrical Schiff base complexes of cobalt(II)

The electronic spectra of all the cobalt(II) complexes in $CHCl_3$ are very similar to each other and consist of three bands, one each at 18 587−18 939, 22 272−22 779 and 24 876–25 575 cm^{-1} regions, which clearly indicate the low-spin square planar/distorted square planar geometry of the complexes [180]. This is also corroborated by the observed effective magnetic moment of the complexes. The other intense bands between 28 902 and 41 494 cm^{-1} are due to charge transfer transitions. The electronic spectra of all the complexes in DMSO displayed a single *d-d* transition at 25 063−25 445 cm^{-1} and a charge transfer transition at 29 412−36 101 cm^{-1}. The appearance of a single *d*−*d* transition in DMSO is attributed to the effect of the coordination of solvent which alters the stereochemistry to form low spin six-coordinate distorted octahedral [181]. The slight differences in the peaks observed in the spectra of these complexes in both solvents are due to substituent effects of the different substituents on the salicylaldehyde ring

4.4.1.2 Unsymmetrical Schiff base complexes of nickel(II)

The solution spectra of all the nickel(II) complexes in both solvents are very similar to each other and consist of four bands. The electronic spectra of the complexes in $CHCl_3$ show two bands at 20 619−20 747 and 25 773−26 178 cm^{-1} assignable to $^1A_{1g}\rightarrow{}^1B_{1g}$ and $^1A_{1g}\rightarrow{}^1E_g$ transitions in a square-planar geometry [177]. The assignment of square-planar geometry is supported by the zero BM effective magnetic moment the complexes. The stereochemistry of these complexes was unchanged when moving from a non-coordinating solvent to a coordinating solvent (DMSO) except for the complex [NiL^2], whose ligand contains the nitro group, which

shows a slightly deviation from the other. The observed bands in this complex were still in conformity with a squre-planar geometry. The solution spectra of the complexes in DMSO also show two bands at 20 619−20 877 and 25 974−26 178 cm^{-1}. At higher energy, two more strong absorptions are observed in the range 30 303−38 760 ($CHCl_3$) and 30 395−39 063 cm^{-1} (DMSO) which are likely due to charge transfer or intra-ligand transitions.

4.4.1.3 Unsymmetrical Schiff base complexes of copper(II)

The electronic spectra of all the copper(II) complexes in both $CHCl_3$ and DMSO show a broad unsymmetrical band centred at 22 831−24 038 cm^{-1} and 23 095−24 038 cm^{-1} respectively. This broad band is assigned to $^2B_{1g}\rightarrow{}^2A_{1g}$ transition of four-coordinate square-planar geometry [60, 177]. This *d-d* transition is in the region of that observed for structurally well-characterized complexes of coper(II) N-alkylsalicyladiminates with square-planar geometry [60]. The other intense bands between 27 778 and 40 816 cm^{-1} in $CHCl_3$ and 28 490−37 313 cm^{-1} in DMSO are due to charge transfer or intra-ligand transitions

4.4.1.4 Unsymmetrical Schiff base complexes of oxovanadium(IV)

Three structural types can be identified from the solution spectra of this series. VOL^1 and VOL^4 have similar spectra in both solvents. VOL^2 and VOL^3 are distinctively different in chloroform and DMSO. The electronic spectra in both solvents for 10^{-3} M solution displayed a broad d-d transition similar to the one observed by Kolawole, *et al.* [182] for symmetric napthaldiimine complexes. The authors also proposed the possibility of pseudoaromatization of the rings around V when the azomethine N atoms are bridged with aromatic groups. In such instances

the d^1 electron of the V could be delocalised into the ring system. Similar scenario is suspected in these complexes because the salicylidiimine group is also bridged with a phenyl ring in each case. Such a conjugation would cause ligand based electronic transition to shift to red overlapping with the d-d transition resulting in complex spectra, like the one recorded here in solution.

At 10^{-3} and 10^{-5} M solutions only bands II and III could be observed in these complexes. The high extinction co-efficient observed for band III corroborate the borrowing of intensities from the ligand (as a result of the hyperconjugation) by the vanadium. The d-d bands are assigned as follows: $b_2 \rightarrow b_1^*$: 16 207–16 393 ($CHCl_3$), 15 748–16 129 (DMSO) and $b_2 \rightarrow a_1^*$: 21 598–24 096 ($CHCl_3$), 23 474–24 096 (DMSO). The bands in the region 27 701–41 322 ($CHCl_3$) and 27 473–38 610 (DMSO) are assigned to either a metal-ligand charge transfer band or to an electronic transition within the ligand. The observed shift in band II of this series with a lowering of intensity in the molar absorptivity from $CHCl_3$ to DMSO is indicative of solvent interaction in DMSO while they remain five-coordinate in $CHCl_3$. The above observation may indicate a facile formation of six-coordinate species in DMSO.

4.4.2 Symmetrical Schiff base complexes of oxovanadium(IV)

4.4.2.1 Benzophenoneimino complexes

The spectra of the chloroform solutions of VOL^5 and VOL^6 show two d-d transition in the visible region, the first at 16 026–17 182 cm^{-1} and the other at 20 747–21 277 cm^{-1} (often as a shoulder). The spectrum in DMSO of VOL^5 is characterized by two bands at 13 870–17 575 cm^{-1} and a shoulder at 21 277 cm^{-1} while the spectrum of VOL^6 gave only one band at 17 123 cm^{-1} and a shoulder at 21 276 cm^{-1}. The spectra of the solutions in DMSO of these two complexes were

notably different. The two bands observed in chloroform solutions were shifted to 17 123-19 231 cm^{-1} and 21 097-21 277 cm^{-1} respectively, in DMSO.

Complex VOL^3 displayed the three spectral peaks predicted for VO^{2+} complexes and appears to assume octahedral geometry in DMSO. Most trimethylene-bridged Schiff base complexes reported were, like this compound, orange, but more planar, polymeric, (with ····V=O····V=O···· linkages) and distorted octahedral [182]. The only evidence that supports the planarity of this compound is that it is yellow and it was formed with associated methanol molecule, which reduces the νV=O to 959 cm^{-1} as evidence of the solvent perturbation of the V=O bond (unsolvated νV=O for the other complexes occur at about 990 cm^{-1}).

The change of solvent from chloroform to DMSO resulted in some shifts in band positions and resulted in enhanced intensity in some of the d-d and CT transitions. The bands are assigned as follows: $b_2 \rightarrow b_1^*$: 12 555–13 263 ($CHCl_3$), 12 555–12 970 (DMSO); $b_2 \rightarrow e_\pi^*$: 17 182–17 544 ($CHCl_3$), 17 123–19 231 (DMSO) and $b_2 \rightarrow a_1^*$: 20 747-21 186 ($CHCl_3$), 21 097–21 277 (DMSO). The bands in the region 27 027–41 322 cm^{-1} are assigned to charge-transfer or intra-ligand transitions. The above spectral characteristics indicate that VOL^5 and VOL^6 exhibit five-coordinate geometry in non-coordinating solvent, $CHCl_3$, whereas they exhibit six coordination number in coordinating solvent, DMSO, in which the sixth coordination site is occupied by the solvent molecule. VOL^7 displayed six-coordinate geometry in both non-coordinating and coordinating solvents.

4.4.2.2 Naphthaldiimino complexes

Two characteristic bands out of the three predicted for oxovanadium(IV) complexes in the visible region were displayed in the solution spectra of this series

except complex VOL[9] which exhibits only band III in $CHCl_3$. A considerable reduction in molar absorptivities was observed on going from $CHCl_3$ to DMSO in the solution spectra of VOL[8] and VOL[10]. These complexes are five-coordinate square pyramidal in $CHCl_3$ and the reduction in molar absorptivity in DMSO indicates a facile formation of six-coordinate species in this solvent.

Distinct spectral change was observed in the solution spectrum of VOL[9] when this complex was treated with DMSO. Band III disappears and two new bands appear at 12 887 and 19 455 cm^{-1} which are assigned as band I and band II respectively. Band II transition has a greater intensity than band I in this complex, indicative of inversion of the e_π^* and b_1^* energy-levels [40]. This complex appears to be six-coordinate in DMSO and like most derivatives of trimethylene-brigded complexes, it is polymeric (with ····V=O····V=O···· linkages) and distorted octahedral geometry in the solid state. The bands are assigned as follows: $b_2 \rightarrow b_1^*$: 12 887 (DMSO); $b_2 \rightarrow e_\pi^*$: 15 942–16 155 ($CHCl_3$), 15 528–19 455 (DMSO) and $b_2 \rightarrow a_1^*$: 21 749–25 840 ($CHCl_3$), 21 786–23 641 (DMSO). In the UV region, some charge-transfer or intra-ligand bands are observed between 26 178 and 40 650 cm^{-1}.

4.4.2.3 Chlorosalicylaldiimino complexes

Complex VOL[12] displayed the three spectral peaks predicted for VO^{2+} complexes in DMSO and two bands in $CHCl_3$. The shift and reduction in molar absorptivities in the band II of complex VOL[12] observed on going from $CHCl_3$ to DMSO is indicative of different stereochemistry in both solvents. It appears to exhibit five-coordinate geometry in $CHCl_3$ whereas, it exhibits six coordination in DMSO in which the sixth coordination site is occupied by the solvent molecule. Band I and III were absent in the solution spectra of VOL[11] and the band II observed was shifted to

higher energy with a reduction in the molar absorptivities. The similarity in the band II in the spectra of VOL^{12} and VOL^{11} might be as a result of both possessing similar structures in these solvents.

Complex VOL^{13} was not soluble in both solvents and complex VOL^{14} was only sparingly soluble in both solvents. The spectrum VOL^{14} was noisy in the visible region run on 10^{-3} M solution and some of the bands in the region could not be extracted. Only band III was observed in the spectrum of VOL^{14}. The bands are assigned as follows: $b_2 \rightarrow b_1^*$: 13 263 ($CHCl_3$), 12 970 (DMSO); $b_2 \rightarrow e_\pi^*$: 16 778–16 892 ($CHCl_3$), 17 544–17 699 (DMSO) and $b_2 \rightarrow a_1^*$: 21 186 (DMSO). In the UV region, some charge-transfer or intra-ligand bands are observed at 26 178–41 152 cm^{-1}.

4.4.2.4 Methoxysalicylaldiimino complexes

The spectra solutions of VOL^{15} in both solvents show only two d-d transitions out of the three predicted for oxovanadium(IV) complexes. Band I transition was absent in the solution spectra of VOL^{15} in both solvents and band II experiences a shift of ~197 cm^{-1} with a lowering of intensity in the molar absorptivity from $CHCl_3$ to DMSO which is indicative of six-coordination geometry in DMSO solution but five coordinate geometry in $CHCl_3$. Complex VOL^{16} formed with associated methanol molecule, which reduces the $\nu V{=}O$ to 848 cm^{-1} appears to be polymeric with ····V=O····V=O···· linkages and a distorted octahedral coordination geometry in the solid state. This complex displayed all three bands predicted for VO^{2+} complexes in the visible region in both solvents. This is due to dissociation of the complex in solution to form five-coordinate species. A facile interaction of DMSO with vanadium is indicated by the reduction in the molar absorptivity of band II in this solvent. The above spectral characteristics indicate that VOL^{16} is six-coordinate in solid and in

DMSO. It may be concluded that this complex also exhibit six-coordinate geometry in $CHCl_3$ due to the observation of band I transition and it appeared that the ····V=O····V=O···· linkages was not broken in this solvent.

Complex VOL[17]exhibits only band III at 22 422 cm^{-1} in $CHCl_3$ and two bands at 15 649-22 624 cm^{-1} in DMSO. It is difficult, on the strength of this result, to deduce the absolute stereochemistry of this complex but it appeared to exhibit six-coordinate geometry in DMSO and five-coordinate in $CHCl_3$. The bands are assigned as follows: $b_2 \rightarrow b_1^*$: 14 728 ($CHCl_3$), 13 850–15 649 (DMSO); $b_2 \rightarrow e_\pi^*$: 16 694–19 685 ($CHCl_3$), 16 891–18 762 (DMSO) and $b_2 \rightarrow a_1^*$: 22 422–24 876 ($CHCl_3$), 22 624–25 445 (DMSO). The bands in the region 31 348–39 370 cm^{-1} are attributed to charge-transfer or intra-ligand transitions.

4.4.2.5 Ethoxysalicylaldiimino complexes

The solutions spectra of this series are similar to those of methoxysalicylaldiimino complexes discussed above. Two d-d transitions were observed in the solution spectra of this series in the visible region except VOL[19] which is characterized by a single band in DMSO. Transition corresponding to band I was absent in the solution spectra in both solvents. A shift in band II with a slight lowering in the molar absorptivities of complexes VOL[18] and VOL[19] is indicative of six-coordinate geometry in DMSO but five-coordinate geometry in $CHCl_3$. A slight shift was observed in the spectrum of VOL[20] moving from $CHCl_3$ to DMSO. This indicates different stereochemistry in both solvents. The bands are assigned as follows: $b_2 \rightarrow e_\pi^*$: 16 051–16 694 ($CHCl_3$), 16 155 –17 065 (DMSO) and $b_2 \rightarrow a_1^*$: 22 831–25 510 ($CHCl_3$), 23 641 (DMSO). Some charge-transfer or intra-ligand bands were observed at 26 110–40 984 cm^{-1}.

4.5 Magnetic moment of the metal(II) complexes

4.5.1 Unsymmetrical Schiff base complexes of cobalt(II)

The observed values of magnetic moment for cobalt(II) complexes are generally diagnostic of the coordination geometry about the metal ion. The room temperature magnetic moments of low-spin square-planar cobalt(II) complexes are between 1.9−2.9 BM, arising from one unpaired electron plus an apparently large orbital contribution. Both tetrahedral and high-spin octahedral cobalt(II) complexes possess three unpaired electrons but may be distinguished by the magnitude of the deviation of effective magnetic moment from the spin-only value. The octahedral and tetrahedral cobalt(II) complexes are reported to have magnetic moments between 4.9−5.2 and 4.2−4.8 BM. respectively [39]. The effective magnetic moments of all the cobalt(II) complexes reported here lie in the range of 2.23–2.61 BM. (Table 4.5.1), corresponding to one unpaired electron for square-planar stereochemistry around d^7 cobalt(II) ion [180].

4.5.2 Unsymmetrical Schiff base complexes of nickel(II)

Nickel(II) has the electronic configuration $3d^8$ and should exhibit a magnetic moment higher than expected for two unpaired electrons in octahedral (2.8–3.2 BM) and tetrahedral (3.4–4.2 B.M.) complexes. Deviations from spin-only moment of 2.83 BM. due to two unpaired electrons are attributed to orbital contribution. Nickel(II) square-planar complexes are generally diamagnetic [177]. The observed zero magnetic moments confirm the square-planar environment for the nickel(II) complexes in conformity with the fact that all known square-planar complexes of nickel(II) are diamagnetic (Table 4.5.1).

4.5.3 Unsymmetrical Schiff base complexes of copper(II)

The room temperature magnetic moments of copper(II) complexes are expected to be higher than the spin-only value of 1.73 BM. as a result of orbital contribution and spin-orbit coupling, which mixes in the higher T terms into the ground term. Consequently a magnetic moment of 1.7–2.2 BM. is usually observed for mononuclear copper(II) complexes, regardless of stereochemistry. The magnetic moments of 1.56–2.20 BM. observed for the copper(II) complexes is assigned to four-coordinate, square-planar geometry [60] (Table 4.5.1). The low magnetic moment of CuL^2 can be attributed to the possible dimeric structure in which two Cu-Cu atoms interact [183].

4.5.4 Symmetrical and unsymmetrical Schiff base complexes of oxovanadium(IV)

The oxovanadium(IV) ion belongs to the S=½ system. The magnetically dilute oxovanadium(IV) complexes usually exhibit magnetic moments corresponding to their spin-only value of 1.73 B.M. The observed magnetic moments of the complexes under study are found in the range 1.60-1.84 BM. and they are presented in Table 4.5.2.

4.6 EPR spectra of oxovanadium(IV) complexes

EPR spectroscopy is a useful technique as it provides information on the stereochemistry, ligand type and degree of covalency of oxovanadium(IV) complexes. The unpaired electron responsible for EPR spectrum is confined largely to the oxovanadium(IV) centre. When this unpaired electron interacts with the nuclear spin of ^{51}V ($I = {}^{7}/_{2}$), the result is (2I+1) or 8 lines separated by coupling constants with different intensities. The EPR spectra of the oxovanadium(IV)

complexes were measured using a Bruker EMX Micro Premium X Spectrometer at X-band of 9.4 GHz on the powder and on the fluid and frozen solutions in toluene/dichloromethane (90:10 v/v). The Spin Hamiltonian parameters were obtained from the simulation of the spectra using a commercial Bruker X Sophe program and all the data are reported in Table 4.6.1-4.6.2 The EPR experimental and simulated spectra are depicted in Figure 4.6.1-4.6.2.

Symmetry also has an effect on EPR spectra. The point symmetry at the metal determines whether or not any of the principal values of g or of A are required to be equal to each other and it also determines whether or not any of the principal axes of g and A are required to be coincident. If the spectra are obtained from frozen solutions or as a powder, where the anisotropy is not averaged away by motion of the molecule, a complex pattern can emerge. For example, the electronic configuration around a metal ion may have a unique axis of symmetry. In the commonly employed first derivative display, two superimposed spectra with different hyperfine splittings will be obtained from frozen solutions (‘axial symmetry’). If all three axes in the molecular frame of reference are electronically distinct, three different splittings may be obtained (‘rhombic symmetry’). Due to the strong vanadium–oxygen interaction in the oxovanadium unit, axial or nearly axial EPR spectra are usually observed for oxovanadium(IV) complexes. The parallel transitions, (representing the orientation of the V=O bond parallel to the applied magnetic field), exhibit hyperfine coupling constants that are larger than those for the perpendicular orientation.

4.6.1 Unsymmetrical Schiff base complexes of oxovanadium(IV)

The EPR spectra of the compounds under consideration were obtained as solid and in toluene-dichloromethane (9:1, v/v) solutions, at room temperature and at 120 K. The powder spectra of the complexes at room temperature and 120 K show a broad single line around g = 2. The g values are all very close to the spin-only value (free electron value) of 2.0023, suggesting minima spin-orbital coupling. The fluid solution spectra of the complexes at room temperature exhibit eight equally spaced lines due to the hyperfine interaction of the unpaired electron with the vanadium nucleus (^{51}V, I = $^{7}/_{2}$). The frozen solution spectra of the complexes at 120 K display axial vanadium(IV) spectra ($g_z = g_{\parallel} < g_{\perp} = g_x = g_y$ and $A_z = A_{\parallel} > A_{\perp} = A_x = A_y$). The g values, g_o = 1.971, $g_{\parallel}$ = 1.978 and $g_{\perp}$ = 1.950, are essentially the same for all the complexes examined. The vanadium nuclear hyperfine splitting, A_o = 101-99, $A_{\parallel}$ = 65-64, $A_{\perp}$ = 179-177, vary slightly with substituents on the salicylaldehyde. The EPR data for these complexes are in agreements with previously published data for similar complexes with tetradentate bis(Schiff base) ligands [184]. The A_o values are satisfactorily matched with A_{av} = 99.7-100.7 in all cases, indicating that the configuration of the complexes in solution at room temperature is the same as in frozen state at 120 K. The orders $g_{\parallel} < g_{\perp}$ and $A_{\parallel} > A_{\perp}$ are consistent with the oxovanadium(IV) square pyramidal complexes with a C_{4v} symmetry and with the unpaired electron reciding in the d_{xy} orbital [159].

4.6.2 Symmetrical Schiff base complexes of oxovanadium(IV)

Five out of the eleven symmetrical oxovanadium(IV) complexes analysed exhibit axial EPR symmetry ($g_z = g_{\parallel} < g_{\perp} = g_x = g_y$ and $A_z = A_{\parallel} > A_{\perp} = A_x = A_y$) while four of the complexes exhibit rhombic EPR symmetry ($g_x \neq g_y \neq g_z$ and $A_x \neq A_y \neq A_z$).

Complex VOL^{13} was not measured as fluid solution because it did not dissolve in the mixed solvent used. Two of the complexes, VOL^{17} and VOL^{19}, did not show any hyperfine interaction and they were not simulated. The powder spectra of the complexes at room temperature and 120 K show a broad single line around g = 2. The fluid solution spectra of the complexes at room temperature exhibit eight equally spaced lines due to the hyperfine interaction of the unpaired electron with the vanadium nucleus (^{51}V, $I = {}^{7}/_{2}$). The frozen solution spectra of the complexes VOL^{5}-VOL^{7}, VOL^{9} and VOL^{12} at 120 K display axial vanadium(IV) spectra with hyperfine structure where $g_{\perp} \sim 1.98$ with $A_{\perp} \sim 60$ G and $g_{\parallel} \sim 1.95$ with $A_{\parallel} \sim 179$ G ($g_z = g_{\parallel} < g_{\perp} = g_x = g_y$ and $A_z = A_{\parallel} > A_{\perp} = A_x = A_y$). The Spin Hamiltonian parameters are reported in Table 4.5.1. The EPR experimental and simulated spectra are reported in Figure 4.5. The $g_{\parallel} < g_{\perp}$ and $A_{\parallel} > A_{\perp}$ relations are consistent with square pyramidal complexes with C_{4V} symmetry with the unpaired electron in the d_{xy} orbital [159].

The frozen solution spectra of the complexes VOL^{10}, VOL^{14} and VOL^{19} at 120 K display rhombic vanadium(IV) spectra with three g ($g_z < g_x < g_y$) and three A values ($A_z > A_x > A_y$) characteristic for C_{2V} symmetry [185]. Usually, this is due to a distortion of the square-pyramidal geometry towards a trigonal-bipyramidal, with the two longer bonds in the axial direction and the three shorter ones in the equatorial plane. Simulation gave the following parameters: $g_x = 1.976$, $g_y = 1.978$-1.980, $g_z = 1.948$-1.950 and $A_x = 63.0$-64.0, $A_y = 58.0$-60.0, $A_z = 178.0$-179.0. The Hamiltonian parameters obtained for the oxovanadium(IV) complexes with rhombic symmetry are presented in Table 4.5.2.

4.7 Cyclic voltammetry

The cyclic voltammetric data for all the complexes are presented in Fig. 4.7 and Table 4.7. At a scan rate of 100 mV/s on a 10^{-3} M solution of each complex in DMSO containing 0.1 M tetrabutylammonium perchlorate as supporting electrolyte, all the complexes display one well defined oxidation-reduction wave at positive potentials. In an ideal reversible process the peak-to-peak separation, $\Delta E_p \approx 59$ mV and 30 mV for a one-electron and two-electron processes respectively and $i_a/i_c \approx 1$ for a reversible process. In our complexes $\Delta E_p = 78 \pm 1.8$ mV and $i_a/i_c = 0.94 \pm 0.04$ (approximately 1). Because of the deviation in ΔE_p, which is greater than 59 mV in all the complexes but the i_a/i_c being approximately 1, we conclude that these complexes are electrochemically pseudo-reversible.

The complexes appear to remain stable on a prolonged storage as no significant difference was observed in the voltammogram of VOL^{12} when it was re-run 24 h after the first reading on the same solution, stored in an air-tight container. The positive $E_{½}$ values of 401-480.5 mV may be assigned to metal-centred oxidation of V^{IV} to V^{V} in which there appears not to be any change in the structure of parent complex when oxidized [186] and falls within the range reported in the literature for similar complexes [187]. The electrode process can therefore be represented as:

$$[VO^{IV}L]^0 \rightleftharpoons [VO^{V}L]^+$$

4.8 Thermal analysis of oxovanadium(IV) complexes

Differential scanning calorimetry (DSC) gives information about thermal stability, melting, crystallization, decomposition, desolvation, sublimation, and glass transition. Any reaction or transformation involving absorption or release of heat can also be detected with this technique. The thermal characteristic data of the

complexes were determined from DSC thermograms (melting points, taken as the temperature corresponding to the minimum of the endothermic peak) and the results are summarized in Table 4.8 and Figure 4.8.1.1-4.8.2.5.3. The analysis of the DSC thermograms indicates that all the oxovanadium(IV) complexes under study are thermally stable at constant ambient pressure between 25 and 300 ^{o}C. The DSC analyses were carried out mainly to determine the melting and the decomposition temperatures of the oxovanadium(IV) complexes because their melting points were outside the range covered by the melting point instrument.

4.8.1 Unsymmetrical Schiff base complexes of oxovanadium(IV)

Four peaks were observed in the DSC thermogram of VOL^1, corresponding to three different endothermic peaks followed by an exothermic peak representing the decomposition of the complex (Fig. 4.8.1.1). The complex showed some morphology transformations [188] between 350 and 365 ^{o}C, followed by the sharp endothermic peak at 385 ^{o}C corresponding to the melting point of the complex. A close examination of the DSC peaks show that there is a hump near the onset temperature of the exothermic peak. This may be due to the competition between the melting and decomposition processes while the latter process predominates. The exothermic peak at 455 ^{o}C corresponds to the decomposition of the complex.

The DSC curve of VOL^3 (Fig. 4.8.1.3) shows a sharp endothermic peak with a minimum at 310 ^{o}C corresponding to the melting process. Immediately after melting, decomposition occurs and a broad exothermic peak was observed at 365 ^{o}C. VOL^4 gave a moderate exothermic peak at 455 ^{o}C, after an endothermic peak at 335 ^{o}C (Fig. 4.8.1.4), corresponding to the melting point of the complex. The hump observed near the onset temperature of the exothermic peaks of both VOL^3 and VOL^4 is

indicative of competition between the melting and decomposition processes while the latter process predominates. The DSC curve (Fig. 4.8.1.2) of VOL^2 showed no melting but a sharp exothermic decomposition at 380 ^oC. Thus this complex decomposed without melting.

4.8.2 Symmetrical Schiff base complexes of oxovanadium(IV)

4.8.2.1 Benzophenoneimino complexes

The DSC thermogram of VOL^5 (Fig. 4.8.2.1.1) shows a sharp endothermic peak with a minimum at 401 ^oC corresponding to the melting point of the complex. There was no exothermic peak observed which indicates that the complex did not decompose up to 500 ^oC. Two endothermic peaks were observed in the thermogram of VOL^7. The DSC curve (Fig. 4.8.2.1.3) presented an endothermic peak (broad) which we provisionally assign to the loss of the MeOH, followed by a melting process at 345 ^oC represented by a sharp endothermic peak.

4.8.2.2 Naphthaldiimino complexes

The DSC thermograms of the members of this series all show single sharp endothermic peaks at 390, 330 and 420 ^oC (Fig. 4.8.2.2.1-4.8.2.2.3). These peaks correspond to the melting points of the complexes VOL^8, VOL^9 and VOL^{10} respectively. The melting points of the members of this series do not correspond to the order of their molecular masses.

4.8.2.3 Chlorosalicylaldiimino complexes

The DSC thermograms of the complexes VOL^{11} and VOL^{13} show one sharp endothermic peak and one exothermic peak. It can be observed that the

melting and the onset of the decomposition are partially superposed (Fig 4.8.2.3.1 and 4.8.2.3.3). The endothermic peaks which correspond to their melting points has its minimum at 420 and 415 ^{o}C while the exothermic peaks occur at 430 and 425 ^{o}C respectively. The DSC curve of complex VOL^{12} (Fig. 4.8.2.3.2) shows three peaks, two of the peaks correspond to an exothermic processes and one corresponds to an endothermic process. The sharp endothermic peak at 315 ^{o}C corresponds to melting which is followed by broad exothermic peaks at 360 and 395 ^{o}C; the peaks immediately after the melting is due to stepwise decomposition of the complex. The DSC thermogram of VOL^{14} (Fig. 4.8.2.3.4) shows a sharp endothermic peak at 460 ^{o}C corresponding to the melting point of the compound.

4.8.2.4 Methoxysalicylaldiimino complexes

The DSC thermogram of VOL^{17} shows three peaks, the weak endothermic peak at about 120 ^{o}C is due to morphological transformation, while the sharp endothermic peak at 345 ^{o}C corresponds to melting. This is followed by a strong exothermic peak at 415 ^{o}C. In the DSC curve of VOL^{16} (Fig. 4.8.2.4.2), a sharp endothermic peak was observed at about 348 ^{o}C. This was followed by decomposition process which corresponds to a broad exothermic peak with the maximum at 390 ^{o}C. In the DSC curve of VOL^{15}, a sharp endothermic peak, with the minimum at 325 ^{o}C corresponding to the melting process was observed. A broad exothermic peak at 440 ^{o}C is observed in the thermogram of the complex which corresponds to the decomposition procress.

4.8.2.5 Ethoxysalicylaldiimino complexes

An endothermic peak at 240 ^{o}C was observed in the thermogram of complex VOL^{19} which corresponds to its melting point. The exothermic peak at 360 ^{o}C represents the decomposition of the complex (Fig. 4.8.2.5.2). Three peaks were observed in the DSC curve of VOL^{18}, two endothermic peaks and one exothermic peak. The first endothermic peak might be an evaporation process because the complex did not melt when heated to 250 ^{o}C and this peak is observed at 245 ^{o}C. The second endothermic peak at 290 ^{o}C corresponds to the melting point of the complex (Fig. 4.8.2.5.1). The exothermic peak is observed at about 360 ^{o}C which corresponds to the decomposition of the complex.

The DSC thermogram of VOL^{20} (Fig. 4.8.2.5.3) shows two sharp peaks and two broad and weak peaks. The two weak and broad endothermic peaks were between 75 - 140 ^{o}C and they are due to morphological transformations [188]. A sharp endothermic peak with minimum at 310 ^{o}C corresponds to the melting point of the complex. The complex decomposed at about 375 ^{o}C.

In general, the DSC thermograms of the complexes reveal a sharp endothermic process corresponding to sharp melting points followed by an exothermic decomposition processes. Few of the complexes show some weak endothermic peaks before the melting processes and these peaks are due to morphological transformation in the complexes.

CHAPTER 5

INSULIN-MIMETIC STUDIES ON THE OXOVANADIUM(IV) COMPLEXES

5.1 *In vitro* analysis

The use of *in vitro* studies to evaluate the glucose uptake in cell lines following stimulation with insulin and other active compounds is a direct and sensitive method of determining the antidiatogenic effect of these compounds [189, 190]. It allows for rapid screening of compounds in terms of their efficacy and toxicity in an ethically acceptable manner. Although the *in vitro* environment does not accurately mimic the *in vivo* situation, it offers unique opportunities and insights into the biochemical pathways which control the utilization of glucose by different cell types following exposure to various agents with potential diabetogenic effects. At the cellular level glucose uptake is mediated through glucose transporters. Glucose transporter subtype 4 (GLUT4) is the insulin-responsive transporter of glucose in various cell types in the body [189, 190]. Muscle and fat derived cell lines including C2C12 and L6 myoblast have been shown to be sensitive to insulin stimulation in culture resulting in an increase of GLUT4 and glucose uptake from the culture medium [189, 190].

Metformin and insulin were included in this analysis for comparative purposes. Metformin is an oral anti-diabetic drug from the biguanide family. It is the first-line drug for the treatment of type 2 diabetes, particularly in overweight and obese people and those with normal kidney function. Metformin improves hyperglycemia primarily through its suppression of hepatic glucose production (hepatic gluconeogenesis). In addition to suppressing hepatic glucose production, metformin increases insulin sensitivity, enhances peripheral glucose uptake, increases fatty acid oxidation [191],

and decreases absorption of glucose from the gastrointestinal tract. Increased peripheral utilization of glucose may be due to improved insulin binding to insulin receptors [192]. AMP-activated protein kinase (AMPK) probably also plays a role, as metformin administration increases AMPK activity in skeletal muscle [193]. AMPK is known to cause GLUT4 translocation, resulting in insulin-independent glucose uptake.

C2C12 cells were pre-exposed to the oxovanadium(IV) compounds, insulin and metformin respectively in glucose and serum-free media for 3 h before the glucose uptake experiments. Basal glucose uptake i.e. solvent vehicle only (DMSO) is represented as 100% and the subsequent increase or decrease induced by the compounds is reflected as ± 100%. Cytotoxic test carried out on all the complexes using 3-(4, 5-dimethylthiazo)-2-yl)-2, 5-diphenyltetrazolium bromide (MTT) assay showed that the complexes were not toxic to the cells at both low (0.05 µL) and high (0.25 µL) concentrations.

5.1.1 Unsymmetrical Schiff base complexes of oxovanadium(IV)

The insulin-like capacity of vanadium compounds is usually related to their ability to lower the blood glucose level by activating the glucose transport into the cell of the peripheral tissues. In this study, the *in vitro* glucose uptake by C2C12 muscle cells following exposure to four unsymmetrical tetradentate Schiff base complexes of oxovanadium(IV) has been investigated. Insulin-mimetic test on C2C12 muscle cells shows that all the complexes significantly stimulated cell glucose uptake when compared to the basal glucose uptake of the solvent vehicle (DMSO) with negligible cytotoxicity at the concentration of 0.05 µg/mL (Figure 5.1.1 and Table 5), but not at the same levels as insulin and metformin.

It seems that substitution on the salicylaldehyde group lowers the insulin enhancing activity as VOL^4 gave the largest effect. It was also observed that the electronic state of the substituents has some effects on the effectiveness. The order of activity, $VOL^4 > VOL^1 \sim VOL^3 > VOL^2$ correspond to H, Cl (-I, +M), OEt (+I, +M), NO_2 (-I, -M) substituents on the salicylaldehyde ring. The lowest percentage glucose utilization for complex VOL^2 may therefore be attributed to the greater negative electron withdrawing effect (-I and –M) of the nitro group on the salicylaldehyde when compared to the other substituents.

5.1.2 Symmetrical Schiff base complexes of oxovanadium(IV)

5.1.2.1 Benzophenoneimino complexes

All tested complexes in the series increased glucose utilization in C2C12 cells over basal values except VOL^6 whose percentage glucose uptake was lower than the basal glucose uptake (DMSO). Two of the complexes VOL^5 and VOL^7 significantly increased glucose uptake (p=0.001) over basal values. VOL^7, which shows the highest activity when compared to the other members of this series, could be attributed to the presence of an adduct (MeOH) in the molecule. The percentage glucose uptake of VOL^7 was comparable close to that of metformin as shown in Fig. 5.1.1 and Table 5.

5.1.2.2 Naphthaldiimino complexes

All the complexes increased glucose uptake in C2C12 cells over basal glucose uptake. Complex VOL^8 significantly increased glucose uptake (p= 0.001) when compared to the basal glucose uptake (DMSO). The ethylenediamine-bridged complexes in the whole series studied showed some increase in activity when

compared to the other diamines used. The results are presented in Table 5 and Fig. 5.1.1.

5.1.2.3 Chlorosalicylaldiimino complexes

All tested complexes in the series significantly increased glucose uptake in C2C12 cells if compared to the basal glucose uptake (DMSO). It seems from the above observation that the +M and –I effect of the chlorine atom plays an important role in the increased activities of the complexes in this series as shown in Fig. 5.1.2 and Table 5.

5.1.2.4 Methoxysalicylaldiimino complexes

All the complexes tested in the series also significantly increased glucose uptake if compared to the basal glucose uptake (solvent vehicle). The percentage glucose uptake of VOL^{18} was higher than that of metformin but less than that of insulin (Fig. 4.9.2 and Table 4.9). The complex VOL^{16} showed a remarkable glucose uptake activity in that its percentage glucose uptake was higher than those of insulin and metformin. The activities of this series may be attributed to the presence of the methoxy substituent on the salicylaldehyde because the same set of diamines that was used in the other series was also used in this series.

5.1.2.5 Ethoxysalicylaldiimino complexes

Two of the complexes increased glucose consumption in C2C12 cells over basal values but VOL^{20} recorded a lower percentage glucose uptake than the basal glucose uptake (DMSO). The presence of the ethoxyl substituent on the salicylaldehyde did not seem to affect the activities of this complex as much as the

methoxyl group did in the series above but complex VOL[18] significantly increased glucose (p= 0.001) in C2C12 cells if compared to the basal glucose uptake as shown in Fig. 5.1.2 and Table 5.

5.2 *In vivo* analysis

Vandate(V) and oxovanadium(IV) compounds have been well documented to mimic many of the actions of insulin [77]. Vanadium compounds have been shown to increase glucose transport and oxidation, to stimulate glycogen synthesis in the liver and to inhibit gluconeogenesis, i.e., vanadium is able to mimic most of the biological effects of insulin in various cell types[92]. Great efforts have therefore been made to prepare vanadium*(*IV*)* and vanadium*(V)* complexes of high biological activity and low toxicity which are readily absorbed. Many oxovanadium*(*IV*)* complexes with various coordination modes like $VO(O_4)$, $VO(S_2N_2)$, $VO(S_4)$, $VO(N_4)$ and $VO(N_2O_2)$,[93, 132] have been prepared, and the relationship between their structures and insulin-mimetic activities has also been examined by evaluating both *in vitro* and *in vivo* experimental results. As mentioned in Chapter 1, $VO(maltolate)_2$, $VO(picolinate)_2$, and $VO(6\text{-}Me\text{-}picolinate)_2$ proved to be potent in decreasing the blood glucose level with high efficiency.

A detailed literature review show that till date, only [$VO(sal_2\text{-}en)$] [126] and [$VO(sal_2\text{-}1,3\text{-}pn)$] [127] among complexes of the type reported in this work have been tested for insulin mimetic. [$VO(sal_2\text{-}en)$] was reported to be orally effective for glucose lowering in alloxan-induced diabetic rats, with a tendency for rats to be hypoglycemic; withdrawal of treatment results in the reversal to hyperglycemia. On the other hand [$VO(sal_2\text{-}1,3\text{-}pn)$] normalized glucose and lipid values without an increase in insulin levels, and improved glucose tolerance.

In this study, rats were injected with STZ to reduce or deplete the number of B cells to induce an insulin deficient non-ketoacidotic hyperglycaemia at levels typical of a stable Type 1, or late stage Type 2 diabetes. This is to test the effect of oxovanadium(IV) complexes in reducing fasting glucose levels in the absence (T1D) or presence of a compromised insulin production (late stage T2D). If the complexes do show a lowering effect of blood glucose it might be possible that the complexes have an insulin-like effect or extra-pancreatic actions. The extra-pancreatic actions could be stimulation of peripheral glucose utilization or enhancing glycolytic and glycogenic processes with a decrease glycogenlysis and gluconeogenesis.

Nine of the twenty oxovanadium(IV) complexes were tested *in vivo* for their insulin mimetic activities. An acute oral administration of the four unsymmetrical Schiff base complexes of oxovanadium(IV) elicited a progressive reduction in plasma glucose over 6 h in STZ rats. Two of the unsymmetrical Schiff base complexes of oxovanadium(IV) induced a significant reduction in plasma glucose over a 6 h period.

5.2.1 Unsymmetrical Schiff base complexes of oxovanadium(IV)

An acute oral administration of the unsymmetrical complexes at a dose of 0.2 mmol/kg to STZ rats elicited a progressive reduction in plasma glucose over 6 h periods. Acute oral administration of VOL^1 and VOL^4 to STZ rats induced a significant reduction in plasma glucose over a 6 h period. The complex VOL^1, significantly reduced plasma glucose by 20.48 % after 6 h (p = 0.04) while complex VOL^4 also significantly reduced plasma glucose by 28.87 % at 5 h (p = 0.03) and by 31.91 % at 6 h (p = 0.007). The percentage reduction in plasma glucose after treatment of the STD rats with the complexes is shown in Fig. 5.2.1

The above results confirm the structural activities proposed under the *in vitro* analysis, that substitution on the salicylaldehyde ring lowers the insulin enhancing activity as VOL^4 also gave the largest effect in the *in vivo* analysis. Almost the order of activity, VOL^4 > VOL^1 > VOL^2 > VOL^3 corresponding to H, Cl (-I, +M), OEt (+I, +M), NO_2 (-I, -M) substituents on the salicylaldehyde ring proposed under the *in vitro* discussion was observed in the *in vivo* experiments. These results demonstrate that oral administration of the complexes is effective in lowering diabetic hyperglycemia.

5.2.2 Symmetrical Schiff base complexes of oxovanadium(IV)

An acute oral administration of the complexes VOL^5, VOL^6, VOL^7, VOL^{12} and VOL^{13} elicited a progressive reduction in plasma glucose over 6 h in STZ rats. Acute oral administration of VOL^7 and VOL^{13} to STZ rats induced a significant reduction in plasma glucose during the 6 h period. Complex VOL^7 significantly reduced plasma glucose by 26.23 % (p=0.01) after 5 h and by 24.56 % (p=0.05) after 6 h. Complex VOL^{13} was found to significantly reduced plasma glucose by 10.58 % (p=0.03) after 1 h. The electronic effect of the chlorine substituent (-I, +M) on the salicylaldehyde, like in the *in vitro* studies, might be responsible for the high activity of VOL^{13}. The percentage reduction in plasma glucose after treatment of the STD rats with the complexes is shown in Fig. 5.2.2. The optimal time-course procedure used in this study to investigate the short-term insulin-mimetic effect of these complexes showed a significant hypoglycaemic effect from 0 to 6 h when compared to the control. From the results obtained from the *in vitro* and *in vivo* analyses, it may be inferred that the complexes under observation will also enhance glucose utilization or lowering of glucose serum level if they are administered over a long-term period.

It is very difficult to compare the efficacy of insulin-mimetic activities of vanadium complexes in published studies unless the studies are carried out for the specific purpose of comparison. These are due to variables such as method of administration, dose, diet, liquid consumption, gravity of the disease and the genetics, metabolism and environment of the animal model. Comparison and evaluation can therefore only be done if a reference compound has been included in the study for the purpose of comparison. BMOV has been experimentally used as a representative standard in several biological studies due to its approval for clinical experimient [194]. But BMOV was not included in this study because the pharmacological beneficial dose is associated with some toxicity and hence attempts are underway to evolve vanadium complexes with fewer side effects while retaining their enhanced therapeutic activities.

CHAPTER 6

CONCLUSIONS AND FUTURE PROSPECTS

6.1 Conclusions

The involvement of azomethine *N* and phenolic *O* of the tertadentate Schiff bases to the metal ions was confirmed by comparing the IR data of the ligands with those of the metal(II) complexes. Further conclusive evidence of the coordination of these Schiff-bases with the metal ions was shown by the appearance of new bands due to ν(M—N) and ν(M—O) in the metal complexes. The unsymmetrical nature of the unsymmetrical Schiff bases and their metal(II) complexes was confirmed by their IR spectra where two bands were observed for each of ν(C=N), ν(C—O), ν(V—N) and ν(V—O), taking their origin from the different aldehydes contained in each ligand. Most of the oxovanadium(IV) complexes exhibit a strong band in the range 959−989 cm^{-1}, which have been assigned to ν(V=O) in a monomeric square pyramidal environment. The oxovanadium(IV) complexes with trimethylene bridge, in which the ν(V=O) appeared at 848−860 cm^{-1}, have been assigned polymeric structure with ····V=O····V=O···· interactions, which afforded distorted octahedral coordination geometry.

The electronic spectral and magnetic susceptibility measurements were used for assigning the stereochemistry of each metal(II) complexes. For four-coordinate metal(II) complexes, either a square planar or a tetrahedral configuration is possible. On the basis of electronic spectra, together with the magnetic moments, it was possible for us to assign the preffered configuration for the metal(II) complexes reported herein.

The electronic spectra indicate a low spin square-planar geometry for all the cobalt(II) complexes. This was also corroborated by the effective magnetic moment of

the complexes, which lie in the range of 2.23–2.61 B.M., corresponding to one unpaired electron for low spin square-planar cobalt(II) complexes. The appearance of a single *d*−*d* transition in DMSO is attributed to solvent effect, indicating the possibility of formation of five- or six-coordinate species.

A square-planar geometry was assigned to all the red nickel(II) complexes. The observed zero magnetic moment confirms the square-planar environment in conformity with the fact that all known square-planar complexes of nickel(II) are diamagnetic. The stereochemistry of these complexes was unchanged in coordinating solvent (DMSO), except for NiL^2 containing nitro group on the aromatic ring, where some changes were observed even though the observed bands in the complex were still in conformation with a squre-planar geometry.

For the copper(II) complexes, a distorted square-planar N_2O_2 coordination chromophore was assigned. The distorted square-planar geometry of these complexes was also supported by their effective magnetic moments in the range 1.56–2.20 B.M. The low magnetic moment value of CuL^2 can be attributed to possible dimerization in the complex.

A multiple spectroscopic techniques were used to established the stereochemistry of the oxovanadium(IV) complexes. The electronic spectra of the oxovanadium(IV) complexes suggest a diversity of geometries. The electronic spectra indicate a square-pyramidal geometry for the five-coordinate species and distorted octahedral geometry for the six-coordinate species. The room temperature magnetic moments of 1.6–1.8 B.M. are normal for V(IV) d^1 configuration. In chloroform, the complexes are most probably five-coordinate with square-pyramidal geometry. The observed shift in band II of most these complexes with a lowering of

intensity in the molar absorptivity from $CHCl_3$ to DMSO are indicative of six-coordinate geometry in DMSO.

The frozen solution EPR spectra of the complexes VOL^{10}, VOL^{14}, and VOL^{19} at 120 K display rhombic vanadium(IV) spectra with three g ($g_z < g_x < g_y$) and three A values ($A_z > A_x > A_y$) characteristic for C_{2V} symmetry. Usually, this is due to a distortion of the square-pyramidal geometry towards a trigonal-bipyramidal. The solution EPR spectra of the other oxovanadium(IV) study are consistent with square pyramidal complexes with C_{4v} symmetry.

The cyclic voltammetry revealed only one quasi-reversible wave for each oxovanadium(IV) complex and they all showed redox couples with peak-to-peak separation values ranging from 74 to 83 mV, indicating a single step one-electron transfer process.

In vitro glucose uptake was carried out on all the oxovanadium(IV) complexes using C2C12 cell line. All the complexes tested increased glucose utilization in C2C12 cells over basal values except two of the complexes whose percentage glucose uptake was lower than the basal glucose uptake (DMSO). Eighteen of the oxovanadium(IV) complexes significantly increased glucose uptake when compared to the basal glucose uptake of the solvent vehicle (DMSO). Cytotoxic test carried out on all the complexes using MTT assay showed that the complexes were not toxic to the cells at both low and high concentrations. Two of the complexes showed activities comparable or greater than that of insulin.

Among the symmetrical oxovanadium(IV) complexes subjected to *in vitro* studies, the methoxysalicylaldiimines and chlorosalicylaldiimines complexes showed remarkable glucose uptake activity in that their percentage glucose uptake were higher than basal glucose uptake. All the members of the two series significantly

increased glucose uptake in C2C12 cells on comparison to the basal glucose uptake. We have proposed that the +M and –I effects of the chlorine and the +M and +I effects of the methoxy group play important roles in the enhanced activities of this series. It was also observed that all the ethylenediamine-bridged complexes showed enhanced activities.

Four unsymmetrical and five symmetrical Schiff base complexes of oxovanadium(IV) have been tested *in vivo* for their insulin mimetic activities. An acute oral administration of the four unsymmetrical Schiff base complexes of oxovanadium(IV) elicited a progressive reduction in plasma glucose over 6 h in STZ rats. Two of the unsymmetrical Schiff base complexes of oxovanadium(IV) induced a significant reduction in plasma glucose over a 6 h period. Oral administration of the five symmetrical complexes also elicited a progressive reduction in plasma glucose over 6h. Two of these complexes induced a significant reduction in plasma glucose during the 6 h period. The *in vitro* and *in vivo* studies carried out on the unsymmetrical complexes show structure-activity relationships brought about by the substituents on the salicylaldehyde group. The results show that substitution on the salicylaldehyde group lowers the insulin enhancing activity of the complexes as the complex without substitution gave the largest effect.

6.2 Suggestion for future work

Novel symmetrical and unsymmetrical Schiff base complexes of oxovanadium(IV) suitable for insulin-enhancing biological studies were successfully synthesized. The results from this work show that most of the complexes are promising insulin-enhancing agents. To get a better understanding of the insulin-mimetic properties of these compounds, further studies would need to be carried out

to determine their mechanism of action. *In vitro* and *in vivo* glucose uptake studies should be carried out using the radioactive 2-deoxyglucose (DOG) to monitor their mode of actions. Furthermore, all the complexes need to be screened for the anti-microbial properties using different strain of micro organisms to explore other areas of possible application.

The synthetic methodology for preparation of the unsymmetrical Schiff bases (Chapter three) will find application in the synthesis of more unsymmetrical Schiff bases with more substituents on the aromatic 2-hydroxyaldehydes. There is therefore room for the synthesis of more unsymmetrical Schiff bases and their metal complexes and further exploration of their biological activities.

The need to obtain good crystals for structural studies, lacking in this work, cannot be over-emphasized.

References

[1] J. Hine, C.Y. Yeh, Equilibrium in formation and conformational isomerization of imines derived from isobutyraldehyde and saturated aliphatic primary amines, J. Am. Chem. Soc. 89 (1967) 2669.

2] R.J. Fessenden, J.S. Fessenden, Organic Chemistry, Brooks/Cole Publishing Company, USA, 1998.

[3] Z. Cimerman, S. Miljanic, N. Galic, Schiff bases derived from aminopyridines as spectrofluorimetric analytical reagents, Croatica Chemica Acta 73 (1) (2000) 81.

[4] A. Elmali, M. Kabak, Y. Elerman, Conformational study and structure of bis-N,N′-p-bromo-salicylideneamine-1,2-diaminobenzene, J. Mol. Struct. 477 (2000) 151.

[5] M. Valcarcel, M.D. Laque de Castro, Flow-throgh Biochemical Sensors, Elsevier, Amsterdam., 1994.

[6] U. Spichiger-Keller, Chemical Sesors and Biosensors for Medical and Biological Applications, Wiley-VCH, Weinheim, 1998.

[7] J.F. Lawrence, R.W. Frei, Chemical Derivatization in Chromatography, Elsevier, Amsterdam, 1976.

[8] S. Patai (Ed.), The Chemistry of the Carbon-Nitrogen Double Bond, J. Wiley & Sons, London, 1970.

[9] E. Jungreis, S. Thabet, Analytical Applications of Schiff bases, Marcell Dekker, New York, 1969.

[10] C.M. Metzler, A. Cahill, D.E. Metzler, Equilibriums and absorption spectra of Schiff bases, J. Am. Chem. Soc. 102 (1980) 6075.

[11] C. Spinu, M. Pleniceanu, C. Tigae, Biologically Active Transition Metal Chelates with a 2-Thiophenecarboxaldehyde-Derived Schiff Base: Synthesis, Characterization, and Antibacterial Properties, Turk. J. Chem. 32 (2008) 487.

[12] B. Clarke, N. Clarke, D. Cunningham, T. Higgins, P. McArdle, M. Ni Cholchu, M. O'Gara, Transition-metal Schiff-base complexes as ligands in tin chemistry. Part 7. Reactions of organotin(IV) Lewis acids with [M(L)]2 [M-Ni, Cu and Zn; H2L-N,N%-bis(3- methoxysalicylidene)benzene-1,3-diamine and its -1,4-diamine analog], J. Organometallic Chem. 559 (1998) 55.

[13] A.L. Lehlinger, Principles of biochemistry, Worth, New York, 1975.

[14] P. Otto, J. Ladik, A. Szent-Gyorgyi, Internal charge transfer in proteins to the Schiff bases of their lysine side chains, Proc. Nat. Acad. Sci. USA 75 (1978) 3548.

[15] T. McKee, J. McKee, Biochemistry, Wm. C. Brown Publishers, Dubuque, 1996.

[16] S.N. Pandeya, D. Sriram, G. Nath, E. De Clercq, Synthesis, antibacterial, antifungal and antiviral activity evaluation of some new bis-Schiff bases of isatin and their derivatives, Pharm. Acta Helv. 74 (1999) 11.

17] S.N. Pandeya, D. Sriram, G. Nath, E. de Clercq, Synthesis, antibacterial, antifungal and anti-HIV evaluation of Schiff and Mannich bases of isatin and its derivatives with triazole, Arzneimittel Forsch. 50 (2000) 55.

[18] W.M. Singh, B.C. Dash, Synthesis of some new schiff bases containing thiazole and oxazole nuclei and their fungicidal activity, Pesticides 22 (1988) 33.

[19] J.L. Kelley, J.A. Linn, D.D. Bankston, C.J. Burchall, F.E. Soroko, B.R. Cooper, 8-Amino-3-benzyl-1,2,4-triazolo[4,3-α]pyrazines.Synthesis and anticonvulsant activity, J. Med. Chem. 38 (1995) 3676.

[20] G. Turan-Zitouni, Z.A. Kaplancikli, A. Özdemir, P. Chevallet, Studies on 1,2,4-triazole derivatives as potential anti-ıInflammatory agents, Arch. Pharm. Chem. Life Sci. 340 (2007) 586.

[21] M.T.H. Tarafder, A. Kasbollah, N. Saravanan, K.A. Crouse, A.M. Ali, K.T. Oo, S-methyldithiocarbazate and its schiff bases: Evaluation of bondings and biological properties, J. Biochem. Mol. Biol. Biophys. 6 (2002) 85.

[22] G.H. Schmid, Organic Chemistry, New York, 1996.

[23] F.A. Carry, Organic Chemistry', McGraw-Hill, 1992.

[24] D.H. Brown, W.E. Smith, Enzyme Chemistry- impact and Applications, Chapmann and Hall, London, 1990.

[25] K. Singh, M.S. Barwa, P. Tyagi, Synthesis and characterization of cobalt(II), nickel(II), copper(II) and zinc(II) complexes with Schiff base derived from 4-amino-3-mercapto-6-methyl-5-oxo-1,2,4-triazine, Eur. J. Med. Chem. 42 (2007) 394.

[26] P.G. Cozzi, Metal–Salen Schiff base complexes in catalysis: Practical aspects, Chem. Soc. Rev. 33 (2004) 410.

[27] S. Chandra, J. Sangeetika, EPR and electronic spectral studies on copper(II) complexes of some N-O donor ligands, J. Indian Chem. Soc. 81 (2004) 203.

[28] M.B. Ferrari, S. Capacchi, G. Pelosi, G. Reffo, P. Tarasconi, R. Albertini, S. Pinelli, P. Lunghi, Synthesis, structural characterization and biological activity of helicin thiosemicarbazone monohydrate and a copper(II) complex of salicylaldehyde thiosemicarbazone, Inorg. Chim. Acta 286 (1999) 134.

[29] E. Canpolat, M. Kaya, Studies on mononuclear chelates derived from substituted Schiff-base ligands (part 2): synthesis and characterization of a new 5-bromosalicyliden-paminoacetophenone oxime and its complexes with Co(II), Ni(II), Cu(II) and Zn(II), J. Coord. Chem. 57 (2004) 1217.

[30] M. Yildiz, B. Dulger, S.Y. Koyuncu, B.M. Yapici, Synthesis and antimicrobial activity of bis(imido) Schiff bases derived from thiosemicarbazide with some 2-hydroxyaldehydes and metal complexes, J. Indian Chem. Soc. 81 (2004) 7.

[31] H. Schiff, Untersuchungen uber salicinderirate, Ann. Chem. Pharm. 150 (1869) 193.

[32] C.K. Jørgensen, Comparative ligand field studies - IV. Vanadium(IV), titanium (III), molybdenium(V) and other system with one d-electron, Acta Chem. Scand. 11 (1957) 73.

[33] P. Pfeiffer, T. Hesse, H. Pfitzinger, W. Scholl, H. Thielert Inner Komplexsalze der aldeimin und azoreihe, J. Prakt., Chem. 149 (1937) 217.

[34] P. Pfeiffer, E. Buchholz , O. Baver, Inner complex salts from hydroxyaldimines and hydroxyketimines, J. Prakt. Chem. 129 (1931) 163.

[35] M. Calligaris, G. Nardin , L. Randaccio, Structural aspects of metal complexes with some tetradentate schiff bases, Coord. Chem. Rev. 7 (1972) 385.

36] M. Hariharan, F.L. Urbach, The stereochemistry of tetradentate Schiff base complexes of cobalt(II), Inorg. Chem. 8 (1969) 556.

[37] L.C. Nathan, J.E. Koehne, J.M. Gilmore, K.A. Hannibal, W.E. Dewhirst, T.D. Mai, The X-ray structures of a series of copper(II) complexes with tetradentate Schiff base ligands derived from salicylaldehyde and polymethylenediamines of varying chain length, Polyhedron 22 (2003) 887.

[
38] M.K. Taylor, J. Reglinski, D. Wallace, Coordination Geometry of Nickel Complexes with Tetradentate Schiff Base Ligands: the Effects of Donors, Backbone Length and Hydrogenation, Polyhedron 23 (2004) 3201.

[39] S. Yamada, Recent Aspects of the Stereochemistry of Schiff base Metal Complexes, Coord. Chem. Rev. 1 (1966) 415.

[40] G.A. Kolawole, K.S. Patel, The stereochemistry of Oxovanadium(IV) Complexes derived from Salicylaldehyde and Polymethylenediamines, J. Chem. Soc. (Dalton Trans.) (1981) 1241.

[41] K.S. Patel, G.A. Kolawole, A. Earnshaw, Spectroscopic and Magnetic Properties of Schiff base Complexes of Oxovanadium(IV) Derived from 3-methoxysalicylaldehyde and Aliphatic Diamines, J. Inorg. Nucl. Chem. 43 (1981) 3107.

[42] K.S. Patel, G.A. Kolawole, Magnetic and Spectral Properties of Oxovanadium(IV) Complexes of Quadridentate Naphthaldimine Ligands, J. Coord. Chem. 11 (1982) 231.

[43] G.A. Kolawole, K.S. Patel, Spectroscopic and Magnetochemical Investigation of Oxovanadium(IV) 5-Chlorosalicylaldiimines, J. Coord. Chem. 12 (1982) 121.

[44] F.L. Urbach, R.D. Bereman, J.A. Topich, M. Hariharan, B.J. Kalbacher, Stereochemistry and electronic structure of low-spin, square-planar cobalt(II) chelateswith tetradentate Schiff Base ligands, J. Am. Chem. Soc. 96 (1974) 5063.
[45] L.M. Engelhardt, J.D. Duncan, M. Green, The ESR of some low spin cobalt(II)-N_4 and -N_2O_2 complexes Inorg. Nucl. Chem. Lett. 8 (1972) 725.

[46] S. Yamada, Advancement in stereochemical aspects of Schiff base metal complexes, Coord. Chem. Rev.
190–192 (1999) 537.

[47] B.J. Hathaway, Comprehensive Coordination Chemistry Pergamon Press, Oxford, 1987.

[48] N. Raman, J. Dhaveethu Raja, A. Sakthivel, Synthesis, spectral characterization of Schiff base transition metal complexes: DNA cleavage and antimicrobial activity studies, J. Chem. Sci. 119 (2007) 303.

[49] S.M. Ben Saber, M. A.A., H. S.S., E.-a. M.M., Complexation behavior of some Schiff base complexes towards transition metal ions, Microchemical J. 81 (2005) 191.

[50] R. Nair, A. Shah, S. Baluja, S. Chanda, Synthesis and antibacterial activity of some Schiff base complexes, J. Serb. Chem. Soc. 71 (2006) 733.

[51] N. Raman, S. Ravichandran, C. Thangaraja, Copper(II), cobalt(II), nickel(II) and zinc(II) complexes of Schiff base derived from benzil-2,4-dinitrophenylhydrazone with aniline, J. Chem. Sci. 116 (2004) 215.

[52] M.A. Ali, A.H. Mirza, R.J. Butcher, M. Rahman, Nickel(II), copper(II), palladium(II) and platinum(II) complexes of bidentate SN ligands derived from S-alkyldithiocarbazates and the X-ray crystal structures of the [Ni(tasbz)$_2$] and [Cu(tasbz)$_2$] · $CHCl_3$ complexes, Trans. Met. Chem. 25 (2000) 430.

[53] F.M. Morad, M.M. EL.ajaily, S. Ben Gweirif, Preparation, Physical Characterization and Antibacterial Activity of Ni (II) Schiff Base Complex, J. Sci. and Its Applications 1 (2007) 72.

[54] N. Raman, V. Muthuraj, S. Ravichandran , A. Kulandaisamy, Synthesis, characterisation and electrochemical behaviour of Cu(II), Co(II), Ni(II) and Zn(II) complexes derived from acetylacetone andp-anisidine and their antimicrobial activity Proc. Indian Acad. Sci. 115 (2003) 161.

[55] R. Atkins, G.A. Brewer, E. Kokot, G.M. Mockler, E. Sinn, Copper(II) and Nickel(II) Complexes of some Unsymmetrical Tetradentate Schiff Base Ligands., Inorg. Chem. 24 (1985) 127.

[56] M.S. Co, K.O. Hodgson, T.K. Eccles, R. Lontie, Copper site of molluscan oxyhemocyanins. Structural evidence from x-ray absorption spectroscopy., J. Am. Chem. Soc. 103: (1981) 984.

[57] I. Rousso, N. Friedman, M. Sheves, M. Ottolenghi, pKa of the Protonated Schiff Base and Aspartic 85 in the Bacteriorhodopsin Binding Site Is Controlled by a Specific Geometry between the Two Residues, Biochemistry 34 (1995) 12059.

[58] J.P. Costes, M.I. Fernandes-Garcia, Easy synthesis of 'half-units': their use as ligands or as precursors of non-symmetrical Schiff base complexes, Inorg. Chim. Acta 237 (1995) 57.

[59] A.A. Osowole, G.A. Kolawole, O.E. Fagade, Synthesis, Physicochemical and Biological Properties of Nickel(II), Copper(II) and Zinc(II) Complexes of Unsymmetrical Tetradentate Schiff Base and Their Adducts, Synth. React. Inorg. Met.-Org. Chem. 35 (2005) 829.

[60] X.R. Bu, C.R. Jackson, D. Van Derveer, X.Z. You, Q.J. Meng, R.X. Wang, New copper(II) complexes incorporating unsymmetrical tetradentate ligands with cis-N_2O_2 chromophores: synthesis, molecular structure, substituent effect and thermal stability, Polyhedron 16 (1997) 2991.

[61] D.M. Boghaei, S. Mohebi, Non-symmetrical tetradentate vanadyl Schiff base complexes derived from 1,2-phenylenediamine and 1,3-naphthalenediamine as catalysts for the oxidation of cyclohexene, Tetrahedron 58 (2002) 5357.

[62] D. Rehder, The coordination chemistry of vanadium as related to its biological functions, Coord. Chem. Rev. 182 (1999) 297.

[63] J.O. Nriagu, Vanadium in the Environment, Part One: Chemistry and Biochemisty, John Wiley & Sons, New York, 1998.

[64] B.J. Wallar, J.D. Lipscomb, Dioxygen activation by enzymes containing binuclear non-heme iron clusters, Chem. Rev. 96 (1996) 2625.

[65] D. Rehder, The Bioinorganic Chemistry of Vanadium, Angew. Chem. 30 (1991) 148.

[66] E.M. Oltz, R.C. Brüning, M.J. Smith, K. Kustin, K. Nakanishi, The tunichromes. A class of reducing blood pigments from sea squirts: isolation, structures, and vanadium chemistry, J. Am. Chem. Soc. 110 (1988) 6162.

[67] H. Vilter, Peroxidases from Phaeophyceae: a Vanadium(V)-dependent Peroxidase from *Ascophyllum Nodosum*, Phytochemistry 23 (1984) 1387.

[68] H. Vilter, Vanadium-dependent haloperoxidases, Met. Ions Biol. Syst. 31 (1995) 325.

[69] M. Casny, D. Rehder, H. Schmidt, H. Vilter, V. Conte, A (17)O NMR study of peroxide binding to the active centre of bromoperoxidase from *Ascophyllum nodosum*, J. Inorg. Biochem. 80 (2000) 157.

[70] A. Butler, Bioinorganic Catalysis, Marcel Dekker, New York, 1993.

71] R. Wever, W. Hemrika, Vanadium in the Environment, Part One: Chemistry and Biochemistry, John Wiley & Sons, New York, 1998.

[72] J.W.P.M. Van Schijndel, E.G.M. Vollenbroek, R. Wever, The chloroperoxidase from the fungus *Curvularia inaequalis*; a novel vanadium enzyme, Biochim. Biophys. Acta 1161 (1993) 249.

[73] H. Kneifel, E. Bayer, Determination of the Structure of the Vanadium Compound, Amavadine, from Fly Agaric, Angew. Chem. 12 (1973) 508.

[74] G. Wilkinson (Ed.), Comprehensive Coordination Chemistry, Pergamon Press, Oxford, 1987.

[75] A. Butler, C. Carrano, Coordination chemistry of vanadium in biological system, J. Coord. Chem. Rev. 109 (1991) 61.

[76] N.D. Chasteen, Vanadium in Biological Systems: Physiology and Biochemistry, Kluwer Academic Dordrecht, 1990.

[77] D.C. Crans, Chemistry and insulin-like properties of vanadium(IV) and vanadium(V) compounds, J. Inorg. Biochem. 80 (2000) 123.

[78] F.A. Cotton, G. Wilkinson, Advanced Inorg. Chemistry, Wiley-Interscience, New York, (1999).

[79] N.D. Chasteen, Biological Magnetic Resonance, Plenum, New York, 1981.

[80] E.M. Page, S.A. Wass, Vanadium 1995, Coord. Chem. Rev. 164 (1997) 203.

81] M. Mathew, A.J. Carty, G.J. Palenik, An unusual complex containing bridging vanadyl groups. The crystal structure of N,N'-propylenebis(salicylaldiminato) oxovanadium(IV), J. Am. Chem. Soc. 92 (1970) 3197.

[82] A. Serrette, P.J. Carrol, T.M. Swager, Tuning the intermolecular dative interactions in vanadium-oxo linear chain compounds: formation of a new type of liquid crystalline polymer, J. Am. Chem. Soc. 114 (1992) 1887.

[83] M. Rangel, A. Tamura, C. Fukushima, H. Sakurai, In vitro study of the insulin-like action of vanadyl-pyrone and pyridinone complexes with a $VO(O_4)$ coordination mode, J. Biol. Inorg. Chem. 6 (2001) 128.

[84] P.R. Klich, A.T. Daniher, P.R. Challen, D.B. McConville, W.J. Youngs, Vanadium(IV) Complexes with Mixed O,S Donor Ligands. Syntheses, Structures, and Properties of the Anions Tris(2-mercapto-4-methylphenolato)vanadate(IV) and Bis(2 mercaptophenolato)oxovanadate(IV), Inorg. Chem. 35 (1996) 347.

[85] A. Hodge, K. Nordquest, E.L. Blinn, Oxovanadium(IV) complexes containing bidentate nitrogen-sulfur and oxygen-sulfur ligands, Inorg. Chim. Acta 6 (1972) 491.

[86] J. Burgess, B. De Castro, C. Oliveira, M. Rangal, W. Schlindwein, Synthesis and characterization of 3-hydroxy-4pyridinone-oxovanadium(IV) complexes, Polyhedron 16 (1997) 789.

[87] C.J. Ballhausen, H.B. Gray, The electronic structure of the vanadyl ion, Inorg. Chem. 1 (1962) 111.

[88] A. Neves, S.M. de Moraes Romanowski, I. Vencato, A.S. Mangrich, A new unsymmetrical N,O-donor hexadentate ligand. Synthesis, structure and properties of its first vanadyl(IV) complex, J. Chem. Soc., Dalton Trans. (1998) 617.

[89] G. Micera, D. Sanna, Vanadium in the Environment, Part One: Chemistry and Biochemisty, John Wiley & Sons, New York, 1998.

[90] B. Lyonnet, M. Martz, E. Martin, Lèmploi therapeutique des derives du vanadium. , La Presse Med. 7 (1899) 191.

[91] E.L. Tolman, E. Barris, M. Burns, A. Pansisni, R. Partridge, Effect of vanadium on glucose metabolism in vitro, Life Sci. 25 (1979) 1159.

[92] C. Orvig, K.H. Thompson, M. Battell, J.H. McNeill, Vanadium compounds as insulin mimics, Metal Ions Biol. Syst. 31 (1995) 575.

[93] K.H. Thompson, J.H. McNeill, C. Orvig, Vanadium compounds as insulin mimics, Chem. Rev. 99 (1999) 2561.

[94] K.H. Thompson, C. Orvig, Coordination chemistry of vanadium in metallopharmaceutical candidate compounds, Coord. Chem. Rev. 219–221 (2001) 1033.

[95] P. Comba, The relation between ligand structures, coordination stereochemistry, and electronic and thermodynamic properties, Coord. Chem. Rev. 123 (1993) 1.

[96] D.J. Clevette, W.O. Nelson, A. Nordin, C. Orvig, S. Sjoberg, The complexation of aluminum with N-substituted 3-hydroxy-4-pyridinones, Inorg. Chem. 28 (1989) 2079.

[97] M.M. Finnegan, S.J. Rettig, C. Orvig, Neutral water-soluble aluminum complex of neurological interest, J. Am. Chem. Soc. 108 (1986) 5033.

[98] W.O. Nelson, T.B. Karpishin, S.J. Rettig, C. Orvig, Physical and structural studies of N-substituted-3-hydroxy-2-methyl-4(1H)-pyridinones, Can. J. Chem. 66 (1988) 123.

[99] J.H. McNeill, V.G. Yuen, H.R. Hoveyda, C. Orvig, Bis (maltolato)oxovanadium (IV) is a potent insulin mimic, J. Med. Chem. 35 (1992) 1489.

[100] B.A. Reul, S.S. Amin, J.-P. Buchet, L.N. Ongemba, D.C. Crans, S.M. Brichard, Effects of vanadium complexes with organic ligands on glucose metabolism: A comparison study in diabetic rats, Br. J. Pharmacol. 126 (1999) 467.

[101] I.A. Setyawati, K.H. Thompson, V.G. Yuen, Y. Sun, M. Battell, D.M. Lyster, C. Vo, T.J. Ruth, S. Zeisler, J.H. McNeill, C. Orvig, Kinetic analysis and comparison of the uptake, distribution and excretion of 48V-labeled compounds in rats, J. Appl. Physiol. 84 (1998) 569.

[102] C.M. Krejsa, S.G. Nadler, J.M. Esselstyn, T.J. Kavanagh, J.A. Ledbetter, G.L. Schieven, Role of Oxidative Stress in the Action of Vanadium Phosphotyrosine Phosphatase Inhibitors, J. Biol. Chem. 272 (1997) 11541.

[103] S.A. Dikanov, B.D. Liboiron, K.H. Thompson, E. Vera, V.G. Yuen, J.H. McNeill, C. Orvig. In Vivo Electron Spin−Echo Envelope Modulation (ESEEM) Spectroscopy: First Observation of Vanadyl Coordination to Phosphate in Bone, J. Am. Chem. Soc. 121 (1999) 11004.

[104] G.T. Morgan, H.W. Moss, J. Chem. Soc. 103 (1914) 78.

[105] K. Kaneda, K. Jitsukawa, T. Itoh, S. Teranishi, Direct epoxy alcohol synthesis from cyclic olefins using molecular oxygen and $VO(acac)_2$-AIBN catalyst system, J.Org. Chem. 45 (1980) 3004.

[106] T. Hirao, Vanadium in modern organic synthesis, Chem. Rev. 97 (1997) 2707.

107] P.A. Wender, K.D. Rice, M.E. Schnute, The first formal asymmetry synthesis of phorbol, J. Am. Chem. Soc. 119 (1997) 7897.

[108] H. Taguchi, K. Isobe, Y. Nakamura, S. Kawaguchi, Some Adducts of Oxobis(acetylacetonato) Vanadium(IV) with Phenol or its Para-substituted Derivatives, Chem. Lett. (1975) 757.

[109] N.M. Atherton, P.J. Gibbon, M.C.B. Shohoji, Interaction of vanadyl acetylacetonate with solvents: the ^{51}V hyperfine interaction in mixtures of ethanol and carbon tetrachloride, J. Chem. Soc. Dalton Trans. (1982) 2289.

[110] J. Seibin, H.R. Manning, G. Cessac, Ligation effects in vanadyl complexes, J. Inorg. Nucl. Chem. 25 (1963) 1253.

[111] N.S. Al-Niaimi, A.R. Al-Karaghouli, S.M. Aliwi, M.G. Jalhoom, Adducts formation between bis(β-diketonato)oxovanadium(IV) complexes and 4-methylpyridine N-oxide, J. Inorg. Nucl. Chem. 36 (1974) 283.

112] B.J. Pandya, P.K. Bhattacharya, Indian J. Chem. 25A (1986) 776.

[113] P.-K. Hon, R.L. Belford, C.E. Pfluger, Bis(1-Phenyl-1,3-Butanedionato) Vanadyl. I. Molecular and Crystal Structure of the cis Form, J. Chem. Phys. 43 (1965) 1323.

[114] S.S. Amin, K. Cryer, B. Zhang, S.K. Dutta, S.S. Eaton, O.P. Anderson, S.M. Miller, B.A. Reul, S.M. Brichard, D.C. Crans, Chemistry and Insulin-mimetic properties of Bis(acetylacetonate)oxovanadium(IV) and derivatives, Inorg. Chem. 39 (2000) 406.

[115] J. Li, G. Elberg, D.C. Crans, Y. Shechter, Evidence for the Distinct Vanadyl(+4)-Dependent Activating System for Manifesting Insulin-Like Effects, Biochemistry 35 (1996) 8314.

[116] R.L. Dhutta, S. Ghosh, S. Lahiry, Sci. Cult. 30 (1964) 551.

[117] M. Melchior, K.H. Thompson, J.M. Jong, S.J. Rettig, E. Shuter, V.G. Yuen, Y. Zhou, J.H. McNeill, C. Orvig, Vanadium complexes as Insulin Mimetic Agents: Coordination chemistry and in vivo studies of oxovanadium(IV) and Dioxovanadium(V) complexes formed from Naturally occurring chelating Oxazolinate, Thiazolinate or Picolinate units, Inorg. Chem. 38 (1999) 2288.

[118] H. Sakurai, K. Fujii, H. Watanabe, H. Tamura, Orally Active and Long-Term Acting Insulin-Mimetic Vanadyl Complex: Bis(Picolinato)oxovanadium(IV), Biochem. Biophys. Res. Commun. 214 (1995) 1095.

[119] Y. Fujisawa, H. Sakurai, Evidence for the improvement of noninsulin-dependent diabetes mellitus in KKA(Y) mice with daily oral administration of bis(6-methylpicolinato)oxovanadium(IV) complex, Chem. Pharm. Bull. 47 (1999) 1668.

[120] T. Kiss, E. Kiss, E. Garribba, H. Sakurai, Speciation of insulin-mimetic VO(IV)-containing drugs in blood serum, J. Inorg. Biochem. 80 (2000) 65.

[121] H. Yasui, K. Takechi, H.J. Sakurai, Metallokinetic analysis of disposition of vanadyl complexes as insulin-mimetics in rats using BCM-ESR method, Inorg. Biochem. 78 (2000) 185.

[122] S. Fujimoto, K. Fujii, H. Yasui, R. Matsushita, J. Takada, H. Sakurai, Long-term acting and orally active vanadyl-methylpicolinate complex with hypoglycemic activity in streptozotocin-induced diabetic rats, J. Clin. Biochem. Nutr. 23 (1997) 113.

[123] M.M. Aly, Recent developments in the metallosupramolecular and molecular structures of the cobalt, iron and vanadium complexes of the dianionic tetradentate Schiff base ligands of salicylideneimine and acetylacetoneimine, J. Coord. Chem. 43 (1998) 89.

[124] A.H. Vetter, A. Berkessel, Schiff-base ligands carrying two elements of chirality: Matched-mismatched effects in the vanadium-catalyzed sulfoxidation of thioethers with hydrogen peroxide, Tetrahedron Lett. 39 (1998) 1741.

[125] D.J. Berrisford, C. Bolm, K.B. Sharpless, Ligand-accelerated catalysis, Angew. Chem. 34 (1995) 1059.

[126] N. Durai, G. Saminathan, Insulin-like effects of bis-salicylidine ethylenediiminato oxovanadium (IV) complex on carbohydrate metabolism, J. Clin. Biochem. Nutr. 22 (1997) 31.

[127] M. Xie, G. Xu, L. Li, W. Liu, Y. Niu, S. Yan, In vivo Insulin-mimetic Activity of [N,N'-1,3-propyl-bis(salicylaldimine)]oxovanadium(IV), Eur. J. Med. Chem. 42 (2007) 817.

[128] H. Sakurai, K. Tsuchiya, M. Nukatsuka, J. Kawada, S. Ishikawa, H.e.a. Yoshida, Insulin-mimetic action of vanadyl complexes, J. Clin. Biochem. Nutr. 8 (1990) 193.

[129] H. Sakurai, Z.-I. Taira, N. Sakai, Crystal Structure of an L-Cysteine Methyl Ester-Vanadyl(IV) Complex, Inorg. Chim. Acta 151 (1988) 85.

[130] S.F. Simon, C.G. Taylor, Dietary zinc supplementation attenuates hyperglycemia in db/db mice, Exp. Biol. Med. 226 (2001) 43.

[131] M.M. James, S.C. Charles, The mechanism of the insulin-like effects of ionic zinc, J. Biol. Chem. 257 (1982) 4362.

[132] H. Sakurai, Y. Kojima, Y. Yoshikawa, K. Kawabe, H. Yasui, Antidiabetic vanadium(IV) and Zinc(II) complexes, Coord. Chem. Rev. 26 (2002) 187.

[133] C.G. Taylor, Zinc, the Pancreas, and Diabetes: Insights from Rodent Studies and Future Directions, BioMetals 18 (2005) 305.

[134] L. Coulson, P. Dandona, Insulin-like effect of zinc on adipocytes, Diabetes 29 (1980) 665.

[135] A. Shisheva, D. Gefel, Y. Shechter, Insulinlike effects of zinc ion in vitro and in vivo. Preferential effects on desensitized adipocytes and induction of normoglycemia in streptozocin-induced rats, Diabetes 41 (1992) 982.

[136] M.D. Chen, S.J. Liou, P.Y. Lin, V.C. Yang, P.S. Alexander, Effects of zinc supplementation on the plasma glucose level and insulin activity in genetically obese (ob/ob) mice, Biol. Trace Elem. Res. 61 (1998) 303.

[137] J. Fugono, K. Fujimoto, H. Yasui, K. Kawabe, Y. Yoshikawa, Y. Kojima, H. Sakurai, Metallokinetic Study of Zinc in the Blood of Normal Rats Given Insulinomimetic Zinc(II) Complexes and Improvement of Diabetes Mellitus in Type 2 Diabetic GK Rats by their Oral Administration., Drug Metab. Pharmacokinet.17 (2002) 340.

[138] H. Sakurai, Y. Adachi, The Pharmacology of the Insulinomimetic Effect of Zinc Complexes, BioMetals 18 (2005) 319.

[139] Y. Yoshikawa, E. Ueda, Y. Suzuki, N. Yanagihara, H. Sakurai, Y. Kojima, New Insulinomimetic Zinc(II) Complexes of α-Amino Acids and Their Derivatives with $Zn(N_2O_2)$ Coordination Mode, Chem. Pharm. Bull. 49 (2001) 652.

[140] Y. Yoshikawa, K. Kawabe, M. Tadokoro, Y. Suzuki, N. Yanagihara, A. Nakayama, H. Sakurai, Y. Kojima, New Zinc(II) Complexes with Tetradentate Amino Acid Derivatives: Structure Characterization, Solution Chemistry, and in vitro Insulinomimetic Activity, Bull. Chem. Soc. Jpn. 75 (2002) 2423.

[141] Y. Yoshikawa, E. Ueda, K. Kawabe, H. Miyake, T. Takino, H. Sakurai, Y. Kojima, Development of new insulinomimetic zinc(II) picolinate complexes with a $Zn(N_2O_2)$ coordination mode: structure characterization, in vitro, and in vivo studies, J. Biol. Inorg. Chem. 7 (2002) 68.

[142] T. Sasagawa, Y. Yoshikawa, K. Kawabe, H. Sakurai, Y. Kojima, Bis(6-ethylpicolinato)oxovanadium(IV) complex with normoglycemic activity in KK-Ay mice, J. Inorg. Biochem. 88 (2002) 108.

[143] R.A. Anderson, Chromium in the prevention and control of diabetes, Diabetes Metabol. 26 (2000) 22.

[144] D.G. Barceloux, Vanadium, J. Toxicol. 37 (1999) 265.

[145] J.L. Domingo, Vanadium and diabetes.What about vanadium toxicity? Mol. Cell Biochem. 203 (2000) 185.

[146] T. Scior, A. Guevara-Garcie, Q.D. Bernard, P. D. Domeyer, S. Laufer, Are vanadium compounds drugable? Structures and effects of antidiabetic vanadium compounds; A critical review. Mini-Reviews, Med. Chem. 5 (2005) 995.

[147] G. Elberg, Z. He, J. Li, N. Sekar, S. Y., Vanadate activates membranous nonreceptor protein tyrosine in rat adipocytes, Diabetes 46 (1997) 1684.

[148] J.L. Domingo, Vanadium: A review of the reproductive and developmental toxicity, Reprod. Toxicol. 10 (1996) 175.

[149] A. Mohammad, V. Sharma, J.H. McNeill Vanadium increases GLUT4 in diabetic rat skeletal muscle, Mol. Cell Biochem. 233 (2002) 139.

[150] S. Dai, K.H. Thompson, E. Vera, J.H. McNeill, Toxicity studies on one-year treatment of non-diabetic and streptozotocin-diabetic rats, Pharmacol. Toxicol. 75 (1994) 265.

[151] C. Taha, A. Klip, The insulin signaling pathway, J. Membrane Biol. 169 (1999) 1.

[152] D. Rehder, J.C. Pessoa, C.F.G.C. Geraldes, M.M.C.A. Castro, T. Kiss, B. Meier, G. Micera, L. Petterson, M. Rangel, A. Salifoglu, I. Turel, D. Wang, In vitro study of the insulin-mimetic behaviour of vanadium(IV,V) coordination compounds, J. Biol. Inorg. Chem. 7 (2002) 384.

[153] D. Rehder, Biological and medicinal aspects of vanadium, Inorg. Chem. Commun. 6 (2003) 604.

[154] S. Wild, G. Roglic, A. Green, R. Sicree, H. King, Global prevalence of diabetes: estimates for the year 2000 and projection for 2030, Diabetes Care 27 (2004) 1047.

[155] M.A.K. Omar, M.A. Seedat, R.B. Dyer, A.A. Motala, L.T. Knight, P.J. Becker, South African Indians show a high prevalence of diabetes and bimodality in plasma glucose distribution, Diabetes Care 17 (1994) 70.

[156] L.J. Berliner, Spin labelling II: Theory and applications, Academic Press, New York, 1979.

[157] R.J. Wasson, Instrumental Analysis, Allyn and Bacon Inc., Boston, 1978.

[158] R.C. Maurya, S. Rajput, Oxovanadium(IV) complexes of bioinorganic and medicinal relevance: synthesis, characterization and 3D molecular modeling and analysis of some oxovanadiun(IV) complexes involving the O, N-donor environment of pyrazolone-based sulfa drug Schiff bases, J. Mol. Str. 794 (2006) 24.

[159] E. Garribba, G. Micera, A. Panzanelli, D. Sanna, Electronic Structure of Oxovanadium(IV) Complexes of α-Hydroxycarboxylic Acids, Inorg. Chem. 42 (2003) 3981.

[160] F.E. Mabbs, Some Aspects of the Electron Paramagnetic Resonance Spectroscopy of d-Transition Metal Compound, Chem. Soc. Rev. (1993) 313.

[161] R.S. Drago, Physical methods in chemistry, W.B. Saunders company, Philadelphia, 1977.

[162] F.E. Mabbs, D.J. Machin, Magnetism and transition metal complexes, Chapman and Hall, London, 1973.

[163] C.J. O'Connor, Magnetochemistry - Advances in Theory and Experimentation, Prog. Inorg. Chem. 29 (1982) 203.

[164] A. Earnshaw, Introduction to magnetochemistry, Academic press, London, 1968.

[165] J. Selbin, The Chemistry of Oxovanadium(IV), Chem. Rev. 65(2) (1965) 153.

[166] C. Furlani, Ric. Sci. 27 (1957) 1141

[167] J. Selbin, Oxovanadium(IV) complexes, Coord. Chem. Rev. 1 (1966) 293.

[168] J. Selbin, Spectral studies of β-ketoenolate complexes of oxovanadium(IV), J. Inorg. Nucl. Chem. 29 (1967) 1735.

[169] C.J. Ballhausen, B.F. Djurinskij, K.J. Watson, The polarized absorption spectra of three crystalline polymorphs of VOSO4 • $5H_2O$, J. Am. Chem. Soc. 90 (1968) 3305.

[170] R.P. Dodge, D.H. Templeton, A. Zalkin, Creystal structure of N,N'-Ethylenebis(acetyacetoiminato)oxovanadium(IV), Inorg. Chem. 9 (1961) 130.

[171] P.J. Haine, Thermal methods of analysis principles, applications and problems, Chapman and Hall, Oxford, 1995.

[172] H.H. Willard, L.L. Merritt Jr., J.A. Dean, F.A. Settle Jr., Instrumental methods of analysis, Wadsworth publishing company, California, 1988.

[173] A.J. Bard, L.R. Faulkner, Electrochemical Methods: Fundamentals and Applications, John Wiley and Sons, New York, 2000.

[174] R.S. Nicholson, I. Shain, Theory of stationary electrode polarography: single scan and cyclic methods applied to reversible, irreversible, and kinetic systems, Anal. Chem. 36 (1964.) 706.

[175] M.M. Abd-Elzar, Spectroscopic characterization of some tetradentate Schiff bases and their complexes with nickel, copper and zinc, J. Chin. Chem. Soc. 48 (2001) 153.

[176] P.E. Aranha, M.P. Do Santo, S. Romera, E.R. Dockal, Synthesis, characterization, and spectroscopic studies of tetradentate Schiff base chromium(III) complexes, Polyhedron 26 (2007) 1373.

[177] D.M. Boghaei, M. Lashanizadegan, Template synthesis, characterization of highly unsymmetrical tetradentate Schiff base complexes of Nickel(II) and Copper(II). J. Sci. I.R. Iran 11 (2000) 301.

[178] R.D. Hancock, D.A. Thornton, Crystal field aspects of vibrational spectral first-row transition metal(III) β-ketonenolates, J. Mol.Struct. 4 (1969) 361.

[179] G.C. Percy, D.A. Thornton, N-Aryl salicyladimine complexes: Infrared and PMR spectra of the ligands and vibrational frequencies of their metal(II) chelates, J. Inorg. Nucl. Chem. 34 (1972) 3357.

[180] B.S. Manhas, B.C. Verma, S.B. Kalia, Spectral and magnetic studies on normal cobalt(II) planar and cobalt(III) octahedral, spin-crossover cobalt(III)octahedral and planar-tetrahedral cobalt(II) carbodithioates, Polyhedron 14 (1995) 3549.

[181] S. Belaid, A. Landreau, O. Benali-Baitich, M.A. Khan, G. Bouet, Synthesis, characterisation and antifungal activity of a series of cobalt(II) and nickel(II) complexes with ligands derived from reduced N, N'-o-phenylenebis(salicylideneimine), Trans. Met. Chem. 33 (2008) 511.

[182] G.A. Kolawole, K.S. Patel, A. Earnshaw, The stereochemistry of oxovanadium(IV) complexes derived from substituted 2-hydroxy aromatic aldehydes and aromatic diamines, J. Coord. Chem. 14 (1985) 57

[183] B.J. Hathaway, D.E. Billing, Copper(II) ammonia complexes, Coord. Chem. Rev. 5 (1970) 143.

[184] A. Sarkar, S. Pal, Dioxovanadium(V) complexes with N,N,O-donor monoanionic ligands: Synthesis, structure and properties, Polyhedron 25 (2006) 1689

[185] F.E. Mabbs, D. Collison, Electron Paramagnetic Resonance of d-Transition Metal Compounds, Elsevier, Amsterdam, 1992.

[186] J. Dai, H. Wang, M. Mikuriya, Electrochemistry of vanadium complexes of o-N-salicylideneaminoethylphenol. A well characterized cyclic mechanism for the gain or loss of vanadyl oxygen, Polyhedron 15 (1996) 1806.

[187] A.H. Kianfar, S. Mohebbi, Synthesis and Electrochemistry of Vanadium(IV) Schiff Base Complexes, J. Iran. Chem. Soc. 4(2) (2007) 215.

[188] C.H. Lee, C.K. Hsu, C.L. Chang, A study on the thermal decomposition behaviours of PETN, RDX, HNS and HMX, Thermochim. Acta 392-393 (2002) 173.

[189] P. Galante, L. Mosthaf, M. Kellerer, L. Berti, S. Tippmer, B. Bossenmaier, T. Fujiwara, A. Okuno, H. Horikoshi, H.U. Haring, Acute hyperglycemia provides an insulin-independent inducer for GLUT4 translocation in C2C12 myotubes and rat skeletal muscle, Diabetes 44 (1995) 646.

[190] T. Nedachi, M. Kanzaki, Regulation of glucose transporters by insulin and extracellular glucose in C2C12 myotubes, Am. J. Physiol. Endocrinol. Metab. 291 (2006) E817.

[191] G. Zhou, R. Myers, Y. Li, Y. Chen, X. Shen, J. Fenyk-Melody, M. Wu, J. Ventre, T. Doebber, N. Fujii, N. Musi, M.F. Hirshman, L.J. Goodyear, D.E. Moller, Role of AMP-activated protein kinase in mechanism of metformin action, J. Clin. Invest. 108 (2001) 1167

[192] Y.D. Kim, K.G. Park, Y.S. Lee, Y.Y. Park, D.K. Kim, B. Nedumaran, W.G. Jang, W.J. Cho, J. Ha, I.K. Lee, C.H. Lee, H.S. Choi, Metformin inhibits hepatic gluconeogenesis through AMP-activated protein kinase–dependent regulation of the orphan nuclear receptor SHP, Diabetes 57 (2008) 306.

[193] L. Zhang, H. He, J.A. Balschi, Metformin and phenformin activate AMP-activated protein kinase in the heart by increasing cytosolic AMP concentration, Am. J. Physiol. Heart Circ. Physiol. 293(1) (2007) H457.

[194] V.G. Yuen, C. Orvig, J.H. McNeill, Comparison of the glucose-lowering properties of
vanadyl sulfate and bis(maltolato)oxovanadium(IV) following acute and chronic administration, Can. J. Physiol. Pharmacol. 73 (1995) 55

APPENDIX I

Table 4.1.1 Physical properties and analytical data for the Schiff bases and oxovanadium(IV) complexes

Compound	Empirical Formula	Formula weight	Yield (%)	Colour	M.P./ ^{o}C	Microanalysis (Calc.) %C	%H	%N
H_2L^1	$C_{24}H_{17}N_2O_2Cl$	400.86	91.5	Orange -Yellow	194-195	71.60 (71.83)	4.27 (4.73)	6.98 (6.60)
VOL^1	$C_{24}H_{15}N_2O_3ClV$	465.79	81.6	Green	>250	62.22 (61.83)	3.15 (3.24)	6.11 (6.01)
H_2L^2	$C_{24}H_{17}N_3O_4$	411.41	86.2	Orange -Yellow	134-135	69.69 (70.07)	4.23 (4.16)	10.12 (10.21)
VOL^2	$C_{24}H_{15}N_3O_5V$	476.34	75.4	Green	>250	60.7 (60.52)	3.38 (3.17)	8.67 (8.82)
H_2L^3	$C_{26}H_{22}N_2O_3$	410.47	71.9	Orange -Yellow	135-136	76.34 (76.08)	5.51 (5.40)	6.79 (6.82)
VOL^3	$C_{26}H_{20}N_2O_4V$	475.40	79.2	Green	>250	65.69 (65.69)	5.51 (5.40)	5.91 (5.89)
H_2L^4	$C_{24}H_{18}N_2O_2$	366.41	78.4	Orange -Yellow	187-188	78.41 (78.67)	4.81 (4.95)	7.62 (7.65)
VOL^4	$C_{24}H_{16}N_2O_3V$	431.34	92.8	Green	>250	66.29 (66.83)	3.86 (3.74)	6.38 (6.49)
H_2L^5	$C_{28}H_{24}N_2O_2$	420.5	90.7	Yellow	164-165	79.98 (79.95)	5.75 (5.77)	6.66 (6.68)
VOL^5	$C_{28}H_{22}N_2O_3V$	485.4	73.3	Green	>250	69.28 (69.06)	4.57 (4.49)	5.77 (5.98)
H_2L^6	$C_{29}H_{24}N_2O_2$	434.5	86.5	Yellow	154-155	80.16 (80.12	6.03 (6.12)	6.45 (6.48)
VOL^6	$C_{29}H_{22}N_2O_3V$	499.5	83.9	Green	>250	69.74 (69.80)	4.84 (4.83)	5.61 (5.64)
H_2L^7	$C_{29}H_{26}N_2O_2$	434.5	82.2	Yellow	123-124	79.92 (80.16)	5.97 (6.03)	6.41 (6.45)
VOL^7	$C_{30}H_{28}N_2O_4V$	531.5	67.0	Orange	>250	67.79 (67.02)	5.31 (5.36)	5.46 (5.29)
H_2L^8	$C_{24}H_{20}N_2O_2$	368.4	95.6	Yellow	>250	78.24 (78.11)	5.47 (5.49)	7.60 (7.62)
VOL^8	$C_{24}H_{18}N_2O_3V$	382.4	93.9	Green	>250	65.72 (65.17)	4.90 (5.13)	5.68 (5.61)
H_2L^9	$C_{25}H_{22}N_2O_2$	382.5	89.2	Yellow	222-223	78.51 (78.52)	5.80 (5.82)	7.32 (7.37)
VOL^9	$C_{25}H_{20}N_2O_3V$	447.4	95.6	Orange	>250	67.12 (67.11)	4.51 (4.41)	6.26 (6.39)
H_2L^{10}	$C_{28}H_{20}N_2O_2$	416.5	86.4	Orange	233-234	80.75 (80.55)	4.84 (4.69)	6.73 (6.72)
VOL^{10}	$C_{28}H_{18}N_2O_3V$	481.4	72.5	Brown	>250	69.86 (70.40)	3.77 (3.66)	5.82 (6.03)

H_2L^{11}	$C_{16}H_{14}N_2O_2Cl$	337.2	88.7	Yellow	178-179	56.84 (57.05)	4.17 (4.13)	8.28 (8.29)
VOL^{11}	$C_{16}H_{12}N_2O_3Cl_2V$	402.1	91.3	Green	>250	47.68 (47.85)	3.00 (2.87)	6.95 (7.06)
H_2L^{12}	$C_{17}H_{16}N_2O_2Cl_2$	351.2	82.4	Yellow	122-123	58.14 (57.77)	4.59 (4.53)	7.98 (7.83)
VOL^{12}	$C_{17}H_{14}N_2O_3Cl_2V$	416.2	76.1	Green	>250	49.07 (48.86)	3.39 (3.31)	6.73 (6.52)
H_2L^{13}	$C_{17}H_{16}N_2O_2Cl_2$	351.2	78.6	Yellow	61-62	58.14 (58.00)	4.59 (4.63)	7.98 (8.00)
VOL^{13}	$C_{17}H_{14}N_2O_3Cl_2V$	416.2	79.0	Orange	>250	49.07 (48.99)	3.39 (3.34)	6.78 (6.88)
H_2L^{14}	$C_{20}H_{14}N_2O_2Cl_2$	385.2	84.2	Orange -Yellow	219-220	62.31 (62.21)	3.57 (3.65)	7.30 (7.25)
VOL^{14}	$C_{20}H_{12}N_2O_3Cl_2V$	450.1	79.5	Orange	>250	53.25 (53.25)	2.59 (2.68)	6.31 (6.21)
H_2L^{15}	$C_{18}H_{20}N_2O_4$	328.4	83.4	Yellow	165-166	65.82 (65.84)	6.14 (6.14)	8.51 (8.53)
VOL^{15}	$C_{20}H_{18}N_2O_5V$	397.3	86.7	Green	>250	54.85 (54.97)	4.61 (4.61)	7.12 (7.12)
H_2L^{16}	$C_{19}H_{22}N_2O_4$	342.4	79.6	Yellow	82-83	66.58 (66.65)	6.50 (6.48)	8.15 (8.18)
VOL^{16}	$C_{20}H_{24}N_2O_6V$	443.4	81.5	Orange	>250	55.80 (56.03)	4.79 (4.95)	6.82 (6.88)
H_2L^{17}	$C_{22}H_{20}N_2O_4$	376.4	65.1	Orange	103-104	70.23 (70.20)	5.29 (5.36)	7.45 (7.44)
VOL^{17}	$C_{22}H_{18}N_2O_5V$	441.3	74.3	Brown	>250	57.92 (58.34)	4.60 (4.68)	5.94 (5.92)
H_2L^{18}	$C_{20}H_{24}N_2O_4$	356.4	80.2	Yellow	138-139	67.52 (67.40)	6.98 (6.79)	7.96 (7.86)
VOL^{18}	$C_{20}H_{22}N_2O_5V$	421.4	91.6	Green	>250	56.93 (57.01)	5.32 (5.26)	6.79 (6.65)
H_2L^{19}	$C_{21}H_{26}N_2O_4$	370.5	89.3	Yellow	70-71	67.73 (68.09)	7.15 (7.07)	7.51 (7.56)
VOL^{19}	$C_{21}H_{24}N_2O_5V$	435.4	88.5	Green	239-240	57.45 (57.93)	5.49 (5.56)	6.40 (6.43)
H_2L^{20}	$C_{24}H_{24}N_2O_4$	404.5	79.7	Orange -Yellow	72-73	71.43 (71.27)	5.98 (5.98)	7.01 (6.93)
VOL^{20}	$C_{24}H_{22}N_2O_5V$	469.4	75.5	Green	>250	59.98 (61.41)	4.93 (4.47)	5.88 (5.64)

Table 4.1.2 Physical properties and analytical data for cobalt(II), nickel(II) and copper(II) the compounds

Complex	Empirical Formula	Formula Mass	% Yield	Colour	M.P./ ^{o}C	Microanalysis (Calc.)		
						%C	%H	%N
CoL^1	$C_{24}H_{15}N_2O_2ClCo$	458.25	93.2	Brown	>250	63.17 (62.91)	3.20 (3.30)	5.81 (6.11)
CoL^2	$C_{24}H_{15}N_3O_4Co$	468.34	89.5	Brown	>250	61.97 (61.55)	3.10 (3.23)	8.63 (8.97)
CoL^3	$C_{26}H_{20}N_2O_3Co$	467.39	94.7	Brown	>250	66.62 (66.82)	4.30 (4.28)	5.91 (5.99)
CoL^4	$C_{24}H_{16}N_2O_2Co$	423.34	91.8	Brown	>250	68.31 (68.09)	3.65 (3.81)	6.16 (6.62)
NiL^1	$C_{24}H_{15}N_2O_2ClNi$	458.00	95.8	Red	>250	63.21 (62.94)	3.22 (3.30)	5.87 (6.12)
NiL^2	$C_{24}H_{15}N_3O_4Ni$	468.10	96.1	Red	>250	61.02 (61.58)	3.16 (3.23)	8.87 (8.98)
NiL^3	$C_{26}H_{20}N_2O_3Ni$	467.15	90.2	Red	>250	66.49 (66.85)	4.17 (4.32)	5.51 (6.00)
NiL^4	$C_{24}H_{16}N_2O_2Ni$	423.10	88.8	Red	>250	68.11 (68.13)	3.70 (3.81)	6.31 (6.62)
CuL^1	$C_{24}H_{15}N_2O_2ClCu$	462.86	90.9	Pale Brown	>250	62.06 (62.28)	3.11 (3.27)	5.68 (6.05)
CuL^2	$C_{24}H_{15}N_3O_4Cu$	472.95	86.3	Pale Brown	>250	60.72 (60.95)	3.47 (3.20)	9.13 (8.88)
CuL^3	$C_{26}H_{20}N_2O_3Cu$	472.01	91.7	Pale Brown	>250	66.03 (66.16)	4.50 (4.27)	5.48 (5.93)
CuL^4	$C_{24}H_{16}N_2O_2Cu$	431.34	94.8	Pale Brown	>250	66.29 (66.83)	3.86 (3.74)	6.38 (6.49)

Table 4.2 ^{1}H NMR data for free ligands (chemical shifts in ppm)

Ligand	δ OH	δ Ar-H	δ CH_3	δ CH_2	δ CH	δ N=CH
H_2L^1	15.5 (s, 1H) 10.2 (s, 1H)	6.9-8.1(m,13H)				8.9 (s, 1H) 9.0 (s, 1H)
H_2L^2	13.9 (s, 1H) 15.2 (s, 1H)	7.1-8.1(m,13H)				8.4 (s, 1H) 8.8 (s, 1H)
H_2L^3	12.9 (s, 1H) 15.0 (s, 1H)	6.8-8.1(m, 13H)	1.5 (t, 3H)	4.1 (q, 2H)		8.2 (s, 1H) 8.7 (s, 1H)
H_2L^4	12.0 (s, 1H) 15.7 (s, 1H)	6.9-8.0 (m, 14H)				8.6 (s, 1H) 8.9 (s, 1H)
H_2L^5	15.2 (s, 2H)	6.6-7.5 (m, 18H)	—	3.7 (t, 4H)	—	—
H_2L^6	15.3 (s, 2H)	6.6-7.5 (m, 18H)	1.3 (d, 3H)	3.7 (d, 2H)	3.5 (m, 1H)	—
H_2L^7	15.5 (s, 2H)	6.6-7.5 (m, 18H)	—	2.0 (m, 2H) 3.4 (t, 4H)	—	—
H_2L^8	14.3 (s, 2H)	7.2-8.0 (m, 12H)	—	4.0 (s, 4H)	—	8.2 (s, 2H)
H_2L^9	14.8 (s, 2H)	7.0-7.9 (m, 12H)	—	2.2 (m, 2H) 3.8 (t, 4H)	—	8.9 (s, 2H)
H_2L^{10}	15.1 (s, 2H)	7.2 -8.1 (m,12H)	—	—	—	9.5 (s, 2H)
H_2L^{11}	13.1 (s, 2H)	6.9-7.3 (m, 6H)	—	4.0 (s, 4H)	—	8.3 (s, 2H)
H_2L^{12}	13.1 (s, 2H)	6.6-7.3 (m, 6H)	1.3 (d, 3H)	3.9 (d, 2H)	3.7 (m, 1H)	8.3 (s, 2H)
H_2L^{13}	13.4 (s, 2H)	6.6-7.3 (m, 6H)	—	2.1 (m, 2H) 3.7 (t, 4H)	—	8.3 (s, 2H)
H_2L^{14}	13.0 (s, 2H)	6.9-7.4 (m, 10H)	—	—	—	8.6 (s, 2H)
H_2L^{15}	12.7 (s, 2H)	6.7-7.3 (m, 6H)	3.8 (s, 3H)	4.0 (s, 4H)	—	8.3 (s, 2H)
H_2L^{16}	12.9 (s, 2H)	6.7-7.3 (m, 10H)	3.8 (s, 3H)	3.7 (t, 4H) 2.2 (m, 2H)	—	8.3 (s, 2H)
H_2L^{17}	12.7 (s, 2H)	6.9-7.7 (m, 10H)	3.8 (s, 3H)	—	—	8.6 (s, 2H)
H_2L^{18}	13.6 (s, 2H)	6.7-7.3 (m, 6H)	1.5 (t, 3H)	4.0 (s, 4H) 4.1 (q, 2H)	—	8.3 (s, 2H)
H_2L^{19}	13.8 (s, 2H)	6.7-7.3 (m, 6H)	1.4 (d, 3H) 1.5 (t, 3H)	3.9 (d, 2H)	3.8 (m, 1H)	8.3 (s, 2H)
H_2L^{20}	13.1 (s, 2H)	6.8-7.3 (m, 10H)	1.5 (t, 3H)	4.2 (q, 2H)	—	8.6 (s, 2H)

Table 4.3.1 Selected infrared spectral bands of the Schiff bases and oxovanadium(IV) complexes

Compounds	ν(C=N)	ν(C—O)	ν(V=O)	ν(V—N)	ν(V—O)
VOL^{1}	1607, 1574	1363,1312	979	485, 537	573, 456
H_2L^{1}	1611, 1583	1313,1276	–	–	–
VOL^{2}	1607, 1576	1362,1315	982	483, 541	581, 457
H_2L^{2}	1621, 1567	1333,1289	–	–	–
VOL^{3}	1604 ,1573	1361,1324	988	498, 540	572, 455
H_2L^{3}	1610, 1569	1316,1283	–	–	–
VOL^{4}	1607, 1574	1366,1321	970	558, 536	488, 458
H_2L^{4}	1615, 1568	1313,1286	–	–	–
VOL^{5}	1599	1337	986	495	406
H_2L^{5}	1604	1334	–	–	–
VOL^{6}	1599	1336	989	519	489
H_2L^{6}	1607	1331	–	–	–
VOL^{7}	1601	1337	959	528	418
H_2L^{7}	1604	1331	–	–	–
VOL^{8}	1606	1343	988	577	506
H_2L^{8}	1634	1284	–	–	–
VOL^{9}	1618	1281	852	549	466
H_2L^{9}	1621	1257	–	–	–
VOL^{10}	1600	1306	979	503	561
H_2L^{10}	1615	1287	–	–	–
VOL^{11}	1616	1297	967	493	546
H_2L^{11}	1633	1278	–	–	–
VOL^{12}	1627	1297	988	498	554
H_2L^{12}	1631	1277	–	–	–
VOL^{13}	1630	1309	860	471	516
H_2L^{13}	1636	1280	–	–	–
VOL^{14}	1612	1322	969	435	524
H_2L^{14}	1615	1275	–	–	–
VOL^{15}	1627	1277	979	491	573

H_2L^{15}	1638	1285	–	–	–
VOL^{16}	1634	1307	848	476	549
H_2L^{16}	1640	1275	–	–	–
VOL^{17}	1599	1289	981	497	544
H_2L^{17}	1622	1272	–	–	–
VOL^{18}	1631	1313	976	483	611
H_2L^{18}	1637	1275	–	–	–
VOL^{19}	1611	1304	982	471	614
H_2L^{19}	1631	1272	–	–	–
VOL^{20}	1602	1315	982	448	541
H_2L^{20}	1614	1283	–	–	–

Table 4.3.2 Selected infrared spectral bands of cobalt(II), nickel(II) and copper(II) complexes

Complex	ν(C=N)	ν(C−O)	ν(M−N)	ν(M−O)
CoL^1	1604, 1578	1326, 1288	453, 508	575, 423
CoL^2	1603, 1574	1363, 1319	454, 539	568, 428
CoL^3	1606, 1577	1342, 1314	475, 548	568, 428
CoL^4	1603, 1571	1337, 1313	580, 554	463, 428
NiL^1	1609, 1582	1331, 1287	457, 554	577, 431
NiL^2	1603, 1580	1366, 1311	457, 510	545, 431
NiL^3	1606, 1577	1346, 1290	478, 507	560, 431
NiL^4	1606, 1577	1343, 1290	583, 507	463, 431
CuL^1	1606, 1582	1325, 1290	457, 548	574, 419
CuL^2	1606, 1580	1363, 1317	472, 501	563, 452
CuL^3	1606, 1580	1340, 1311	498, 542	560, 463
CuL^4	1609, 1577	1340, 1314	574, 545	460, 416

Table 4.4.1 Electronic spectral data of the cobalt(II) complexes

Compound	Solvent	*d-d* transitions/cm^{-1} (ε/$cm^{-1}mol^{-1}$)	C.T	Ligand[#]
CoL^1	$CHCl_3$	18 939 (77), 22 523 (205), 24 876 (273)		31 949 (228) 40 323 (606)
	DMSO	25 126 (236)	29 586 (183)	
CoL^2	$CHCl_3$	18 587 (59), 22 272 (153), 25 575 (227)		31 447 (202) 40 816 (364)
	DMSO	25 063 (333)		36 101 (363)
CoL^3	$CHCl_3$	18 868 (93), 22 523 (233), 24 876 (279)	28 902 (270) 30 675 (274	40 323 (675)
	DMSO	25 063 (228)	29 412 (238)	
CoL^4	$CHCl_3$	18 832 (94), 22 779 (250), 25 189 (337)		31 546 (277) 41 494 (668)
	DMSO	25 445 (263)	29 586 215)	

[#]The spectra were noisy in the UV and some of the bands in the region could not be extracted.

Table 4.4.2 Electronic spectral data of the nickel(II) complexes

Compound	Solvent	*d-d* transitions/cm^{-1} (ε/$cm^{-1}mol^{-1}$)	C.T	Ligand[#]
NiL^1	$CHCl_3$	20 619 (154), 25 840 (361)	30 675 (211)	38 314 (697)
	DMSO	20 790 (145), 26 042 (322)	30 581 (184)	39 063 (658)
NiL^2	$CHCl_3$	20 704 (127), 26 178 (312)	30 769 (204)	38 760 (437)
	DMSO	20 877 (156), 26 178 (384)		31 250 (216) 38 610 (501)
NiL^3	$CHCl_3$	20 619 (162), 25 773 (383)	30 303 (234)	38 314 (700)
	DMSO	20 619 (161), 25 974 (375)	30 395 (232)	38 168 (830)
NiL^4	$CHCl_3$	20 747 (173), 25 840 (402)	30 675 (234)	38 314 (703)
	DMSO	20 877 (150), 26 110 (340)	30 581 (191)	38 168 (638)

[#]The spectra were noisy in the UV and some of the bands in the region could not be extracted.

Table 4.4.3 Electronic spectral data of the copper(II) complexes

Compound	Solvent	*d-d* transitions/cm^{-1} (ε/$cm^{-1}mol^{-1}$)	C.T	Ligand[#]
CuL^1	$CHCl_3$	23 041 (280)	27 778 (176) 29 326 (198)	31 056 (240) 37 736 (482)
	DMSO	23 256 (307)	30 030 (215)	31 646 (223) 37 313 (529)
CuL^2	$CHCl_3$	24 038 (184)	28 571 (213)	31 447 (225) 36 900 (344) 40 816 (371)
	DMSO	23 981 (362)		36 101 (356)
CuL^3	$CHCl_3$	22 831 (262)	29 674 (269)	37 736 (421)
	DMSO	23 095 (262)	30 030 (252)	36 765 (408)
CuL^4	$CHCl_3$	23 419 (308),	27 933 (203)	31 250 (262) 38 168 (438)
	DMSO	23 585 (322),	28 490 (181), 30 395 (244)	

[#]The spectra were noisy in the UV and some of the bands in the region could not be extracted.

Table 4.4.4 Electronic spectral data of the oxovanaduim(IV) complexes

Compound	Solvent	Band maxima/cm^{-1} ($\varepsilon/cm^{-1}mol^{-1}$)			C.T	Ligand#
		Band I	Band II	Band III		
VOL[1]	$CHCl_3$	16 393 (99)	16 393 (99)	23 641(2 390)	27 701(1 380)*	31 447 (18 200) 40 323 (53 800)
	DMSO	16 129 (10)	16 129 (10)	23 753 (2,180)		31 746 (1 690)* 38 610 (1 550)
VOL[2]	$CHCl_3$			21 598*(2,375)	28 329 (860)	31 746 (890) 36 364 (1 220)* 40 323 (1 990)
	DMSO	15 748 (9)	15 748 (9)*		27 473 (4,400)	31 746 (3 640) 36 101 (4 140)
VOL[3]	$CHCl_3$	16 207 (9)	16 207 (9)	23 256 (2 090)	28 736 (2 250)	41 322 (5 000)
	DMSO	15 898 (9)	15 898 (9)	23 474 (2,100)	29 155 (2,230)	38 610 (3 730)
VOL[4]	$CHCl_3$	16 234 (20)	16 234(20)	24 096 (2 270)	27 701(1 450)*	31 348 (1 860) 40 323 (5 000)
	DMSO	16 051 (10)	16 051 (10)	24 096 (2 080)		31 153 (1 700) 38 168 (3 220)
VOL[5]	$CHCl_3$		17 182 (127)	21 097 (82)*	27 473 (4 360)	35 461 (2 697) 40 486 (4 486) 41 152 (4 481)
	DMSO	13 870 (461)	17 575 (484)	21 277 (453)*	27 322 (7 448)	
VOL[6]	$CHCl_3$		16 863 (150)	20 747 (154)*	27 027 (1,002)	34 965 (2 563) 35 336 (2 364) 40 486 (3 973) 41 322 (4 051)
	DMSO		17 123 (205)	21 276 (161)*	27 397 (970)	36 765 (2 355)*
	$CHCl_3$	12 255	16 026	21 186 (398)*	27 397 (714)	35 714 (1 929)

VOL[7]		(94)	(24) 16 667 (226)			40 323 (3 849) 40 984 (3 857)
	DMSO	12 225 (37)*	19 231 (140)	21 097 (166)	27 624 (854)	
VOL[8]	$CHCl_3$		16 155 (47)	25 840 (1 660)	29 851 (2 650)	36 900 (3 680)* 41 322 (7 160)
	DMSO		16 269 (18)	24 213 (1 190)	26 110 (1 780) 30 581 (2 600)	37 313 (5 080)
VOL[9]	$CHCl_3$			25 840 (1 490)	30 395 (2 580)	36 900 (3 680)* 41 322 (6 850)
	DMSO	12 887 (6)	19 455 (11)		26 178 (1350)	32 154(2 520) 37 879(5 020)
VOL[10]	$CHCl_3$		15 942 (36)	21 749 (2 950) 23 474 (3 790)	28 169 (2 680)	31 746 (1 920) 36 765 (4 670) 40 650 (8 810)
	DMSO		15 528 (13)	23 641(3 060) 21 786 (2 350)*	28 736 (2 080)	36 630(4 180)
VOL[11]	$CHCl_3$		16,778 (25)		26 178(910)	35 714(2 350)* 39 683(5 220)
	DMSO		17 544 15)		26 882 (910)	
VOL[12]	$CHCl_3$	13 263 (450)	16 892 (25)		26 178 (955)	35 971 (2 440)* 39 841 (5 193) 40 650 (6 234) 41 152 (4 420)
	DMSO	12 970 (46)*	17 699 (14)	21 186 (549)	26 810 (893)	37 879(3 896) 38 610 (4 659) 38 911 (5 517)
VOL[14]	$CHCl_3$			23 753 (1 140)	30 864 (1 410)	39 841 (2 520) 40 816 (2 580)
	DMSO			24 096 (18)	31 447 (1 950)	37 879 (2 750)
	$CHCl_3$		16 694	24 631 (10)	34 722(2 660)*	39 370 (4 210)

VOL[15]			(19)			
	DMSO		16 891 (17)	25 380 (1090)		37 879 (4 270)
VOL[16]	$CHCl_3$	14 728 (76)	19 685 (90)	24 876 (11)	35 336 (2950)*	
	DMSO	13 850 (19)	18 762 (30)	25 445 (1 010)		37 879 (3 350)
VOL[17]	$CHCl_3$			22 422 (1 790)	31 348 (2 590)	39 370 (3 930)
	DMSO	15 649 (9)		22 624 (1 790)	31 646 (2 500)	38 023 (3 390)
VOL[18]	$CHCl_3$		16 694 (15)	25 510 (620)	33 333 (2 280)	40 984 (3 660)
	DMSO		17 065 (14)		26 385 (650) 34 364 (2 150)	38 760 (3 290)
VOL[19]	$CHCl_3$		16 667 (16)	25 316 (6)	33 445 (2 250)	40 816 (3 540)
	DMSO		16 694 (15)		26 110 (650)	34 130 (2 200) 38 314 (2 760)
VOL[20]	$CHCl_3$		16 051 (7)	22 831 (1 180)	28 818 (3 040)	40 650 (3 550)
	DMSO		16 155 (9)	23 641 (1 410)	30 395 (2 990)	37 879 (2 920)

[#]The spectra were noisy in the UV and some of the bands in the region could not be extracted. * = Shoulder

Table 4.5 Room temperature magnetic moments for the complexes

Complex	Magnetic moment/B.M.		Complex	Magnetic moment/B.M.
CoL^1	2.61		VOL^1	1.73
CoL^2	2.59		VOL^2	1.73
CoL^3	2.23		VOL^3	1.60
CoL^4	2.36		VOL^4	1.81
NiL^1	diamagnetic		VOL^5	1.74
NiL^2	diamagnetic		VOL^6	1.68
NiL^3	diamagnetic		VOL^7	1.78
NiL^4	diamagnetic		VOL^8	1.71
CuL^1	2.20		VOL^9	1.79
CuL^2	1.56		VOL^{10}	1.83
CuL^3	1.81		VOL^{11}	1.78
CuL^4	1.78		VOL^{12}	1.84
			VOL^{13}	1.76
			VOL^{14}	1.80
			VOL^{15}	1.72
			VOL^{16}	1.82
			VOL^{17}	1.83
			VOL^{18}	1.77
			VOL^{19}	1.72
			VOL^{20}	1.78

Table 4.6.1 EPR parameters for the oxovanadium(IV) complexes with axial symmetry

Complexes	Solution (290 K)			Solution (120 K)		
	g_{iso}	A_{iso} (G)	$g_{\perp}$	$g_{//}$	$A_{//}$ (G)	$A_{\perp}$ (G)
VOL[1]	1.971	99.5	1.978	1.950	64	179.0
VOL[2]	1.971	101.0	1.978	1.950	65.0	179.0
VOL[3]	1.971	99.0	1.978	1.950	65.0	178.0
VOL[4]	1.971	99.5	1.978	1.950	64.0	177.0
VOL[5]	1.969	98.0	1.978	1.948	60.0	177.5
VOL[6]	1.969	98.0	1.978	1.949	60.0	177.0
VOL[7]	1.967	97.0	1.976	1.947	59.0	176.0
VOL[9]	1.970	96.5	1.972	1.950	58.0	170.0
VOL[12]	1.970	99.0	1.979	1.948	60.0	179.0

Table 4.6.2 EPR parameters for the oxovanadium(IV) complexes with rhombic symmetry

Complexes	solution (290K)		solution (120K)					
	g_{iso}	A_{iso} (G)	g_x	g_y	g_z	A_x (G)	A_y (G)	A_z (G)
VOL[10]	1.972	99.0	1.976	1.980	1.950	63.0	58.0	178.0
VOL[14]	1.970	100.0	1.976	1.978	1.948	64.0	59.0	179.0
VOL[19]	1.97	99.0	1.976	1.978	1.948	64.0	60.0	179.0

Table 4.7 Cyclic voltammetric data for oxovanadium(IV) complexes

Complexes	Redox couple	$E_{p.c}$/mV	$E_{p.a}$/mV	$i_c/10^6$	$i_a/10^6$	i_a/i_c	$E_{½}$/mV	ΔE_p/mV
VOL^1	V^{IV}/V^V	613	530	6.91	5.31	0.77	571.5	83
VOL^3	V^{IV}/V^V	552	469	7.87	6.26	0.80	510.5	83
VOL^4	V^{IV}/V^V	568	490	6.91	5.45	0.79	529	78
VOL^5	V^{IV}/V^V	457	378	8.77	8.65	0.99	417.5	79
VOL^6	V^{IV}/V^V	465	387	8.48	8.47	1.00	426	78
VOL^7	V^{IV}/V^V	438	364	4.75	3.93	0.83	401	74
VOL^8	V^{IV}/V^V	456	379	8.42	6.03	0.72	417.5	77
VOL^9	V^{IV}/V^V	538	458	9.12	8.22	0.90	498	80
VOL^{10}	V^{IV}/V^V	590	507	7.46	5.79	0.78	548.5	83
VOL^{11}	V^{IV}/V^V	521	442	9.31	8.68	0.93	481.5	79
VOL^{12}	V^{IV}/V^V	525	444	10.09	9.39	0.93	484.5	81
VOL^{13}	V^{IV}/V^V	521	440	10.15	9.07	0.89	480.5	81
VOL^{14}	V^{IV}/V^V	662	580	7.90	5.46	0.69	621	82
VOL^{15}	V^{IV}/V^V	380	297	1.07	1.02	0.95	338.5	83
VOL^{16}	V^{IV}/V^V	490	414	8.92	8.45	0.95	452	76
VOL^{17}	V^{IV}/V^V	512	428	8.96	7.27	0.81	470	84
VOL^{18}	V^{IV}/V^V	395	317	9.21	8.81	0.96	356	78
VOL^{19}	V^{IV}/V^V	399	319	8.21	7.93	0.97	359	80
VOL^{210}	V^{IV}/V^V	528	448	8.22	6.45	0.78	488	80

Table 4.8 DSC phenomenological data of oxovanadium(IV) complexes

complex	DSC peak temperature (^{o} C)	
	Endothermic peak	Exothermic peak
VOL^{1}	350, 365,385	455
VOL^{2}	—	380
VOL^{3}	310	365
VOL^{4}	335	455
VOL^{5}	401	—
VOL^{7}	345	—
VOL^{8}	390	—
VOL^{9}	330	—
VOL^{10}	420	—
VOL^{11}	420	430
VOL^{12}	315	360, 395
VOL^{13}	415	425
VOL^{14}	460	—
VOL^{15}	325	440
VOL^{16}	348	390
VOL^{17}	345	415
VOL^{18}	290	360
VOL^{19}	240	360
VOL^{20}	310	375

Table 5 Glucose uptake data for the oxovanadium(IV) complexes

Compound	% glucose uptake	SD	*p*=value
DMSO	100.00	0.07	
Insulin	185.70	0.28	0.010
Metformin	175.58	0.47	0.001
VOL^{1}	154.16	0.34	0.007
VOL^{2}	142.58	0.39	0.001
VOL^{3}	153.38	0.51	0.001
VOL^{4}	167.34	0.72	0.009
VOL^{5}	151.69	0.21	0.001
VOL^{6}	93.84	0.17	-0.07
VOL^{7}	166.77	0.58	0.001
VOL^{8}	158.62	0.46	0.001
VOL^{9}	111.78	0.19	0.2
VOL^{10}	128.77	0.25	0.006
VOL^{11}	155.20	0.36	0.001
VOL^{12}	119.30	0.23	0.4
VOL^{13}	156.04	0.62	0.001
VOL^{14}	130.45	0.33	0.03
VOL^{15}	200.04	0.54	0.01
VOL^{16}	169.33	0.29	0.001
VOL^{17}	179.70	0.36	0.008
VOL^{18}	145.23	0.29	0.001
VOL^{19}	107.24	0.21	0.3
VOL^{20}	90.67	0.18	-0.04

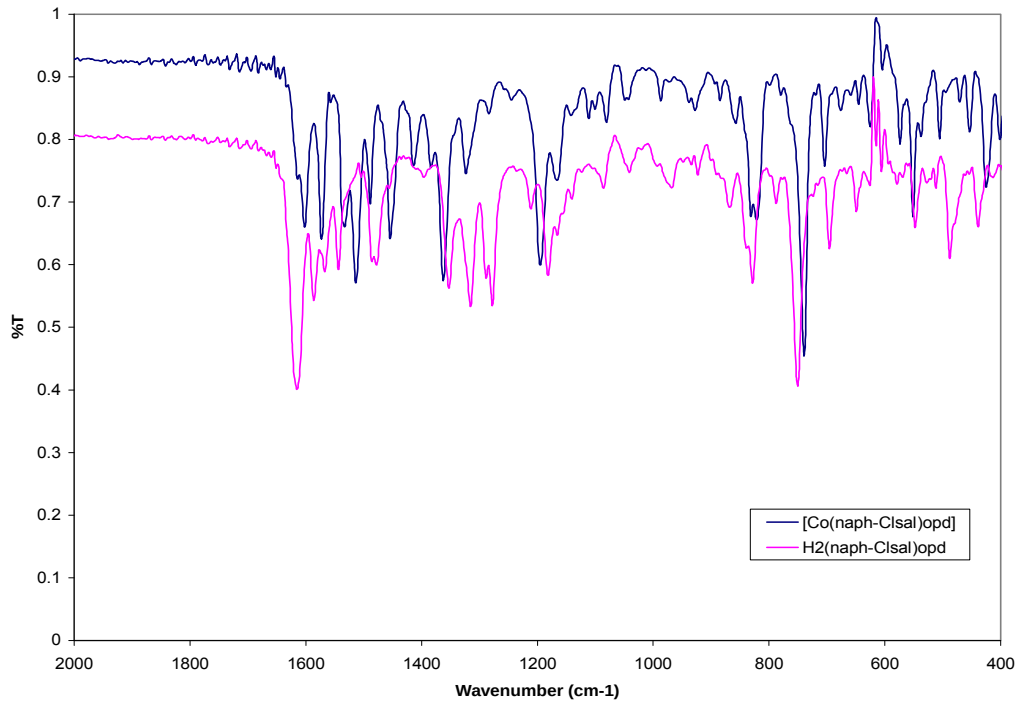

Fig. 4.3.1 IR spectra of complex CoL^1 and its ligand H_2(naph-Clsal)opd: representative spectra for the unsymmetrical complexes of cobalt(II) and the ligands

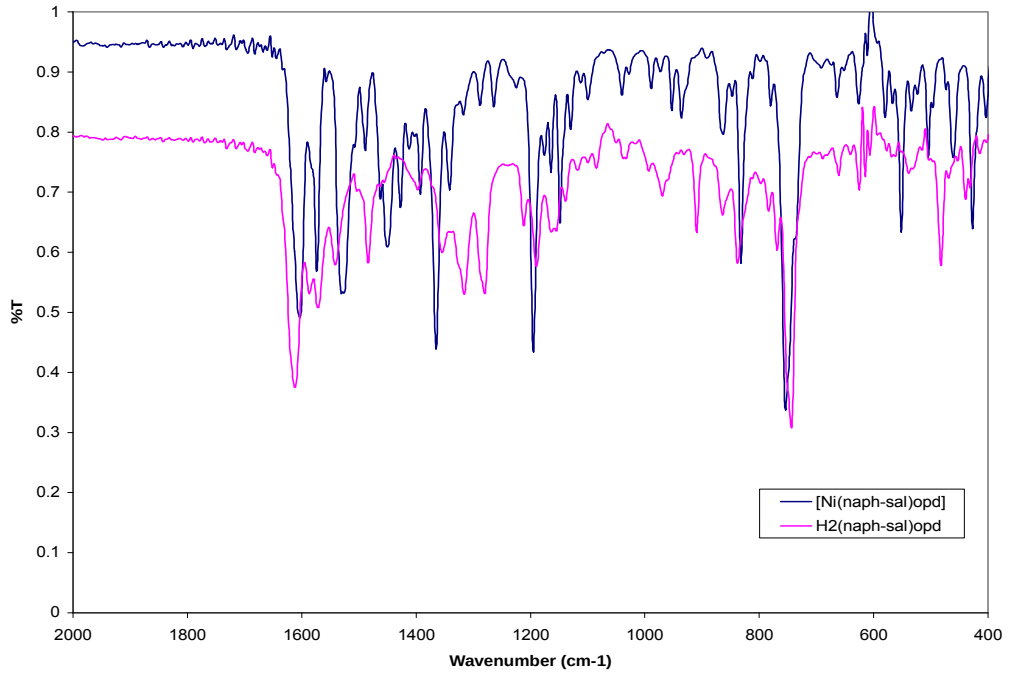

Fig. 4.3.2 IR spectra of complex NiL^4 and its ligand H_2(naph-Clsal)opd: representative spectra for the unsymmetrical complexes of nickel(II) and the ligands

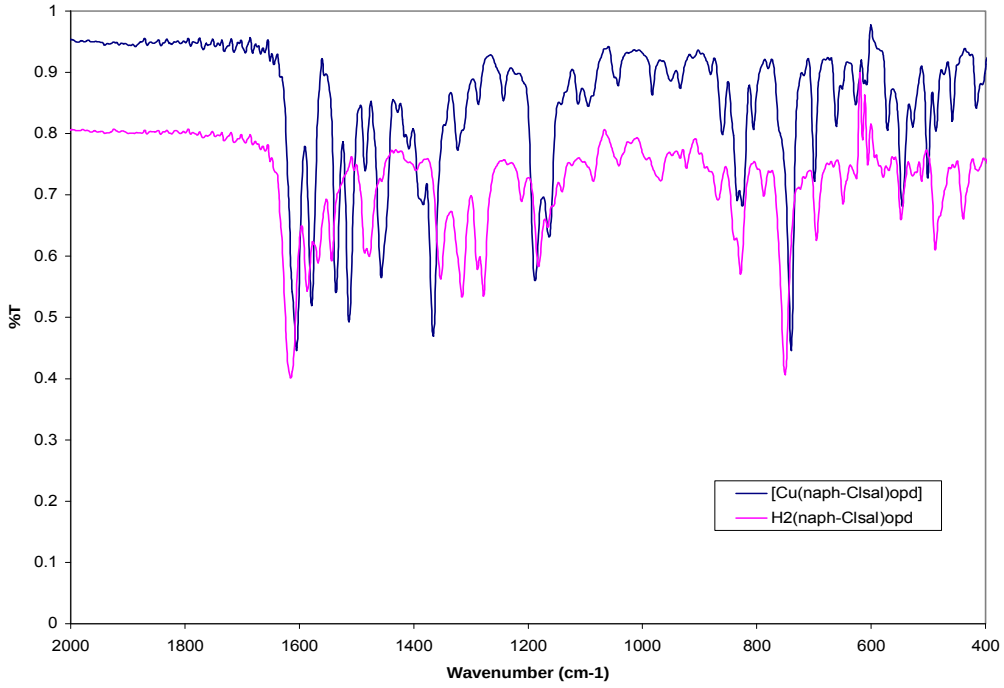

Fig. 4.3.3 IR spectra of complex CuL^1 and its ligand H_2(naph-Clsal)opd: representative spectra for the unsymmetrical complexes of copper(II) and the ligands

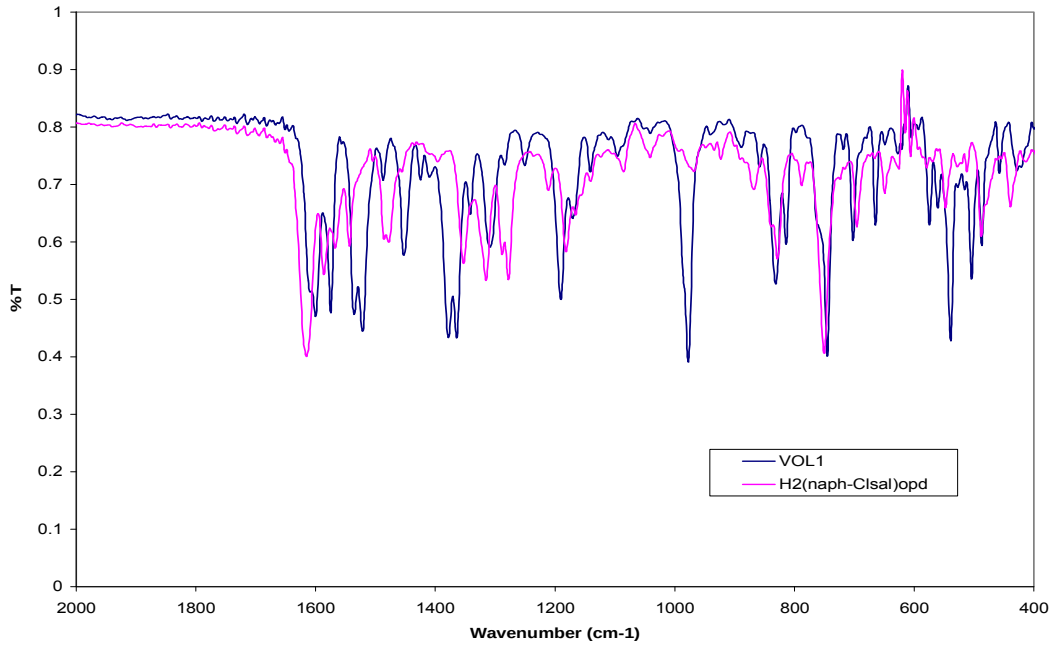

Fig. 4.3.4 IR spectra of complex VOL^1 and its ligand H_2(naph-Clsal)opd: representative spectra for the unsymmetrical complexes of oxovanadium(IV) and the ligands

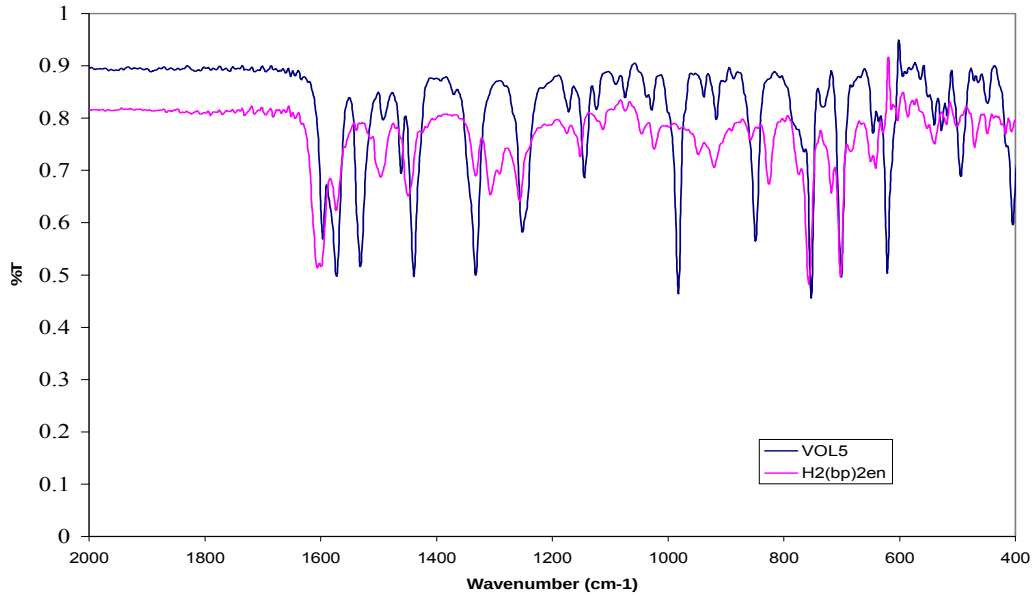

Fig. 4.3.5 IR spectra of complex VOL^5 and its ligand H_2bp_2en: representative spectra for the benzophenoneimine

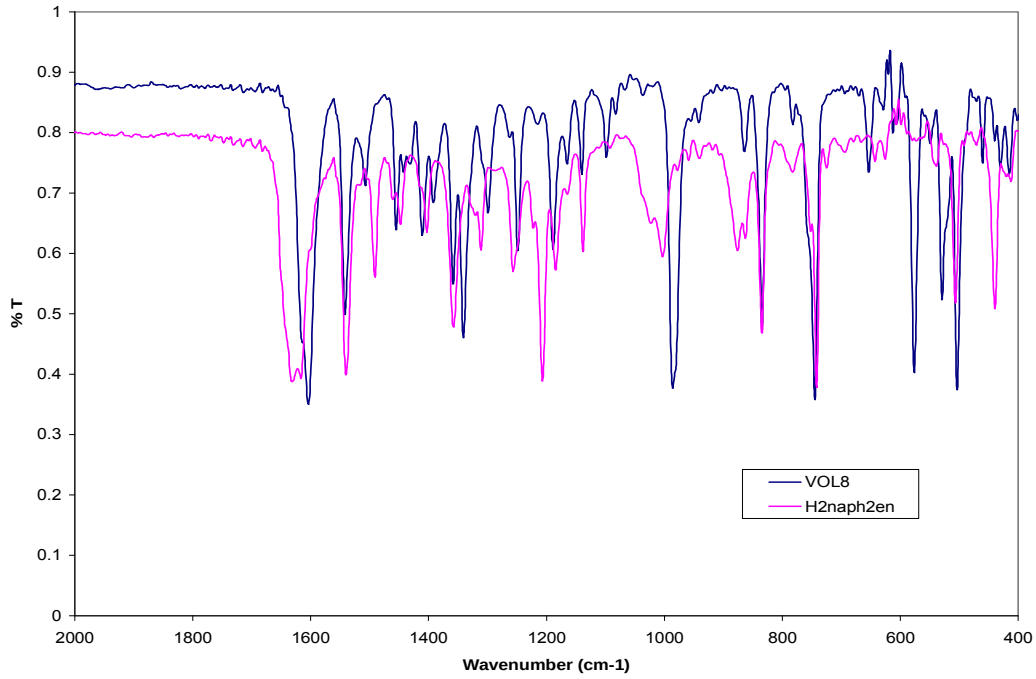

Fig. 4.3.6 IR spectra of complex VOL^8 and its ligand H_2naph_2en: representative Spectra for the naphthaldiimine

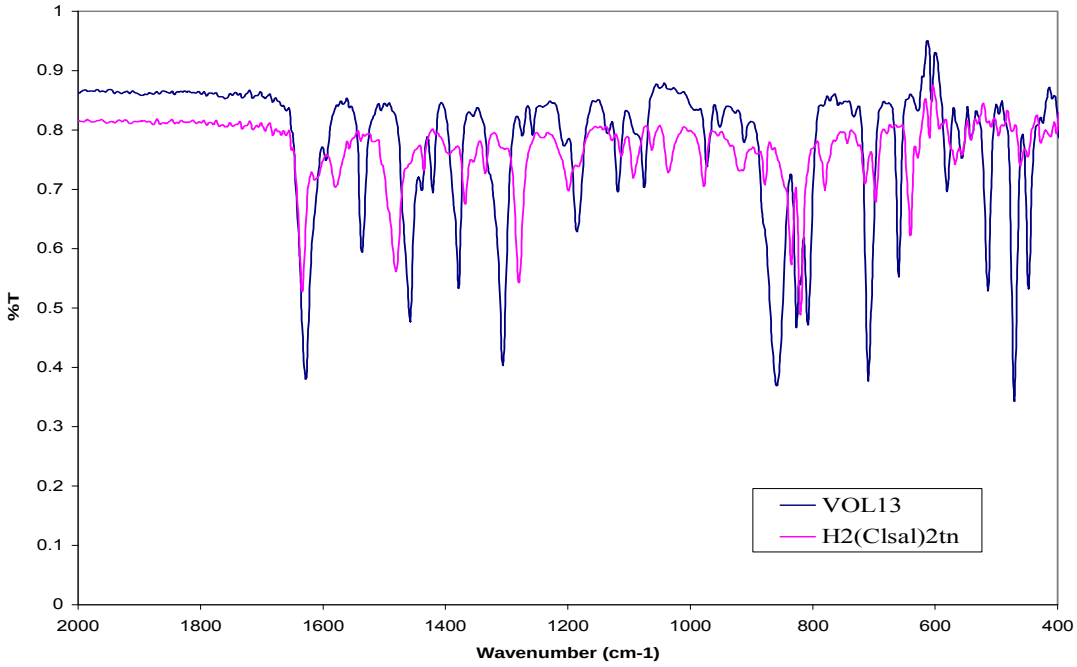

Fig. 4.3.7 IR spectra of complex VOL[13] and its ligand H_2Clsal_2tn: representative spectra for the chlorosalicylaldiimine

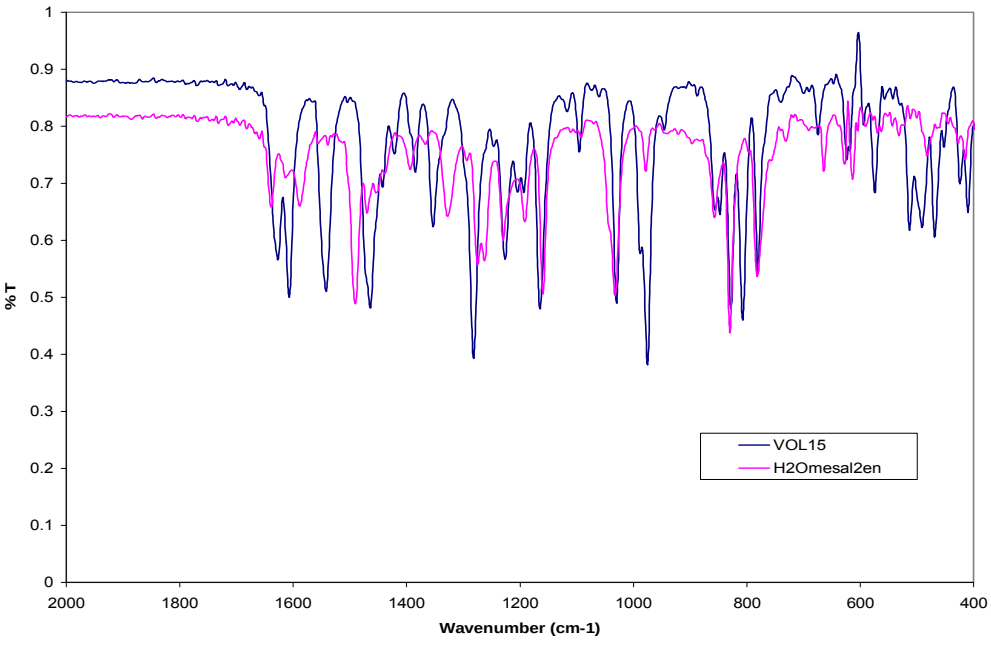

Fig. 4.3.8 IR spectra of complex VOL[15] and its ligand $H_2Omesal_2en$: representative spectra for the methoxysalicylaldiimine

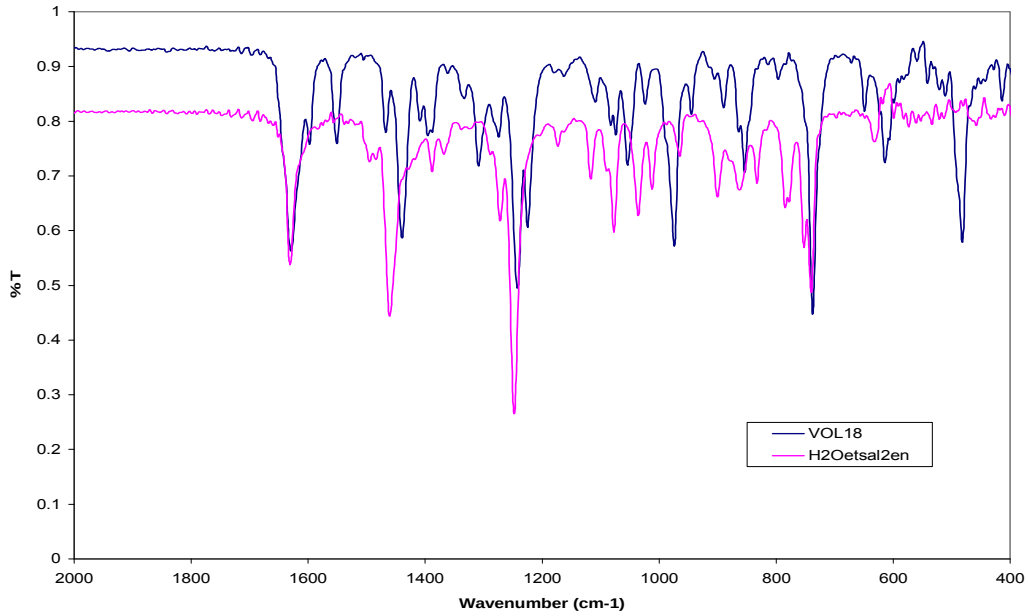

Fig. 4.3.9 IR spectra of complex VOL[18] and its ligand H_2Oetsal$_2$en: representative spectra for the ethoxysalicylaldiimine

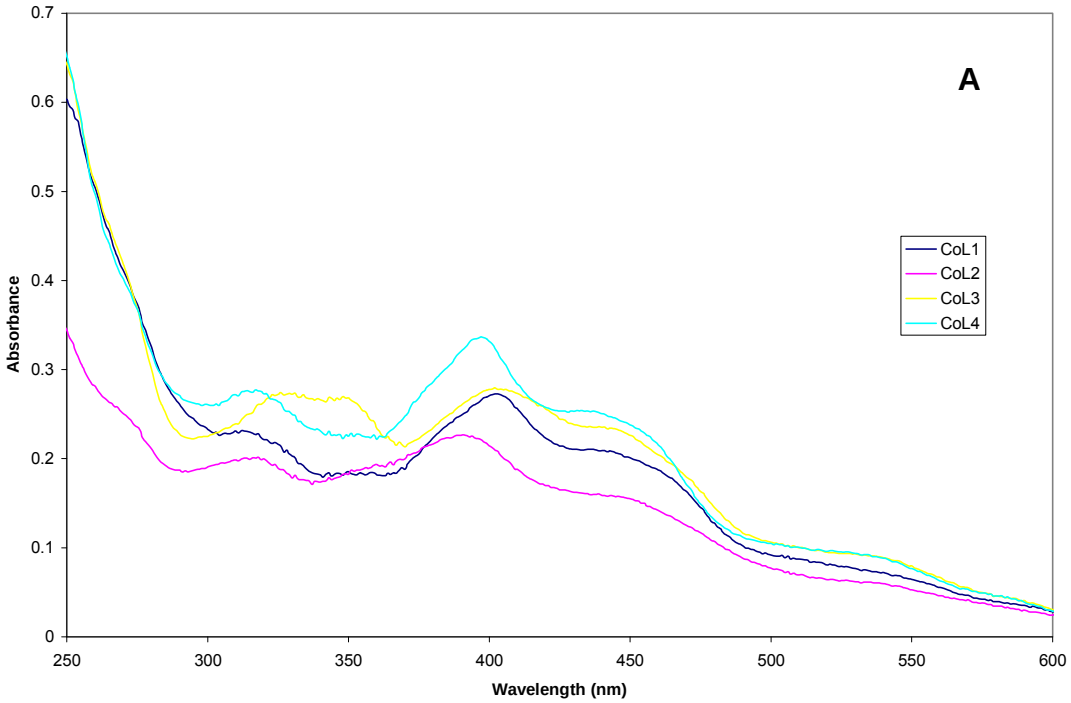

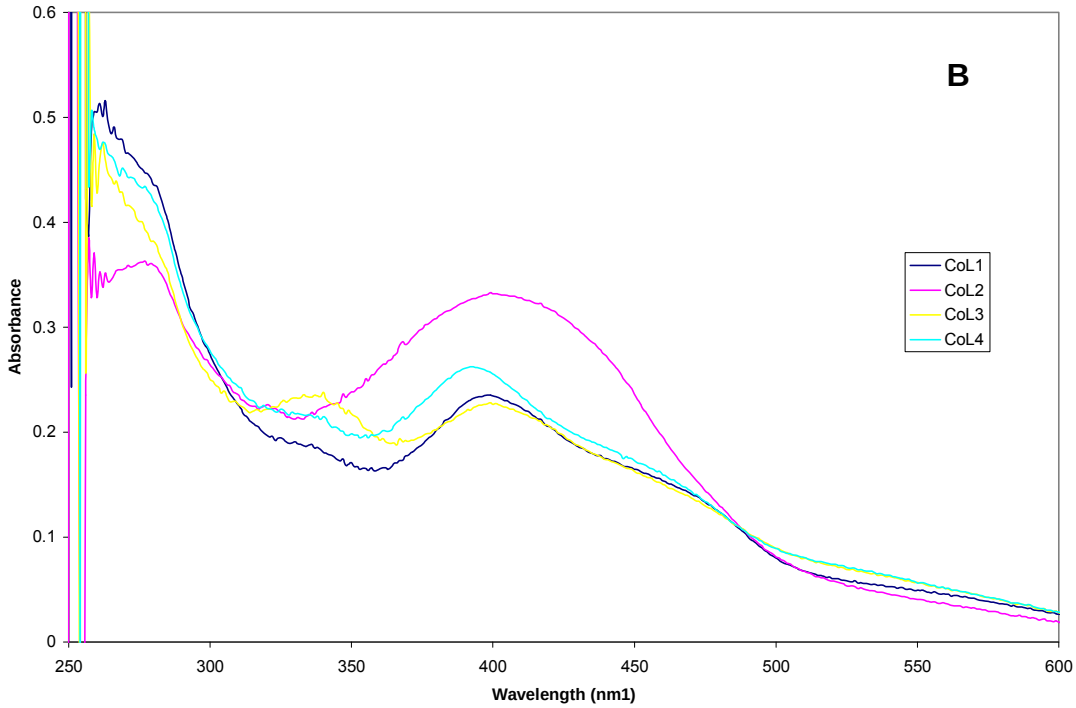

A: [complexes] = 10^{-5} in $CHCl_3$; B: [complexes] = 10^{-5} in DMSO

Fig. 4.4.1 Electronic spectra of the unsymmetrical cobalt(II) complexes

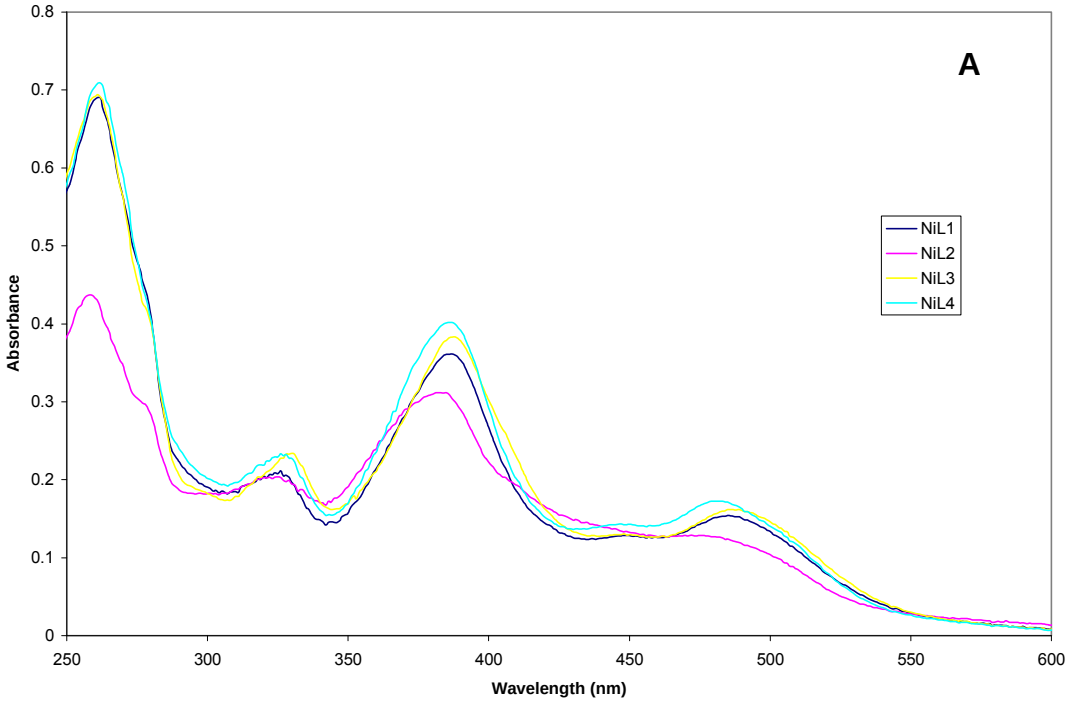

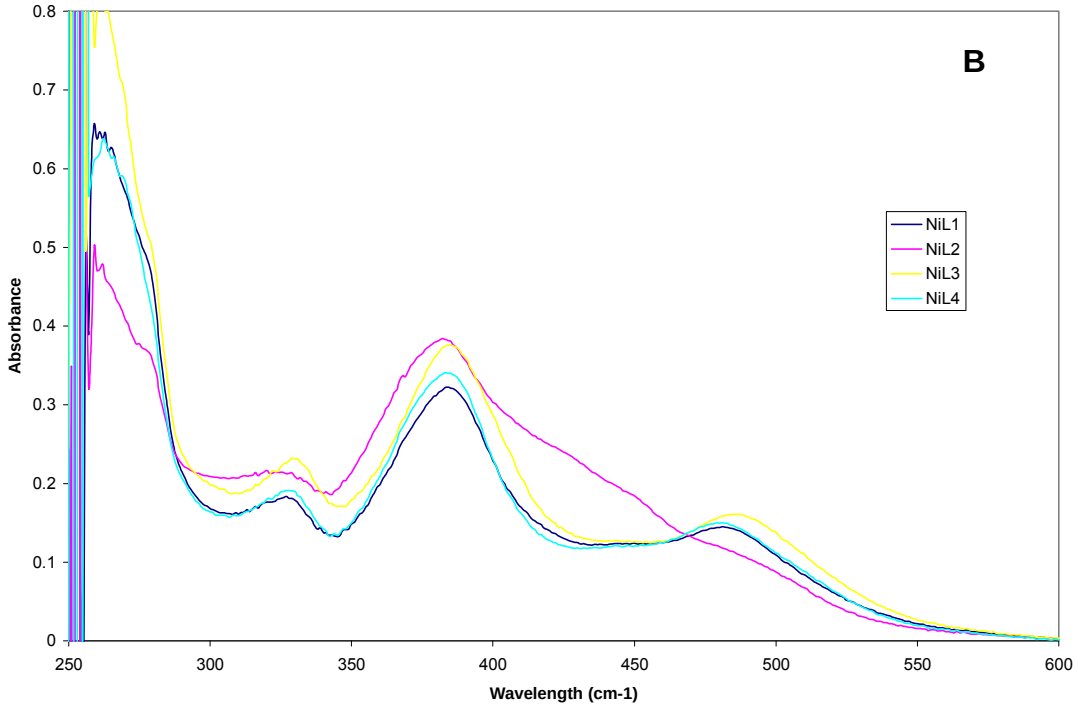

A: [complexes] = 10^{-5} in $CHCl_3$; B: [complexes] = 10^{-5} in DMSO

Fig. 4.4.2 Electronic spectra of the unsymmetrical nickel(II) complexes

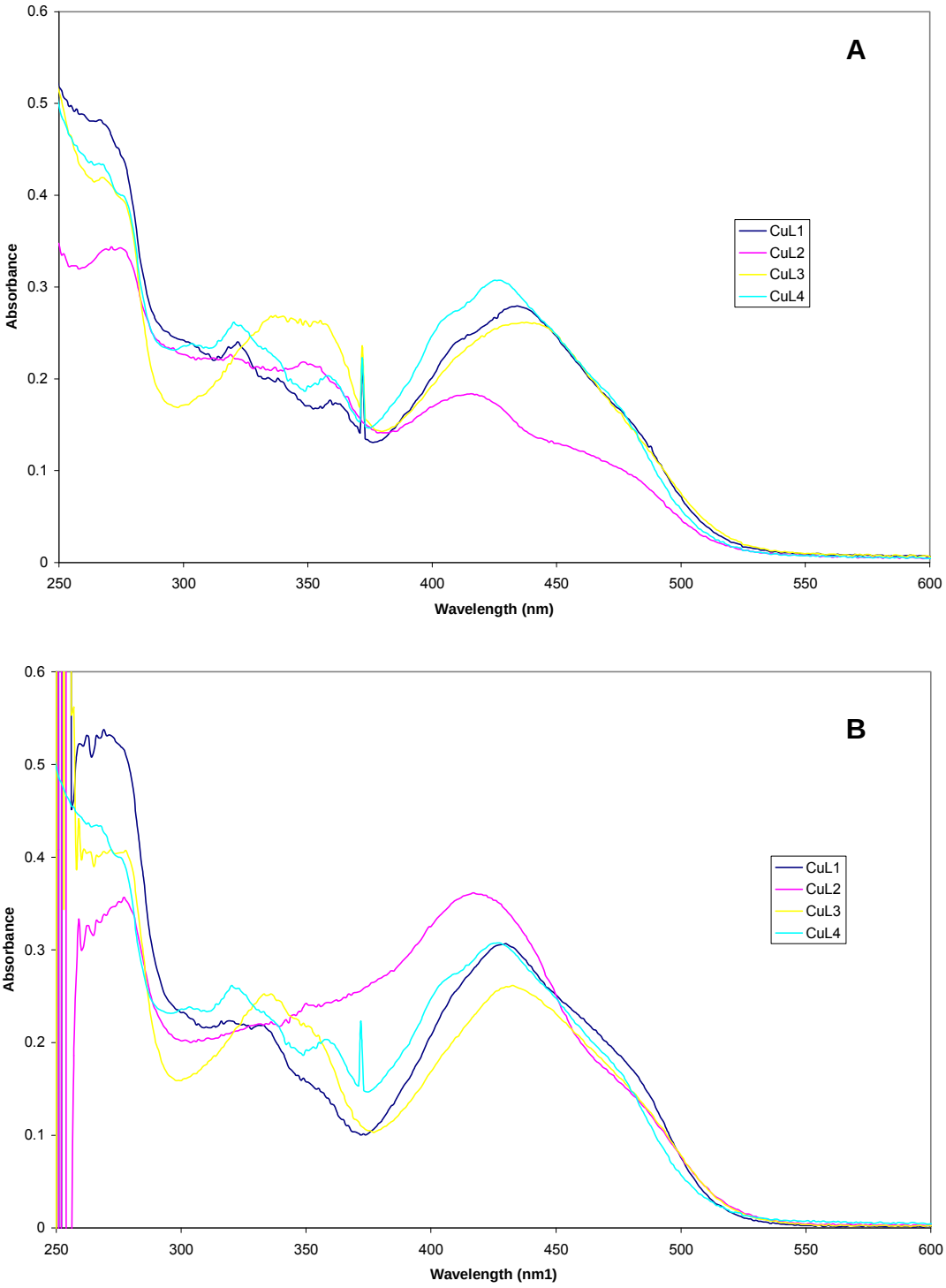

A: [complexes] = 10^{-5} in $CHCl_3$; B: [complexes] = 10^{-5} in DMSO

Fig. 4.4.3 Electronic spectra of the unsymmetrical copper(II) complexes

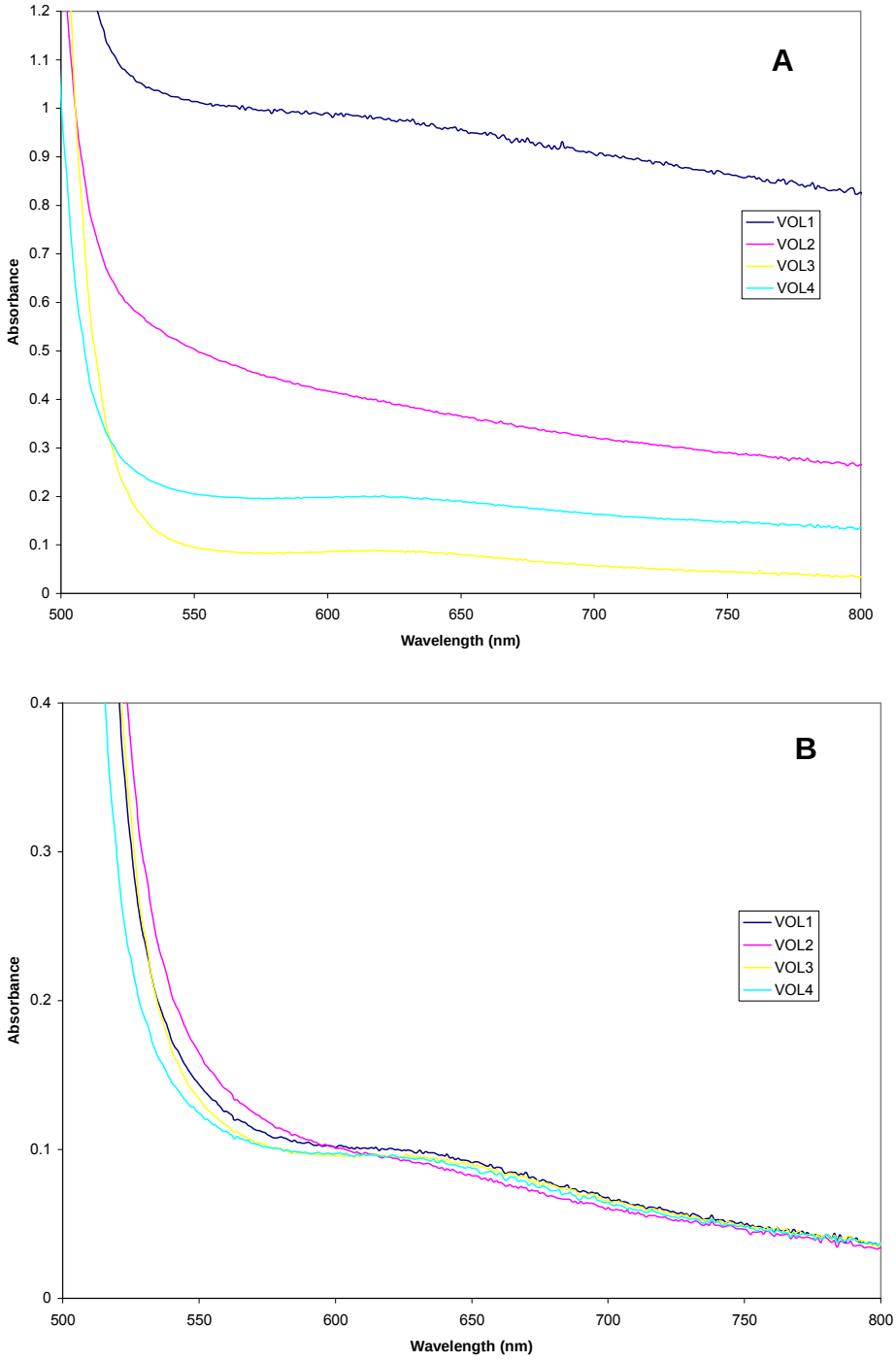

A: [complexes] = 10^{-3} in $CHCl_3$; B: [complexes] = 10^{-3} in DMSO

Fig. 4.4.4 Electronic spectra of the unsymmetrical oxovanadium(IV) complexes

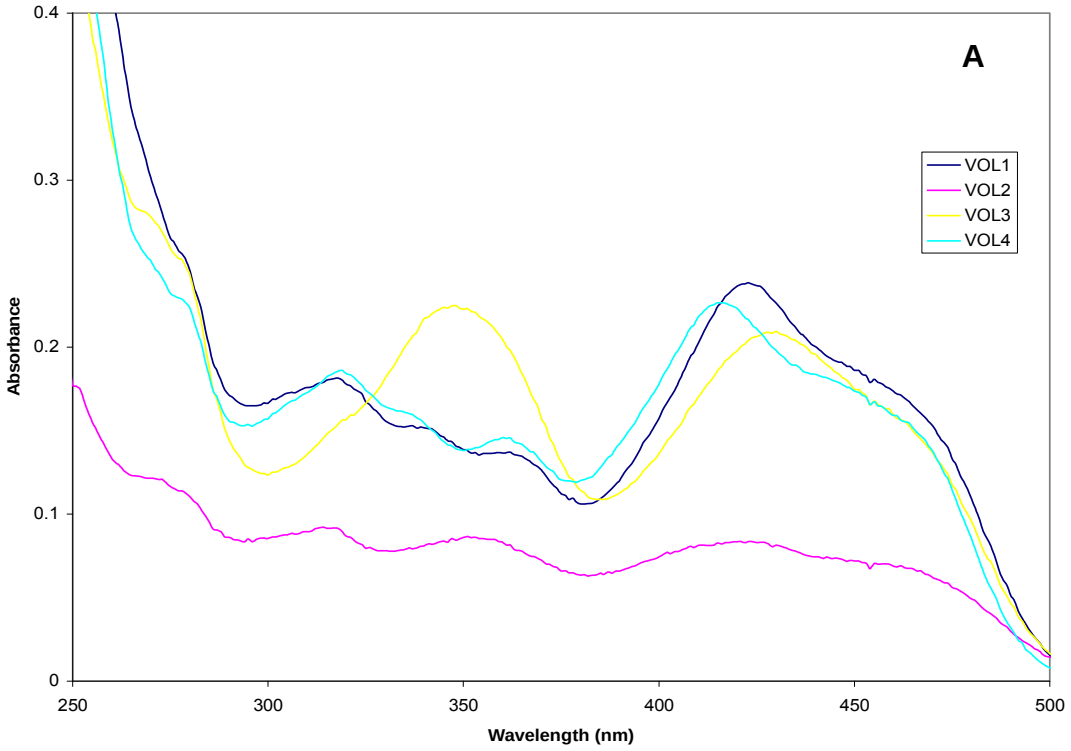

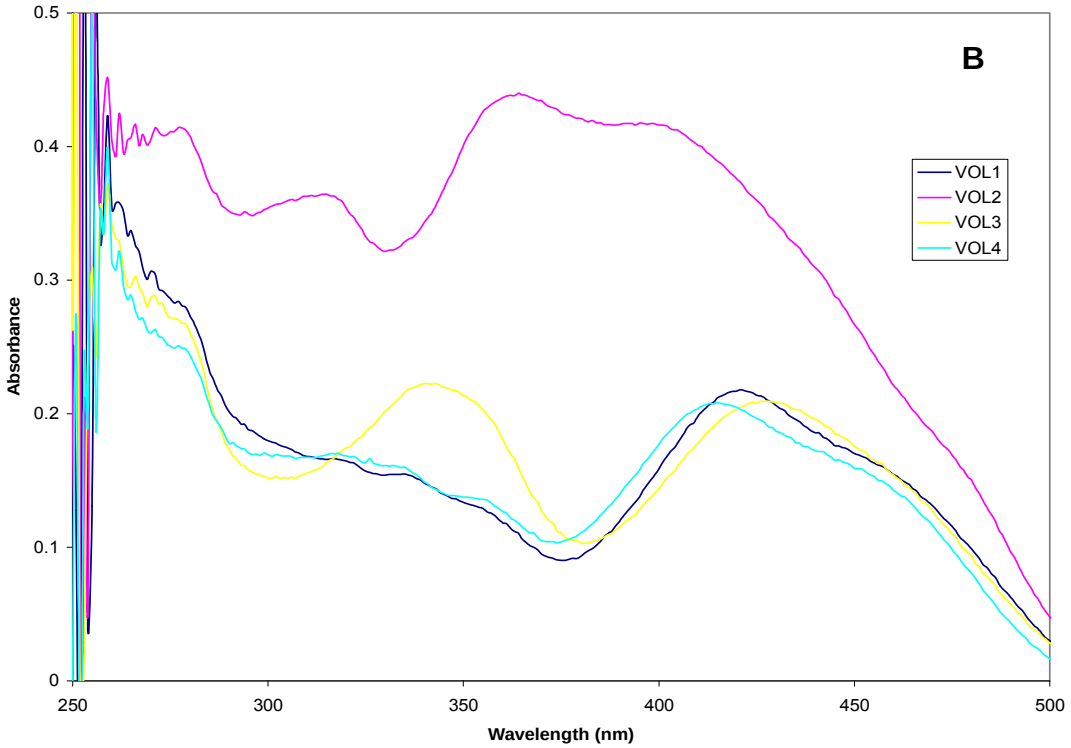

A: [complexes] = 10^{-5} in $CHCl_3$; B: [complexes] = 10^{-5} in DMSO

Fig. 4.4.5 Electronic spectra of the unsymmetrical oxovanadium(IV) complexes

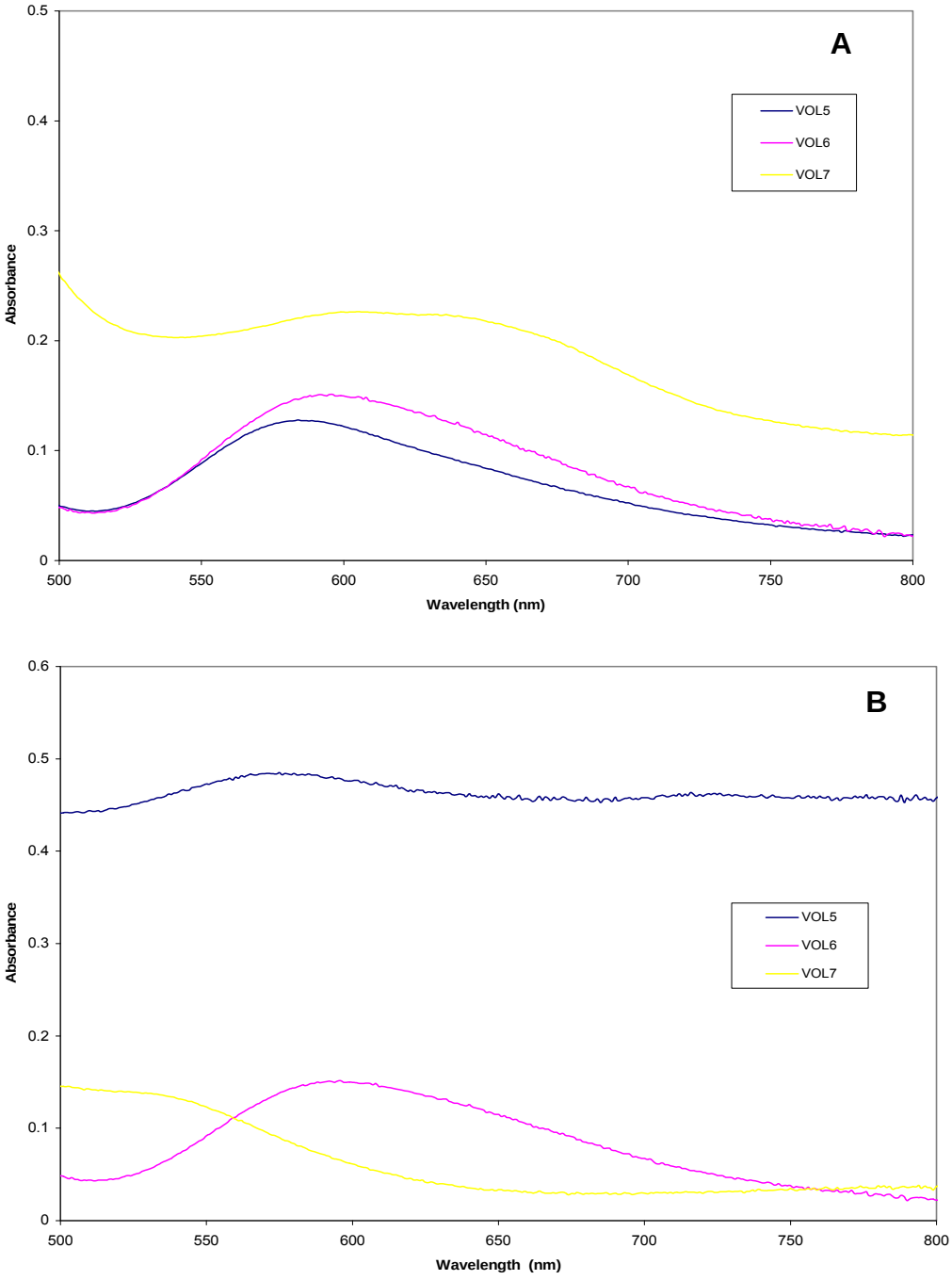

A: [complexes] = 10^{-3} in $CHCl_3$; B: [complexes] = 10^{-3} in DMSO

Fig. 4.4.6 Electronic spectra of the benzophenoneiminatooxovanadium(IV) complexes

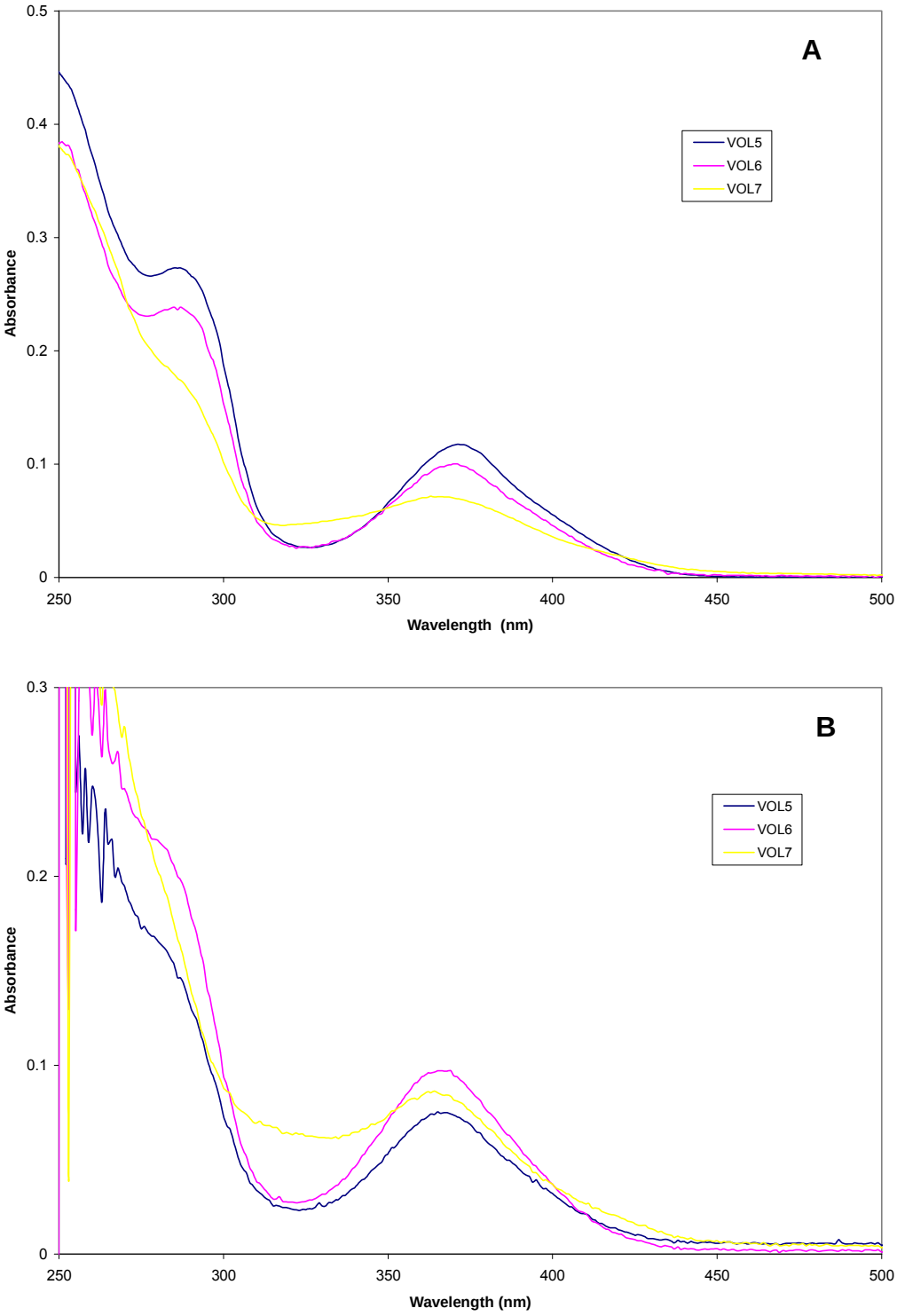

A: [complexes] = 10^{-5} in $CHCl_3$; B: [complexes] = 10^{-5} in DMSO

Fig. 4.4.7 Electronic spectra of the benzophenoneiminatooxovanadium(IV) complexes

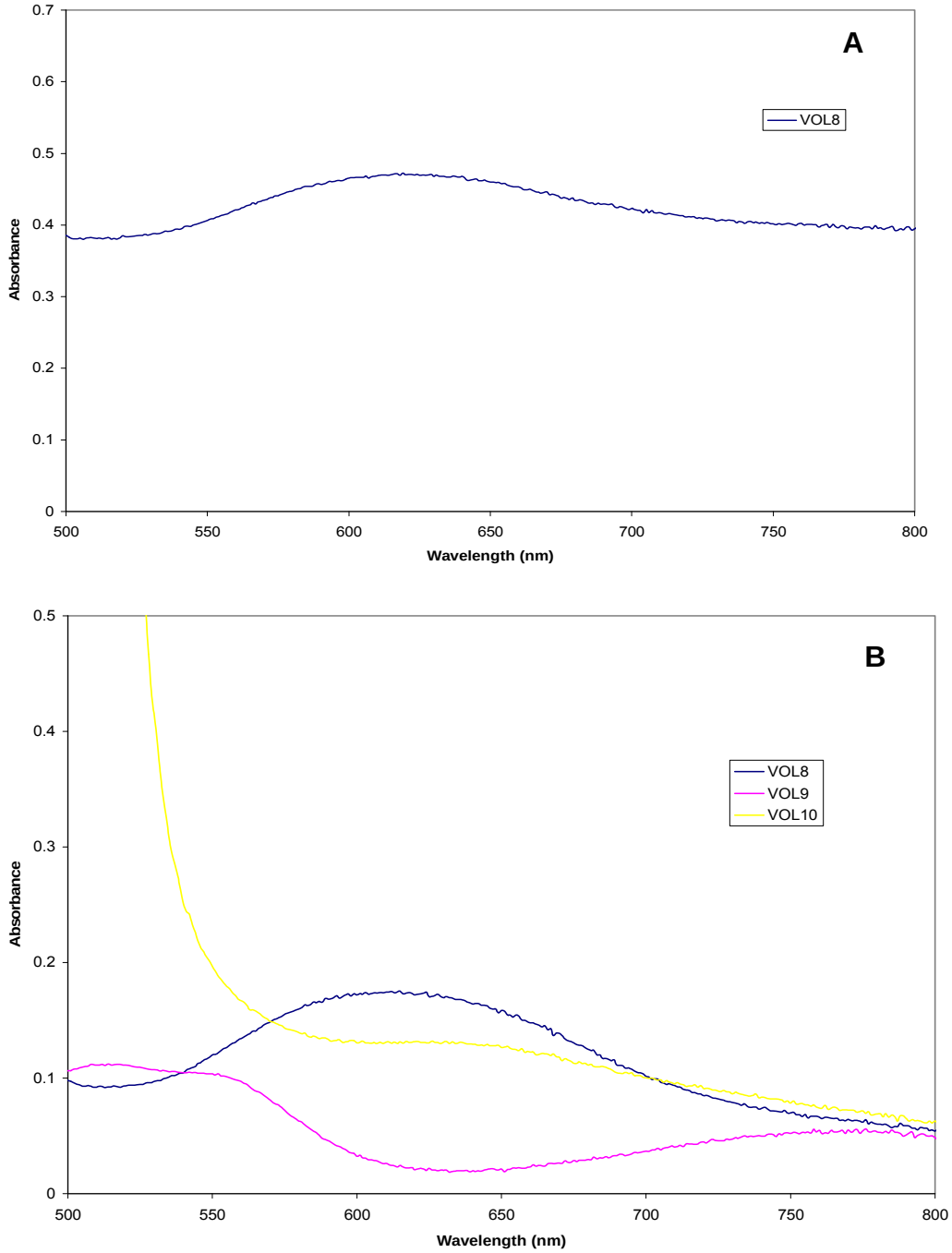

A: [complexes] = 10^{-3} in $CHCl_3$; B: [complexes] = 10^{-3} in DMSO

Fig. 4.4.8 Electronic spectra of the napthaldimiinatooxovanadium(IV) complexes

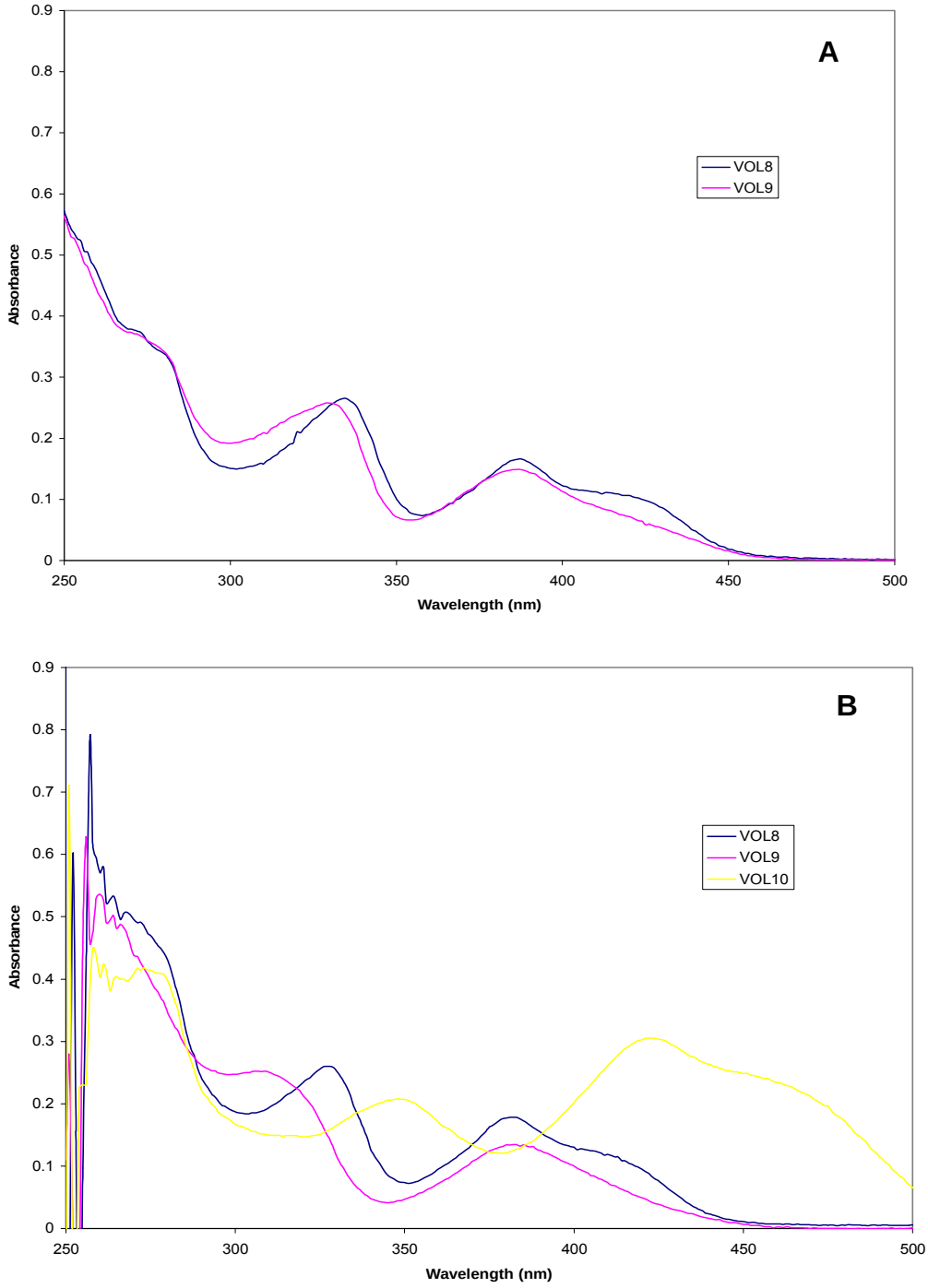

A: [complexes] = 10^{-5} in $CHCl_3$; B: [complexes] = 10^{-5} in DMSO

Fig. 4.4.9 Electronic spectra of the napthaldiiminatooxovanadium(IV) complexes

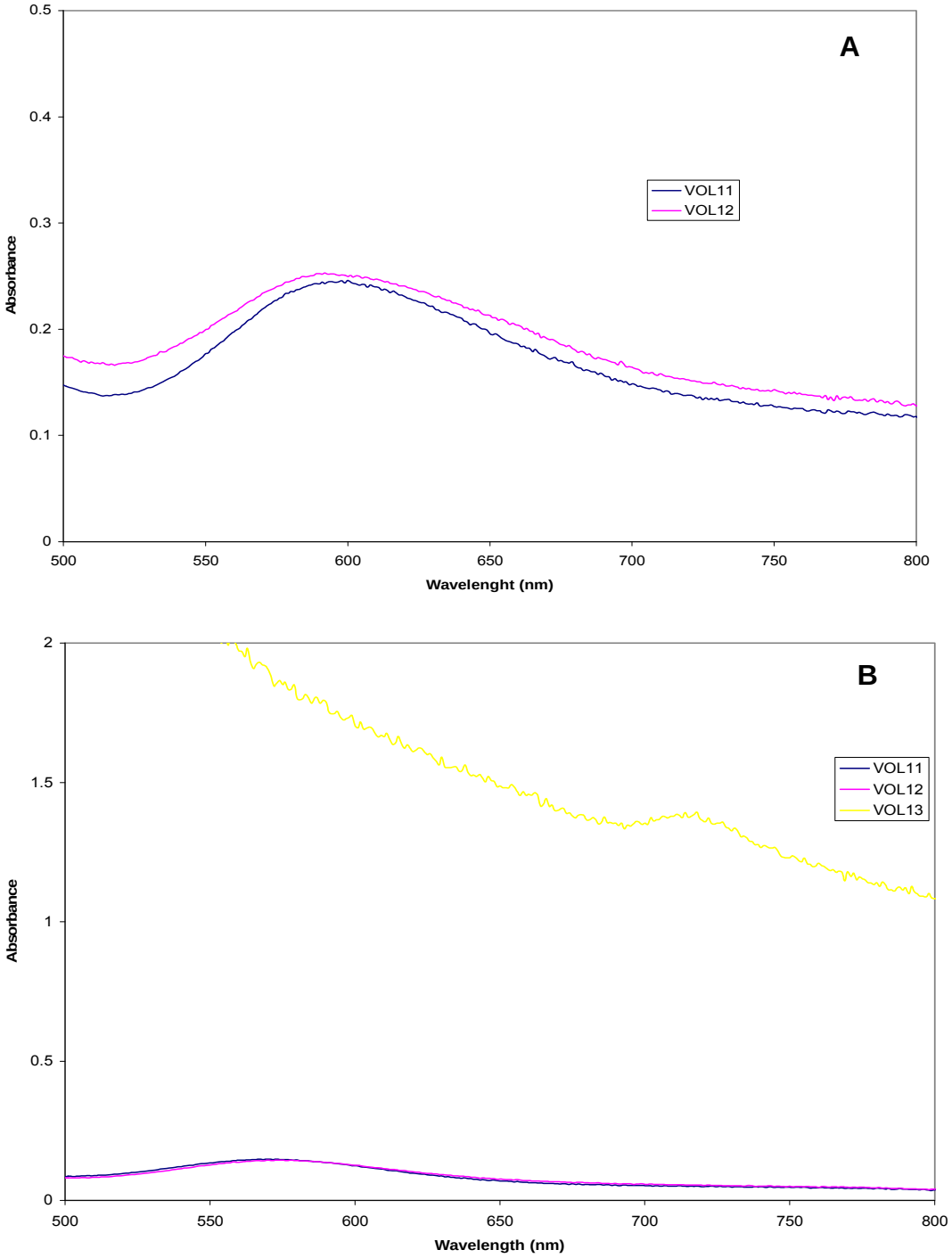

A: [complexes] = 10^{-3} in $CHCl_3$; B: [complexes] = 10^{-3} in DMSO

Fig. 4.4.10 Electronic spectra of the chlorosalicylaldiiminatooxovanadium(IV) complexes

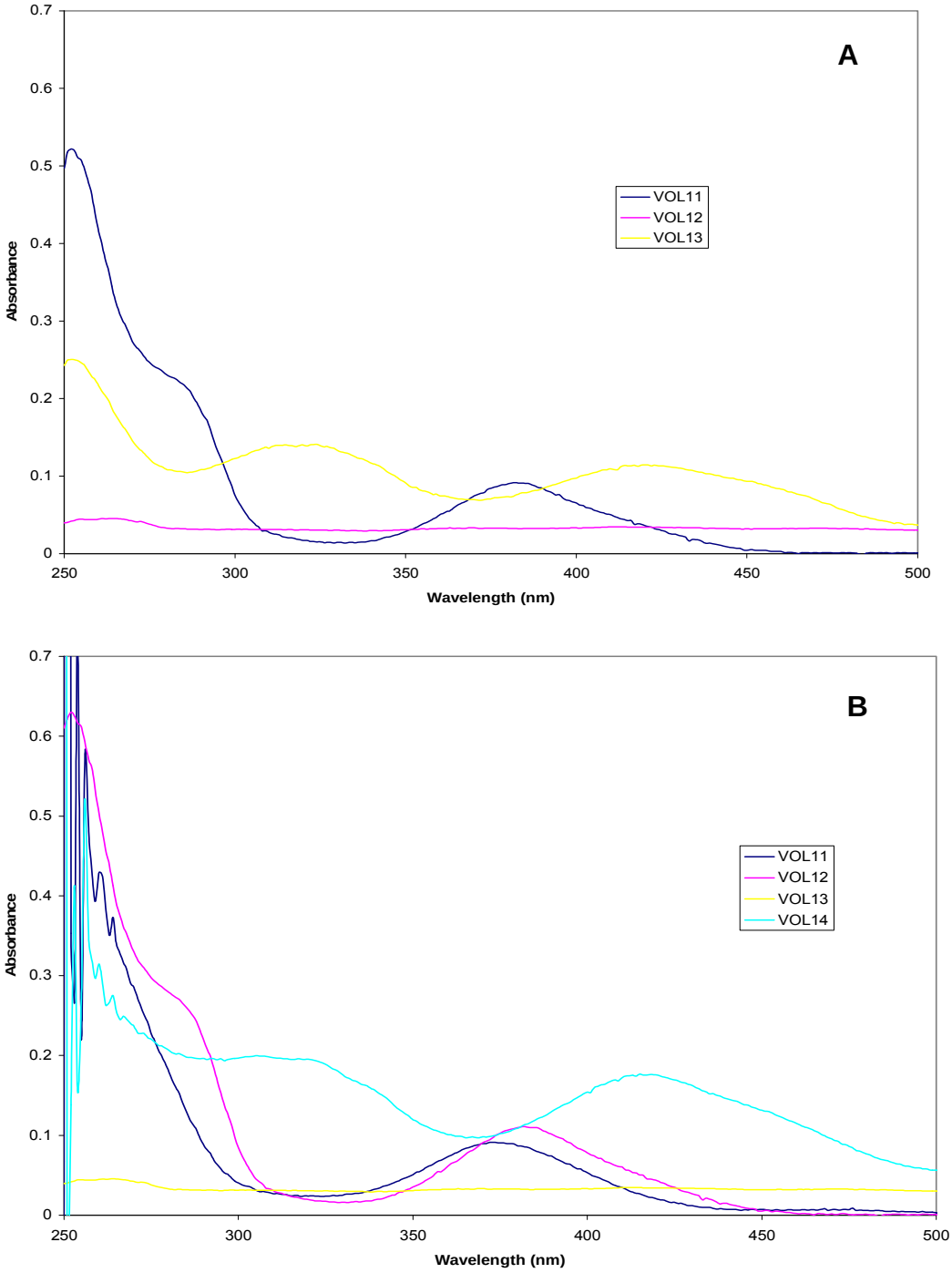

A: [complexes] = 10^{-5} in $CHCl_3$; B: [complexes] = 10^{-5} in DMSO

Fig. 4.4.11 Electronic spectra of the chlorosalicylaldiiminatooxovanadium(IV) complexes

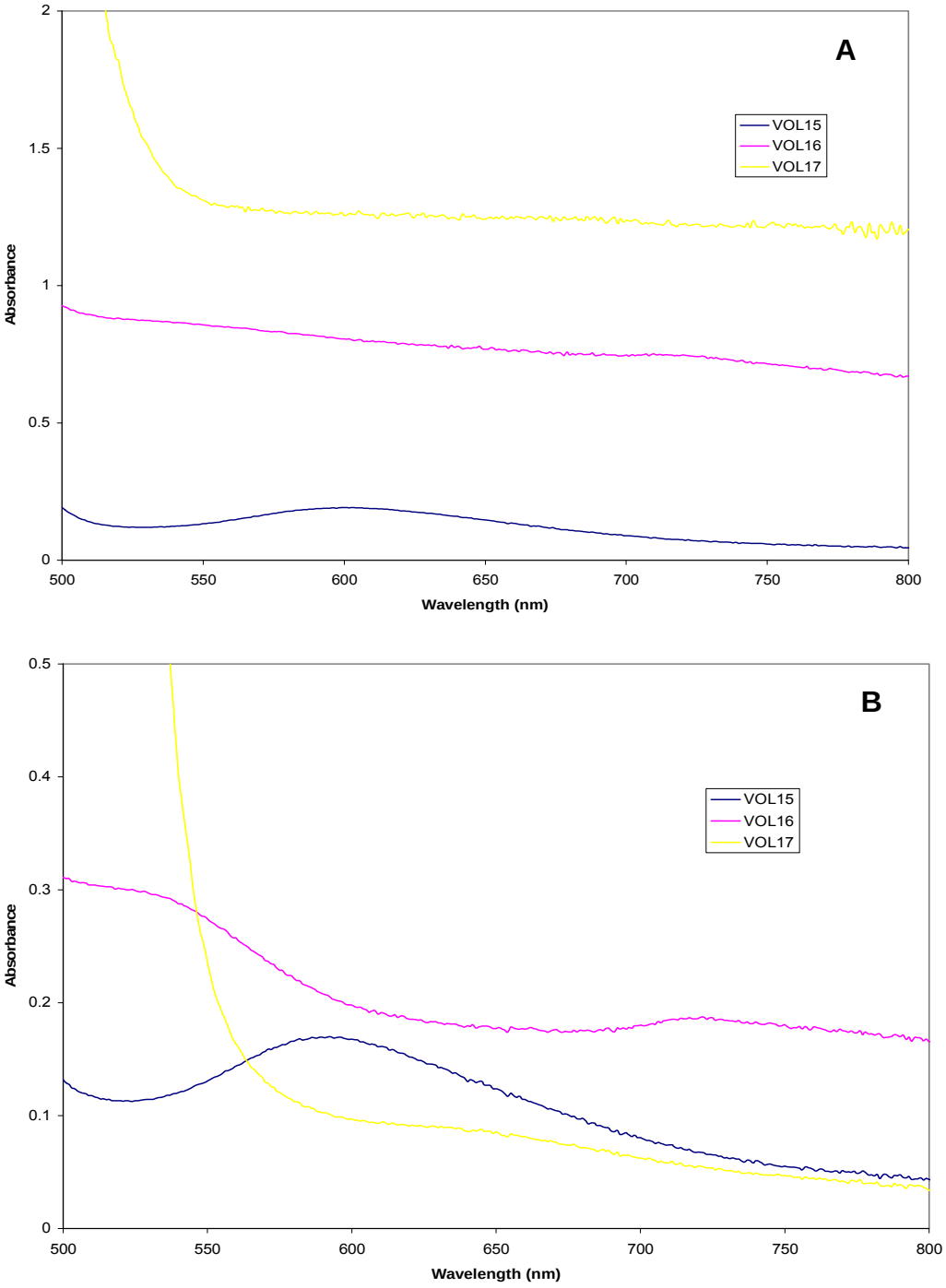

A: [complexes] = 10^{-3} in $CHCl_3$; B: [complexes] = 10^{-3} in DMSO

Fig. 4.4.12 Electronic spectra of the methoxysalicylaldiiminatooxovanadium(IV) complexes

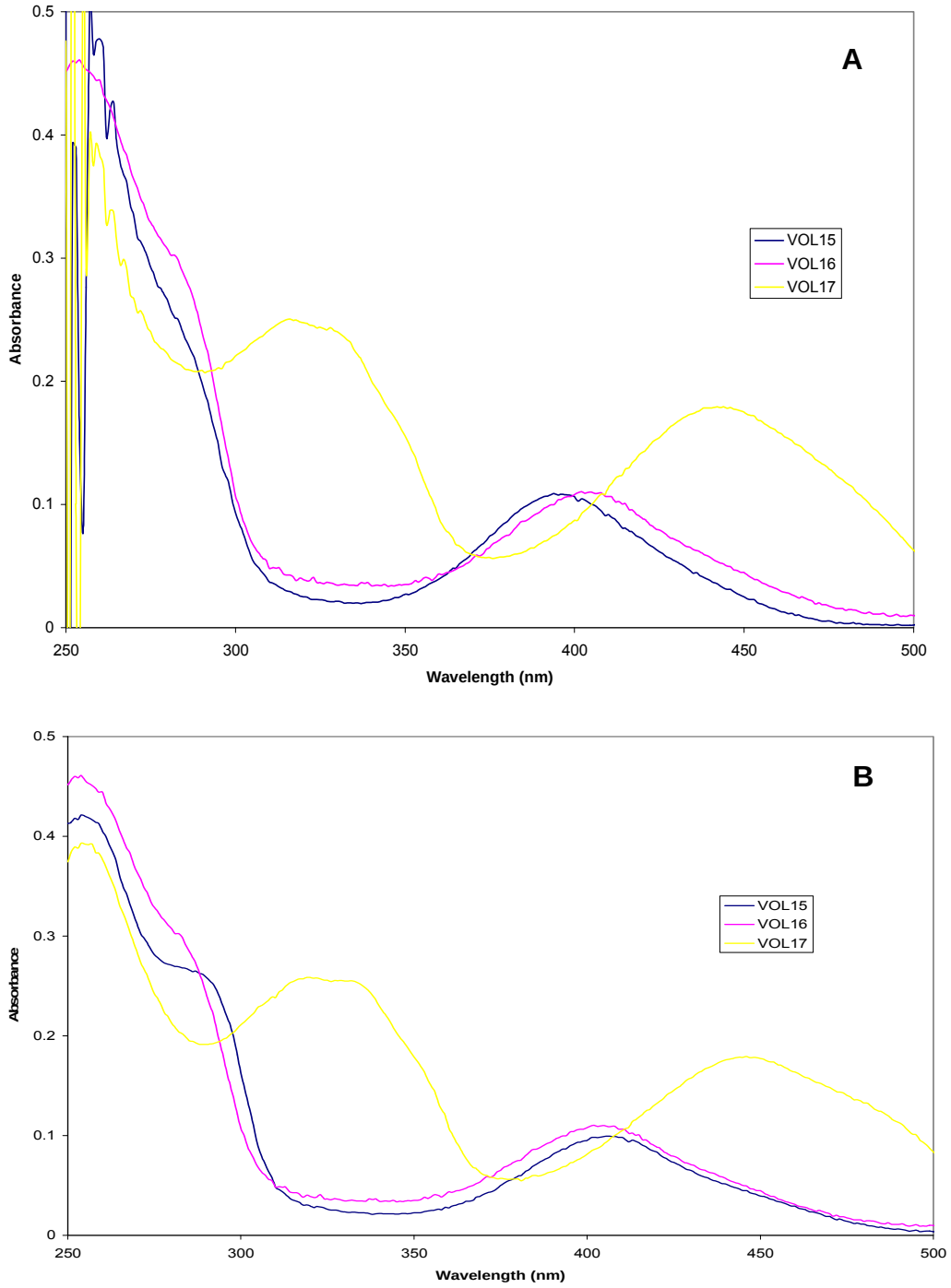

A: [complexes] = 10^{-5} in $CHCl_3$; B: [complexes] = 10^{-5} in DMSO

Fig. 4.4.13 Electronic spectra of the methoxysalicylaldiiminatooxovanadium(IV) complexes

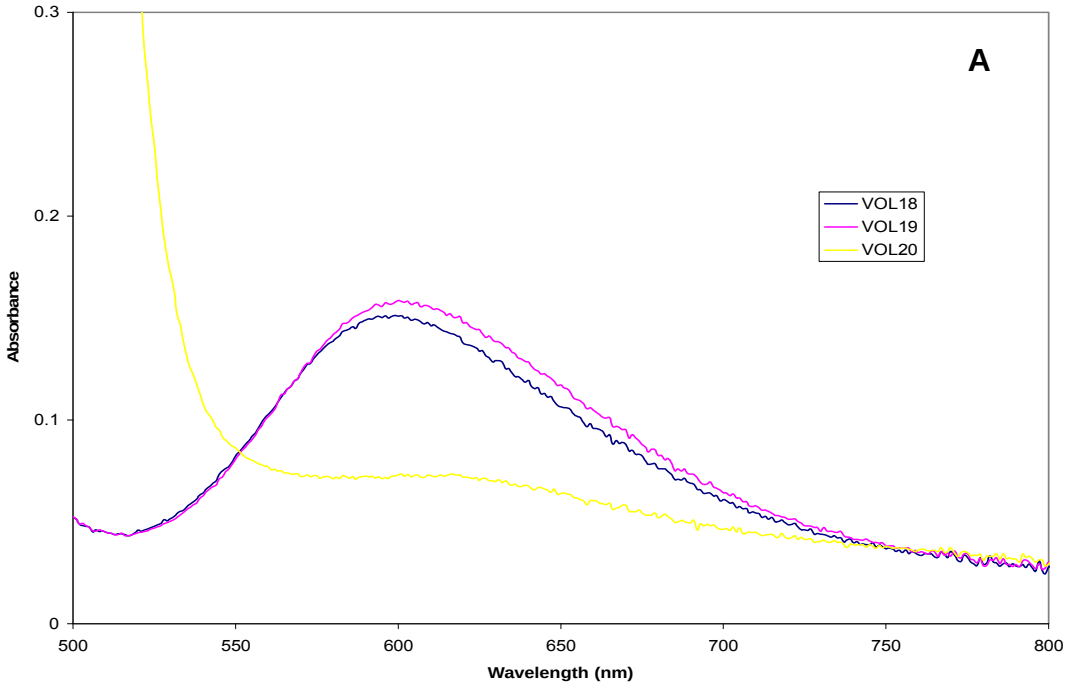

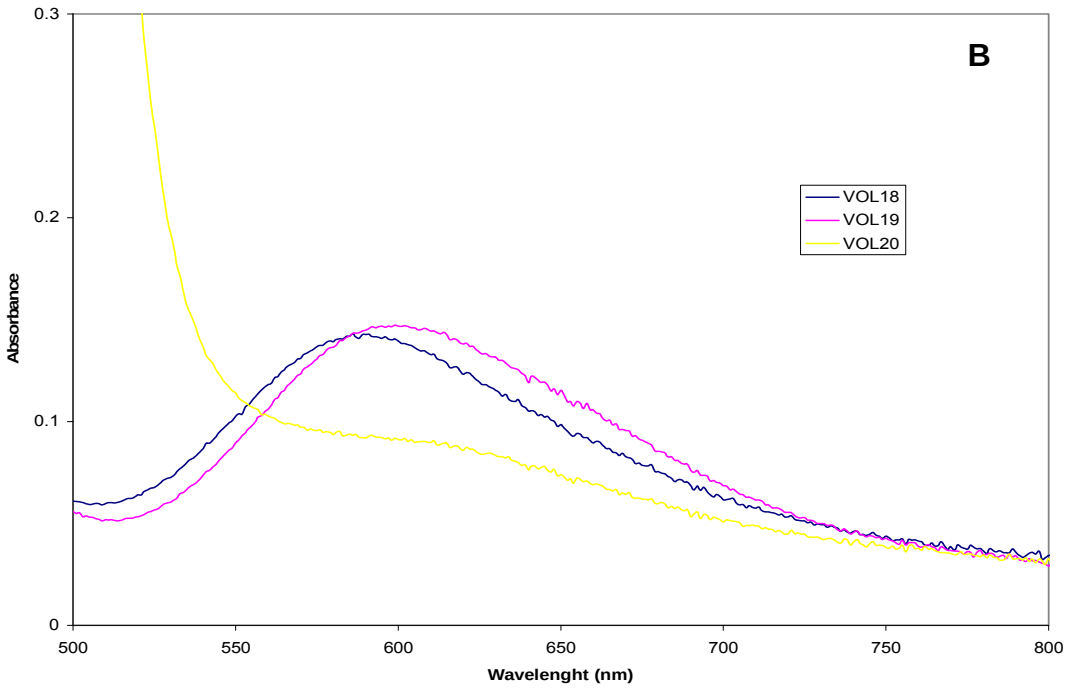

A: [complexes] = 10^{-3} in $CHCl_3$; B: [complexes] = 10^{-3} in DMSO

Fig. 4.4.14 Electronic spectra of the ethoxysalicylaldiiminatooxovanadium(IV) complexes

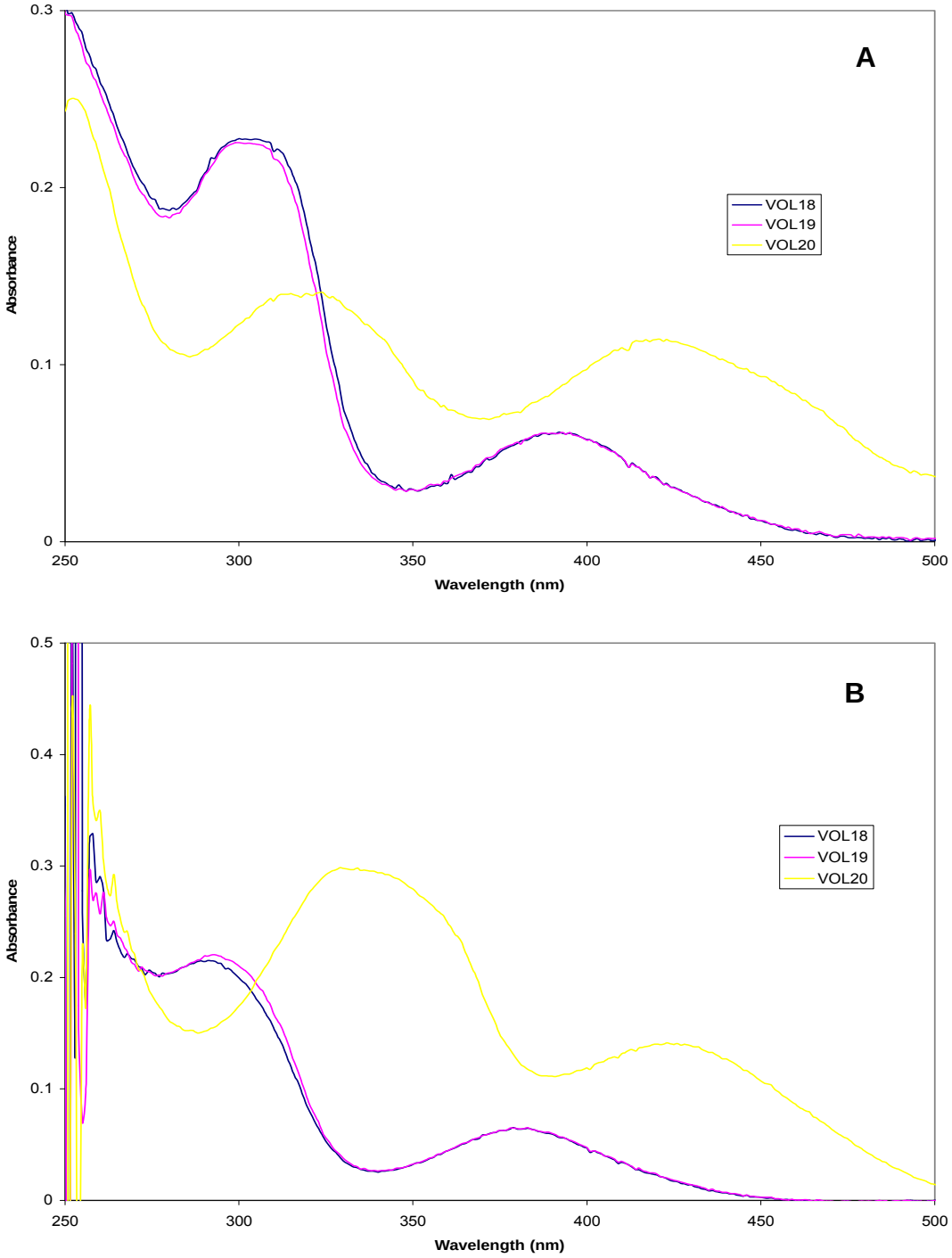

A: [complexes] = 10^{-5} in $CHCl_3$; B: [complexes] = 10^{-5} in DMSO

Fig. 4.4.15 Electronic spectra of the ethoxysalicylaldiiminatooxovanadium(IV) complexes

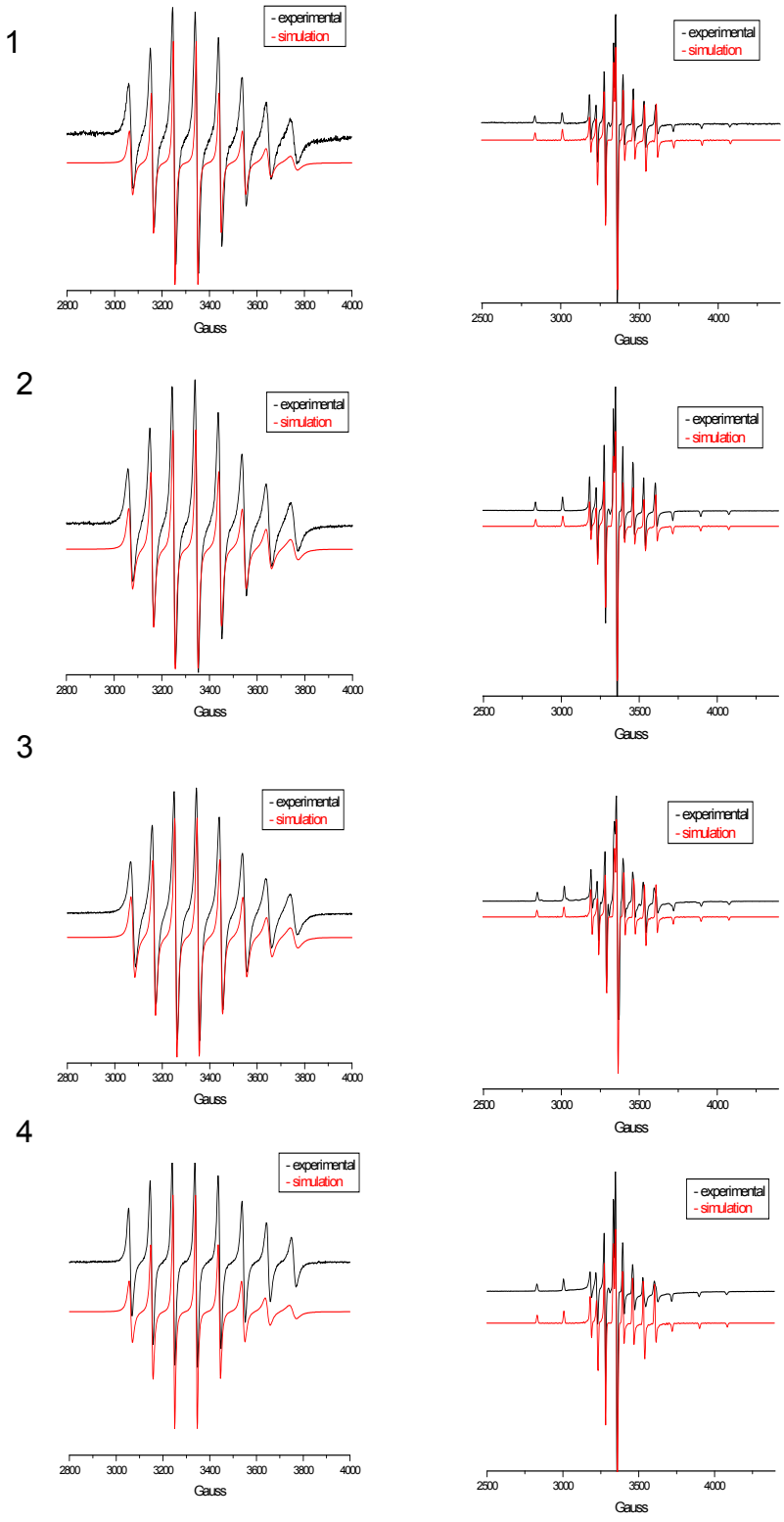

Fig. 4.5.1 EPR spectra of complexes 1 [VOL^1], 2 [VOL^2], 3 [VOL^3] and 4 [VOL^4] at 290K (left) and 120 K (right) in toluene/CH_2Cl_2

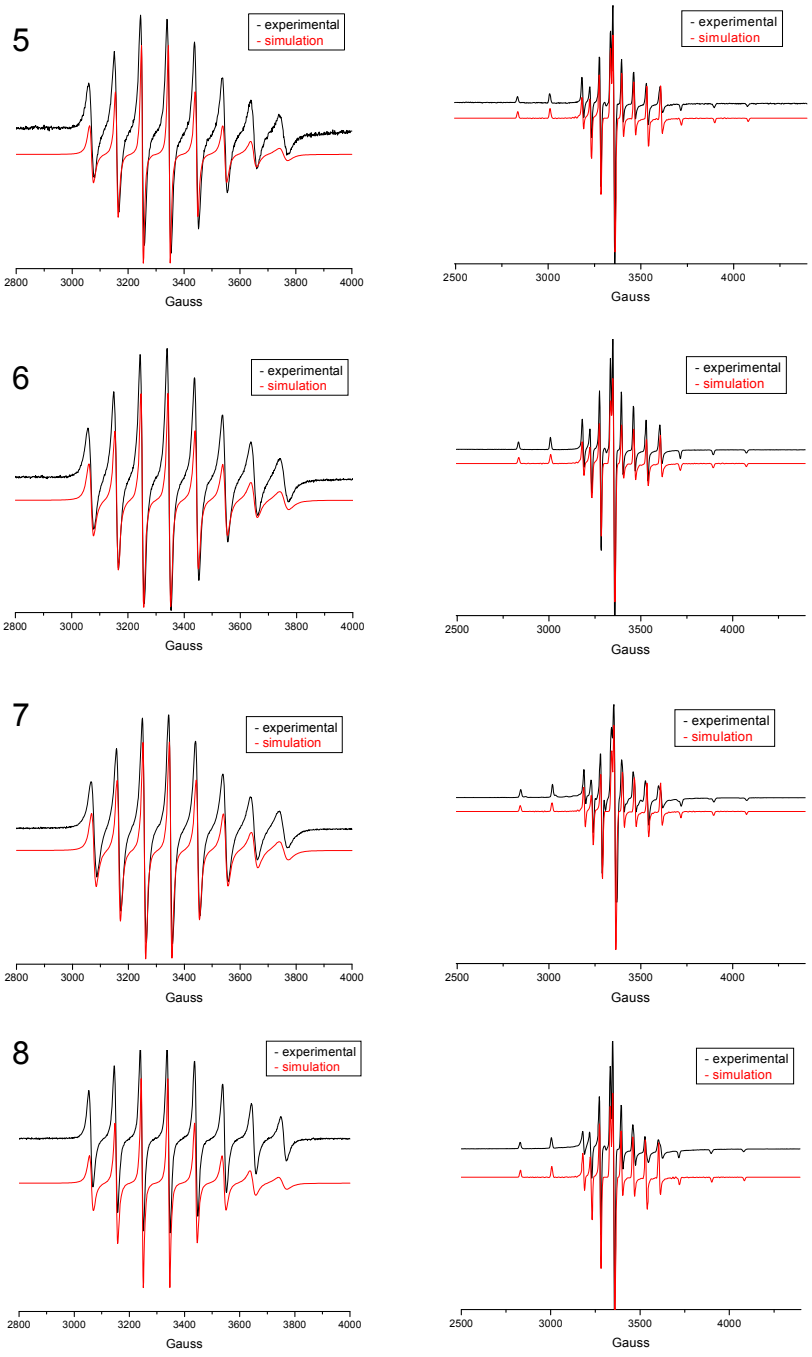

Fig. 4.5.2 EPR spectra of complexes 5 [VOL^5], 6[VOL^6], 7 [VOL^7] and 8 [VOL^{12}] at 290K (left) and 120 K (right) in toluene/CH_2Cl_2

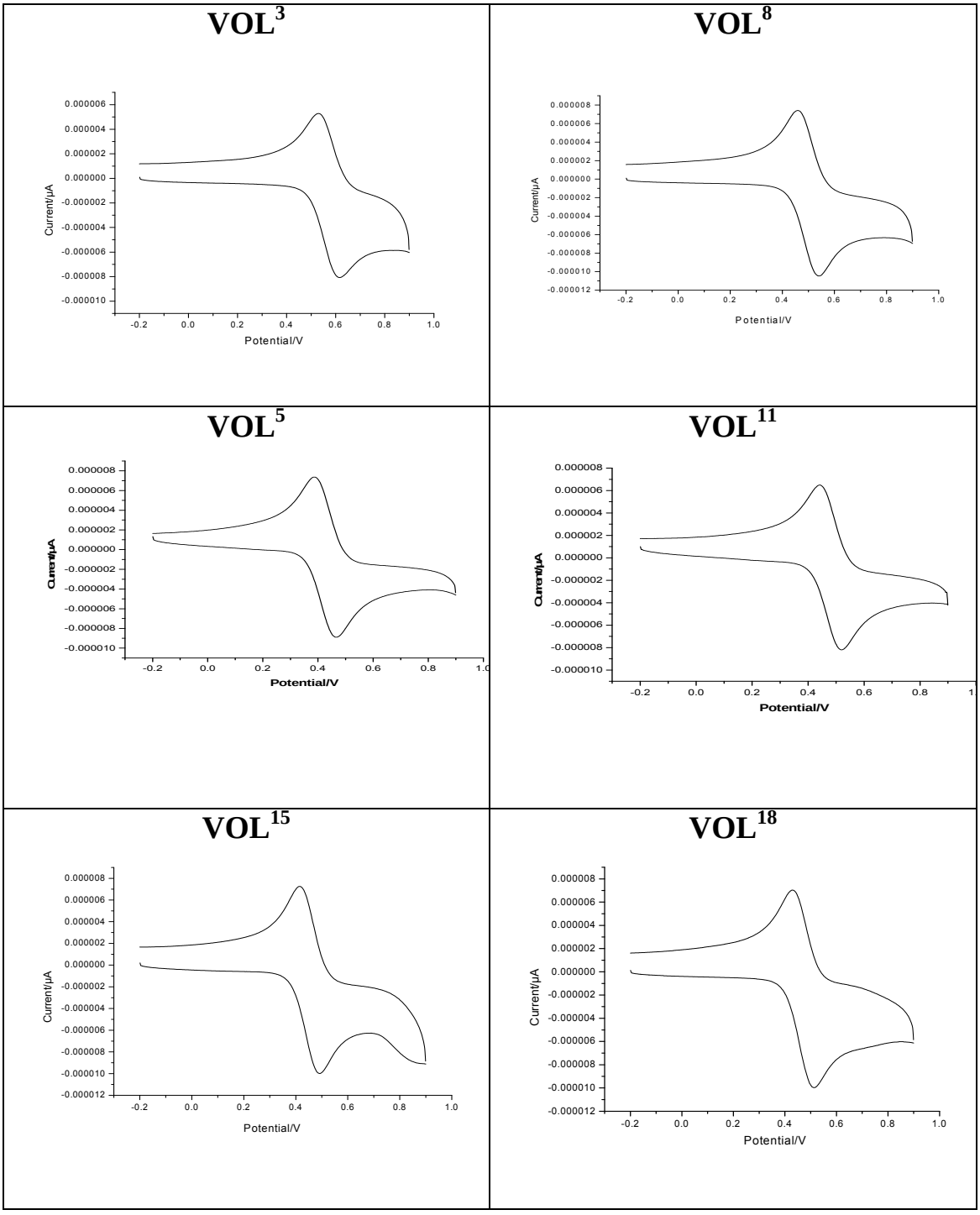

Fig. 4.6 Cyclic voltammograph of the oxovanadium(IV) complexes: Representative voltammograph for each of the series

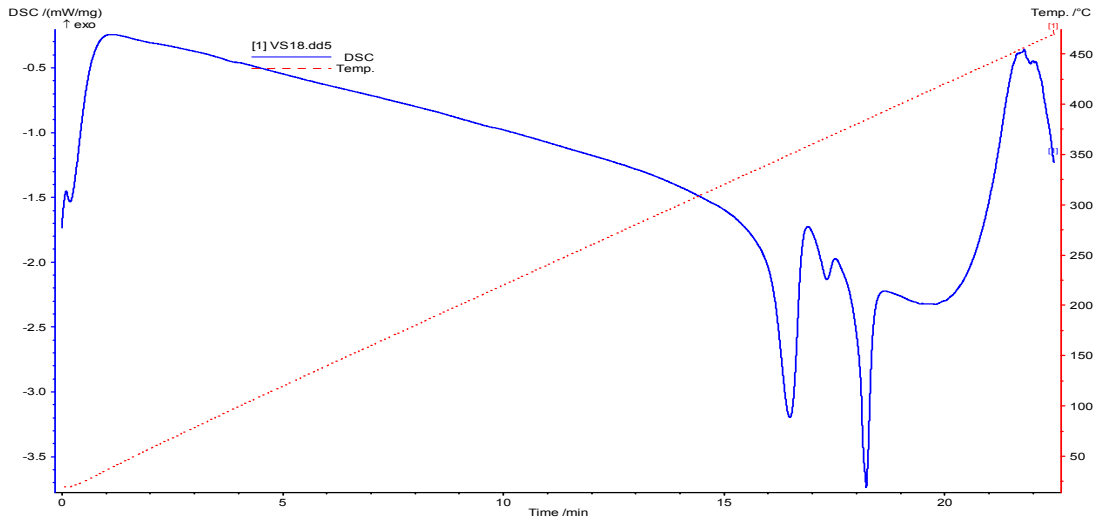

Fig. 4.7.1.1 DSC curves of VOL[1]

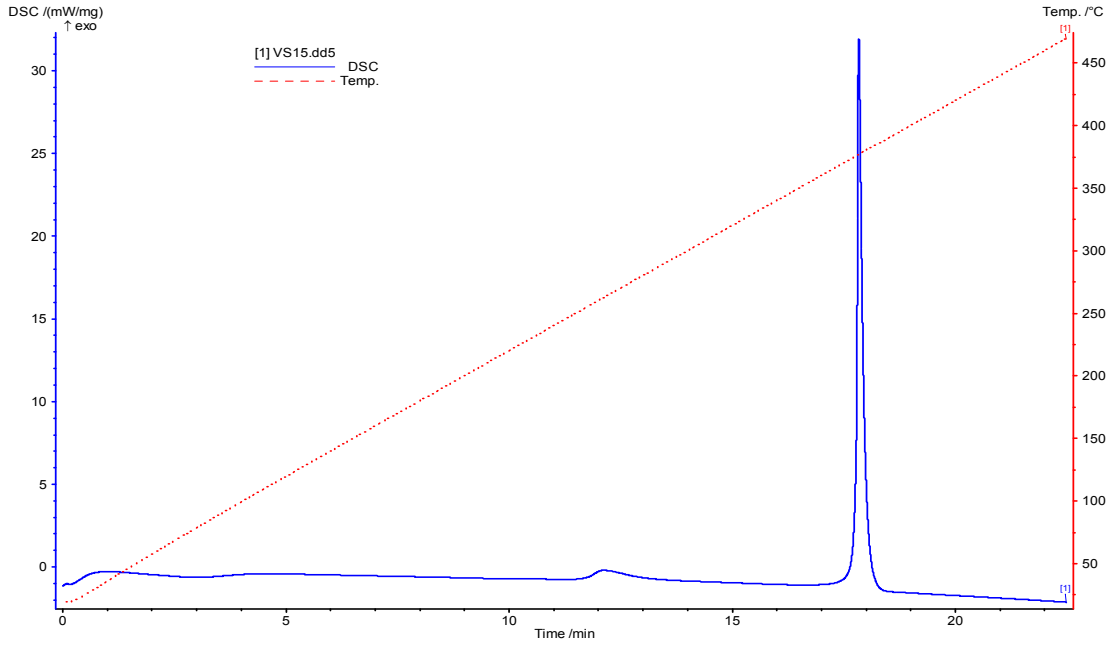

Fig. 4.7.1.2. DSC curves of VOL[2]

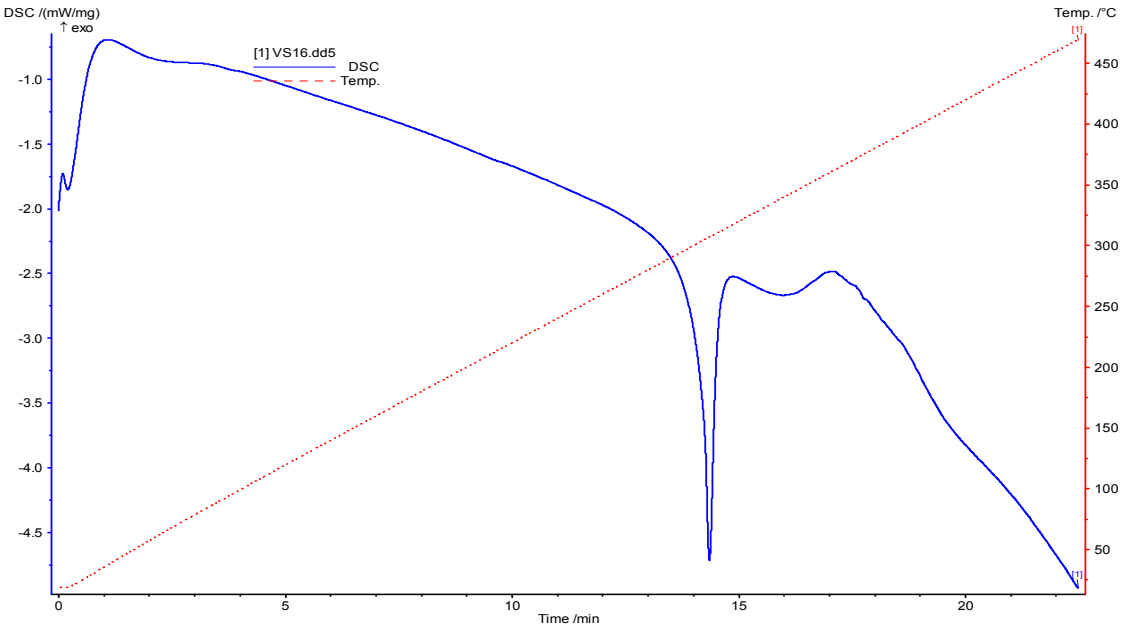

Fig. 4.7.1.3. DSC curves of VOL[3]

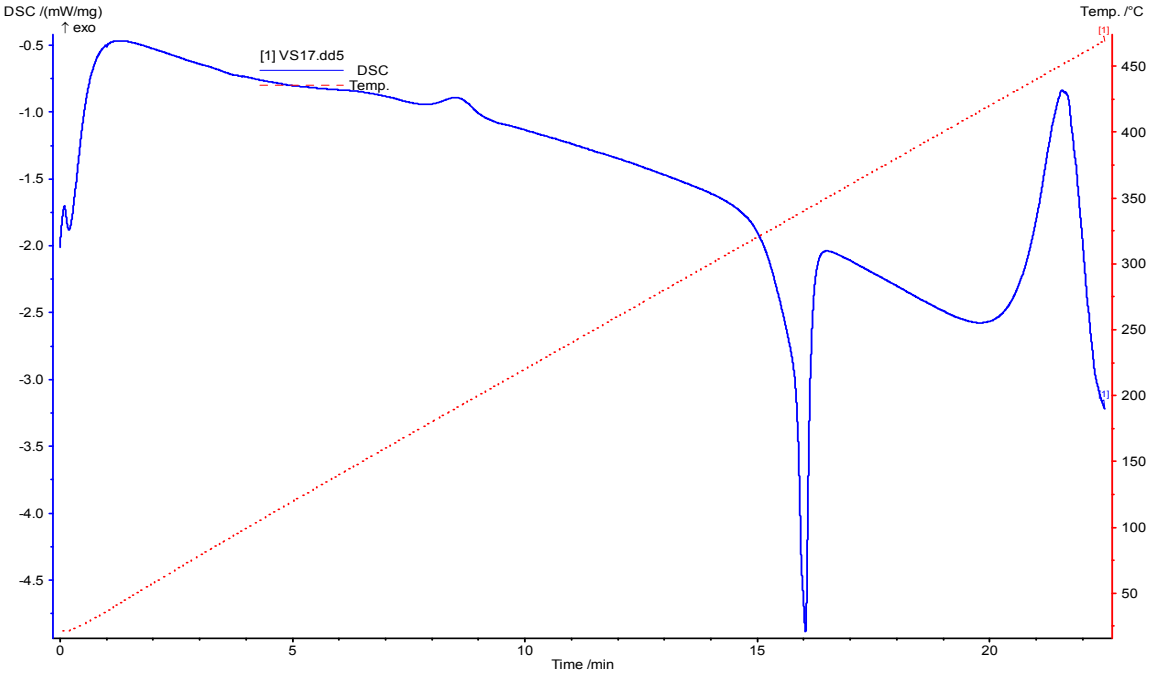

Fig. 4.7.1.4. DSC curves of VOL[4]

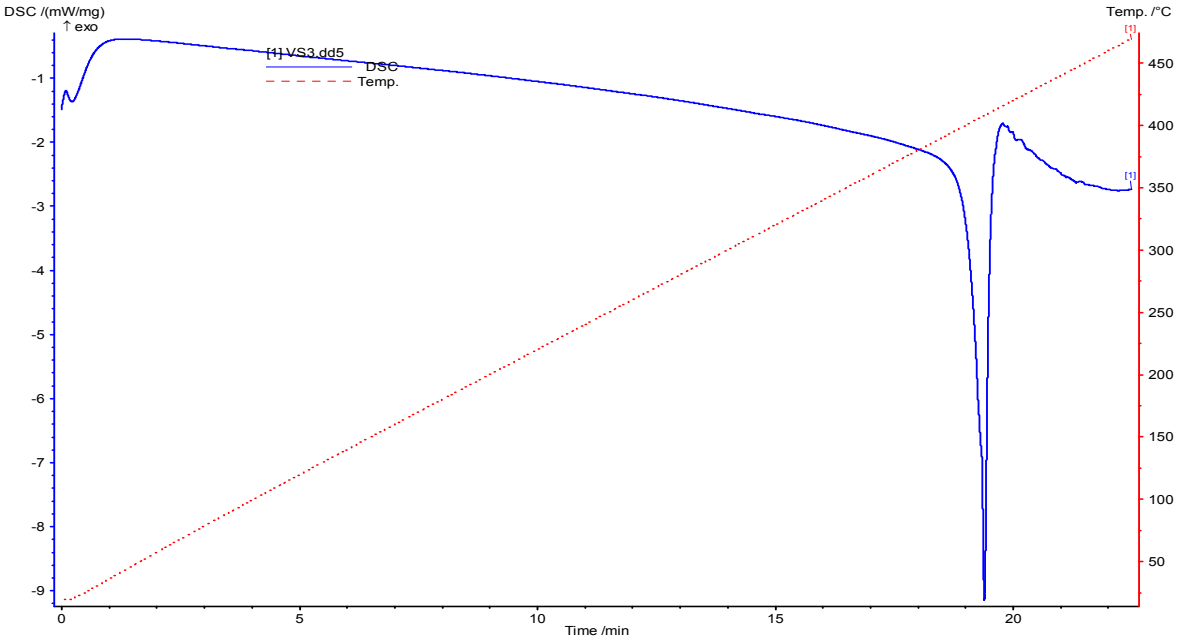

Fig. 4.7.2.1.1. DSC curves of VOL[5]

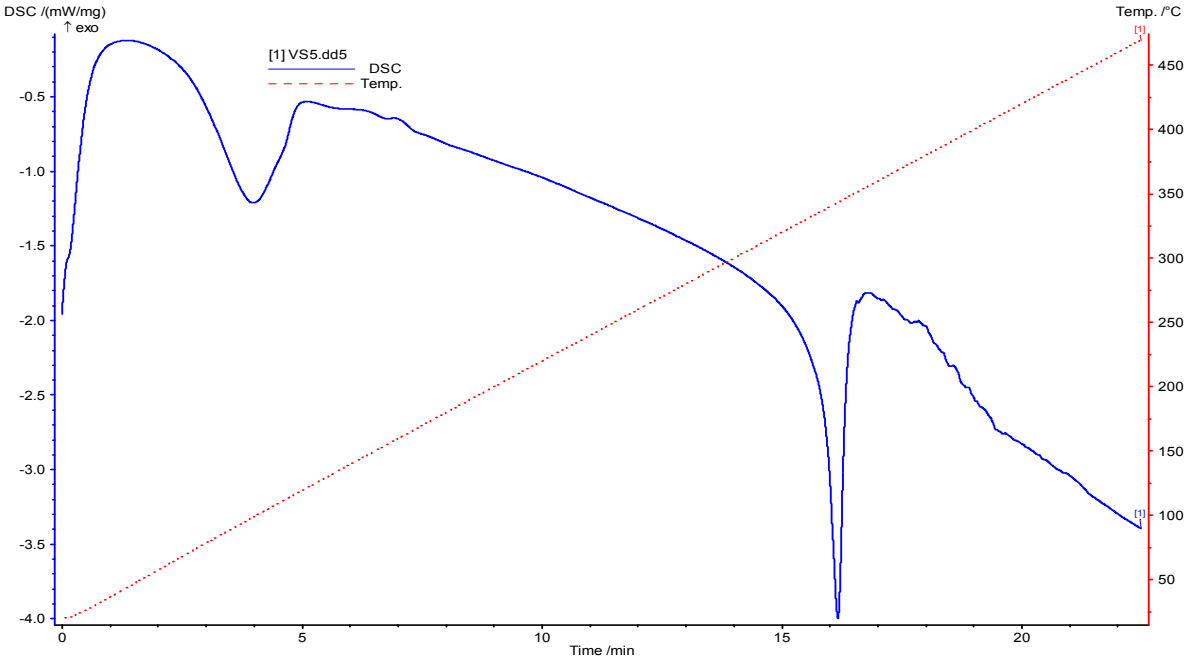

Fig. 4.7.2.1.3. DSC curves of VOL[7]

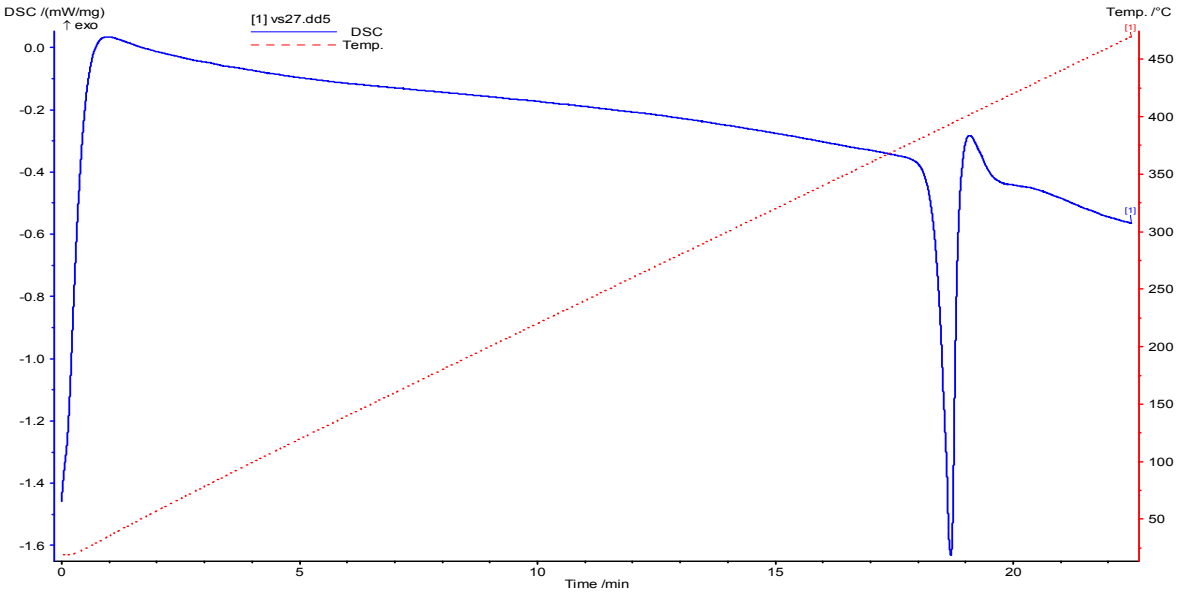

Fig. 4.7.2.2.1. DSC curves of VOL[8]

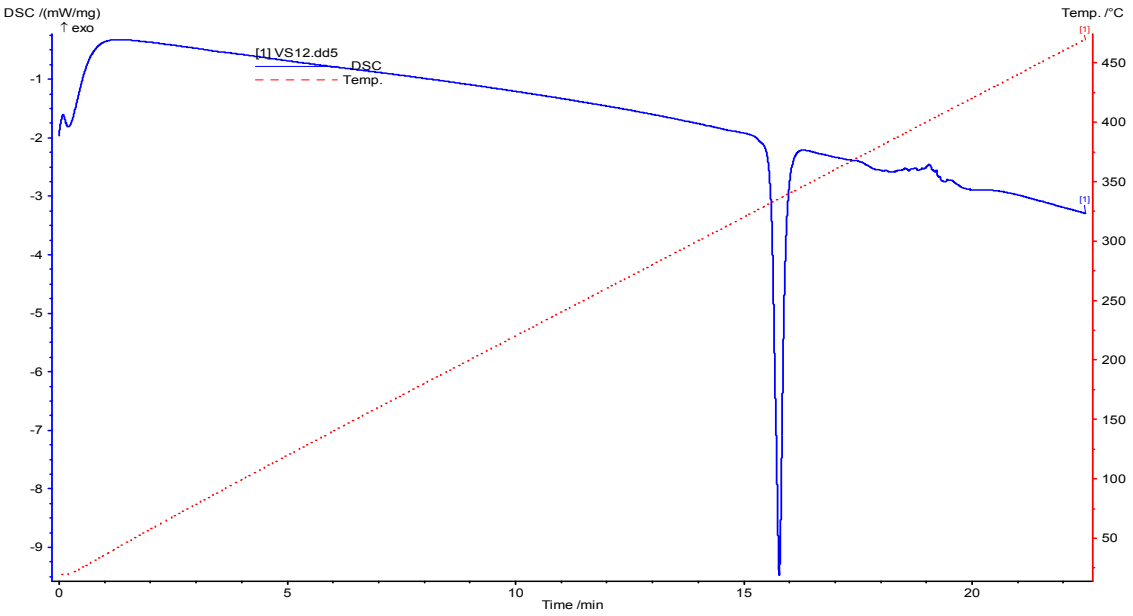

Fig. 4.7.2.2.2. DSC curves of VOL[9]

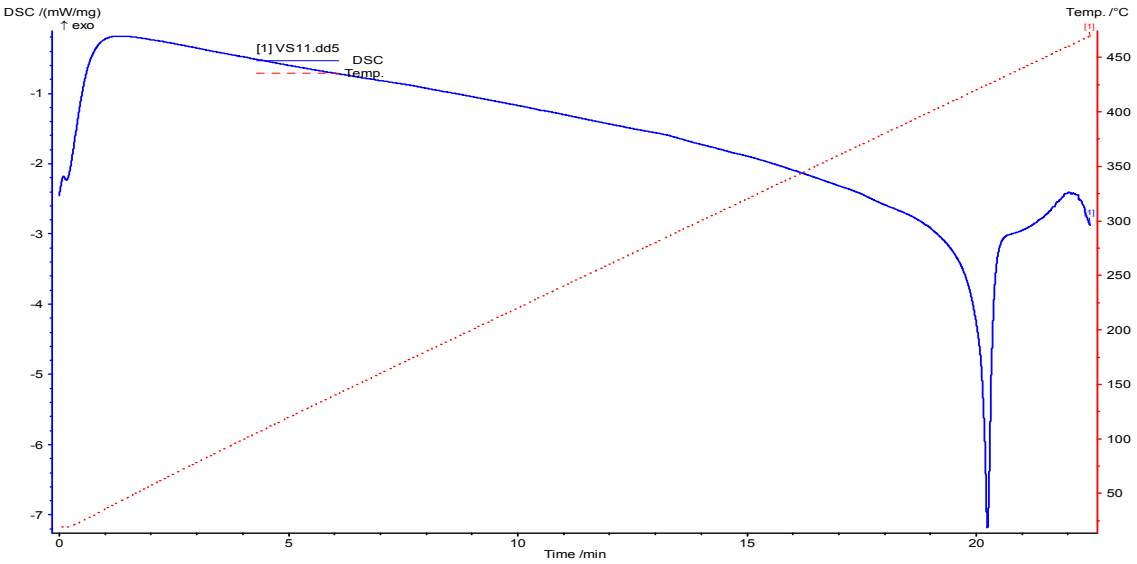

Fig. 4.7.2.2.3. DSC curves of VOL[10]

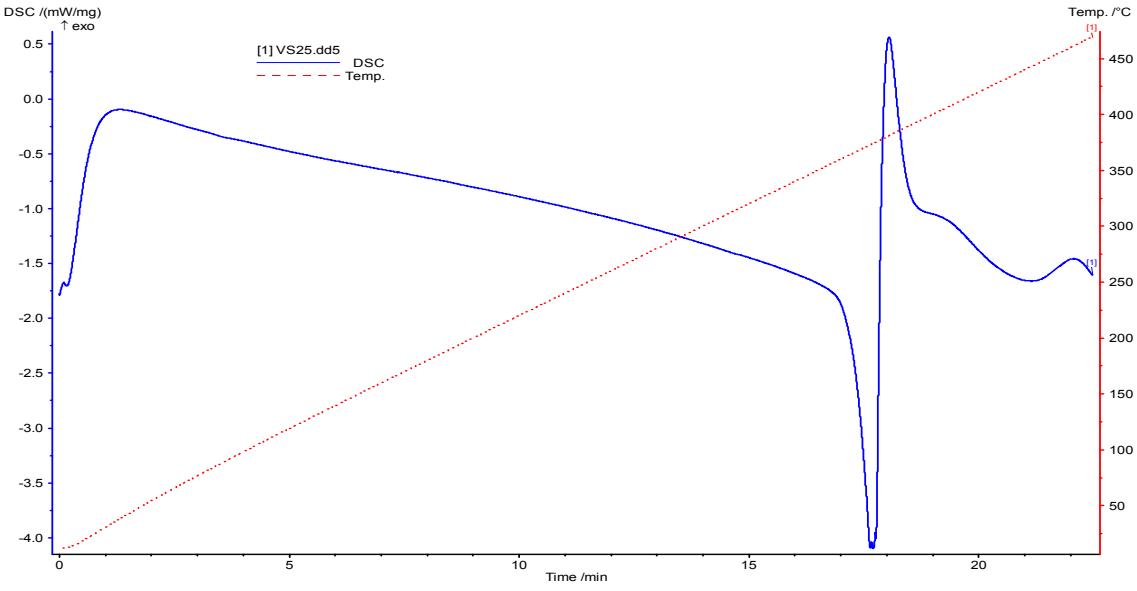

Fig. 4.7.2.3.1. DSC curves of VOL[11]

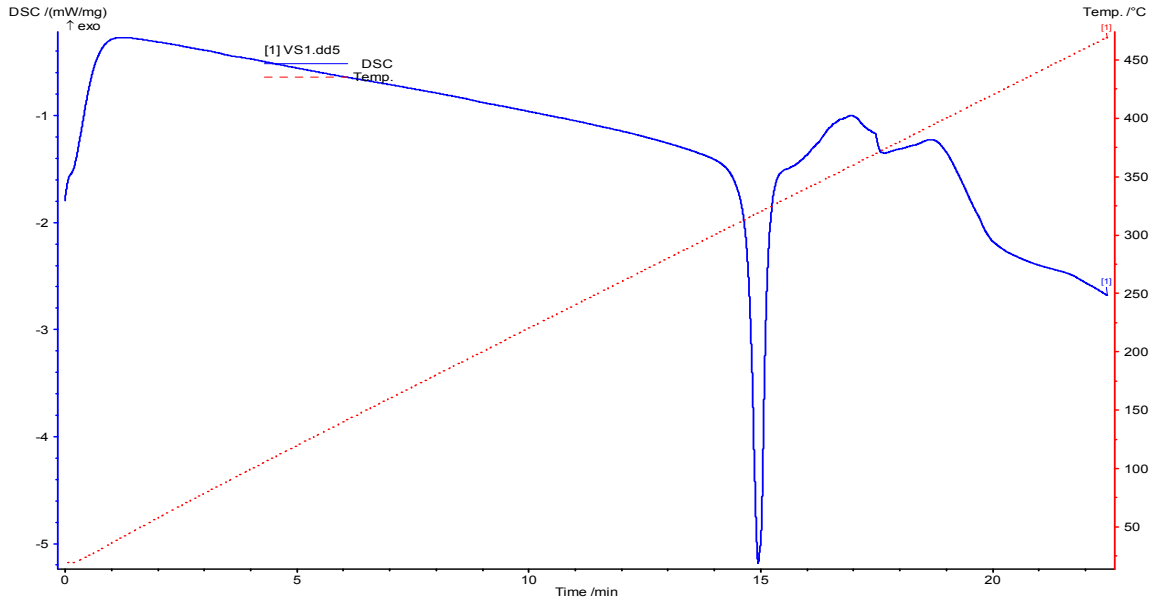

Fig. 4.7.2.3.2. DSC curves of VOL[12]

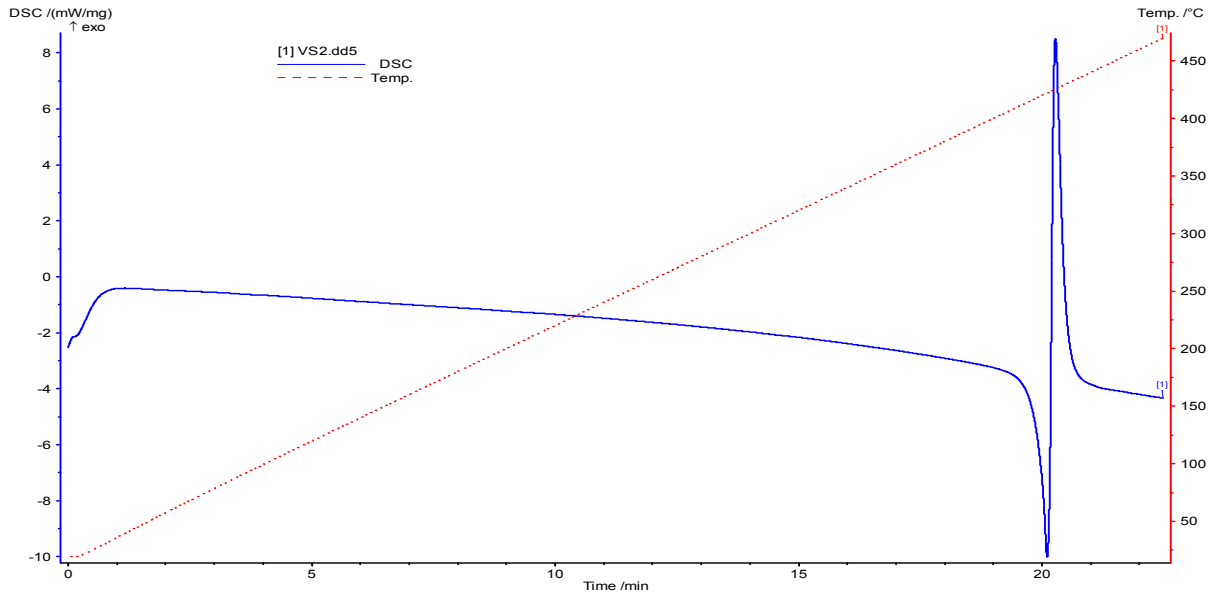

Fig. 4.7.2.3.3. DSC curves of VOL[13]

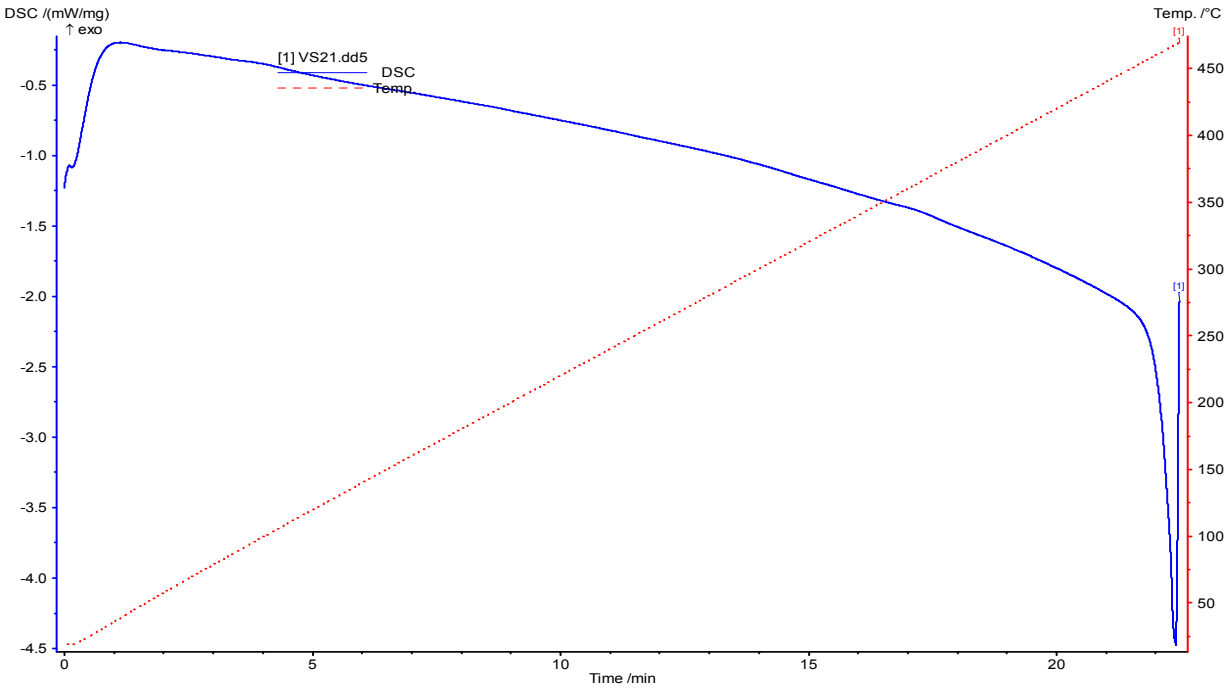

Fig. 4.7.2.3.4. DSC curves of VOL[14]

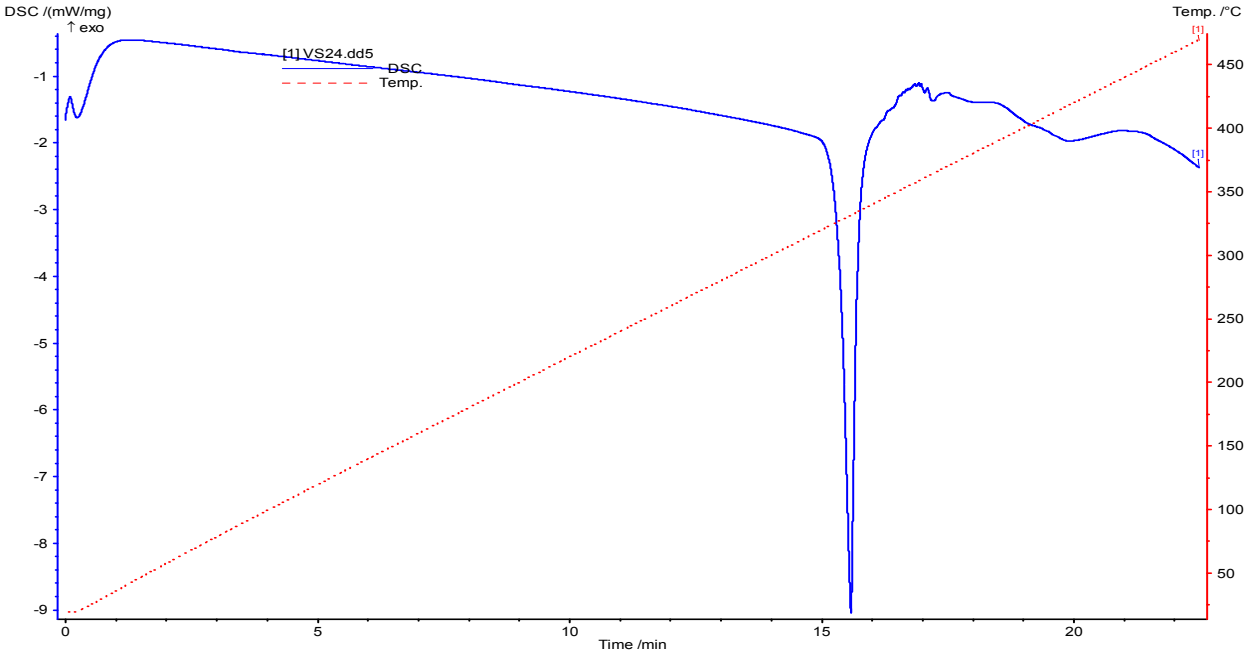

Fig. 4.7.2.4.1. DSC curves of VOL[15]

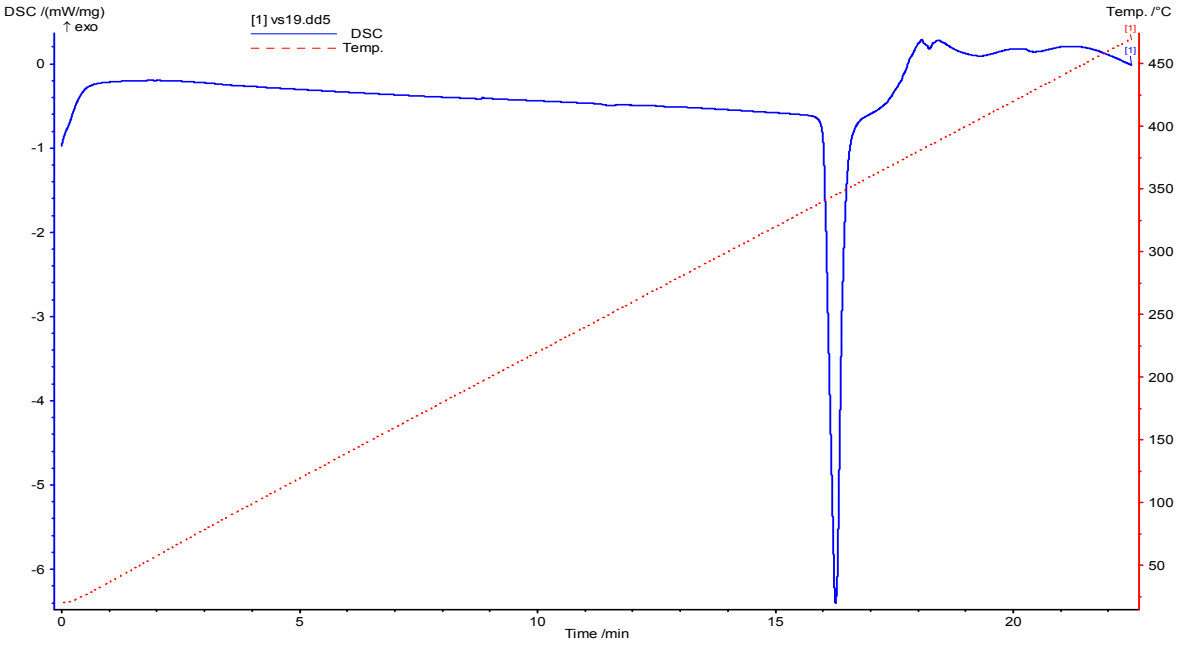

Fig. 4.7.2.4.2. DSC curves of VOL[16]

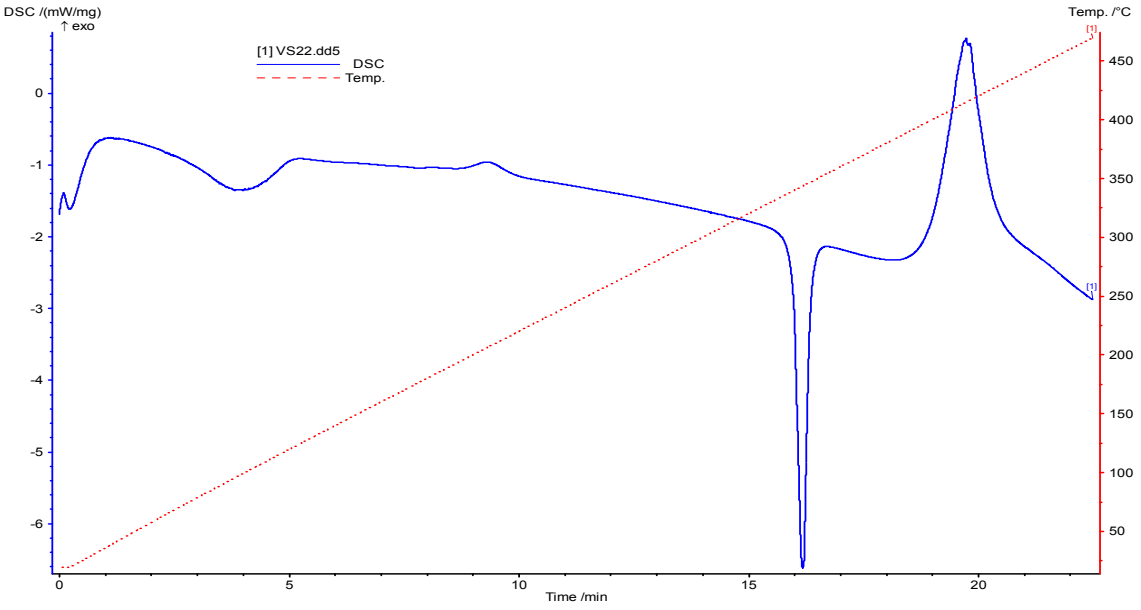

Fig. 4.7.2.4.3. DSC curves of VOL[17]

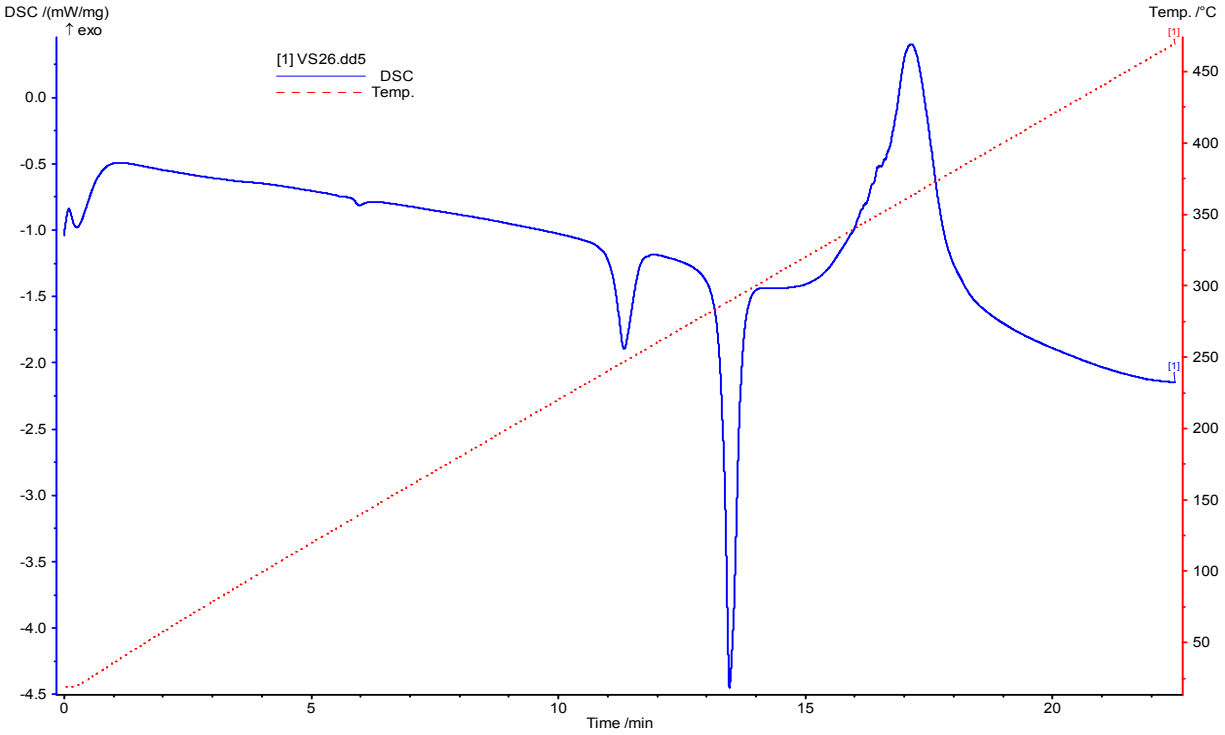

Fig. 4.7.2.5.1. DSC curves of VOL[18]

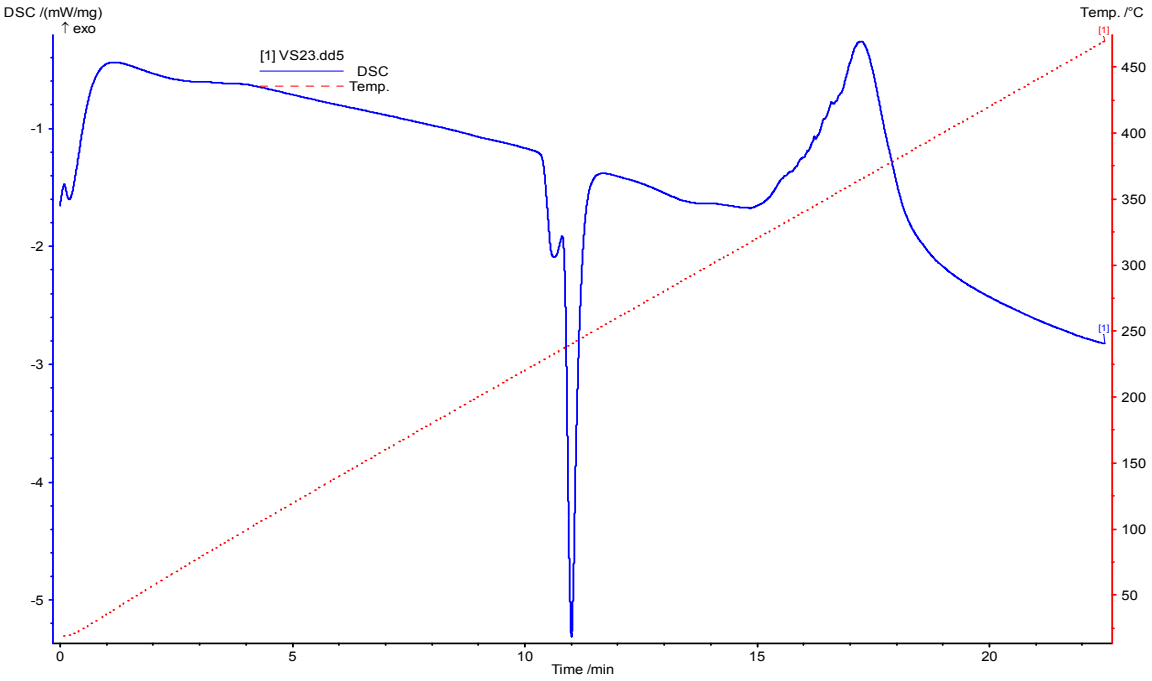

Fig. 4.7.2.5.2. DSC curves of VOL[19]

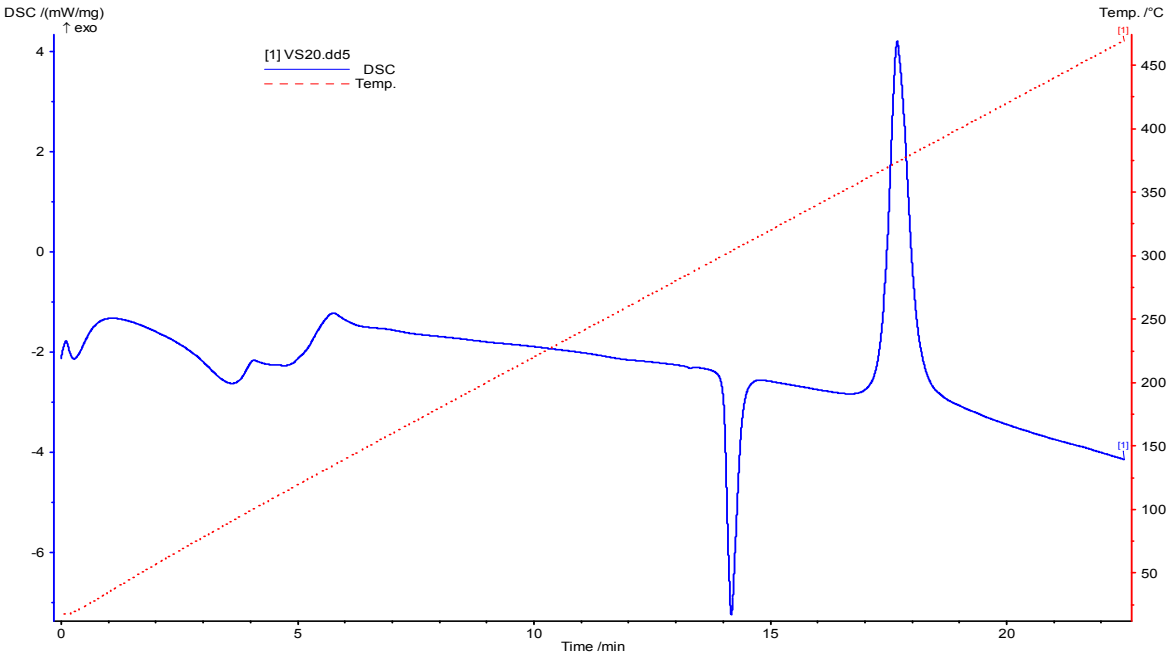

Fig. 4.7.2.5.3. DSC curves of VOL^{20}

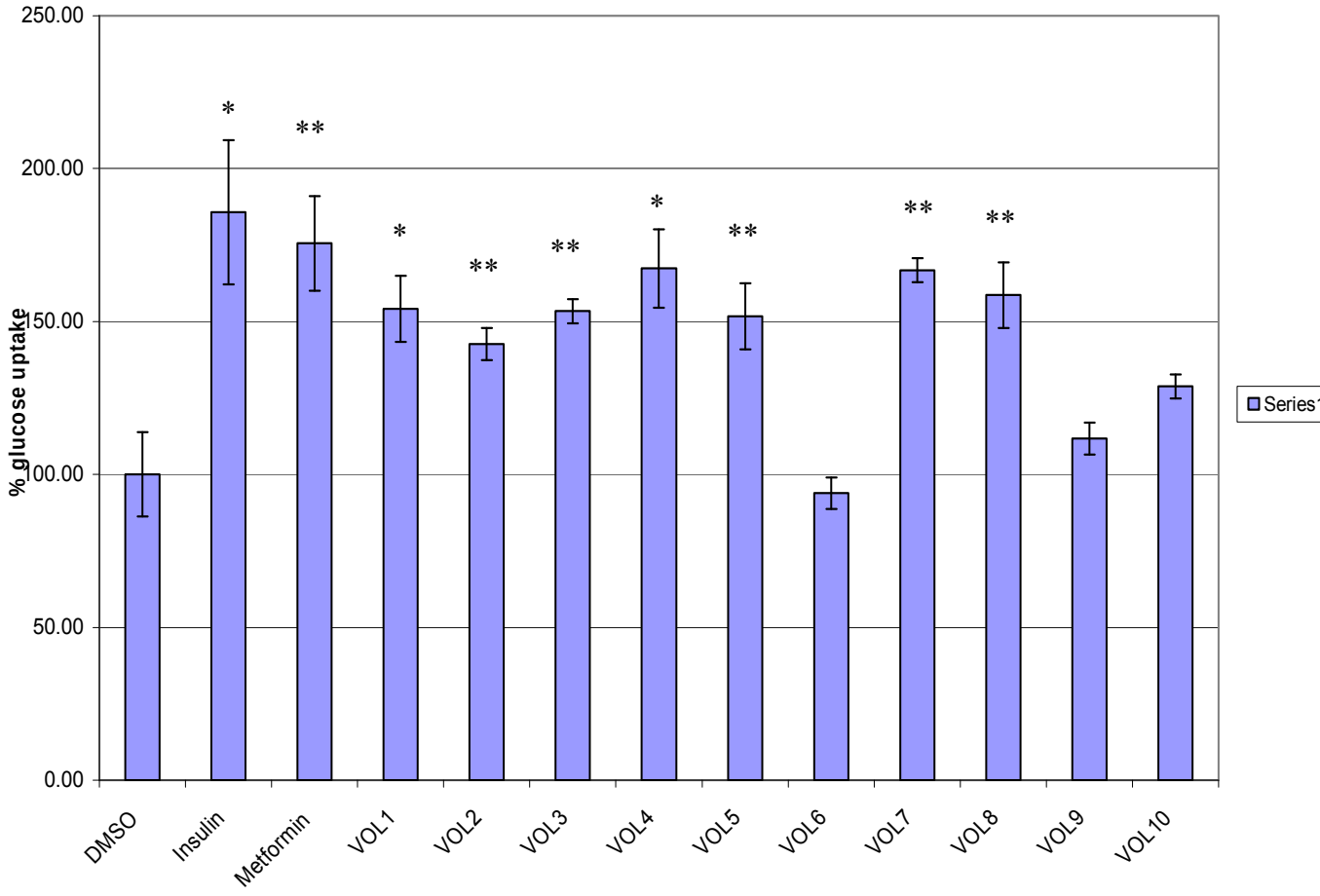

Fig. 5.1.1 Glucose uptake from the culture media containing 8mM glucose by C2C12 cells over one 1 **h.** C2C12 cells were pre-exposed to the complexes, insulin and metformin respectively in glucose and serum free media for 3 h before the glucose uptake experiments. Basal glucose uptake, i.e. solvent vehicle only (DMSO), is represented as 100% and the subsequent increase or decrease induced by the compounds is reflected as ± 100%. Statistical significances of p≤0.01 and 0.001 are indicated by * and ** respectively.

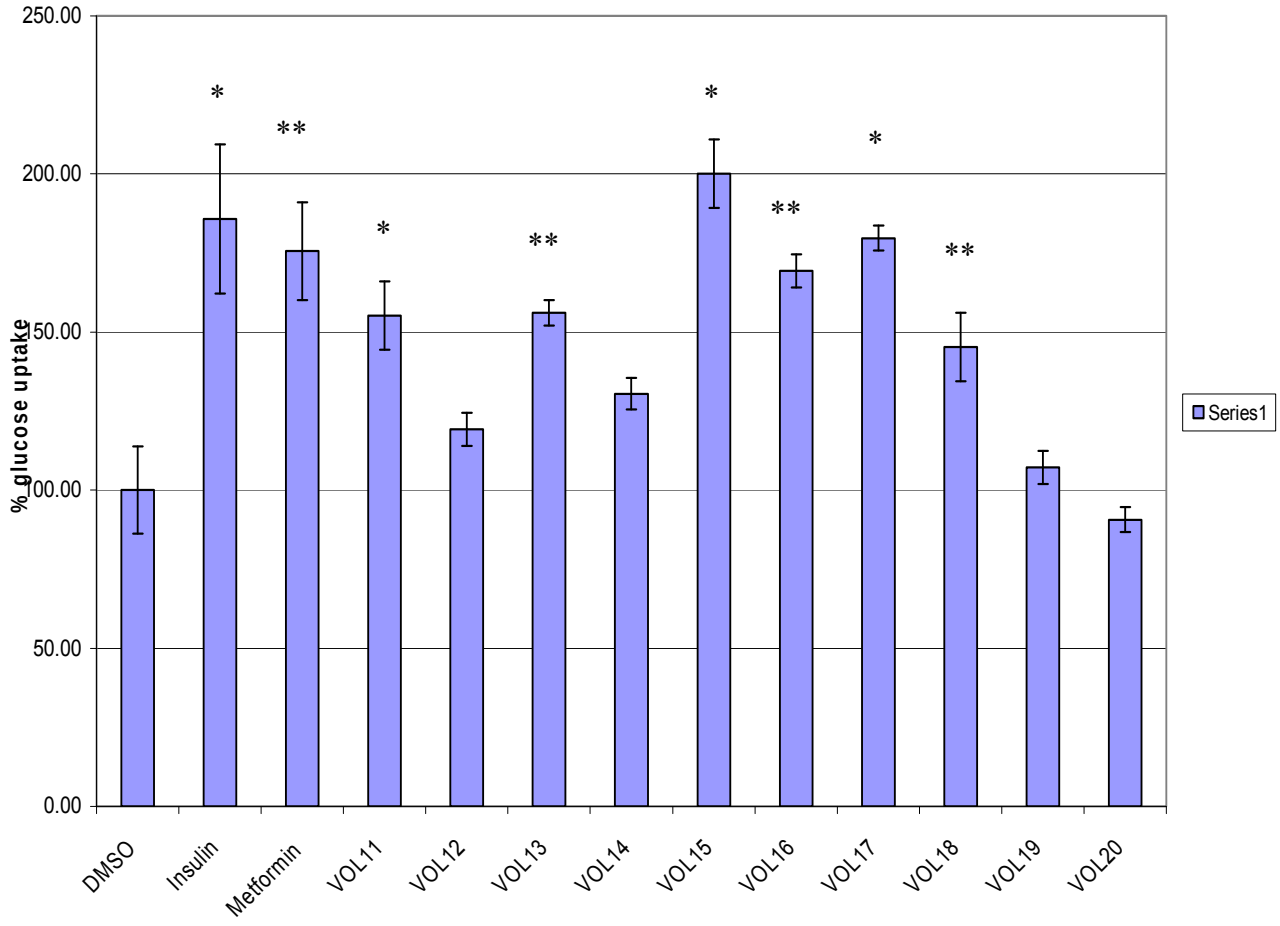

Fig. 5.1.2 Glucose uptake from the culture media containing 8mM glucose by C2C12 cells over one 1 h**.** C2C12 cells were pre-exposed to the complexes, insulin and metformin respectively in glucose and serum free media for 3 h before the glucose uptake experiments. Basal glucose uptake, i.e. solvent vehicle only (DMSO), is represented as 100% and the subsequent increase or decrease induced by the compounds is reflected as ± 100%. Statistical significances of p≤0.01 and 0.001 are indicated by * and ** respectively.

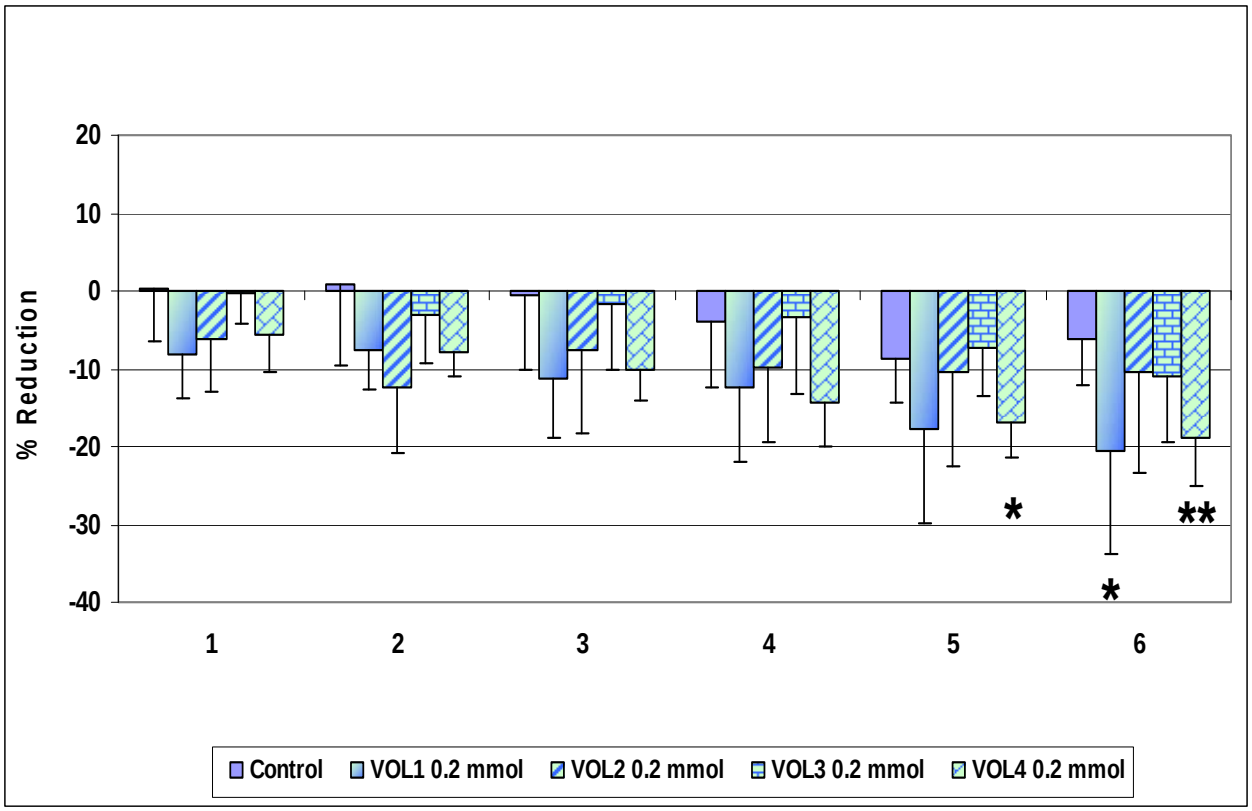

Fig. 5.2.1 The effect of the unsymmetrical complexes on hyperglycemia in Wistar outbred rats with STZ-induced diabetes is shown. A bar-graph with SEM error bars represents the hourly percentage changes in the whole blood glucose values over the 6-hour monitoring period.The percentage changes in the plasma glucose values of the treatment groups in the STZ rat model were calculated for each hour and then subtracted from the percentage changes in the control values (normalized against the control) at each time-point. A statistical significance of $p \leq 0.05$ is indicated by *, statistical significance 0.01 – 0.0001 is indicated by ** and statistical significance $p \leq 0.0001$ is indicated by ***.

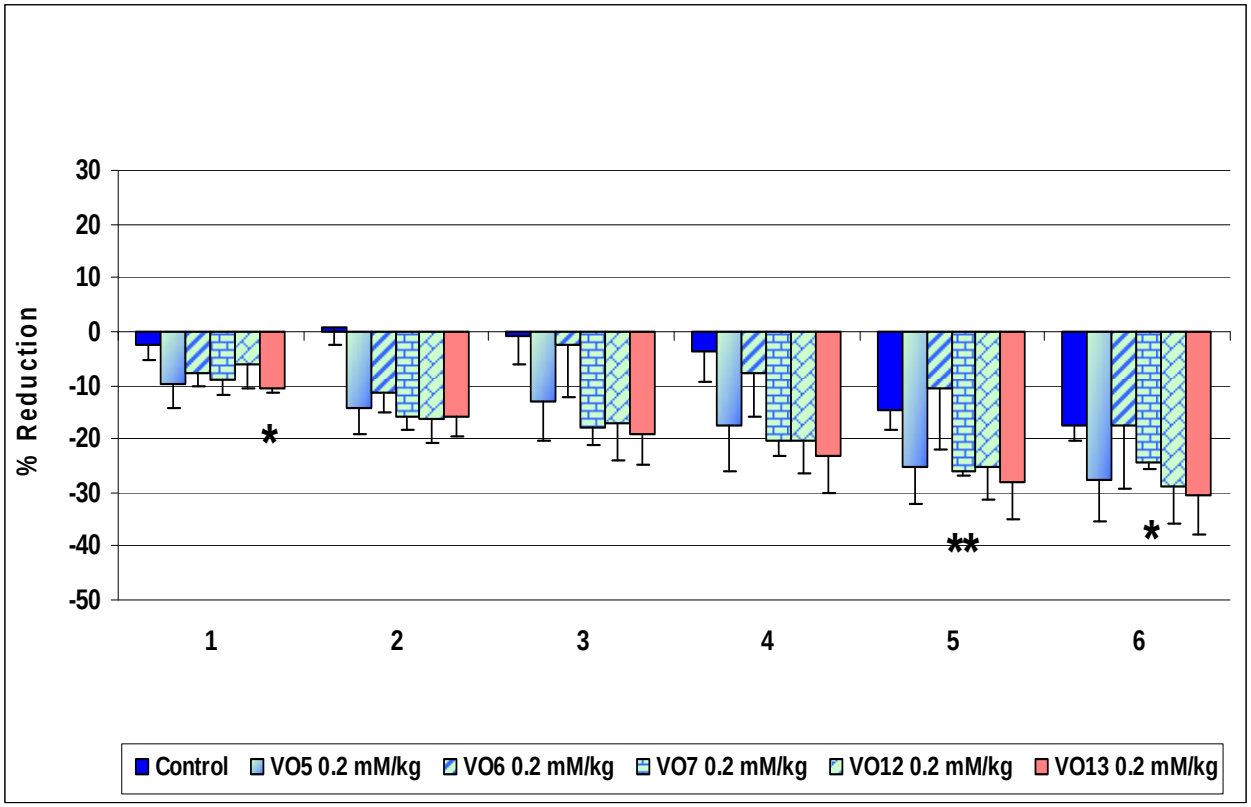

Fig. 5.2.2 The effect of five symmetrical complexes on hyperglycemia in Wistar outbred rats with STZ-induced diabetes is shown. A bar-graph with SEM error bars represents the hourly percentage changes in the whole blood glucose values over the 6-hour monitoring period.The percentage changes in the plasma glucose values of the treatment groups in the STZ rat model were calculated for each hour and then subtracted from the percentage changes in the control values (normalized against the control) at each time-point. A statistical significance of $p \leq 0.05$ is indicated by *, statistical significance 0.01 – 0.0001 is indicated by ** and statistical significance $p \leq 0.0001$ is indicated by ***.